Influence of Phonons on Semiconductor Quantum Emission

Dissertation

zur

Erlangung des Doktorgrades
der Naturwissenschaften
(Dr. rer. nat.)

dem Fachbereich Physik
der Philipps-Universität Marburg
vorgelegt

von

THOMAS FELDTMANN
aus Cuxhaven

Marburg (Lahn), 2009

Zusammenfassung

Viele Halbleitermaterialien weisen Bandlücken von einigen wenigen Elektronenvolt auf, was ihnen die Absorption oder Emission von sichtbarem Licht ermöglicht. Diese Eigenschaft bildet die Grundlage für zahlreiche technische Anwendungen, zu denen Solarzellen, LEDs und Laserdioden als Beispiele von besonderer wirtschaftlicher Bedeutung gehören. Doch auch in der Grundlagenforschung bedienen sich Physiker häufig optischer Experimente, um die Eigenschaften wechselwirkender Vielteilchensysteme in Halbleiterstrukturen zu untersuchen. Hierbei wird ausgenutzt, dass sowohl die Elektron-Elektron- als auch die Elektron-Phonon-Wechselwirkung Form und Dynamik der optischen Spektren beeinflussen. Um aus den experimentellen Ergebnisse auf den quantenmechanischen Zustand des Vielteilchensystems schließen zu können, benötigt man eine mikroskopische Theorie der gekoppelten Ladungsträger, Gitterschwingungen und Lichtfelder. Bei der kohärenten Spektroskopie erweist sich in der Regel eine semi-klassische Beschreibung der Licht-Materie-Wechselwirkung [1] als angemessen. Photolumineszenz wird hingegen häufig im inkohärenten Regime untersucht, wo das klassische Strahlungsfeld bereits verschwunden und die Polarisation des Materials zerfallen ist. Unter diesen Bedingungen stellt die Emission von Licht einen rein quantenmechanischen Prozess dar, dessen theoretische Beschreibung die Quantisierung des Lichtfeldes erfordert. Eine Möglichkeit, die verschiedenen Wechselwirkungen zwischen Elektronen, Phononen und Photonen einheitlich zu behandeln, ist die Heisenbergschen Bewegungsgleichungen für die relevanten Erwartungswerte zu lösen. Hierbei werden die auftretenden Operatorkombinationen über die Wechselwirkungsterme an immer kompliziertere Kombinationen gekoppelt, was auf das bekannte *Hierarchie-Problem* der Vielteilchenphysik führt. Eine konsistente Abbruchbedingung für die Gleichungshierarchie lässt sich z.B. mit Hilfe der sogenannten *Cluster-Entwicklung* [2–7] formulieren, bei der N-Teilchen-Erwartungswerte in unabhängige Einteilchengrößen, korrelierte Paare, korrelierte Drei-Teilchen-Cluster usw. bis hin zu den korrelierten N-Teilchen-Clustern faktorisiert werden. Man erhält dann ein geschlossenes System von Differentialgleichungen, indem man nur Cluster bis zu einer bestimmten Ordnung berücksichtigt. Mit dieser Methode konnten in jüngerer Zeit bereits Vielteilchenkorrelationen in ein- und zweidimensionalen Halbleitersystemen erfolgreich berechnet werden [7–9]. In der vorliegenden Arbeit wenden wir den allgemeinen theoretischen Rahmen auf zwei verschiedene Arten von Systemen an. Der erste Teil beschäftigt sich mit der Absorption und Emission in Halbleiter-Quantenpunkten, während im zweiten Teil phononenassistierte Resonanzen in den Lumineszenzspektren polarer Halbleiter untersucht werden.

Als *Quantenpunkte* bezeichnet man mesoskopische Heterostrukturen, in denen die Elektronen in allen drei räumlichen Richtungen in ihrer Bewegung eingeschränkt sind, was zu einer Diskretisierung ihrer Einteilchenenergien führt. In vielfacher Hinsicht lässt sich solch ein quasi nulldimensionales System als eine Art künstliches Atom betrachten. Ein Reihe kürzlich durchgeführter Experimente [10–15] hat eindrucksvoll gezeigt, dass Quantenpunkte Licht mit ausgeprägt nicht-klassischen Eigenschaften emittieren können. Bereits bei Dauerstrichanregung können sogenannte Photon-Antibunching-Effekte zu Abweichungen von der Poisson-Statistik führen [14]. Im Fall gepulster Anregung wurde sogar die Emission eines einzelnen Photons [11–13] oder eines Paares stark korrelierter Photonen [15] pro Periode beobachtet. Solch ein fundamental quantenmechanisches Verhalten macht Quantenpunkte zu vielverspre-

chenden Kandidaten für zukünftige Anwendungen in der Quantenkryptografie [16], in Quantencomputern [17,18] oder bei der Datenspeicherung [19]. Bereits ohne Kopplung an ein Lichtfeld stellt die theoretische Beschreibung des Ladungsträgersystems in einem Quantenpunkt ein anspruchsvolles Vielteilchenproblem dar [20–33]. Die eingeschränkte Dimensionalität des Systems führt im Allgemeinen zu einer beträchtlichen Verstärkung der Coulomb-Korrelationen zwischen den Elektronen und Löchern. Der Einfluss dieser Korrelationen auf die optischen Resonanzen des Systems wurden in früheren Veröffentlichungen mit Hilfe von Diagonalisierungsmethoden [20–27] und Konfigurations-Wechselwirkungs-Rechnungen [28–30] studiert. Die Eigenschaften eines isolierten Quantenpunktes lassen sich auf diese Weise sehr genau berechnen. Allerdings steigt der rechnerische Aufwand beträchtlich, wenn die Wechselwirkung mit mehreren quantisierten Lichtmoden berücksichtigt werden muss. Darüberhinaus sind Halbleiter-Quantenpunkte in der Regel in eine Festkörperumgebung eingebettet, so dass die eingesperrten Elektronen und Löcher sowohl mit propagierenden Ladungsträgern [34–37] als auch mit Gitterschwingungen [38–41] wechselwirken können.

Zur Modellierung all dieser Kopplungseffekte bietet sich die Cluster-Entwicklungs-Methode an, da sie sich in ähnlichen Situationen bei Systemen höherer Dimension bewährt hat. Wir bedienen uns dieses Verfahrens, um eine vollständig mikroskopische Theorie wechselwirkender Elektronen, Löcher und Photonen in einem Halbleiter-Quantenpunkt zu entwickeln. Die Gleichungshierarchie wird in zweiter Ordnung der Cluster-Entwicklung abgebrochen, was eine konsistente Berechnung der Dynamik von Teilchendichten, Polarisationen, klassischen Lichtfeldern sowie allen Coulomb- und quantenoptischen Zweiteilchenkorrelationen ermöglicht. Bei der Behandlung der internen Freiheitsgrade des Quantenpunktes muss sich unsere Herangehensweise an den oben erwähnten Methoden messen lassen, mit deren Hilfe die Eigenenergien des wechselwirkenden Ladungsträgersystems in vielen Fällen sogar exakt berechnet werden können. Unsere numerischen Ergebnisse zeigen, dass die Kenntnis der Ein- und Zweiteilchenkorrelationen ausreicht, um stabile Konfigurationen des Ladungsträgersystems zu beschreiben, die wohl-definierte optischen Resonanzen aufweisen. Wie in homogenen Systemen können auch in Quantenpunkten gebundene Elektron-Loch-Paare, d.h. Exzitonen, und Elektron-Loch-Plasma anhand der Coulomb-Korrelationen charakterisiert werden. Es stellt sich heraus, dass in einem schwach angeregten Quantenpunkt stabile Vielteilchenkonfigurationen von reinem Plasma bis zu vollständig korrelierten Elektron-Loch-Paaren auftreten können.

In Abhängigkeit von den zu untersuchenden Phänomenen müssen zwei verschiedene Sätze von Bewegungsgleichungen gelöst werden. Die *Halbleiter-Bloch-Gleichungen* (SBE) beschreiben die kohärente Anregung des Ladungsträgersystems durch ein klassisches Lichtfeld, während die Photoemission im inkohärenten Regime aus den *Halbleiter-Lumineszenzgleichungen* (SLE) berechnet werden kann. Mit Hilfe einer geeigneten Basistransformation lassen sich analytische Näherungsformeln sowohl für die lineare Absorption als auch für das stationäre Lumineszenzspektrum aufstellen. Aus der Struktur der SLE lässt sich erkennen, dass sowohl exzitonische Korrelationen als auch unkorreliertes Plasma Beiträge zur Photoemission liefern, die in einem gewöhnlichen Lumineszenz-Experiment nicht unterschieden werden können.

Die besondere Stärke des Cluster-Entwicklungs-Zugangs zur Beschreibung von Halbleiter-Quantenpunkten besteht darin, dass der Einfluss der Umgebung auf einfache Weise berücksichtigt werden kann. Zu diesem Zweck brauchen die Bewegungsgleichungen nicht neu formuliert, sondern lediglich durch zusätzliche Terme ergänzt zu werden. Als konkretes Beispiel betrachten wir die Kopplung an ein Reservoir von akustischen Gitterschwingungen. Nach einer resonanten optischen Anregung des Quantenpunktes führen phononenassistierte Prozesse zur Dephasierung kohärenter Größen wie der Polarisation, zur Bildung exzitonischer Populationen und zur Thermalisierung der Ladungsträger. Unsere Berechnungen machen deutlich, dass all diese Prozesse im Prinzip ähnlich wie in Quantenfilmen ablaufen, die betreffenden Zeitskalen

jedoch stark abweichen können.

Die in dieser Arbeit vorgestellte Theorie lässt sich in verschiedene Richtungen erweitern. Zum einen könnte der Einfluss der Festkörperumgebung des Quantenpunktes genauer untersucht werden, indem auch die Kopplung an propagierende Ladungsträger berücksichtigt wird. Auf der anderen Seite könnte man quantenoptische Korrelationen höherer Ordnung berechnen mit dem Ziel, die Quantenstatistik der Emission zu analysieren. Um das oben erwähnte Photon-Antibunching zu beschreiben, müsste man z.B. bedingte Detektionswahrscheinlichkeiten auswerten, bei denen es sich in der Sprache der Cluster-Entwicklung um Vierteilchengrößen handelt.

Im zweiten Teil dieser Arbeit spielt die Elektron-Phonon-Wechselwirkung eine zentrale Rolle. Longitudinale optische (LO) Phononen in Halbleitern tragen nicht nur zur Ladungsträgerstreuung bei, sondern können sich auch direkt an der Rekombination von Elektron-Loch-Paaren beteiligen, was zu einer Folge zusätzlicher Resonanzen im Lumineszenzspektrum führt. Bei hinreichend starker Kopplung lassen sich diese Resonanzen als Repliken der Exzitonlinie beobachten, die auch unter dem Namen *Phononen-Seitenbanden* bekannt sind, während die Exzitonlinie in diesem Zusammenhang häufig als *Nullphononlinie* bezeichnet wird [42–48].

Es existiert eine allgemein anerkannte störungstheoretische Behandlung der phononenassistierten Lumineszenz [49], die bereits in den Siebzigerjahren entwickelt worden ist und die bis in die Gegenwart in zahlreichen Veröffentlichungen verwendet wird. Diese Theorie basiert auf dem sogenannten Exziton-Bild, in dem der angeregte Zustand des Halbleiters ausschließlich als System von gebundenen Elektron-Loch-Paaren, d.h. Exzitonen, beschrieben wird. Theoretische und experimentelle Studien jüngeren Datums haben gewisse Schwächen eines solchen Zugangs aufgedeckt. Insbesondere kann, wie oben bereits erwähnt, Lumineszenz an der exzitonischen Resonanz nicht als Nachweis gewertet werden, dass sich tatsächlich Exzitonen in dem System gebildet haben, da unkorrelierte Elektron-Loch-Paare bei der selben Wellenlänge rekombinieren. Dieser überraschende Befund wurde zum ersten Mal in Ref. [50] dargelegt und konnte anschließend in einer Reihe von Experimenten bestätigt werden [51–53]. Eine der zentralen Fragen dieser Arbeit lautet daher, ob unkorreliertes Plasma auch zur phononenassistierten Lumineszenz beitragen kann. Um dieser Frage nachzugehen, verallgemeinern wir die SLE aus Ref. [50, 54], so dass spontane Emission an der ersten Exziton-Phonon-Resonanz berechnet werden kann. In der Tat zeigen unsere Ergebnisse, dass sowohl Plasma als auch gebundene Elektron-Loch-Paare zum Seitenband beitragen können. Dabei sind zumindest bei niedrigen Temperaturen die Linienformen und relativen Intensitäten so ähnlich, dass sich die beiden Quellen der Emission in einem gewöhnlichen Photolumineszenz-Experiment nicht auseinander halten lassen.

Es gibt jedoch noch weitere Gründe, einen neuen Blick auf das Phononen-Seitenband-Problem zu werfen. Kürzlich veröffentlichte Arbeiten haben gezeigt, dass die Seitenbandintensitäten vergleichbar zur Nullphononlinie oder sogar deutlich stärker werden können. Zu den eindrucksvollsten Beispielen gehören an ZnO-Nanodrähten gemessene Spektren, die zahlreiche Repliken mit einem weit von der Nullphononlinie entfernten Intensitätsmaximum aufweisen [55]. Derartige Experimente haben das Interesse an einer theoretischen Beschreibung von Phononen-Seitenbanden höherer Ordnung neu aufleben lassen. Die etablierte Theorie der phononenassistierten Lumineszenz gründet sich auf einer störungstheoretischen Behandlung der Elektron-Phonon-Wechselwirkung, wobei der n-te Summand der Störungsreihe die n-te Phononenreplik liefert. Die Eigenschaften der ersten beiden Seitenbanden lassen sich mit einem solchen Ansatz akkurat berechnen [49, 56–58]. Allerdings wird die Auswertung der Störungsreihe für große n sehr aufwendig. Um Repliken höherer Ordnung zu untersuchen, verwenden wir deshalb das sogenannte Polaron-Bild, in dem propagierende Kristallelektronen mit den von ih-

nen hervorgerufenen Gitterverzerrungen zu neuen Quasiteilchen vereinigt werden. Formal wird dies mit Hilfe einer unitären Transformation erreicht, die den Hamiltonoperator der Elektron-Phonon-Wechselwirkung eliminiert, während Phononoperator-Kombinationen beliebiger Ordnung Eingang in den Hamiltonoperator der Licht-Materie-Wechselwirkung finden [59]. Diese neue Struktur hat zur Folge, dass die phononenassistierten SLE im Polaron-Bild für alle Phononen-Seitenbanden getrennt ausgewertet werden können. Im stationären Limes erhalten wir eine kompakte Lumineszenzformel für Seitenbanden beliebiger Ordnung, in der Plasma und Exzitonen additiv zur Gesamtintensität beitragen.

Für einen direkten Vergleich mit der störungstheoretischen Behandlung führen wir die Cluster-Entwicklung auch im Exziton-Bild durch, wo nicht die Elektron-Phonon-, dafür aber die Coulomb-Wechselwirkung eliminiert ist. Da auf diese Weise das Hierarchie-Problem beträchtlich entschärft wird, lassen sich die phononenassistierten SLE im Exziton-Bild im stationären Limes rekursiv lösen, um Seitenbanden beliebiger Ordnung zu berechnen. Allerdings werden bei diesem Zugang nur die korrelierten Quellen der Emission berücksichtigt. Es stellt sich heraus, dass die Cluster-Entwicklungs-Methode für diese Beiträge sehr ähnliche Ergebnisse produziert wie der störungstheoretische Ansatz. Eine Weiterentwicklung der etablierten Theorie erreichen wir dadurch, dass wir unsere verschiedenen Ansätze miteinander kombinieren. Durch einen Vergleich der Lumineszenzformeln im Polaron- und im Exziton-Bild finden wir ein einfaches Verfahren, mit dem sich beliebige Repliken analytisch auswerten lassen.

Der kurzreichweitige Anteil der Elektron-Phonon-Wechselwirkung kann mit Hilfe von Deformationspotentialen modelliert werden. Eine LO Gitterschwingung in einem polaren Medium erzeugt ein oszillierendes, makroskopisches elektrisches Feld, dem die Kristallelektronen als geladene Teilchen ausgesetzt sind. Dieser Effekt liefert einen weiteren, langreichweitigen Beitrag zur Elektron-Phonon-Wechselwirkung, der unter dem Namen Fröhlich-Kopplung bekannt ist. Streuprozesse innerhalb eines Energiebandes werden für gewöhnlich von der Fröhlich-Wechselwirkung dominiert. Im Gegensatz hierzu legen unsere Berechnungen den Schluss nahe, dass der kurzreichweitige Anteil der Wechselwirkung selbst in stark polaren Halbleitern den Hauptbeitrag zu den Phononenrepliken liefern kann. Für dreidimensionale Halbleiterstrukturen sollte sich sowohl anhand der Amplitude als auch anhand der Temperaturabhängigkeit des Intensitätsverhältnisses der ersten beiden Repliken erkennen lassen, ob die Seitenbandemission von Fröhlich- oder Deformationspotential-Wechselwirkung herrührt.

Um unsere Theorie auszuwerten und zu prüfen, führen wir eine Reihe numerischer Fallstudien durch. Unsere Ergebnisse zeigen, dass oberhalb einer gewissen kritischen Temperatur die Phononenrepliken in einem Volumenhalbleiter stärker ausgeprägt sind als in einem Quantenfilm aus dem gleichen Material. Seitenbanden aufgrund von freien und an Störstellen gebundenen Exzitonen lassen sich anhand ihrer Linienformen und ihrer Temperaturabhängigkeit unterscheiden. Das Entstehen der außerordentlich starken Phononenrepliken in den erwähnten Nanodrähten lässt sich im Rahmen unserer Theorie deuten.

Die in dieser Arbeit vorgestellten Untersuchungen werfen eine Reihe von Fragen an zukünftige Experimente auf. So steht ein experimenteller Nachweis von Seitenbandemission aus unkorreliertem Plasma noch aus. Der Beitrag der optischen Deformationspotential-Wechselwirkung zu den Phononenrepliken in polaren Materialien ist in der Literatur bislang kaum diskutiert worden. Eine denkbare technische Anwendung der Seitenbandemission besteht in der Konstruktion eines Lasers, der an der Exzitonresonanz gepumpt wird, aber beim ersten Seitenband emittiert. Da phononenassistierte Absorption vornehmlich auf der Hochenergieseite der Exzitonlinie stattfindet, die Emission dagegen auf der Niedrigenergieseite, würde sich ein solcher Aufbau durch eine extrem niedrige Laserschwelle auszeichnen. Zur theoretischen Beschreibung der Eigenschaften eines Seitenbandlasers müssten die phononenassistierten Lumineszenzgleichungen an die Halbleiter-Bloch-Gleichungen gekoppelt werden.

Author's contributions

Publications

[I] T. FELDTMANN, L. SCHNEEBELI, M. KIRA, AND S.W. KOCH. Quantum theory of light emission from a semiconductor quantum dot. *Phys. Rev. B*, **73**:155319, 2006.

[II] T. FELDTMANN, M. KIRA, AND S.W. KOCH. Phonon sidebands in semiconductor luminescence. *Phys. stat. sol. (b)*, **246**(2):332, 2009.

[III] T. FELDTMANN, M. KIRA, AND S.W. KOCH. Theoretical analysis of higher-order phonon sidebands in semiconductor luminescence spectra. Submitted for publication, 2009.

[IV] T. FELDTMANN, M. KIRA, S.W. KOCH, ET AL. Microscopic theory of LO-phonon assisted semiconductor luminescence. (In preparation.)

[V] T. FELDTMANN, L. SCHNEEBELI, M. KIRA, AND S.W. KOCH. (In preparation.)

Original contributions

The first project in the framework of my Ph.D. thesis concerned the quantum dynamics of interacting charge carriers in a semiconductor quantum dot. L. Schneebeli[1] and I adopted the cluster-expansion based equation-of-motion approach that was used earlier in this group to analyze quantum wells and quantum wires. The central idea was to check the convergency of the cluster-expansion scheme for an isolated dot and to generalize the theory to open dot systems that are coupled to quantized light modes, phonons, or wetting-layer states. The underlying quantum-dot model was previously analyzed by F. Jahnke and coworkers (University of Bremen) with whom we discussed the single-particle wave functions and matrix elements. We developed a microscopic theory of spontaneous emission and characterized the generic phase space of the quantum-dot carriers in the incoherent regime. This analysis is summarized in Ref. [I] and was presented as a poster at the CLEO/QELS conference 2007.

Afterwards, L. Schneebeli and I worked on different aspects of quantum-dot theory. I extended the equations of motion to include coupling of the dot carriers to a phonon bath. The aim was to model processes like phonon-induced dephasing and build-up of excitonic correlations after coherent optical excitation with a classical light field. While my approach recovered a number of phenomena that are well known from higher-dimensional hetero structures, recent works on the polaron problem in quantum dots have shown that alternative approaches are necessary to describe the role of optical phonons quantitatively. Moreover, it turned out that the quantum-dot equations are more sensitive to numerical errors than the corresponding quantum-well dynamics. Thus, I finally switched the focus of my research to a different topic.

---

[1]Unless otherwise stated, all scientists mentioned in this section were members of the theoretical semiconductor physics group at the Phillips University in Marburg at the time of our collaboration.

Starting in summer 2007, I analyzed LO-phonon assisted emission in polar semiconductors that can lead to phonon sidebands, i.e. replica of the exciton peak, in the luminescence spectrum. Well-established perturbational theories that can successfully describe the first few sidebands had already been developed in the seventies. However, previous works in this group had shown that both excitonic populations and uncorrelated electron-hole plasma can lead to luminescence at the excitonic resonance and that these contributions cannot be distinguished by a standard luminescence experiment. It was therefore interesting to investigate whether plasma can also participate in phonon-assisted emission. Moreover, recent publications had reported on strong sideband emission from ZnO systems where numerous replica could be detected. To analyze these spectra, a compact theoretical description of higher-order phonon-assisted recombination would be desirable.

My first approach to the phonon-sideband problem was based on a unitary-transformation method that had been employed previously by K. Hannewald and P. A. Bobbert (Eindhoven University of Technology) to calculate exciton-phonon resonances in the absorption spectrum. I used the semiconductor Hamiltonian in the polaron picture to derive phonon-assisted luminescence equations. W. Hoyer and I arrived independently and in different ways at a closed steady-state luminescence formula for arbitrary-order replica where plasma and excitons contribute additively to the total intensity like for the exciton peak. Because prominent phonon sidebands are only observed with polar semiconductors, the LO-phonon assisted emission is almost always related to Fröhlich interaction in the literature. It turned out that the polaron-picture formula clearly underestimated the role of this coupling mechanism.

To shed some light on this problem, I also tried a different approach and generalized the well-known semiconductor luminescence equations to compute the first phonon replicum in the stationary limit. Similar results had been obtained earlier by A. Moskalenko, but I was able to find a more consistent truncation scheme. While the new results also took Fröhlich interaction into account, they surprisingly indicated that even in strongly polar media, the optical deformation-potential interaction can yield the dominant contribution to the sideband emission. This assumption is supported by two recent publications that report on the observation of extraordinarily strong phonon replica assigned to non-polar optical modes in ZnO nanowires. Having elaborated the relation between my two approaches, I presented the polaron-picture analysis as a poster at the NOEKS 9 workshop in 2008 and published it in Ref. [II]. The corresponding steady-state luminescence formula will be presented in Ref. [III].

To gain further insight into the relation between perturbative, polaron-picture, and cluster-expansion results, I also derived phonon-assisted luminescence equations in the exciton picture that could be solved in steady state for arbitrary-order replica. I was able to identify the limiting cases in which all three treatments produce comparable results for the excitonic contribution to the sideband luminescence. In a number of numerical case studies, I concentrated on the questions how plasma and exciton emission could be identified experimentally and whether Fröhlich and optical deformation-potential interaction lead to different temperature dependencies of the luminescence spectra. Furthermore, I considered free versus impurity-bound excitons and qualitatively compared emission from bulk and quantum-well systems. For the theory-experiment comparison, I was provided InGaN quantum-well spectra by OSRAM Opto Semiconductors (Regensburg). In view of the results of my case studies, the sideband luminescence in these systems could be traced back to bound excitons. I obtained quantitative agreement with ZnO bulk spectra found in the literature and could interpret the extraordinarily strong sideband emission observed with ZnO nanowires. In an ongoing collaboration with A. Chernikov and S. Horst from the experimental semiconductor physics group in Marburg, we seek to detect signatures of plasma emission in the transients of ZnO bulk spectra. Based on my generalized semiconductor luminescence equations, C. Böttge develops a microscopic

theory of lasing at the first exciton-phonon resonance.

Shortly before finishing this thesis, I collaborated with L. Schneebeli in another quantum-dot project. Using an elementary model of the exciton-to-biexciton transition in CdSe-based quantum dots, we proposed a device design for Zeno-based optoelectronics. This work will be summarized in Ref. [V].

Contents

List of Figures

1 Introduction

Many semiconductor materials have band gaps of a few electron Volts, which enables them to absorb or emit light in the visible range. On the one hand, this opens the door to a multitude of technical applications such as photovoltaic cells, LEDs, and lasers diodes. On the other hand, optical experiments with semiconductors are of fundamental interest for solid-state physicists as they provide a means to scan the properties of an interacting many-particle system. This is possible because the temporal evolution of the optical spectra as well as the positions and line shapes of the optical resonances are influenced by both the electron-electron and the electron-phonon interaction in the active material. In order to relate the experimental results to the quantum dynamics of the many-particle system, a microscopic theory of coupled charge carriers, lattice vibrations, and light field is needed. For coherent spectroscopy, a semi-classical description of the light-matter interaction constitutes an appropriate theoretical background [1]. Photoluminescence experiments, however, are often performed in the incoherent regime where the classical radiation field and the material polarization vanish. Under these conditions, the emission becomes a genuinely quantum-mechanical process such that the theoretical analysis requires a quantization of the light field. One possibility to treat electrons, phonons, and photons consistently on the same level of approximation is given by the Heisenberg equation-of-motion approach together with a cluster-expansion scheme that truncates the hierarchy of coupled differential equations [2–7]. Previously, this approach was successfully used to calculate many-body correlations in one- and two-dimensional semiconductor structures [7–9]. In the present thesis, we apply this theoretical framework to two different kinds of systems. The first part concerns the absorption and emission of semiconductor quantum dots while in the second part, phonon-assisted resonances in the luminescence spectra of polar semiconductors are investigated.

Quantum dots are mesoscopic hetero structures where the band-gap mismatch at the interfaces confines the electron movement in all three spatial directions, which results in a discrete single-particle spectrum for the charge carriers. In many aspects, this makes a quantum dot comparable to an artificial atom. A number of recent experiments [10–15] have demonstrated that the light emission from such a quasi zero-dimensional system can feature strikingly non-classical signatures. Already for continuous-wave excitation, so-called photon-antibunching effects can lead to sub-Poissonian emission statistics [14]. In case of a pulsed excitation, emission of a single photon [11–13] or one pair of strongly correlated photons [15] per pulse have been observed. This truly quantum-mechanical behavior makes quantum dots promising candidates for future applications in quantum cryptography [16] as well as quantum computing [17,18] and data storing [19]. Already in the absence of transverse electromagnetic fields, the theoretical description of the quantum-dot carrier system is a sophisticated many-body problem [20–33]. As a general tendency, the three-dimensional confinement strongly enhances the Coulomb correlations between the dot electrons and holes. To investigate the properties of these correlations and their effect on the optical resonances of the system, both partial and full diagonalization techniques [20–27] as well as configuration-interaction calculations [28–30] have been applied. These methods can successfully solve the specific details of an isolated dot. For instance, one can accurately describe emission and absorption lines. However, the

computations become rather involved when the interaction with a quantized multi-mode light field is included. Moreover—and here the analogy to atomic systems ends—semiconductor quantum dots are usually embedded in a solid-state environment such that the dot carriers become coupled to wetting-layer carriers [34–37] and phonons [38–41].

In view of its successful application to higher-dimensional systems, the cluster-expansion method lends itself to the consistent description of all these coupling effects. We therefore adopt that approach to develop a fully microscopical theory of Coulomb-interacting charge carriers in a quantum dot that are coupled to a light field. The backbone of our theory will be formed by the *semiconductor Bloch equations* (SBE) and the *semiconductor luminescence equations* (SLE) for the quantum dot. The SBE describe the excitation of the carrier system when it is driven by a coherent light field [60] whereas the SLE describe the emission from the dot under incoherent conditions [50, 54]. While we concentrate here on the internal electronic interaction, our theory can straightforwardly be extended to include all kinds of phenomena related to open quantum-dot systems. In order to demonstrate the potential of our approach, we implement the interaction with a generic reservoir of lattice vibrations to study phonon-assisted phenomena such as dephasing of polarization and thermalization of the carrier system.

The electron-phonon interaction plays a central role in the second part of this thesis. Longitudinal optical (LO) phonons not only provide scattering for electrons and holes in semiconductors but they can also participate in electron-hole recombination, which gives rise to additional resonances in the luminescence spectrum of a semiconductor. Provided that the coupling is sufficiently strong, these resonances can be observed as replica of the excitonic peak that are commonly referred to as phonon sidebands while the exciton peak is called zero-phonon line in this context [42–48].

There exists a well-established perturbational treatment of phonon-assisted luminescence [49] that was already developed in the seventies and is widely used in the literature till the present day. This theory describes the excited states of the semiconductor purely in terms of bound electron-hole pairs called *excitons*. More recent theoretical and experimental studies have revealed certain shortcomings of such an approach. In particular, luminescence at the excitonic resonance may not be considered as unique evidence that excitons are present in the system because uncorrelated electron-hole plasma emits at the same wave lengths. This surprising result was first pointed out in Ref. [50] and subsequently confirmed in a number of experiments [51–53]. One of the main goals of this work is to investigate whether uncorrelated plasma can also contribute to phonon-assisted luminescence. To this end, we generalize the SLE from Refs. [50, 54] such that spontaneous emission at the first exciton-phonon resonance can be calculated.

However, there are further reasons why we reconsider the phonon-sideband problem. Recent experimental publications report that the sideband intensities can be of the same order of magnitude or even larger than the intensity of the zero-phonon line. Among the most striking examples are ZnO nanorod spectra featuring numerous replica with the intensity maximum far away from the exciton peak [55]. Experiments like these have renewed the interest in the theoretical description of higher-order sideband emission. The existing theory of LO-phonon assisted luminescence is based on a perturbative treatment of the electron-phonon interaction where the n-th term of the perturbation series yields the n-th replicum. The specific details of the first few phonon sidebands can accurately be resolved with such an approach [49, 56–58]. However, the evaluation of the perturbation series becomes very laborious with increasing n. For the analysis of higher-order replica, we therefore prefer a unitary-transformation method [59] that allows us to treat the electron-phonon interaction non-perturbatively. With the phonon-assisted SLE in the new picture, arbitrary-order recombination processes can thus

be evaluated separately.

The thesis is organized as follows. In Chap. 2, we define the many-body Hamiltonian for interacting electrons, phonons, and photons in bulk and confined semiconductor systems, and outline the cluster-expansion approach. The quantum-dot analysis is presented in Chap. 3, and the phonon-sideband problem is treated in Chap. 4. The results of our studies will be summarized in Chap. 5. For the readers convenience, lengthy calculations and formal aspects of the derivations that do not contribute to the understanding of the physical content are generally moved to the appendix.

2 Theoretical description of bulk and confined semiconductor systems

This chapter is organized as follows. In Sec. 2.1, we define the semiconductor Bloch basis for bulk and confined carrier systems. Lattice vibrations are introduced in Sec. 2.2. The carrier-phonon coupling is discussed in considerable detail to provide an appropriate background for the study of phonon-assisted processes in quantum dots and polar semiconductors. Electron-electron and electron-photon interaction are contained in the quantum-electrodynamical Hamiltonian presented in Sec. 2.3. Because this part of the theory has been thoroughly developed in Refs. [7, 61], we concentrate here on the modifications that are necessary to analyze zero- and three-dimensional semiconductor structures. Finally, we give a brief description of the cluster-expansion approach in Sec. 2.4.

2.1 Single-particle wave functions

For practical computations in second quantization, the electronic field operator $\hat{\Psi}(\mathbf{r})$ is usually expanded into an appropriate single-particle basis. A useful choice that accounts for the discrete translational symmetry of the ionic equilibrium potential is provided by the semiconductor Bloch basis. Before explicitly defining the wave functions, we must briefly introduce some basic notations regarding the periodicity of the crystal. In crystalline solids, the equilibrium positions of the ions are arranged periodically in three linearly independent spatial directions. A minimal building block that fills the crystal volume completely when stacked is called *unit cell*. *Lattice vectors* $\mathbf{R}$ translate one unit cell of an infinite crystal onto another. After fixing the origin of the coordinate system, these vectors define the *crystal lattice*. The *reciprocal lattice* is the set of all wave vectors $\mathbf{G}$ with the property that $e^{i\mathbf{G}\cdot\mathbf{R}} = 1$ for an arbitrary lattice vector $\mathbf{R}$. The shape of the unit cell is not uniquely determined by the above definition. Because it displays all the symmetries of the crystal, one often uses the so-called *Wigner-Seitz cell* that is defined as the set of points in space which are closer to a given lattice point than to any other lattice point. The (first) *Brillouin zone* is the Wigner-Seitz cell of the reciprocal lattice that is centered at the origin. High-symmetry points in the Brillouin zone are marked by capital Greek or Latin letters. In particular, the zone center is always referred to as Γ point, irrespective of the crystal symmetry.

When the ions are at their equilibrium positions, they provide a lattice-periodic potential $V_{\text{ion}}^0(\mathbf{r}) = V_{\text{ion}}^0(\mathbf{r} + \mathbf{R})$. According to the *Bloch theorem*, non-interacting electrons moving through such a potential can be described by single-particle wave functions

$$\psi_{\lambda,\mathbf{k}}(\mathbf{r}) = \frac{e^{i\mathbf{k}\cdot\mathbf{r}}}{\sqrt{\mathscr{L}^3}} u_{\lambda,\mathbf{k}(\mathbf{r})} \tag{2.1}$$

that separate into a plane-wave part with wave vector $\mathbf{k}$ and a lattice-periodic *Bloch function* $u_{\lambda,\mathbf{k}}(\mathbf{r}) = u_{\lambda,\mathbf{k}}(\mathbf{r}+\mathbf{R})$ that is specified by an additional quantum number λ. The wave functions are normalized with respect to a cube of side length $\mathscr{L}$. Periodic boundary conditions restrict

the allowed values of the components of $\mathbf{k}$ to integer multiples of $2\pi/\mathscr{L}$. Surface effects can be eliminated by considering the limit $\mathscr{L} \to \infty$ under the assumption of a constant electron density.[1] One can show that $\psi_{\lambda,\mathbf{k}+\mathbf{G}}(\mathbf{r}) = \psi_{\lambda,\mathbf{k}}(\mathbf{r})$ for every reciprocal lattice vector $\mathbf{G}$. The wave vectors $\mathbf{k}$ may thus be restricted to the Brillouin zone. With this choice, Eq. (2.1) defines a complete orthogonal set. The Brillouin zone contains as many wave vectors as there are unit cells in the quantization volume. *In the remainder of this thesis, the letters $\mathbf{k}$, $\mathbf{p}$, $\mathbf{q}$ will always denote Brillouin-zone vectors unless otherwise stated.* When electrons and other elementary excitations such as phonons or photons that are characterized by a wave vector $\mathbf{k}$ participate in a scattering process, the total wave vector is conserved up to a reciprocal lattice vector $\mathbf{G}$. This conservation law is a consequence of the discrete translational symmetry of the system and motivates to call $\hbar\mathbf{k}$ the *crystal momentum*. A scattering process is called *normal process* for $\mathbf{G} = \mathbf{0}$ and *umklapp process* for $\mathbf{G} \neq \mathbf{0}$. In this work, we exclusively consider electrons with small momenta that interact with photons in the optical regime and long-wavelength phonons. It is then justified to neglect umklapp processes completely. A fixed quantum number λ defines an electronic *energy band*. For our purposes, it will mostly be sufficient to include only one *valence band* $\lambda = \mathrm{v}$ and one *conduction band* $\lambda = \mathrm{c}$ in the analysis. The ground state of the electron system is characterized by a completely filled valence band and an empty conduction band. All materials that we will investigate are *direct semiconductors* where both the upper valence-band edge and the lower conduction-band edge are located at $\mathbf{k} = \mathbf{0}$. The energy spacing between the bands is the *gap energy* E_{g}. In lowest non-vanishing order, the single-particle energies $\varepsilon_{\lambda,\mathbf{k}}$ have parabolic dispersions in the vicinity of the Γ point,

$$\varepsilon_{\mathrm{v},\mathbf{k}} = \frac{\hbar^2 k^2}{2m_{\mathrm{v}}}, \tag{2.2}$$

$$\varepsilon_{\mathrm{c},\mathbf{k}} = E_{\mathrm{g}} + \frac{\hbar^2 k^2}{2m_{\mathrm{c}}}, \tag{2.3}$$

where we assume that $\varepsilon_{\lambda,\mathbf{k}}$ only depends on $k = |\mathbf{k}|$. The Bloch electrons then behave like quasi-free particles with *effective masses*

$$m_\lambda \equiv \hbar^2 \left(\left. \frac{\mathrm{d}^2\varepsilon_{\lambda,\mathbf{k}}}{\mathrm{d}k^2} \right|_{k=0} \right)^{-1}. \tag{2.4}$$

As usual in semiconductor physics, we will often refer to conduction-band electrons and missing valence-band electrons as *electrons* and *holes*, respectively. Holes are positively charged and have a positive effective mass $m_{\mathrm{h}} \equiv -m_{\mathrm{v}}$ in direct semiconductors while the electron effective mass is written as $m_{\mathrm{e}} \equiv m_{\mathrm{c}}$. One can assign positive single-particle energies $\varepsilon_{\mathbf{k}}^{\mathrm{e}} \equiv \varepsilon_{\mathrm{c},\mathbf{k}}$ and $\varepsilon_{\mathbf{k}}^{\mathrm{h}} \equiv -\varepsilon_{\mathrm{v},\mathbf{k}}$ to the electrons and holes, respectively.

Besides the bulk case where the electron system is genuinely three-dimensional, we will also consider confined systems in this work. Here, the movement of the charge carriers is restricted in one, two or all three spatial directions. The corresponding systems are referred to as *quantum wells* (QW), *quantum wires* (QWI), and *quantum dots* (QD), respectively. These geometries can be realized as semiconductor hetero structures that are composed of regions of different semiconductor materials the band gaps of which do not match. Hence, the valence- and conduction-band edges of the two materials do not align with each other at the interfaces. The energy spacing of the band edges defines the *band offset* and produces the potential that is responsible for the carrier confinement. We will exclusively consider hetero structures where

---

[1]The quantization volume is usually chosen to have the same proportions as the unit cell. Nevertheless, we will stick to the cube so as not to overburden the notation.

electrons and holes are confined at the same side of the interface (*type-I structures*) although the opposite case can also occur.

Typically, the confined systems are mesoscopic in the sense that the lateral extensions of the hetero structure are small compared to the length scales of the bulk crystal, but still large compared to the unit cell. A simple and intuitive approach to calculating the single-particle states and energies for such a mesoscopic structure is provided by the so-called *envelope-function approximation* [1, 62, 63]. This approach is based on the assumption that the wave functions of the confined carriers can still be written as the product of a lattice-periodic Bloch function and an envelope function. Deviating from the bulk case, the plane-wave parts for the motion perpendicular to the hetero structure are replaced by the eigenfunctions of a single valence- or conduction-band electron exposed to a *confinement potential* V^{conf}. The bulk case would be recovered for vanishing V^{conf} when these eigenfunctions were plane waves again.

For the description of d-dimensional structures, it is useful to decompose three-dimensional vectors $\mathbf{x} = (x_\parallel, x_\perp)$ into their components $x_\parallel$ and $x_\perp$ parallel and perpendicular to the hetero structure, respectively. Hence, $x_\parallel$ is a d-dimensional and $x_\perp$ a $(3-d)$-dimensional vector where $d = 0, 1, 2$ for QD, QWI and QW. With this notation, the single-particle wave functions in envelope-function approximation can be written as

$$\psi_{\lambda,\beta,k_\parallel}(\mathbf{r}) = \frac{\mathrm{e}^{\mathrm{i}k_\parallel \cdot r_\parallel}}{\sqrt{\mathscr{L}^d}} \zeta_{\lambda,\beta}(r_\perp) u_{\lambda,k_\parallel}(\mathbf{r}) \tag{2.5}$$

with the Bloch functions from the bulk case $u_{\lambda,\mathbf{k}}(\mathbf{r}) = u_{\lambda,(k_\parallel,k_\perp)}(\mathbf{r})$ where we use the abbreviation $u_{\lambda,k_\parallel}(\mathbf{r}) \equiv u_{\lambda,(k_\parallel,k_\perp \simeq 0)}(\mathbf{r})$. Due to the broken translational symmetry perpendicularly to the hetero structure, only the parallel component $\hbar k_\parallel$ of the crystal momentum $\hbar \mathbf{k}$ has to be conserved in scattering processes. The *confinement functions* $\zeta_{\lambda,\beta}(r_\perp)$ are determined from the stationary Schrödinger equations

$$\left[-\frac{\hbar^2}{2m_\lambda} \frac{\partial^2}{\partial r_\perp^2} + V_\lambda^{\mathrm{conf}}(r_\perp) \right] \zeta_{\lambda,\beta}(r_\perp) = E_{\lambda,\beta}^{\mathrm{conf}} \zeta_{\lambda,\beta}(r_\perp), \tag{2.6}$$

that is, the envelope-function approximation relies on the assumption that the Bloch electrons can be treated as quasi-free particle with effective masses m_λ as described above. The additional quantum numbers introduced by the confinement define the sub-band index β. An electron with crystal momentum $\hbar k_\parallel$ in sub-band β of band λ has the single-particle energy

$$\varepsilon_{\lambda,\beta,k_\parallel} \equiv \varepsilon_{\lambda,(k_\parallel,k_\perp \simeq 0)} + E_{\lambda,\beta}^{\mathrm{conf}}. \tag{2.7}$$

Owing to the approximative character of the ansatz, the $V_\lambda^{\mathrm{conf}}(r_\parallel)$ do not reflect the actual potential landscape in the hetero structure but describe the confinement phenomenologically. Quantum wells, for instance, can often be modeled as infinite potential wells where the well width L is a fit parameter that can be quite different from the diameter of the hetero structure.

Equations (2.1) and (2.5) define the semiconductor Bloch basis for bulk and confined systems, respectively. Expanding the electronic field operator into this basis leads to

$$\hat{\Psi}(\mathbf{r}) = \sum_{\lambda,\mathbf{k},\sigma} \psi_{\lambda,\mathbf{k}}(\mathbf{r}) \left| \sigma \right\rangle \hat{a}_{\lambda,\mathbf{k},\sigma} \tag{2.8}$$

for bulk and

$$\hat{\Psi}(\mathbf{r}) = \sum_{\lambda,\beta,k_\parallel,\sigma} \psi_{\lambda,\beta,k_\parallel}(\mathbf{r}) \left| \sigma \right\rangle \hat{a}_{\lambda,\beta,k_\parallel,\sigma} \tag{2.9}$$

7

for confined systems where σ denotes the spin quantum number. The fermionic annihilation operators $\hat{a}_{\lambda,\mathbf{k}}$ and creation operators $\hat{a}^{\dagger}_{\lambda,\mathbf{k}}$ obey *fermionic commutation relations*

$$[\hat{a}_{\lambda,\mathbf{k},\sigma}, \hat{a}^{\dagger}_{\lambda',\mathbf{k}',\sigma'}]_{+} = \delta_{\lambda,\lambda'}\delta_{\mathbf{k},\mathbf{k}'}\delta_{\sigma,\sigma'}, \tag{2.10a}$$

$$[\hat{a}_{\lambda,\mathbf{k},\sigma}, \hat{a}_{\lambda',\mathbf{k}',\sigma'}]_{+} = 0 = [\hat{a}^{\dagger}_{\lambda,\mathbf{k},\sigma}, \hat{a}^{\dagger}_{\lambda',\mathbf{k}',\sigma'}]_{+}. \tag{2.10b}$$

For confined electrons, the corresponding relations read

$$[\hat{a}_{\lambda,\beta,k_{\|},\sigma}, \hat{a}^{\dagger}_{\lambda',\beta',k'_{\|},\sigma'}]_{+} = \delta_{\lambda,\lambda'}\delta_{\beta,\beta'}\delta_{k_{\|},k'_{\|}}\delta_{\sigma,\sigma'}, \tag{2.11a}$$

$$[\hat{a}_{\lambda,\beta,k_{\|},\sigma}, \hat{a}_{\lambda',\beta',k'_{\|},\sigma'}]_{+} = 0 = [\hat{a}^{\dagger}_{\lambda,\beta,k_{\|},\sigma}, \hat{a}^{\dagger}_{\lambda',\beta',k'_{\|},\sigma'}]_{+}. \tag{2.11b}$$

2.2 Dynamics of the crystal lattice

The following information is condensed from a number of textbooks and original papers and supplemented with our own considerations. Since the material is not presented in a coherent fashion throughout the different sources, we organize this section such that it is self-contained. Still, we only derive relations and properties that are explicitly referred to in later parts of this work.

The Hamiltonian of the interacting electron-ion system can be written in the form

$$\hat{H}_{\mathrm{mat}} = \hat{H}_{\mathrm{el}} + \hat{H}_{\mathrm{ion}} + \hat{H}_{\mathrm{el-ion}} \tag{2.12}$$

where $\hat{H}_{\mathrm{el}}$ and $\hat{H}_{\mathrm{ion}}$ denote the kinetic energy plus the interaction energy of the electrons and ions, respectively, while $\hat{H}_{\mathrm{el-ion}}$ describes the electron-ion interaction. In general, the corresponding Schrödinger equation can neither be solved analytically nor numerically with the exact form of the material Hamiltonian $\hat{H}_{\mathrm{mat}}$. The so-called *Born-Oppenheimer approximation* [64–67] makes use of the fact that the ion masses exceed the electron masses by three or four orders of magnitude such that the motions of electrons and ions take place on different time scales. The electrons are affected by the instantaneous potential of the ions and quickly adjust themselves to the new positions of the ions whereas the ions only feel the potential of a time-averaged electron distribution. This allows an adiabatic decoupling of electron and ion degrees of freedom. More explicitly, the electron dynamics follows from the Schrödinger equation

$$\left(\hat{H}_{\mathrm{el}} + \hat{H}_{\mathrm{el-ion}}\right) \Phi_{\mathrm{el}}\left(\{\hat{\mathbf{r}}^{(i)}_{\mathrm{el}}\}; \{\hat{\mathbf{r}}^{(j)}_{\mathrm{ion}}\}\right) = E_{\mathrm{el}}\left(\{\hat{\mathbf{r}}^{(j)}_{\mathrm{ion}}\}\right)\Phi_{\mathrm{el}}\left(\{\hat{\mathbf{r}}^{(i)}_{\mathrm{el}}\}; \{\hat{\mathbf{r}}^{(j)}_{\mathrm{ion}}\}\right) \tag{2.13}$$

where $\hat{\mathbf{r}}^{(i)}_{\mathrm{el}}$ is the position operator of the ith electron. The wave function Φ_{el} and the eigen energy E_{el} parametrically depend on the ion positions $\hat{\mathbf{r}}^{(j)}_{\mathrm{ion}}$. The Schrödinger equation for the ion subsystem then takes the form

$$\left[\hat{H}_{\mathrm{ion}} + E_{\mathrm{el}}\left(\{\hat{\mathbf{r}}^{(j)}_{\mathrm{ion}}\}\right)\right] \Phi_{\mathrm{ion}}\left(\{\hat{\mathbf{r}}^{(j)}_{\mathrm{ion}}\}\right) = E_{\mathrm{ion}}\Phi_{\mathrm{ion}}\left(\{\hat{\mathbf{r}}^{(j)}_{\mathrm{ion}}\}\right). \tag{2.14}$$

Because the electronic potential is expressed in terms of ion coordinates, the electron degrees of freedom do not enter the ion dynamics anymore. Thus, the total wave function of the interacting electron-phonon system can partially be separated,

$$\Phi_{\mathrm{mat}}\left(\{\hat{\mathbf{r}}^{(i)}_{\mathrm{el}}\}, \{\hat{\mathbf{r}}^{(j)}_{\mathrm{ion}}\}\right) = \Phi_{\mathrm{el}}\left(\{\hat{\mathbf{r}}^{(i)}_{\mathrm{el}}\}; \{\hat{\mathbf{r}}^{(j)}_{\mathrm{ion}}\}\right)\Phi_{\mathrm{ion}}\left(\{\hat{\mathbf{r}}^{(j)}_{\mathrm{ion}}\}\right). \tag{2.15}$$

For small deviations from the periodically arranged equilibrium positions, the ions can be treated as a system of coupled harmonic oscillators. We present the canonically quantized form of the lattice-vibration Hamiltonian

$$\hat{H}_{\mathrm{vib}} \equiv \hat{H}_{\mathrm{ion}} + E_{\mathrm{el}}\!\left(\{\hat{\mathbf{r}}_{\mathrm{ion}}^{(j)}\}\right) \tag{2.16}$$

in Sec. 2.2.1. The vibration field can be expanded into normal modes that describe collective oscillations of the ions. In a quantized theory, the normal modes become elementary excitations called *phonons* that are introduced in Sec. 2.2.2. We discuss some important properties of the phonon spectrum in Sec. 2.2.3. Finally, in Sec. 2.2.4, the interaction Hamiltonian $\hat{H}_{\mathrm{el-ion}}$ is expressed in terms of phonons and Bloch electrons. The introductory material summarized in Secs. 2.2.1–2.2.3 is mainly extracted from Refs. [65, 68, 69].

2.2.1 Quantization of the lattice-vibration field

The position of a unit cell relative to the origin of the coordinate system cell can be identified by a lattice vector $\mathbf{R}$. We assume that each unit cell contains Z atoms. Individual ions can then be labeled by $\mathbf{R}$ and an index $j = 1, \ldots, Z$. The position vector $\mathbf{S}_j(\mathbf{R}) = \mathbf{R} + \boldsymbol{\xi}_j(\mathbf{R})$ of the jth ion in the unit cell at $\mathbf{R}$ can uniquely be decomposed into $\mathbf{R}$ and a position vector $\boldsymbol{\xi}_j(\mathbf{R})$ relative to the unit cell. The equilibrium position is denoted as $\mathbf{S}_j^0(\mathbf{R}) = \mathbf{R} + \boldsymbol{\xi}_j^0$. For the description of the lattice vibrations, the displacements $\mathbf{Q}_j(\mathbf{R}) = \mathbf{S}_j(\mathbf{R}) - \mathbf{S}_j^0(\mathbf{R}) = \boldsymbol{\xi}_j(\mathbf{R}) - \boldsymbol{\xi}_j^0$ and their conjugate momenta will serve as dynamical variables. In the following, Cartesian coordinates are always labeled by subscripts $\mu, \mu', \ldots$

Both the ion-ion and the ion-electron interaction contribute to the potential energy U of the lattice. Within the Born-Oppenheimer approximation, U can be written as function of the ion positions alone. A Taylor expansion around the equilibrium configuration of the crystal results in $U = U_0 + U_{\mathrm{harm}} + \cdots$ where U_0 denotes the equilibrium energy that can be set to zero by means of a renormalization of the energy scale. Since the linear terms in $\mathbf{Q}_j(\mathbf{R})$ vanish, the lowest-order contribution to the potential energy is given by the harmonic term

$$U_{\mathrm{harm}} = \frac{1}{2} \sum_{\mathbf{R}, \mathbf{R}'} \sum_{\substack{j, \mu \\ j', \mu'}} Q_{j,\mu}(\mathbf{R}) W_{(j,\mu),(j',\mu')}(\mathbf{R} - \mathbf{R}') Q_{j',\mu'}(\mathbf{R}') \tag{2.17}$$

where the Hessian matrix

$$W_{(j,\mu),(j',\mu')}(\mathbf{R} - \mathbf{R}') = \left.\frac{\partial^2 U}{\partial Q_{j,\mu}(\mathbf{R}) \partial Q_{j',\mu'}(\mathbf{R}')}\right|_{\mathbf{Q}=\mathbf{0}} \tag{2.18}$$

only depends on the difference vector $\mathbf{R} - \mathbf{R}'$ owing to the translational symmetry of the crystal. Moreover,

$$\sum_{\mathbf{R}} W_{(j,\mu),(j',\mu')}(\mathbf{R}) = 0 \tag{2.19}$$

since a translation of the entire crystal, i.e. $\mathbf{Q}_j(\mathbf{R}) = \mathbf{const}$, does not change the potential energy of the ions. We restrict the analysis to lattice temperatures far away from the melting point of the crystal such that only small displacements $\mathbf{Q}_j(\mathbf{R})$ occur. The Taylor expansion of the potential energy can thus be truncated after the quadratic term which characterizes the *harmonic approximation*. With this approach, the ions are treated as a set of coupled harmonic

oscillators. The interaction forces are conservative such that the Hamiltonian $H_{\text{vib}} = T + U_{\text{harm}}$ of the lattice-vibration field is just the sum of the kinetic energy T and the potential energy U_{harm} of the ions. When we use Cartesian coordinates, the canonical momenta are given by $\mathbf{P}_j(\mathbf{R}) = M_j\dot{\mathbf{Q}}_j(\mathbf{R})$ where M_j denotes the mass of the jth ion in each unit cell, and the Hamiltonian takes the form

$$H_{\text{vib}} = \sum_{\mathbf{R}} \sum_j \frac{\mathbf{P}_j^2(\mathbf{R})}{2M_j} + U_{\text{harm}}\big(\{\mathbf{Q}_j(\mathbf{R})\}\big). \tag{2.20}$$

Eliminating the momenta from the Hamilton equations of motion produces the Newton equation for the jth ion in the unit cell at $\mathbf{R}$

$$M_j\ddot{Q}_{j,\mu}(\mathbf{R}) = -\sum_{\mathbf{R}'} \sum_{j',\mu'} W_{(j,\mu),(j',\mu')}(\mathbf{R} - \mathbf{R}')Q_{j',\mu'}(\mathbf{R}'). \tag{2.21}$$

The quantization procedure turns the lattice displacements and momenta into field operators $\hat{\mathbf{Q}}_j(\mathbf{R})$, $\hat{\mathbf{P}}_j(\mathbf{R})$ that obey *canonical commutation relations*

$$\left[\hat{Q}_{j,\mu}(\mathbf{R}), \hat{P}_{j',\mu'}(\mathbf{R}')\right]_- = i\hbar\delta_{\mathbf{R},\mathbf{R}'}\delta_{j,j'}\delta_{\mu,\mu'}, \tag{2.22a}$$

$$\left[\hat{Q}_{j,\mu}(\mathbf{R}), \hat{Q}_{j',\mu'}(\mathbf{R}')\right]_- = 0 = \left[\hat{P}_{j,\mu}(\mathbf{R}), \hat{P}_{j',\mu'}(\mathbf{R}')\right]_-. \tag{2.22b}$$

2.2.2 Phonon operators

It is often useful in practical computations to express the lattice-vibration field in terms of *phonon operators*. To this end, we observe that the equation of motion (2.21) allows plane-wave solutions

$$\mathbf{Q}_j(\mathbf{R}) = \frac{\varepsilon_j^{\alpha,\mathbf{p}}}{\sqrt{M_j}}e^{i(\mathbf{p}\cdot\mathbf{R}-\Omega_{\alpha,\mathbf{p}}t)} \tag{2.23}$$

with wave vector $\mathbf{p}$ and polarization α. In general, the frequency $\Omega_{\alpha,\mathbf{p}}$ and the direction $\varepsilon_j^{\alpha,\mathbf{p}}$ of the amplitude vector can depend on both the wave vector and the polarization of the wave. The explicit separation of a mass-dependent factor will prove useful in the following. Inserting this ansatz into Eq. (2.21) leads to

$$\Omega_{\alpha,\mathbf{p}}^2\varepsilon_{j,\mu}^{\alpha,\mathbf{p}} = \sum_{j',\mu'} D_{(j,\mu),(j',\mu')}(\mathbf{p})\varepsilon_{j',\mu'}^{\alpha,\mathbf{p}} \tag{2.24}$$

where we have defined the *dynamical matrix*

$$D_{(j,\mu),(j',\mu')}(\mathbf{p}) \equiv \frac{1}{\sqrt{M_jM_{j'}}}\sum_{\mathbf{R}} W_{(j,\mu),(j',\mu')}(\mathbf{R})e^{-i\mathbf{p}\cdot\mathbf{R}}. \tag{2.25}$$

Equation (2.24) constitutes a $3Z$-dimensional eigenvalue problem for each wave vector $\mathbf{p}$ in the Brillouin zone. The dispersion relation can be determined via the secular equation

$$\det\left[D_{(j,\mu),(j',\mu')}(\mathbf{p}) - \delta_{j,j'}\delta_{\mu,\mu'}\Omega_{\alpha,\mathbf{p}}^2\right] = 0. \tag{2.26}$$

It follows from the symmetry of the Hessian matrix $W_{(j,\mu),(j',\mu')}(\mathbf{R})$ that the dynamical matrix is Hermitian. Consequently, $\Omega_{\alpha,\mathbf{p}}^2$ must be a real number, and the normalized amplitude vectors

$\varepsilon_j^{\alpha,\mathbf{P}}$ fulfill the orthogonality relation

$$\sum_{j,\mu}\left(\varepsilon_{j,\mu}^{\alpha,\mathbf{P}}\right)^*\varepsilon_{j,\mu}^{\alpha',\mathbf{P}}=\delta_{\alpha,\alpha'} \tag{2.27}$$

and the completeness relation

$$\sum_{\alpha}\left(\varepsilon_{j,\mu}^{\alpha,\mathbf{P}}\right)^*\varepsilon_{j',\mu'}^{\alpha,\mathbf{P}}=\delta_{j,j'}\delta_{\mu,\mu'}. \tag{2.28}$$

Since $W_{(j,\mu),(j',\mu')}(\mathbf{R})$ is real-valued, the same frequencies belong to $\mathbf{p}$ and $-\mathbf{p}$, i.e. $\Omega_{\alpha,\mathbf{p}}^2 = \Omega_{\alpha,-\mathbf{p}}^2$, and we may impose the symmetry $(\varepsilon_{j,\mu}^{\alpha,\mathbf{P}})^* = -\varepsilon_{j,\mu}^{\alpha,-\mathbf{P}}$ without loss of generality. Finally, $\Omega_{\alpha,\mathbf{p}}^2$ must be positive since the equilibrium configuration of the crystal corresponds to a local minimum of the potential energy. We choose $\Omega_{\alpha,\mathbf{p}}$ as the positive root of $\Omega_{\alpha,\mathbf{p}}^2$.

Phonons can now be introduced by expanding the field variables $\hat{Q}_j(\mathbf{R})$, $\hat{P}_j(\mathbf{R})$ in terms of the polarization vectors $\boldsymbol{\varepsilon}_j^{\alpha,\mathbf{P}}$. Explicitly, we obtain $\hat{Q}_j(\mathbf{R}) = \sum_{\alpha,\mathbf{p}}\hat{Q}_j^{\alpha,\mathbf{P}}(\mathbf{R})$ and $\hat{P}_j(\mathbf{R}) = \sum_{\alpha,\mathbf{p}}\hat{P}_j^{\alpha,\mathbf{P}}(\mathbf{R})$ with

$$\hat{\mathbf{Q}}_j^{\alpha,\mathbf{P}}(\mathbf{R}) \equiv -\mathrm{i}\sqrt{\frac{\hbar}{2\mathcal{N}M_j\Omega_{\alpha,\mathbf{p}}}}\left(\hat{D}_{\alpha,-\mathbf{p}}^\dagger + \hat{D}_{\alpha,\mathbf{p}}\right)\mathrm{e}^{\mathrm{i}\mathbf{p}\cdot\mathbf{R}}\varepsilon_j^{\alpha,\mathbf{P}}, \tag{2.29}$$

$$\hat{\mathbf{P}}_j^{\alpha,\mathbf{P}}(\mathbf{R}) \equiv \sqrt{\frac{\hbar\Omega_{\alpha,\mathbf{p}}M_j}{2\mathcal{N}}}\left(\hat{D}_{\alpha,-\mathbf{p}}^\dagger - \hat{D}_{\alpha,\mathbf{p}}\right)\mathrm{e}^{\mathrm{i}\mathbf{p}\cdot\mathbf{R}}\varepsilon_j^{\alpha,\mathbf{P}}, \tag{2.30}$$

where $\mathcal{N}$ denotes the number of unit cells contained in the quantization volume $\mathscr{L}^3$. The constant factors appearing on the right-hand sides are chosen such that the canonical commutation relations for $\hat{Q}_j(\mathbf{R})$ and $\hat{P}_j(\mathbf{R})$ lead to *bosonic commutation relations*

$$[\hat{D}_{\alpha,\mathbf{p}},\hat{D}_{\alpha',\mathbf{p}'}^\dagger]_- = \delta_{\alpha,\alpha'}\delta_{\mathbf{p},\mathbf{p}'}, \qquad [\hat{D}_{\alpha,\mathbf{p}},\hat{D}_{\alpha',\mathbf{p}'}]_- = 0 = [\hat{D}_{\alpha,\mathbf{p}}^\dagger,\hat{D}_{\alpha',\mathbf{p}'}^\dagger]_- \tag{2.31}$$

for the phonon operators. With the help of these relations, the Hamiltonian of the lattice-vibration field can be cast into form

$$\hat{H}_{\mathrm{vib}} = \sum_{\alpha,\mathbf{p}}\hbar\Omega_{\alpha,\mathbf{p}}\left(\hat{D}_{\alpha,\mathbf{p}}^\dagger\hat{D}_{\alpha,\mathbf{p}} + \frac{1}{2}\right) \tag{2.32}$$

which formally corresponds to a set of *independent* harmonic oscillators. The quantized normal modes $(\alpha,\mathbf{p})$ are called *phonons*, and the energy quanta $\hbar\Omega_{\alpha,\mathbf{p}}$ are referred to as *phonon energies*. Similarly, $\hbar\mathbf{p}$ can be regarded as the crystal momentum of the phonon. A fixed value of α defines a so-called *phonon branch*. In view of Eqs. (2.31) and (2.32), $\hat{D}_{\alpha,\mathbf{p}}^\dagger$ and $\hat{D}_{\alpha,\mathbf{p}}$ are interpreted as *bosonic creation and annihilation operators*, respectively, for a phonon with wave vector $\mathbf{p}$ and polarization α.

2.2.3 Acoustic and optical phonons

If the unit cell contains more than one atom, the phonon spectrum can be divided into acoustic and optical branches. By definition, *acoustic* branches have vanishing frequency $\Omega_{\alpha,\mathbf{p}}$ in the limit $\mathbf{p} \to \mathbf{0}$. When we insert this condition into the eigenvalue equation (2.24), we find in view of definition (2.25) and the symmetry relation (2.19) that the vectors $\varepsilon_j^{\alpha,\mathbf{P}}/\sqrt{M_j}$ must be

independent of j for $\mathbf{p} = \mathbf{0}$. Long-wavelength acoustic phonons are thus characterized by all ions in a unit cell oscillating with the same phase and same amplitude. Hence, they correspond to the elastic waves of a continuous medium. The common direction of the vibration can be described by the unit vector

$$\boldsymbol{\varepsilon}^{\alpha,\mathbf{p}} \equiv \sqrt{\frac{M}{M_j}} \varepsilon_j^{\alpha,\mathbf{p}} \tag{2.33}$$

where $M \equiv \sum_j M_j$ is the total ion mass per unit cell. The contribution of an acoustic phonon $(\alpha, \mathbf{p})$ to the displacement $\hat{\mathbf{Q}}(\mathbf{R})$ of an ion in the unit cell at $\mathbf{R}$ can thus be written as

$$\hat{\mathbf{Q}}^{\alpha,\mathbf{p}}(\mathbf{R}) = -\mathrm{i}\sqrt{\frac{\hbar}{2\varrho\mathscr{L}^3\Omega_{\alpha,\mathbf{p}}}} \left(\hat{D}_{\alpha,-\mathbf{p}}^{\dagger} + \hat{D}_{\alpha,\mathbf{p}}\right) \mathrm{e}^{\mathrm{i}\mathbf{p}\cdot\mathbf{R}} \boldsymbol{\varepsilon}^{\alpha,\mathbf{p}} \tag{2.34}$$

where $\varrho = \mathcal{N}M/\mathscr{L}^3$ denotes the mass density of the crystal. Since the vectors $\boldsymbol{\varepsilon}^{\alpha,\mathbf{p}}$ are orthogonal for different modes, the phonon spectrum always contains three acoustic branches, irrespective of the number of ions per unit cell. When the crystal lattice has cubic symmetry, $\boldsymbol{\varepsilon}^{\alpha,\mathbf{p}}$ is parallel to $\mathbf{p}$ for one of the branches and perpendicular to $\mathbf{p}$ for the others in the vicinity of the Γ point. The corresponding branches are called *longitudinal acoustic* (LA) and *transverse acoustic* (TA), respectively, although the geometry is usually more complicated away from the symmetry points of the Brillouin zone. In the long-wavelength limit, LA modes correspond to sound waves while TA modes correspond to shear waves. Acoustic branches have linear dispersion relations close to the Γ point,

$$\Omega_{\alpha,\mathbf{p}} = c_\alpha |\mathbf{p}|. \tag{2.35}$$

LA modes typically have about twice as large phase velocities c_α as the TA modes.

Besides the three acoustic branches, the phonon spectrum contains $3(Z-1)$ *optical* branches with non-vanishing frequencies $\Omega_{\alpha,\mathbf{p}}$ for $\mathbf{p} \to \mathbf{0}$. Evaluating the orthogonality relation (2.27) between an acoustic branch α and an optical branch α', we find that $\boldsymbol{\varepsilon}^{\alpha,\mathbf{p}} \cdot \sum_j \sqrt{M_j}\varepsilon_j^{\alpha'\mathbf{p}} = 0$ for each of the three independent directions $\boldsymbol{\varepsilon}^{\alpha,\mathbf{p}}$. Consequently,

$$\sum_j M_j \hat{\mathbf{Q}}_j^{\alpha',\mathbf{p}}(\mathbf{R}) = \mathbf{0}. \tag{2.36}$$

In long-wavelength optical vibrations, the ions in a unit cell thus move in different directions such that their center of mass remains at rest. For a diatomic basis, i.e. $Z = 2$, the operator of the relative displacement $\Delta\hat{\mathbf{Q}}^{\alpha',\mathbf{p}}(\mathbf{R}) = \hat{\mathbf{Q}}_2^{\alpha',\mathbf{p}}(\mathbf{R}) - \hat{\mathbf{Q}}_1^{\alpha',\mathbf{p}}(\mathbf{R})$ in mode $(\alpha', \mathbf{p})$ can be written as

$$\Delta\hat{\mathbf{Q}}^{\alpha',\mathbf{p}}(\mathbf{R}) = \mathrm{i}\sqrt{\frac{\hbar}{2\varrho\mathscr{L}^3\Omega_{\alpha',\mathbf{p}}}} \frac{M_1 + M_2}{\sqrt{M_1 M_2}} \left(\hat{D}_{\alpha',-\mathbf{p}}^{\dagger} + \hat{D}_{\alpha',\mathbf{p}}\right) \mathrm{e}^{\mathrm{i}\mathbf{p}\cdot\mathbf{R}} \boldsymbol{\varepsilon}^{\alpha',\mathbf{p}}. \tag{2.37}$$

The $3(Z-1) = 3$ linearly independent directions of the relative displacement are specified by the pairwise orthogonal unit vectors

$$\boldsymbol{\varepsilon}^{\alpha',\mathbf{p}} \equiv \sqrt{\frac{M}{M_2}} \varepsilon_1^{\alpha',\mathbf{p}} = -\sqrt{\frac{M}{M_1}} \varepsilon_2^{\alpha',\mathbf{p}}. \tag{2.38}$$

Analogously to the acoustic case, optical modes can be divided into *longitudinal optical* (LO) and *transverse optical* (TO) branches. Close to the Γ point, the optical phonon frequencies can be approximated by the *Einstein dispersion*

$$\Omega^{\alpha',\mathbf{P}} \simeq \Omega^{\alpha'} = \text{const.} \tag{2.39}$$

LO modes in ionic crystals have higher frequencies than the TO modes because they induce macroscopic polarizations that generate additional restoring forces on the moving ions. These oscillating polarizations also lead to strong electron-phonon interaction as discussed in Sec. 2.2.4.2.

In this work, we will exclusively consider binary compound semiconductors with either *zincblende* or *wurtzite* structure. The former structure has a cubic symmetry and contains one atom of each type in its unit cell while the latter has a hexagonal symmetry and contains two atoms of each type in its unit cell. The corresponding Brillouin zones are shown in the right column of Fig. 1. The III-V compound GaN ranks among the semiconductor materials that can crystallize in either of these structures. It is therefore interesting to compare the phonon spectra in both cases. Due to the higher number of atoms per unit cell and the reduced symmetry of the lattice, the wurtzite structure yields the more complicated spectrum, as can be seen in the left column of Fig. 1. Contrary to the cubic case, the TO modes have non-vanishing longitudinal components at the Γ point [45], and both TO and LO branches split into different frequencies. Moreover, the hexagonal structure allows *non-polar optical modes* (NPO) that can be assigned to vibrations of either the Ga sublattice or the N sublattice alone [70]. As we will see in Sec. 2.2.4.2, the electron-phonon interaction with polar and with non-polar optical modes is based on fundamentally different mechanisms. One important consequence of this fact will be discussed in Sec. 4.4.3.3.

2.2.4 Electron-phonon interaction

Lattice vibrations destroy the periodicity of the crystal, which perturbs the quasi-free movement of the Bloch electrons. As a consequence, scattering between electrons and phonons may occur. This interaction has important physical consequences such as dephasing of polarization, thermalization of the charge-carrier system, and phonon-assisted luminescence. Each of these processes will be analyzed in later parts of this work.

In first quantization, the electron-ion interaction Hamiltonian appearing in the Schrödinger equation (2.13) for the electron subsystem can be written as

$$\hat{H}_{\text{el}-\text{ion}} = \sum_i V_{\text{ion}}\big(\hat{\mathbf{r}}_{\text{el}}^{(i)}\big) \tag{2.40}$$

where the ionic potential $V_{\text{ion}}(\mathbf{r}) = V_{\text{ion}}\big(\mathbf{r}, \{\mathbf{S}_j(\mathbf{R})\}\big)$ depends on the instantaneous positions of the ions. While the equilibrium configuration of the ions provides the lattice-periodic potential $V_{\text{ion}}^0(\mathbf{r})$, the electron-phonon coupling follows from the change of the potential $\Delta V_{\text{ion}}(\mathbf{r}) \equiv V_{\text{ion}}(\mathbf{r}) - V_{\text{ion}}^0(\mathbf{r})$ due to lattice vibrations. The aim of this section is to establish the corresponding interaction Hamiltonian

$$\hat{H}_{\text{el}-\text{vib}} = \sum_i \Delta V_{\text{ion}}\big(\hat{\mathbf{r}}_{\text{el}}^{(i)}\big) = \int \hat{\Psi}^\dagger(\mathbf{r}) \Delta V_{\text{ion}}(\mathbf{r}) \Psi(\mathbf{r})\, \mathrm{d}^3 r \tag{2.41}$$

in second quantization. In the first subsection, the explicit form of $\Delta V_{\text{ion}}(\mathbf{r})$ is derived microscopically. This part generalizes the treatment from Ref. [73] to the case of more than one ion
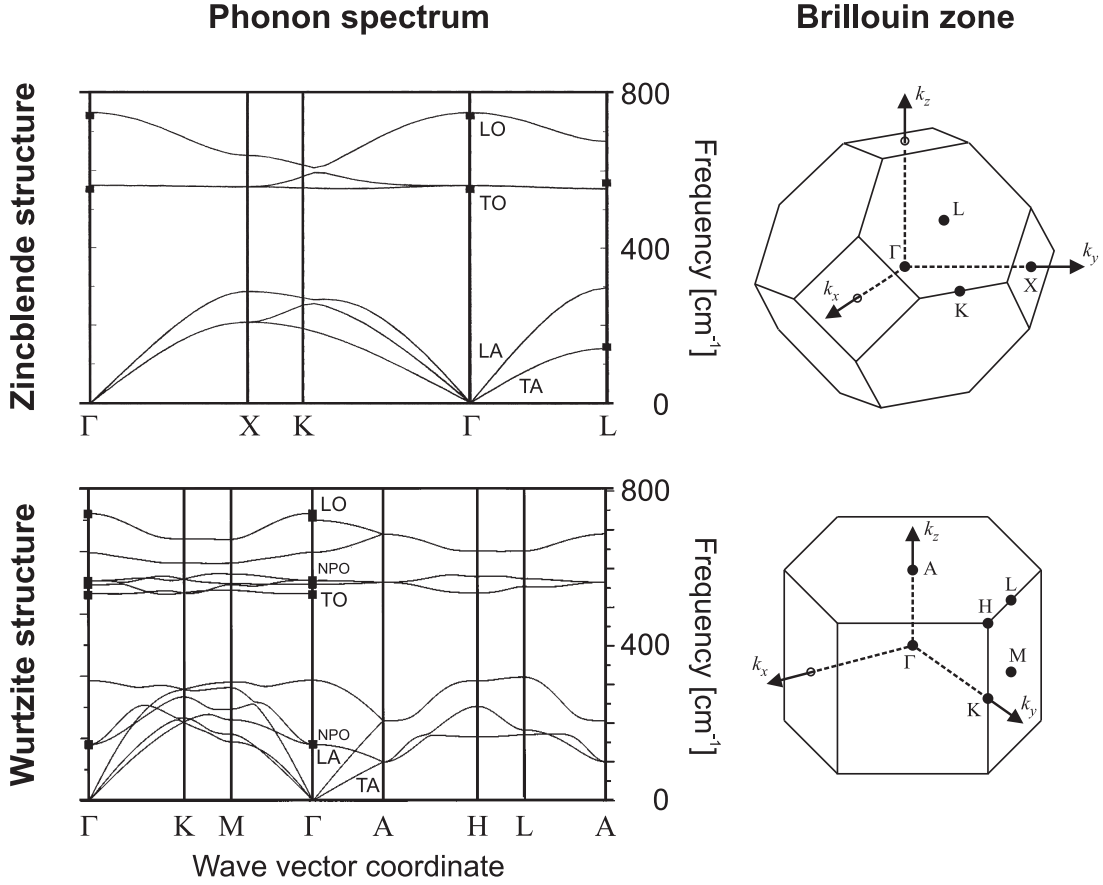
Figure 1: Phonon spectra of cubic (upper row) and hexagonal (lower row) GaN. The corresponding Brillouin zones are shown on the right-hand side where points of high symmetry are labeled by capital Greek or Latin letters. For the horizontal axes of the spectra, the wave vector coordinates are swept in high-symmetry directions of the Brillouin zone. The different types of phonon branches are indicated by the respective acronyms as defined in the text.
The upper curves are taken from Ref. [71] , the lower curves from Ref. [72].

per unit cell. While such an analysis is helpful for the discussion of some fundamental issues, it is very difficult to determine the matrix elements from first principles. However, additional physical insight can be applied to parametrize the interaction, as shown in the second part of this section.

2.2.4.1 Microscopic derivation

The so-called *rigid-ion approximation* [74] assumes that the ions are displaced without distortion. In this case, the ions carry their individual potentials rigidly with themselves when they vibrate around their equilibrium positions. The total potential V_{ion} of the ions can thus be written as

$$V_{\mathrm{ion}}\big(\mathbf{r}, \{\mathbf{S}_j(\mathbf{R})\}\big) = \sum_{\mathbf{R}} \sum_{j} V_j\big(\mathbf{r} - \mathbf{S}_j(\mathbf{R})\big) \qquad (2.42)$$

where $V_j(\mathbf{r})$ denotes the potential of a single ion of type j that is located at $\mathbf{r} = \mathbf{0}$. In lowest non-vanishing order with respect to the ion displacements $\mathbf{Q}_j(\mathbf{R})$, the instantaneous change of the ionic potential due to lattice vibrations is given by

$$
\begin{aligned}
\Delta V_{\text{ion}} &= \sum_{\mathbf{R}} \sum_j \left.\frac{\partial V_{\text{ion}}}{\partial \mathbf{S}_j(\mathbf{R})}\right|_{\mathbf{S}_j(\mathbf{R}) = \mathbf{S}_j^0(\mathbf{R})} \cdot \left[\mathbf{S}_j(\mathbf{R}) - \mathbf{S}_j^0(\mathbf{R})\right] \\
&= \sum_{\mathbf{R}} \sum_j \boldsymbol{\nabla} V_j\left(\mathbf{r} - \mathbf{S}_j^0(\mathbf{R})\right) \cdot \mathbf{Q}_j(\mathbf{R}).
\end{aligned}
\tag{2.43}
$$

The following derivation simultaneously applies to bulk and confined systems. Strictly speaking, not only the charge carriers but also the phonons are affected by the confinement. However, confinement energies are generally proportional to the inverse mass of the confined particle. Owing to the large ratio of ion mass and electron mass, the discrete structure of the confined phonon modes cannot be resolved on the scale of the electronic energies [75]. We may thus model the material system in terms of propagating bulk phonons interacting with an electron gas of reduced dimensionality [76, 77]. With this approach, confinement effects exclusively enter via the electronic field operator (2.9). The electron-phonon interaction Hamiltonian from Eq. (2.41) thus takes the form

$$
\hat{H}_{\text{el-vib}} = \sum_{\substack{\lambda,\beta,k_\parallel \\ \lambda',\beta',k_\parallel'}} \sum_\sigma \sum_{\mathbf{R},j} \mathbf{I}_{\lambda',\beta',k_\parallel'}^{\lambda,\,\beta,\,k_\parallel}(j,\mathbf{R}) \cdot \mathbf{Q}_j(\mathbf{R}) \hat{a}^\dagger_{\lambda,\beta,k_\parallel,\sigma} \hat{a}_{\lambda',\beta',k_\parallel',\sigma}
\tag{2.44}
$$

with the vectorial matrix element

$$
\mathbf{I}_{\lambda',\beta',k_\parallel'}^{\lambda,\,\beta,\,k_\parallel}(j,\mathbf{R}) \equiv \int \psi^*_{\lambda,\beta,k_\parallel}(\mathbf{r}) \boldsymbol{\nabla} V_j\left(\mathbf{r} - \mathbf{S}_j^0(\mathbf{R})\right) \psi_{\lambda,\beta,k_\parallel}(\mathbf{r})\, \mathrm{d}^3 r.
\tag{2.45}
$$

The integral over the entire quantization volume can be expressed as sum over unit-cell (u.c.) integrals,

$$
\mathbf{I}_{\lambda',\beta',k_\parallel'}^{\lambda,\,\beta,\,k_\parallel}(j,\mathbf{R}) = \sum_{\mathbf{R}'} \int_{\text{u.c.}} \psi^*_{\lambda,\beta,k_\parallel}(\mathbf{R}'+\boldsymbol{\xi}) \boldsymbol{\nabla} V_j\left(\mathbf{R}'+\boldsymbol{\xi}-\boldsymbol{\xi}_j^0-\mathbf{R}\right) \psi_{\lambda,\beta,k_\parallel}(\mathbf{R}'+\boldsymbol{\xi})\, \mathrm{d}^3\xi.
\tag{2.46}
$$

Because the Bloch functions are lattice-periodic, i.e. $u_{\lambda,k_\parallel}(\mathbf{R}'+\boldsymbol{\xi}) = u_{\lambda,k_\parallel}(\boldsymbol{\xi})$, while the confinement functions barely change within a unit cell, i.e. $\zeta_{\lambda,\beta}(R'_\perp + \xi_\perp) \simeq \zeta_{\lambda,\beta}(R'_\perp)$, we can rewrite this sum as

$$
\begin{aligned}
\mathbf{I}_{\lambda',\beta',k_\parallel'}^{\lambda,\,\beta,\,k_\parallel}(j,\mathbf{R}) \simeq &\frac{1}{\mathscr{L}^d} \sum_{R'_\parallel, R'_\perp} \zeta^*_{\lambda,\beta}(R'_\perp) \zeta_{\lambda',\beta'}(R'_\perp) \mathrm{e}^{\mathrm{i}(k_\parallel'-k_\parallel)R'_\parallel} \\
&\times \int_{\text{u.c.}} u^*_{\lambda,k_\parallel}(\boldsymbol{\xi}) \boldsymbol{\nabla} V_j\left(\mathbf{R}'-\mathbf{R}+\boldsymbol{\xi}-\boldsymbol{\xi}_j^0\right) u_{\lambda',k_\parallel'}(\boldsymbol{\xi}) \mathrm{e}^{\mathrm{i}(k_\parallel'-k_\parallel)\xi_\parallel}\, \mathrm{d}^3\xi.
\end{aligned}
\tag{2.47}
$$

Such an approximation is often referred to as *separation of length scales*. To complete this procedure, we also separate the ionic potentials $V_j(\mathbf{R}+\boldsymbol{\xi})$ into microscopic and mesoscopic

parts by means of the Fourier transform on the lattice[2]

$$V_{j,\mathbf{q}}(\boldsymbol{\xi}) = \sum_{\mathbf{R}} V_j(\mathbf{R} + \boldsymbol{\xi}) e^{-i\mathbf{q}\cdot\mathbf{R}}, \tag{2.48a}$$

$$V_j(\mathbf{R} + \boldsymbol{\xi}) = \frac{1}{\mathcal{N}} \sum_{\mathbf{q}} V_{j,\mathbf{q}}(\boldsymbol{\xi}) e^{i\mathbf{q}\cdot\mathbf{R}}. \tag{2.48b}$$

In view of $\boldsymbol{\nabla} V_j(\boldsymbol{\xi} + \mathbf{R}) = i\mathbf{q} \sum_{\mathbf{q}} V_{j,\mathbf{q}}(\boldsymbol{\xi}) e^{i\mathbf{q}\cdot\mathbf{R}}/\mathcal{N}$, we thus obtain

$$\mathbf{I}_{\lambda',\beta',k_\parallel'}^{\lambda,\,\beta,\,k_\parallel}(j,\mathbf{R}) = \frac{i}{\mathcal{N}} \sum_{\mathbf{q}} A_{\lambda',k_\parallel'}^{\lambda,\,k_\parallel}(j,\mathbf{q}) B_{\lambda',\beta',k_\parallel'}^{\lambda,\,\beta,\,k_\parallel}(\mathbf{q}) e^{-i\mathbf{q}\cdot\mathbf{R}}\mathbf{q} \tag{2.49}$$

with the unit-cell integral

$$A_{\lambda',k_\parallel'}^{\lambda,\,k_\parallel}(j,\mathbf{q}) \equiv \frac{1}{V_{\text{uc}}} \int_{\text{u.c.}} u_{\lambda,k_\parallel}^*(\boldsymbol{\xi}) V_{j,\mathbf{q}}(\boldsymbol{\xi} - \boldsymbol{\xi}_j^0) u_{\lambda',k_\parallel'}(\boldsymbol{\xi}) e^{i(k_\parallel' - k_\parallel)\xi_\parallel} \, \mathrm{d}^3\xi \tag{2.50}$$

where $V_{\text{uc}} = \mathcal{L}^3/\mathcal{N}$ denotes the volume of the unit cell. The confinement functions enter the quantity

$$B_{\lambda',\beta',k_\parallel'}^{\lambda,\,\beta,\,k_\parallel}(\mathbf{q}) \equiv \frac{V_{\text{uc}}}{\mathcal{L}^d} \sum_{R_\parallel'} e^{i(k_\parallel' - k_\parallel + q_\parallel)R_\parallel'} \sum_{R_\perp'} \zeta_{\lambda,\beta}^*(R_\perp') \zeta_{\lambda',\beta'}(R_\perp') e^{iq_\perp R_\perp'}. \tag{2.51}$$

When umklapp processes are neglected, the $R_\parallel'$ sum vanishes unless $k_\parallel' = k_\parallel - q_\parallel$. Given that the lattice constant can be considered infinitesimal on the mesoscopic length scale, we may convert the $R_\perp'$ sum into an integral. Thus, the above expression simplifies to

$$B_{\lambda',\beta',k_\parallel'}^{\lambda,\,\beta,\,k_\parallel}(\mathbf{q}) = \delta_{k_\parallel',k_\parallel - q_\parallel} \gamma_{\lambda',\beta'}^{\lambda,\,\beta}(q_\perp) \tag{2.52}$$

where we have introduced the form factor

$$\gamma_{\lambda',\beta'}^{\lambda,\,\beta}(q_\perp) \equiv \int \zeta_{\lambda,\beta}^*(r_\perp) \zeta_{\lambda',\beta'}(r_\perp) e^{iq_\perp r_\perp} \, \mathrm{d}^{3-d} r_\perp. \tag{2.53}$$

With these results, Eq. (2.44) becomes

$$\hat{H}_{\text{el-vib}} = \frac{i}{\mathcal{N}} \sum_{\substack{\lambda,\beta \\ \lambda',\beta'}} \sum_{k_\parallel,\sigma,\mathbf{q}} \sum_{\mathbf{R},j} F_{\lambda'}^{\lambda}(j,\mathbf{q}) \gamma_{\lambda',\beta'}^{\lambda,\,\beta}(q_\perp) \mathbf{q} \cdot \hat{\mathbf{Q}}_j(\mathbf{R}) e^{-i\mathbf{q}\cdot\mathbf{R}} \hat{a}_{\lambda,\beta,k_\parallel,\sigma}^\dagger \hat{a}_{\lambda',\beta',k_\parallel',\sigma}. \tag{2.54}$$

One can show that the unit-cell integral

$$F_{\lambda'}^{\lambda}(j,\mathbf{q}) \equiv \frac{1}{V_{\text{uc}}} \int_{\text{u.c.}} u_{\lambda,k_\parallel}^*(\boldsymbol{\xi}) V_{j,\mathbf{q}}(\boldsymbol{\xi} - \boldsymbol{\xi}_j^0) u_{\lambda',k_\parallel - q_\parallel}(\boldsymbol{\xi}) e^{-iq_\parallel \xi_\parallel} \, \mathrm{d}^3\xi \tag{2.55}$$

barely changes with the electron wave vector $k_\parallel$ and decreases when $|\mathbf{q}|$ gets larger [67]. By inserting the normal-mode expansion (2.29) of the displacement operator $\hat{\mathbf{Q}}_j(\mathbf{R})$, we can express the interaction Hamiltonian in terms of electron and phonon operators,

$$\hat{H}_{\text{el-vib}} = \sum_{\substack{\lambda,\beta \\ \lambda',\beta'}} \sum_{\alpha,\mathbf{p},k_\parallel,\sigma} G_{\lambda',\beta'}^{\lambda,\,\beta}(\mathbf{p}) \left(\hat{D}_{\alpha,-\mathbf{p}}^\dagger + \hat{D}_{\alpha,\mathbf{p}} \right) \hat{a}_{\lambda,\beta,k_\parallel,\sigma}^\dagger \hat{a}_{\lambda',\beta',k_\parallel',\sigma}, \tag{2.56}$$

---

[2]On the textbook level, most authors use the Fourier transform on the quantization volume instead of the mesoscopic version. When umklapp processes are neglected, such an approach yields the qualitatively wrong result that the electron-phonon matrix elements cannot be band-dependent.

where again, we exclusively consider normal scattering processes that conserve the crystal momentum. The matrix element

$$G_{\lambda',\beta'}^{\lambda,\beta}(\mathbf{p}) \equiv \sum_j \sqrt{\frac{\hbar}{2\mathcal{N}M_j\Omega_{\alpha,\mathbf{p}}}} F_{\lambda'}^{\lambda}(j,\mathbf{p})\gamma_{\lambda',\beta'}^{\lambda,\beta}(p_\perp)\mathbf{p}\cdot\boldsymbol{\varepsilon}_j^{\alpha,\mathbf{p}} \tag{2.57}$$

only depends on the phonon but not on the electron momentum. If $|\mathbf{p}|$ is small, the polarization vector $\boldsymbol{\varepsilon}_j^{\alpha,\mathbf{p}}$ is parallel to $\mathbf{p}$ for longitudinal and perpendicular to $\mathbf{p}$ for transverse modes. The explicit form of the matrix element shows that in the long-wavelength limit, electrons can only be scattered by longitudinal phonons.[3] All information about the confinement of the electrons is contained in the form factor $\gamma_{\lambda',\beta'}^{\lambda,\beta}(p_\perp)$. The bulk case is recovered from the general formulas (2.56), (2.57) when we eliminate the subband indices β, β' and set $k_\parallel = \mathbf{k}$, $p_\parallel = \mathbf{p}$, and $\gamma_{\lambda',\beta'}^{\lambda,\beta}(p_\perp) = 1$. We find that under the assumption that the confinement effects on the phonon spectrum can be neglected, the interaction matrix elements in the bulk and in the confined case are related via

$$G_{\text{conf}}{}_{\lambda',\beta'}^{\lambda,\beta}(\mathbf{p}) = \gamma_{\lambda',\beta'}^{\lambda,\beta}(p_\perp)G_{\text{bulk}}{}_{\lambda'}^{\lambda}(\mathbf{p}). \tag{2.58}$$

2.2.4.2 Semi-phenomenological treatment

The microscopic derivation from the previous section yields the generic structure how bulk electrons and confined electrons couple to long-wavelength phonons. However, the ionic potentials $V_j(\mathbf{r})$ are very difficult to determine in general. For practical purposes, one usually applies semi-heuristic arguments to obtain physically meaningful approximations for the change $\Delta V_{\text{ion}}(\mathbf{r})$ of the total ionic potential. This approach enables to express the electron-phonon interaction in terms of a small number of parameters that can either be fitted to experimental data or related to directly measurable macroscopic quantities. In the main part of this thesis, we will analyze optical experiments where only carriers close to the band edge have to be considered. We may therefore restrict the following derivations to the long-wavelength limit where the ion displacements $\hat{\mathbf{Q}}_j(\mathbf{R})$ can be treated as continuous fields $\hat{\mathbf{Q}}_j(\mathbf{r})$. Moreover, we will exclusively discuss the bulk case. The interaction matrix elements for low-dimensional electron systems can then be calculated via Eq. (2.58).

Interaction with acoustic phonons
The propagation of long-wavelength LA phonons periodically deforms the crystal. The ion displacement breaks the local charge neutrality, which induces local variations of the electron density. This charge redistribution leads to an additional potential $\Delta V_{\text{ion}}(\mathbf{r})$ for the electrons that is called *acoustic deformation potential* [78, 79] in this context. In a lowest-order approximation, $\Delta V_{\text{ion}}(\mathbf{r})$ is proportional to the local *volume dilation*, i.e. to the fractional volume change $\delta \equiv \Delta\mathcal{V}/\mathcal{V}$ at position $\mathbf{r}$. In general, the proportionality constant d_{ac}^λ will depend on the band index λ, resulting in band-dependent potentials $\Delta V_{\text{ion}}^\lambda(\mathbf{r}) = d_{\text{ac}}^\lambda\delta(\mathbf{r})$. In order to relate the volume dilation to the displacement field $\mathbf{Q}(\mathbf{r}) = \sum_{\mathbf{p}}\mathbf{Q}^{\text{LA},\mathbf{P}}(\mathbf{r})$ as defined in Eq. (2.34), we consider a small cube with edge length a that lies parallel to the coordinate axes at position $\mathbf{r}$. Under deformation, the cube volume $\mathcal{V} = a^3$ is changed to

$$\begin{aligned}
\mathcal{V} + \Delta\mathcal{V} = &[a + Q_x(r_x + a, r_y, r_z) - Q_x(r_x, r_y, r_z)] \\
&\times [a + Q_y(r_x, r_y + a, r_z) - Q_y(r_x, r_y, r_z)] \\
&\times [a + Q_z(r_x, r_y, r_z + a) - Q_z(r_x, r_y, r_z)].
\end{aligned} \tag{2.59}$$

---

[3]As mentioned in Sec. 2.2.3, the TO modes in wurtzite-structure crystals provide a notable exception to this rule.

If a is very small compared to the length scale on which the displacement field varies, we can replace $[Q_\mu(r_\mu + a) - Q_\mu(r_\mu)]/a$ by $\partial Q_\mu/\partial r_\mu$. Neglecting higher-order terms in $\partial Q_\mu/\partial r_\mu$, we find $\delta(\mathbf{r}) = \boldsymbol{\nabla} \cdot \mathbf{Q}(\mathbf{r})$. Hence, the additional potential $\Delta V_{\text{ion}}^\lambda(\mathbf{r})$ is proportional to the divergence of the ion-displacement field. The deformation-potential coupling to LA phonons must be calculated separately for valence- and conduction-band electrons,

$$\hat{H}_{\text{el-vib}}^{\text{LA(def)}} = \hat{H}_{\text{el-vib}}^{\text{LA(def),v}} + \hat{H}_{\text{el-vib}}^{\text{LA(def),c}} \tag{2.60}$$

with

$$\hat{H}_{\text{el-vib}}^{\text{LA(def)},\lambda} \equiv \int \hat{\Psi}_\lambda^\dagger(\mathbf{r}) \Delta V_{\text{ion}}^\lambda(\mathbf{r}) \hat{\Psi}_\lambda(\mathbf{r}) \, \mathrm{d}^3 r \tag{2.61}$$

where $\hat{\Psi}_\lambda(\mathbf{r})$ denotes the field operator for electrons in band λ. A calculation similar to the general derivation presented in the previous section finally leads to

$$\hat{H}_{\text{el-vib}}^{\text{LA(def)}} = \sum_{\lambda,\mathbf{k},\sigma,\mathbf{p}} G_{\lambda,\mathbf{p}}^{\text{ac.def}} \left(\hat{D}_{\text{LA},-\mathbf{p}}^\dagger + \hat{D}_{\text{LA},\mathbf{p}} \right) \hat{a}_{\lambda,\mathbf{k},\sigma}^\dagger \hat{a}_{\lambda,\mathbf{k}-\mathbf{p},\sigma}. \tag{2.62}$$

The matrix element

$$G_{\lambda,\mathbf{p}}^{\text{ac.def}} \equiv d_{\text{ac}}^\lambda \sqrt{\frac{\hbar|\mathbf{p}|}{2\varrho \mathscr{L}^3 c_{\text{LA}}}} \tag{2.63}$$

depends on the mass density ϱ and the sound speed c_{LA} of the material. In the limit $\mathbf{p} \to \mathbf{0}$, the coupling vanishes because zero-wavelength LA phonons correspond to uniform translations of the lattice that do not deform the crystal. Acoustic deformation-potential coupling can be considered *short-ranged* as the coupling strength is not reduced for large phonon momenta. The deformation-potential constants d_{ac}^λ can be determined experimentally by measuring the shift of the electronic energies induced by hydrostatic pressure [80]. For typical binary compound semiconductors, d_{ac}^c has a value of a few eV and exceeds d_{ac}^v by one order of magnitude [81].

When the crystal lattice lacks an inversion center, a macroscopic electric field can be generated by squeezing the crystal. This phenomenon is known as *piezoelectric effect*. Acoustic vibrations are then accompanied by oscillating macroscopic fields that act on the electrons, which provides an additional mechanism for the electron-phonon interaction [79, 82]. In this work, phenomena related to acoustic phonons will only be investigated for GaAs-based structures where the piezoelectric effect is particularly weak. We therefore do not need to determine the corresponding interaction matrix elements.

Interaction with optical phonons

For simplicity, we restrict the following derivations to the diatomic case. Long-wavelength LO phonons are then characterized by a relative displacement field $\Delta\hat{\mathbf{Q}}(\mathbf{r}) = \sum_{\mathbf{p}} \hat{\mathbf{Q}}^{\text{LO},\mathbf{p}}(\mathbf{r})$ with the single-mode contributions defined in Eq. (2.37).

Longitudinal optical vibrations in ionic crystals shift the oppositely charged ions in a unit cell against each other. As illustrated in the left frame of Fig. 2, such a relative displacement generates a macroscopic polarization field $\hat{\mathbf{P}}(\mathbf{r})$ that affects the motion of the electrons. This coupling mechanism is known as *Fröhlich interaction* [83] and can be compared to the piezoelectric interaction with acoustic modes. For small deviations of the ions from their equilibrium positions, the induced polarization can be considered proportional to $\Delta\hat{\mathbf{Q}}(\mathbf{r})$. In the long-wavelength limit, we thus have

$$\hat{\mathbf{P}}(\mathbf{r}) = \mathrm{i}F \sum_{\mathbf{p}} \left(\hat{D}_{\text{LO},-\mathbf{p}}^\dagger + \hat{D}_{\text{LO},\mathbf{p}} \right) \mathrm{e}^{\mathrm{i}\mathbf{p}\cdot\mathbf{r}} \frac{\mathbf{p}}{|\mathbf{p}|} \tag{2.64}$$

where the proportionality constant F must be a real number so that $\hat{\mathbf{P}}(\mathbf{r})$ is Hermitian. Here, we have used that $\boldsymbol{\varepsilon}^{\mathrm{LO},\mathbf{p}} = \pm\mathbf{p}/|\mathbf{p}|$. The sign of F thus depends on how the direction of $\Delta\hat{\mathbf{Q}}(\mathbf{r})$ has been defined. In the absence of free charges, the divergence of the displacement field $\hat{\mathbf{D}}(\mathbf{r}) = \epsilon_0\hat{\mathbf{E}}(\mathbf{r}) + \hat{\mathbf{P}}(\mathbf{r})$ vanishes. Since the induced polarization field is longitudinal (i.e. irrotational), the macroscopic electric field $\hat{\mathbf{E}}(\mathbf{r}) = -\boldsymbol{\nabla}[\Delta\hat{V}_{\mathrm{ion}}(\mathbf{r})]/e$ to which the electrons are exposed follows from $\hat{\mathbf{E}}(\mathbf{r}) = -\hat{\mathbf{P}}(\mathbf{r})/\epsilon_0$. The corresponding potential reads

$$\Delta\hat{V}_{\mathrm{ion}}(\mathbf{r}) = -\frac{eF}{\epsilon_0}\sum_{\mathbf{p}}\left(\hat{D}_{\mathrm{LO},-\mathbf{p}}^\dagger + \hat{D}_{\mathrm{LO},\mathbf{p}}\right)\frac{\mathrm{e}^{\mathrm{i}\mathbf{p}\cdot\mathbf{r}}}{|\mathbf{p}|}. \tag{2.65}$$

With this result, the Fröhlich interaction Hamiltonian can be cast into form

$$\hat{H}_{\mathrm{el-vib}}^{\mathrm{LO(Fr)}} = \sum_{\lambda,\mathbf{k},\sigma,\mathbf{p}} G_{\mathbf{p}}^{\mathrm{Fr}}\left(\hat{D}_{\mathrm{LO},-\mathbf{p}}^\dagger + \hat{D}_{\mathrm{LO},\mathbf{p}}\right)\hat{a}_{\lambda,\mathbf{k},\sigma}^\dagger\hat{a}_{\lambda,\mathbf{k}-\mathbf{p},\sigma}. \tag{2.66}$$

Because the potential energy of a particle in an electric field only depends on the charge of the particle but not, for instance, on its effective mass, the matrix element

$$G_{\mathbf{p}}^{\mathrm{Fr}} = \frac{eF}{\epsilon_0}\frac{1}{|\mathbf{p}|} \tag{2.67}$$

is identical for valence- and conduction-band electrons. The Fröhlich interaction can be considered *long-ranged* since the coupling strength decreases rapidly for large wave vectors. To fully determine the interaction strength, the proportionality constant F has to be fixed. This can be achieved by examining quantitatively how the medium is polarized [78, 83, 84]. Alternatively, we can anticipate the so-called polaron transformation that will be introduced explicitly in Sec. 4.4.2. There, the lattice distortion induced by an electron moving through the crystal is incorporated into the electron movement to create a new quasi-particle called *polaron*. This is formally accomplished by means of a unitary transformation that eliminates the electron-phonon interaction Hamiltonian. As a further consequence, the strength of the electron-electron interaction is modified. The Coulomb matrix elements $\bar{V}_{\mathbf{p}}$ after the transformation follow from the original matrix elements $V_{\mathbf{p}}$ via

$$\bar{V}_{\mathbf{p}} = V_{\mathbf{p}} - \frac{2|G_{\mathbf{p}}^{\mathrm{Fr}}|^2}{\hbar\Omega}. \tag{2.68}$$

In view of the momentum dependence of the Fröhlich matrix elements, this modification can be interpreted as statical screening due to LO phonons. The effective matrix element in the dielectric medium is related to the vacuum matrix element $V_{\mathbf{q}}^{\mathrm{vac}} = e^2/(\epsilon_0\mathscr{L}^3|\mathbf{q}|^2)$ via $\bar{V}_{\mathbf{p}} = V_{\mathbf{p}}^{\mathrm{vac}}/\epsilon(0)$. In ionic crystals, not only the orbital polarization of the individual atoms but also the polarization owing to the relative displacement of oppositely charged ions contribute to the dielectric function $\epsilon(\omega)$. Because the latter contribution is consistently included in the polaron picture, we must choose $V_{\mathbf{p}} = V_{\mathbf{p}}^{\mathrm{vac}}/\tilde{\epsilon}(0)$ in the original Hamiltonian where $\tilde{\epsilon}(0)$ denotes the static permittivity of a fictitious system without lattice vibrations. At high frequencies, the ions cannot follow the exciting fields anymore due to their large inertia. The permittivity in this limit is identical to the phonon-free case. Consequently, $\tilde{\epsilon}(0) = \epsilon(\infty)$. By inserting these relations into Eq. (2.68), we find an explicit form for the Fröhlich matrix element that agrees with the result from the literature:

$$|G_{\mathbf{p}}^{\mathrm{Fr}}|^2 = \frac{\hbar\Omega V_{\mathbf{p}}^{\mathrm{vac}}}{2}\left[\frac{1}{\epsilon(\infty)} - \frac{1}{\epsilon(0)}\right]. \tag{2.69}$$
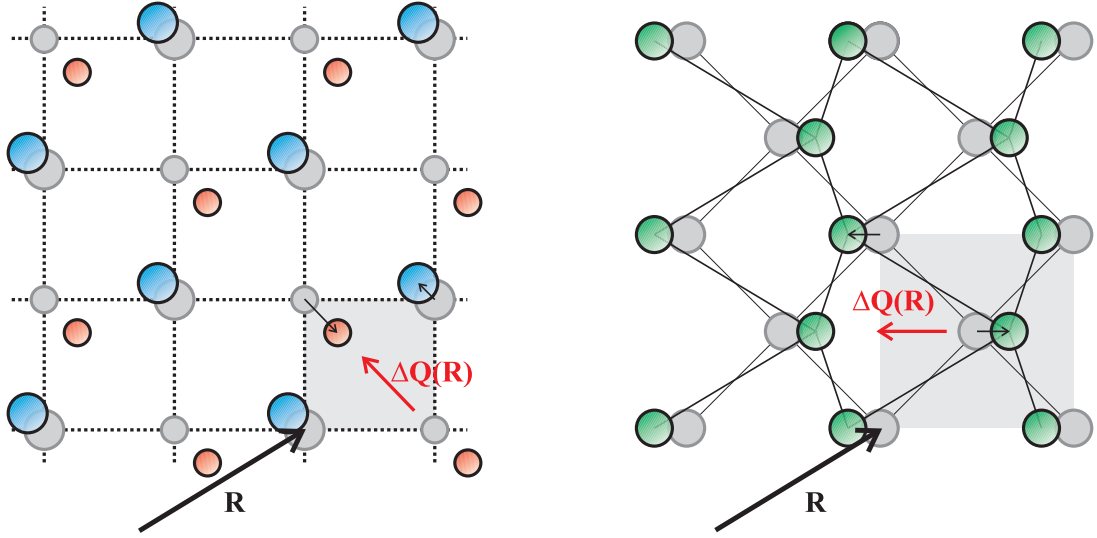
Figure 2: Longitudinal optical phonons in ionic crystals generate macroscopic polarization fields (left picture). Large balls indicate the anions and small balls the cations. The induced polarization in the unit cell at **R** is thus parallel to the relative displacement **Q(R)**.
In both polar and non-polar crystals, optical vibrations change bond lengths and bond angles (right picture). The resulting change of the ionic potential is linear in **Q(R)** for small displacements.
In both pictures, the equilibrium positions of the atoms are marked by gray balls, and the unit cell at **R** by a gray square. (Strictly speaking, the two-dimensional lattice on the right-hand side would have a smaller unit cell than indicated.)

The coupling strength of the electron-phonon interaction can thus be calculated from easily measurable macroscopic quantities.

It it obvious from the above discussion that there is no Fröhlich interaction in non-polar crystals such as covalent elementary semiconductors. Still, LO phonons distort the lattice, thus changing the electronic energies, which effectively gives rise to electron-phonon interaction. This mechanism can be modeled through deformation potentials [78, 79, 85, 86]. Contrary to the acoustic case, optical vibrations do not compress or stretch the unit cell but change the bond lengths and bond angles, as illustrated in the right frame of Fig. 2. In lowest order, the corresponding change of the ionic potential is proportional to the relative displacement vector $\Delta\hat{\mathbf{Q}}(\mathbf{r})$. More explicitly, the *optical deformation potential* can be written as [85]

$$\Delta\hat{V}_{\text{ion}}^{\lambda}(\mathbf{r}) = d_{\text{opt}}^{\lambda}\mathbf{n} \cdot \frac{\Delta\hat{\mathbf{Q}}(\mathbf{r})}{a_0} \tag{2.70}$$

with band-dependent proportionality constants d_{opt}^{λ} where a_0 denotes the lattice constant. The direction of the unit vector $\mathbf{n}$ is determined by the symmetry of the crystal. In the zincblende structure, for instance, $\mathbf{n}$ is parallel to the [111] body diagonal of the cubic unit cell [79, 81, 85]. Relative displacements in this direction do not change the cubic symmetry of the lattice and are often referred to as *internal strain*. The optical deformation potentials are strongly band dependent. In particular, one can show that for symmetry reasons, there is no deformation-potential interaction between conduction-band electrons and optical phonons in direct semiconductors [79, 87]. For convenience, we further use the generic form (2.70) and set

$d_{\mathrm{opt}}^{\mathrm{c}} = 0$. The electron-phonon interaction Hamiltonian can thus be written as

$$\hat{H}_{\mathrm{el-vib}}^{\mathrm{LO(def)}} = \sum_{\lambda, \mathbf{k}, \sigma, \mathbf{p}} G_{\lambda, \mathbf{p}}^{\mathrm{opt.def}} \left(\hat{D}_{\mathrm{LO},-\mathbf{p}}^{\dagger} + \hat{D}_{\mathrm{LO},\mathbf{p}} \right) \hat{a}_{\lambda, \mathbf{k}, \sigma}^{\dagger} \hat{a}_{\lambda, \mathbf{k}-\mathbf{p}, \sigma} \tag{2.71}$$

with the matrix element

$$G_{\lambda, \mathbf{p}}^{\mathrm{opt.def}} = \pm \mathrm{i} \sqrt{\frac{\hbar}{2 \varrho \mathscr{L}^3 \Omega_{\mathrm{LO}}}} \frac{M_1 + M_2}{\sqrt{M_1 M_2}} \frac{d_{\mathrm{opt}}^{\lambda}}{a_0} \frac{\mathbf{n} \cdot \mathbf{p}}{|\mathbf{p}|}. \tag{2.72}$$

Since $G_{\lambda, \mathbf{p}}^{\mathrm{opt.def}}$ is independent of the absolute value of the phonon momentum, the optical deformation-potential interaction is *short-ranged*. Contrary to the acoustic case, the optical deformation-potential constants cannot be measured directly. Depending on the material system, $d_0 \equiv d_{\mathrm{opt}}^{\mathrm{v}}$ can be estimated, e.g., from the line shapes of Raman spectra [88], the temperature dependence of hole mobilities or phonon-assisted exciton-to-exciton transition rates [89, 90]. Alternatively, the coupling constant can be calculated with the help of the pseudo-potential method [91]. However, experimental and theoretical values often diverge considerably. As a general rule, d_0 is of the order of some $10\,\mathrm{eV}$ in most tetrahedrally coordinated semiconductors.

In ionic crystals, both Fröhlich coupling and optical deformation-potential coupling can contribute to the interaction between electrons and LO phonons. The total interaction strength is then determined by the matrix element [92]

$$G_{\lambda, \mathbf{p}}^{\mathrm{LO}} = G_{\mathbf{p}}^{\mathrm{Fr}} + G_{\lambda, \mathbf{p}}^{\mathrm{opt.def}}. \tag{2.73}$$

Physically relevant quantities like scattering rates or phonon-sideband intensities depend on the absolute values squared of the matrix elements. Because $G_{\mathbf{p}}^{\mathrm{Fr}}$ is a real and $G_{\lambda, \mathbf{p}}^{\mathrm{opt.def}}$ an imaginary number, no mixed terms appear but

$$\left| G_{\lambda, \mathbf{p}}^{\mathrm{LO}} \right|^2 = \left| G_{\mathbf{p}}^{\mathrm{Fr}} \right|^2 + \left| G_{\lambda, \mathbf{p}}^{\mathrm{opt.def}} \right|^2. \tag{2.74}$$

The contributions due to the two different coupling mechanisms can thus be evaluated independently. One should keep in mind, however, that $G_{\mathbf{p}}^{\mathrm{Fr}}$ and $G_{\lambda, \mathbf{p}}^{\mathrm{opt.def}}$ are the long-range and the short-range limits, respectively, of the same matrix element (2.57). To compensate for the possible double counting of the interaction, we assume that the optical deformation-potential constants d_0 for polar modes must be somewhat reduced in comparison with the calculated or measured values for non-polar modes.

In strongly polar media, one usually finds that the Fröhlich interaction clearly dominates the scattering. As will be discussed in Sec. 4.3.3.1, the situation is more complicated when phonon-assisted luminescence is considered. In practical computations, the angle dependence of the optical deformation-potential matrix element is often neglected. Instead of the accurate form of $|G_{\lambda, \mathbf{p}}^{\mathrm{opt.def}}|^2$, we will use the angle averaged quantity

$$|G_{\mathrm{v}}^{\mathrm{opt.def}}|^2 = \frac{\hbar}{2 \varrho \mathscr{L}^3 \Omega_{\mathrm{LO}}} \frac{(M_1 + M_2)^2}{2 M_1 M_2} \frac{|d_0|^2}{a_0^2}. \tag{2.75}$$

2.3 Quantum electrodynamical Hamiltonian

We show in this section how interacting electrons coupled to an electromagnetic field can be treated fully quantum mechanically. In Sec. 2.3.1, we present the quantum electrodynamical

Hamiltonian in first quantization for the electrons. A detailed derivation of the explicit form of the Hamiltonian can be found in Ref. [61]. Second quantization in the semiconductor Bloch basis defined in Sec. 2.1 will then be performed in Sec. 2.3.2.

2.3.1 Quantization of the electromagnetic field

In this work, we will exclusively consider absorption or emission close to the semiconductor band gap. Processes such as light absorption by core electrons or transverse optical phonons can be neglected in this spectral region. However, the ions are polarizable due to their internal degrees of freedom, which results in a background permittivity $\epsilon > 1$. In polar crystals, also the macroscopic lattice polarizations induced by LO phonons can contribute to the dielectric constant. It follows from the Poisson equation that $\epsilon(0)$ enters the Coulomb matrix elements whereas $\epsilon(\infty)$ must be used in connection with transverse electric fields. We will exclusively consider non-magnetic semiconductors with permeability $\mu = 1$. The coupling of the electron spins to the magnetic field is neglected in our analysis because for radiation in the optical domain, this interaction would yield corrections of less than $1\,\%$ to the total energy. Including only the light field and the electronic degrees of freedom, the quantum electrodynamical Hamiltonian can be written in the form

$$\hat{H}_{\mathrm{QED}} = \hat{H}_{\mathrm{kin}} + \hat{H}_{\mathrm{el-el}} + \hat{H}_{\mathrm{em}} + \hat{H}_{\mathrm{el-em}} + \hat{H}_{\mathrm{dip}} \tag{2.76}$$

with the kinetic energy of the electrons

$$\hat{H}_{\mathrm{kin}} = \sum_i \frac{1}{2m_0} \left| \hat{\mathbf{p}}_{\mathrm{el}}^{(i)} \right|^2 \tag{2.77}$$

where m_0 denotes the bare electron mass and $\hat{\mathbf{p}}_{\mathrm{el}}^{(i)}$ the momentum of the i-th electron. We use the *Coulomb gauge* where the vector potential $\mathbf{A}(\mathbf{r})$ is purely transverse, i.e. $\boldsymbol{\nabla} \cdot \mathbf{A}(\mathbf{r}) = 0$. The crucial advantage of this choice lies in the fact that the longitudinal electric field $\hat{\mathbf{E}}_{\mathrm{L}}(\mathbf{r})$ can be expressed in terms of the electron positions $\hat{\mathbf{r}}_{\mathrm{el}}^{(i)}$ and that the contribution of $\hat{\mathbf{E}}_{\mathrm{L}}(\mathbf{r})$ to the electromagnetic field energy yields the instantaneous Coulomb interaction,

$$\hat{H}_{\mathrm{el-el}} = \frac{\epsilon_0 \epsilon}{2} \int \hat{\mathbf{E}}_{\mathrm{L}}^2(\mathbf{r}) \, \mathrm{d}^3 r = \frac{e^2}{4\pi\epsilon_0\epsilon} \frac{1}{2} \sum_{\substack{i,j \\ (i \neq j)}} V\big(\hat{\mathbf{r}}_{\mathrm{el}}^{(i)} - \hat{\mathbf{r}}_{\mathrm{el}}^{(j)}\big), \tag{2.78}$$

with the unscreened Coulomb potential $V(\mathbf{r}) = e^2/4\pi\epsilon_0\epsilon(0)|\mathbf{r}|$. In view of this separation, material properties like band structures or excitonic eigenenergies can be calculated without the need to include electromagnetic field variables. The transverse electric field $\hat{\mathbf{E}}_{\mathrm{T}}(\mathbf{r})$ and magnetic field $\hat{\mathbf{B}}(\mathbf{r}) = \hat{\mathbf{B}}_{\mathrm{T}}(\mathbf{r})$ can be expanded into stationary eigen modes $\mathbf{U}_{\kappa,\mathbf{q}}(\mathbf{r})$ with wave vector $\mathbf{q}$ and polarization κ. These eigen modes solve the *Helmholtz equation*

$$\left[\boldsymbol{\nabla}^2 + n^2(\mathbf{r})\mathbf{q}^2 \right] \mathbf{U}_{\kappa,\mathbf{q}}(\mathbf{r}) = \mathbf{0} \tag{2.79}$$

with the background refractive index $n(\mathbf{r}) = \sqrt{\epsilon(\mathbf{r})}$. They can be orthonormalized to fulfill the orthogonality relation

$$\int \mathbf{U}_{\kappa,\mathbf{q}}^*(\mathbf{r}) \cdot \mathbf{U}_{\kappa',\mathbf{q}'}(\mathbf{r}) \, n^2(\mathbf{r}) \mathrm{d}^3 r = \delta_{\kappa,\kappa'} \delta_{\mathbf{q},\mathbf{q}'}, \tag{2.80}$$

and the completeness relation

$$\sum_{\kappa,\mathbf{q}} n(\mathbf{r})U_{\kappa,\mathbf{q},\mu}(\mathbf{r})U_{\kappa,\mathbf{q},\mu'}^*(\mathbf{r}')n(\mathbf{r}') = \delta_{\mu,\mu'}^{\mathrm{T}}(\mathbf{r}-\mathbf{r}') \tag{2.81}$$

with the transverse delta function $\delta_{\mu,\mu'}^{\mathrm{T}}(\mathbf{r})$ where μ and μ' label the Cartesian components of the mode functions. The expansion of the field operators yields

$$\hat{\mathbf{E}}_{\mathrm{T}}(\mathbf{r}) = \sum_{\kappa,\mathbf{q}} \mathscr{E}_{\mathbf{q}} \left[\mathrm{i}\mathbf{U}_{\kappa,\mathbf{q}}(\mathbf{r})\hat{B}_{\kappa,\mathbf{q}} - \mathrm{i}\mathbf{U}_{\kappa,\mathbf{q}}^*(\mathbf{r})\hat{B}_{\kappa,\mathbf{q}}^\dagger \right], \tag{2.82}$$

$$\hat{\mathbf{B}}(\mathbf{r}) = \sum_{\kappa,\mathbf{q}} \frac{\mathscr{E}_{\mathbf{q}}}{\omega_{\mathbf{q}}} \boldsymbol{\nabla} \times \left[\mathbf{U}_{\kappa,\mathbf{q}}(\mathbf{r})\hat{B}_{\kappa,\mathbf{q}} + \mathbf{U}_{\kappa,\mathbf{q}}^*(\mathbf{r})\hat{B}_{\kappa,\mathbf{q}}^\dagger \right] \tag{2.83}$$

with the *vacuum field amplitude* $\mathscr{E}_{\mathbf{q}} = \sqrt{\hbar\omega_{\mathbf{q}}/2\epsilon_0}$. The frequencies $\omega_{\mathbf{q}}$ are defined via the dispersion relation $\omega_{\mathbf{q}} = c_0|\mathbf{q}|$ where c_0 is the vacuum speed of light. The quantization scheme imposes bosonic commutation relations

$$[\hat{B}_{\kappa,\mathbf{q}}, \hat{B}_{\kappa',\mathbf{q}'}^\dagger]_- = \delta_{\kappa,\kappa'}\delta_{\mathbf{q},\mathbf{q}'}, \quad [\hat{B}_{\kappa,\mathbf{q}}, \hat{B}_{\kappa',\mathbf{q}'}]_- = 0 = [\hat{B}_{\kappa,\mathbf{q}}^\dagger, \hat{B}_{\kappa',\mathbf{q}'}^\dagger]_-. \tag{2.84}$$

on the *photon operators* $\hat{B}_{\kappa,\mathbf{q}}$, $\hat{B}_{\kappa,\mathbf{q}}^\dagger$ while the electron operators in first quantization obey canonical commutation relations

$$\left[\hat{r}_{\mathrm{el},\mu}^{(i)}, \hat{p}_{\mathrm{el},\mu'}^{(i')} \right]_- = \mathrm{i}\hbar\delta_{i,i'}\delta_{\mu,\mu'}, \qquad \left[\hat{r}_{\mathrm{el},\mu}^{(i)}, \hat{r}_{\mathrm{el},\mu'}^{(i')} \right]_- = 0 = \left[\hat{p}_{\mathrm{el},\mu}^{(i)}, \hat{p}_{\mathrm{el},\mu'}^{(i')} \right]_-. \tag{2.85}$$

In the absence of the carrier system, the energy of the transverse fields is given by

$$\hat{H}_{\mathrm{em}} = \frac{\epsilon_0}{2} \int \left[n^2(\mathbf{r})\hat{\mathbf{E}}_{\mathrm{T}}^2(\mathbf{r}) + c_0^2\hat{\mathbf{B}}^2(\mathbf{r}) \right] \mathrm{d}^3r = \sum_{\kappa,\mathbf{q}} \hbar\omega_{\mathbf{q}} \left(\hat{B}_{\kappa,\mathbf{q}}^\dagger\hat{B}_{\kappa,\mathbf{q}} + \frac{1}{2} \right). \tag{2.86}$$

As for the lattice-vibration field, the free-field Hamiltonian corresponds to a set of independent harmonic oscillators. Here, the quantized eigen modes $(\kappa, \mathbf{q})$ are called *photons* and have energies $\hbar\omega_{\mathbf{q}}$ and momenta $\hbar\mathbf{q}$. The light-matter coupling follows from the dipole Hamiltonian

$$\hat{H}_{\mathrm{el-em}} = -e \sum_i \hat{\mathbf{r}}_{\mathrm{el}}^{(i)} \cdot \hat{\mathbf{E}}_{\mathrm{T}}\big(\hat{\mathbf{r}}_{\mathrm{el}}^{(i)}\big) \tag{2.87}$$

where $e = -|e| < 0$ denotes the electron charge. This form of the interaction defines the so-called $r \cdot E$ *picture*. Our Hamiltonian is related to the fundamental *minimal-substitution Hamiltonian* that defines the so-called $p \cdot A$ *picture* via a local gauge transformation [93]. For classical electromagnetic fields, the corresponding change of gauge is known as *Göppert-Mayer transformation* [94] and was originally applied to atomic systems. This approach can be generalized to spatially extended semiconductor structures when the light field changes slowly on the length scale of a unit cell. This assumption characterizes the so-called *dipole approximation* and is well justified when optical experiments are considered. Contrary to the minimal-substitution Hamiltonian, no interaction terms that are quadratic in the field variables appear in $\hat{H}_{\mathrm{QED}}$. Strictly speaking, the right-hand side of Eq. (2.82) should not be interpreted as electric field $\hat{\mathbf{E}}_{\mathrm{T}}(\mathbf{r})$ but as electric displacement field $\hat{\mathbf{D}}_{\mathrm{T}}(\mathbf{r})/\epsilon_0$ after the Göppert-Mayer transformation such that $\hat{\mathbf{D}}_{\mathrm{T}}$ instead of $\hat{\mathbf{E}}_{\mathrm{T}}$ enters the dipole Hamiltonian. Additionally, $\hat{H}_{\mathrm{QED}}$ contains a dipole self-energy $\hat{H}_{\mathrm{dip}}$ which is a two-particle operator like

the Coulomb Hamiltonian $\hat{H}_{\text{el}-\text{el}}$. This self-energy must in principle be included to ensure consistent operator equations for the electron-photon coupling. On the other hand, $\hat{H}_{\text{dip}}$ only leads to small shifts of the optical resonances for materials with large background refractive index n. We will neglect this effect by omitting $\hat{H}_{\text{dip}}$ in the following analysis. When the dipole self-energy is not included, one actually has to use $\hat{\mathbf{E}}_T$ instead of $\hat{\mathbf{D}}_T$ in the dipole Hamiltonian so as to find the correct semi-classical limit of the operator equations [61]. It has been verified in Ref. [7] that also quantum-optical phenomena in semiconductors can be described accurately with the quantum electrodynamical Hamiltonian used in this work.

2.3.2 Second quantization of the electron system

With the results from Secs. 2.2 and 2.3.1, the total system Hamiltonian for interacting electrons, ions, and light modes takes the form

$$
\begin{aligned}
\hat{H} &= \hat{H}_{\text{QED}} + \hat{H}^0_{\text{el}-\text{ion}} + \hat{H}_{\text{vib}} + \hat{H}_{\text{el}-\text{vib}} \\
&= \hat{H}_{\text{kin}} + \hat{H}^0_{\text{el}-\text{ion}} + \hat{H}_{\text{el}-\text{el}} + \hat{H}_{\text{em}} + \hat{H}_{\text{el}-\text{em}} + \hat{H}_{\text{vib}} + \hat{H}_{\text{el}-\text{vib}}
\end{aligned}
\tag{2.88}
$$

where $\hat{H}^0_{\text{el}-\text{ion}} = \sum_i V^0_{\text{ion}}\big(\hat{\mathbf{r}}^{(i)}_{\text{el}}\big)$ is the part of the Hamiltonian (2.40) that contains the lattice-periodic equilibrium potential. We have derived in Secs. 2.2.2 and 2.2.4, respectively, how $\hat{H}_{\text{vib}}$ and $\hat{H}_{\text{el}-\text{vib}}$ can be expressed in terms of fermionic electron operators and bosonic phonon operators. The aim of this section is to give the second-quantized forms of the remaining parts of the total Hamiltonian. The electronic field operator $\hat{\Psi}(\mathbf{r})$ in the semiconductor Bloch basis is defined in Eq. (2.8) for the bulk case and in Eq. (2.9) for confined systems.

By definition, the Bloch basis diagonalizes the Hamiltonian $\hat{H}_{\text{el}} \equiv \hat{H}_{\text{kin}} + \hat{H}^0_{\text{el}-\text{ion}}$ of non-interacting Bloch electrons. In second quantization, we thus obtain

$$
\hat{H}_{\text{el}} = \sum_{\lambda,\mathbf{k},\sigma} \varepsilon_{\lambda,\mathbf{k}} \hat{a}^\dagger_{\lambda,\mathbf{k},\sigma} \hat{a}_{\lambda,\mathbf{k},\sigma}
\tag{2.89}
$$

for the bulk case. For hetero structures, an additional term $\hat{H}_{\text{conf}}$ describing the confinement enters the total Hamiltonian, and $\hat{H}_{\text{el}} \equiv \hat{H}_{\text{kin}} + \hat{H}^0_{\text{el}-\text{ion}} + \hat{H}_{\text{conf}}$ becomes

$$
\hat{H}_{\text{el}} = \sum_{\lambda,\beta,k_\parallel,\sigma} \varepsilon_{\lambda,\beta,k_\parallel} \hat{a}^\dagger_{\lambda,\beta,k_\parallel,\sigma} \hat{a}_{\lambda,\beta,k_\parallel,\sigma}.
\tag{2.90}
$$

Since the Coulomb Hamiltonian $\hat{H}_{\text{el}-\text{el}}$ from Eq. (2.78) is a two-particle operator, the second quantization is performed according to

$$
\hat{H}_{\text{el}-\text{el}} = \frac{1}{2} \iint \hat{\Psi}^\dagger(\mathbf{r}) \hat{\Psi}^\dagger(\mathbf{r}') V(\mathbf{r} - \mathbf{r}') \hat{\Psi}(\mathbf{r}') \hat{\Psi}(\mathbf{r}) \, \mathrm{d}^3 r.
\tag{2.91}
$$

In the Bloch basis for the bulk case, the Coulomb Hamiltonian can be written as Ref. [1, 66]

$$
\hat{H}_{\text{el}-\text{el}} = \frac{1}{2} \sum_{\substack{\lambda,\lambda' \\ \sigma,\sigma'}} \sum_{\mathbf{k},\mathbf{k}',\mathbf{q}} V_{\mathbf{q}} \hat{a}^\dagger_{\lambda,\mathbf{k},\sigma} \hat{a}^\dagger_{\lambda',\mathbf{k}',\sigma'} \hat{a}_{\lambda',\mathbf{k}'+\mathbf{q},\sigma} \hat{a}_{\lambda,\mathbf{k}-\mathbf{q},\sigma'}
\tag{2.92}
$$

with the unscreened Coulomb matrix element

$$
V_{\mathbf{q}} \equiv \frac{1}{\mathscr{L}^3} \int V(\mathbf{r}) \mathrm{e}^{-\mathrm{i}\mathbf{q}\cdot\mathbf{r}} \, \mathrm{d}^3 r = \frac{e^2}{\epsilon_0 \epsilon \mathscr{L}^3} \frac{1}{|\mathbf{q}|^2}
\tag{2.93}
$$

The textbook derivation of this result can straightforwardly be generalized to confined systems. This procedure yields

$$\hat{H}_{\text{el}-\text{el}} = \frac{1}{2} \sum_{\substack{\lambda,\lambda' \\ \sigma,\sigma'}} \sum_{k_\parallel,k_\parallel',q_\parallel} \sum_{\beta,\beta',\beta'',\beta'''} V_{\lambda,\lambda'}{}^{\beta}_{\beta''}{}^{\beta'}_{\beta'''}(q_\parallel)$$
$$\times \hat{a}^\dagger_{\lambda,\beta,k_\parallel,\sigma} \hat{a}^\dagger_{\lambda',\beta',k_\parallel',\sigma'} \hat{a}_{\lambda',\beta'',k_\parallel'+q_\parallel,\sigma} \hat{a}_{\lambda,\beta''',k_\parallel-q_\parallel,\sigma'} \quad (2.94)$$

with the matrix element

$$V_{\lambda,\lambda'}{}^{\beta}_{\beta''}{}^{\beta'}_{\beta'''}(q_\parallel) \equiv \frac{1}{\mathscr{L}^3} \int V^{\text{eff}}_{\lambda,\lambda'}{}^{\beta}_{\beta''}{}^{\beta'}_{\beta'''}(r_\parallel) e^{-iq_\parallel \cdot r_\parallel} \, d^d r_\parallel \quad (2.95)$$

where we introduce an effective d-dimensional Coulomb potential

$$V^{\text{eff}}_{\lambda,\lambda'}{}^{\beta}_{\beta''}{}^{\beta'}_{\beta'''}(r_\parallel - r_\parallel') \equiv$$
$$\iint \zeta^*_{\lambda,\beta}(r_\perp) \zeta^*_{\lambda',\beta'}(r_\perp') V(\mathbf{r} - \mathbf{r}') \zeta_{\lambda',\beta''}(r_\perp) \zeta_{\lambda,\beta'''}(r_\perp) \, d^{3-d}r_\perp \, d^{3-d}r_\perp'. \quad (2.96)$$

A close inspection of the Coulomb self-energy of the interacting electron-ion system shows that the formally infinite terms for $\mathbf{q} = \mathbf{0}$ have to be removed from the Hamiltonians (2.92) and (2.94).

Because the dipole Hamiltonian $\hat{H}_{\text{el}-\text{em}}$ is a single-particle operator with respect to the electronic degrees of freedom, the second quantization starts from

$$\hat{H}_{\text{el}-\text{em}} = -e \int \hat{\Psi}^\dagger(\mathbf{r}) \mathbf{r} \cdot \hat{\mathbf{E}}_{\text{T}}(\mathbf{r}) \hat{\Psi}(\mathbf{r}) \, d^3r. \quad (2.97)$$

First, we consider confined systems. In dipole approximation, we can use separation of length scales as explained in Sec. 2.2.4.1 to obtain

$$\hat{H}_{\text{el}-\text{em}} = -\frac{e}{\mathscr{L}^3} \sum_{\substack{\lambda,\beta,k_\parallel \\ \lambda',\beta',k_\parallel'}} \sum_\sigma \sum_{\kappa,\mathbf{q}} \mathscr{E}_\mathbf{q} \sum_\mathbf{R} \left[i\mathbf{U}_{\kappa,\mathbf{q}}(\mathbf{R}) \hat{B}_{\kappa,\mathbf{q}} - i\mathbf{U}^*_{\kappa,\mathbf{q}}(\mathbf{R}) \hat{B}^\dagger_{\kappa,\mathbf{q}} \right]$$
$$\times \zeta^*_{\lambda,\beta}(R_\perp) \zeta_{\lambda',\beta'}(R_\perp) e^{i(k_\parallel' - k_\parallel)R_\parallel}$$
$$\times \int_{\text{u.c.}} u^*_{\lambda,k_\parallel}(\boldsymbol{\xi})(\mathbf{R} + \boldsymbol{\xi}) u_{\lambda',k_\parallel'}(\boldsymbol{\xi}) e^{i(k_\parallel' - k_\parallel)\xi_\parallel} \, d^3\xi$$
$$\times \hat{a}^\dagger_{\lambda,\beta,k_\parallel,\sigma} \hat{a}_{\lambda',\beta',k_\parallel',\sigma} \quad (2.98)$$

When optical experiments are analyzed, only *interband* transitions where $\lambda \neq \lambda'$ have to be included. For these contributions, the part of the unit-cell (u.c.) integral that is proportional to $\mathbf{R}$ vanishes due to symmetry reasons. To simplify Eq. (2.98), we assume that the refractive index $n(\mathbf{r})$ is constant in each part of the hetero structure and only changes in $r_\perp$ direction. When the in-plane extension of the structure is large compared to the wave length of the light field, an $r_\parallel$-dependent plane-wave part can be separated from the mode functions,

$$\mathbf{U}_{\kappa,\mathbf{q}}(\mathbf{r}) = \frac{e^{iq_\parallel \cdot r_\parallel}}{\sqrt{\mathscr{L}^d}} \tilde{\mathbf{U}}_{\kappa,\mathbf{q}}(r_\perp). \quad (2.99)$$

The $R_\parallel$ sum in Eq. (2.98) can thus be evaluated analytically. After some further steps analogously to the derivation of the electron-phonon Hamiltonian in Sec. 2.2.4.1 the dipole Hamil-

tonian can finally be written as

$$
\hat{H}_{\mathrm{el-em}} = -\sum_{k_{\parallel},\beta,\beta',\sigma} \sum_{\kappa,\mathbf{q}} \mathrm{i}\mathscr{E}_{\mathbf{q}} \Big\{ \tilde{\mathbf{U}}_{\mathrm{c,v}}(\beta,\beta',\kappa,\mathbf{q}) \cdot \mathbf{d}_{\mathrm{c,v}}(k_{\parallel},q_{\parallel}) \hat{a}^{\dagger}_{\mathrm{c},\beta,k_{\parallel}+q_{\parallel},\sigma} \hat{a}_{\mathrm{v},\beta',k_{\parallel},\sigma}
$$

$$
+ \big[\tilde{\mathbf{U}}_{\mathrm{c,v}}(\beta',\beta,\kappa,-\mathbf{q}) \cdot \mathbf{d}_{\mathrm{c,v}}(k_{\parallel},-q_{\parallel}) \big]^{*} \hat{a}^{\dagger}_{\mathrm{v},\beta,k_{\parallel},\sigma} \hat{a}_{\mathrm{c},\beta',k_{\parallel}-q_{\parallel},\sigma} \Big\} \hat{B}_{\kappa,\mathbf{q}}
$$

$$
+ \mathrm{H.C.} \tag{2.100}
$$

with the overlap integral

$$
\tilde{\mathbf{U}}_{\lambda,\lambda'}(\beta,\beta',\kappa,\mathbf{q}) \equiv \int \zeta^{*}_{\lambda,\beta}(r_{\perp}) \tilde{\mathbf{U}}_{\kappa,\mathbf{q}}(r_{\perp}) \zeta_{\lambda',\beta'}(r_{\perp}) \, \mathrm{d}^{3-d}r_{\perp} \tag{2.101}
$$

and the *dipole matrix element*

$$
\mathbf{d}_{\lambda,\lambda'}(k_{\parallel},q_{\parallel}) \equiv \frac{1}{V_{\mathrm{uc}}} \int_{\mathrm{u.c.}} u^{*}_{\lambda,k_{\parallel}+q_{\parallel}}(\boldsymbol{\xi}) e\boldsymbol{\xi} u_{\lambda',k_{\parallel}}(\boldsymbol{\xi}) \mathrm{e}^{-\mathrm{i}q_{\parallel}\cdot\xi_{\parallel}} \, \mathrm{d}^{3}\xi. \tag{2.102}
$$

In the vicinity of the band edge, the wave-vector dependence of $\mathbf{d}_{\lambda,\lambda'}$ can usually be neglected. The bulk case with constant n demands a special treatment because here, the refractive index enters the plane-wave part of the mode functions

$$
\mathbf{U}_{\kappa,\mathbf{q}}(\mathbf{r}) = \frac{\mathrm{e}^{\mathrm{i}n\mathbf{q}\cdot\mathbf{r}}}{n\sqrt{\mathscr{L}^{3}}} \varepsilon_{\kappa,\mathbf{q}}. \tag{2.103}
$$

Hence, the photon momenta must be rescaled to cast the bulk Hamiltonian into a form that is similar to Eq. (2.100),

$$
\hat{H}_{\mathrm{el-em}} = -\sum_{\mathbf{k},\sigma} \sum_{\kappa,\mathbf{q}} \mathrm{i}\frac{\mathscr{E}_{\mathbf{q}}}{\sqrt{\mathscr{L}^{3}}} \Big\{ \varepsilon_{\kappa,\mathbf{q}} \cdot \mathbf{d}_{\mathrm{c,v}}(\mathbf{k},\mathbf{q}) \hat{a}^{\dagger}_{\mathrm{c},\mathbf{k}+\mathbf{q},\sigma} \hat{a}_{\mathrm{v},\mathbf{k},\sigma}
$$

$$
+ \big[\varepsilon_{\kappa,-\mathbf{q}} \cdot \mathbf{d}_{\mathrm{c,v}}(\mathbf{k},-\mathbf{q}) \big]^{*} \hat{a}^{\dagger}_{\mathrm{v},\mathbf{k},\sigma} \hat{a}_{\mathrm{c},\mathbf{k}-\mathbf{q},\sigma} \Big\} \hat{B}_{\kappa,\mathbf{q}} + \mathrm{H.C.} \tag{2.104}
$$

2.4 Equations-of-motion approach

In the Heisenberg picture, wave functions are stationary while the operators $\hat{O}$ evolve in time. The operator dynamics follows from the *Heisenberg equation of motion*

$$
\mathrm{i}\hbar\frac{\mathrm{d}}{\mathrm{d}t}\hat{O} = [\hat{O},\hat{H}]_{-}. \tag{2.105}
$$

In second quantization, all relevant operators can be expressed in terms of electron, phonon, and photon operators. The operator combinations can be classified with respect to the number of fermion or boson operators they contain. An *N-particle operator* has the generic form

$$
\hat{O}_{N} = \hat{a}^{\dagger}_{i_{N}} \cdots \hat{a}^{\dagger}_{i_{1}} \hat{a}_{i'_{1}} \cdots \hat{a}_{i'_{N}}. \tag{2.106}
$$

Both the electron-phonon and the electron-photon interaction Hamiltonian contain operator combinations of the form $(\hat{A}^{\dagger}_{-\mathbf{q}} + \hat{A}_{\mathbf{q}})\hat{a}^{\dagger}_{\mathbf{k}}\hat{a}_{\mathbf{k}-\mathbf{q}}$ where $A_{\mathbf{q}}$ is either a phonon or a photon operator. We find that whenever a boson is created or annihilated, an electron changes its state. Boson

operators thus correspond to pairs of fermion operators. The Heisenberg equations of motion have the structure

$$\frac{\mathrm{d}}{\mathrm{d}t}\hat{O}_N = T[\hat{O}_N] + V[\hat{O}_{N+1}],\tag{2.107}$$

where the functional T mainly results from the non-interacting part $\hat{H}_{\mathrm{el}} + \hat{H}_{\mathrm{vib}} + \hat{H}_{\mathrm{em}}$ of the Hamiltonian while the functional V originates from the interacting part $\hat{H}_{\mathrm{el-el}} + \hat{H}_{\mathrm{el-vib}} + \hat{H}_{\mathrm{el-em}}$. Hence, N-particle operators are coupled to $(N+1)$-particle operators via V, which leads to the well-known hierarchy problem of many-body physics [1, 95].

One successful approach to deal with the hierarchy problem is provided by the so-called *cluster expansion* [2–7]. Here, one factorizes N-particle expectation values in terms of independent single particles (singlets), correlated pairs (doublets), correlated three-particle clusters (triplets) and so on up to correlated N-particle clusters. The hierarchy problem can then be treated consistently by truncating the right-hand side of Eq. (2.107) such that one includes all clusters up to a desired order. In practice, the cluster expansion is performed according to the recursion scheme

$$\langle\hat{O}_2\rangle = \langle\hat{O}_2\rangle_{\mathrm{S}} + \Delta\langle\hat{O}_2\rangle,\tag{2.108a}$$

$$\langle\hat{O}_3\rangle = \langle\hat{O}_3\rangle_{\mathrm{S}} + \langle\hat{O}_1\rangle\Delta\langle\hat{O}_2\rangle + \Delta\langle\hat{O}_3\rangle,\tag{2.108b}$$

$$\vdots$$

$$\begin{aligned}\langle\hat{O}_N\rangle = \langle\hat{O}_N\rangle_{\mathrm{S}} &+ \langle\hat{O}_{N-2}\rangle_{\mathrm{S}}\Delta\langle\hat{O}_2\rangle + \langle\hat{O}_{N-4}\rangle_{\mathrm{S}}\Delta\langle\hat{O}_2\rangle\Delta\langle\hat{O}_2\rangle + \cdots\\ &+ \langle\hat{O}_{N-3}\rangle_{\mathrm{S}}\Delta\langle\hat{O}_3\rangle + \langle\hat{O}_{N-5}\rangle_{\mathrm{S}}\Delta\langle\hat{O}_2\rangle\Delta\langle\hat{O}_3\rangle + \cdots + \Delta\langle\hat{O}_N\rangle\end{aligned}\tag{2.108c}$$

where $\Delta\langle\hat{O}_N\rangle$ denotes the purely correlated part of the N-particle cluster. Each term on the right-hand sides of Eq. (2.108) represents the fully antisymmetrized (for fermionic operators) or symmetrized (for bosonic operators) sum over all possibilities to distribute the N creation and N annihilation operators among the different clusters. As a starting point of the recursion scheme, the singlet part $\langle\hat{O}_N\rangle_{\mathrm{S}}$ leads to the Hartree-Fock factorization for the carrier operators while for the photon and phonon operators, it produces the classical factorization for the light field and the lattice-vibration field, respectively. For instance, the cluster expansion for a two-particle expectation value explicitly reads

$$\langle\hat{a}_{i_2}^\dagger\hat{a}_{i_1}^\dagger\hat{a}_{j_1}\hat{a}_{j_2}\rangle = \langle\hat{a}_{i_2}^\dagger\hat{a}_{j_2}\rangle\langle\hat{a}_{i_1}^\dagger\hat{a}_{j_1}\rangle - \langle\hat{a}_{i_2}^\dagger\hat{a}_{j_1}\rangle\langle\hat{a}_{i_1}^\dagger\hat{a}_{j_2}\rangle + \Delta\langle\hat{a}_{i_2}^\dagger\hat{a}_{i_1}^\dagger\hat{a}_{j_1}\hat{a}_{j_2}\rangle\tag{2.109}$$

while for a three-particle expectation value, we obtain

$$\begin{aligned}\langle\hat{a}_{i_3}^\dagger\hat{a}_{i_2}^\dagger\hat{a}_{i_1}^\dagger\hat{a}_{j_1}\hat{a}_{j_2}\hat{a}_{j_3}\rangle =\ &\langle\hat{a}_{i_3}^\dagger\hat{a}_{j_3}\rangle\langle\hat{a}_{i_2}^\dagger\hat{a}_{j_2}\rangle\langle\hat{a}_{i_1}^\dagger\hat{a}_{j_1}\rangle - \langle\hat{a}_{i_3}^\dagger\hat{a}_{j_3}\rangle\langle\hat{a}_{i_2}^\dagger\hat{a}_{j_1}\rangle\langle\hat{a}_{i_1}^\dagger\hat{a}_{j_2}\rangle\\ &+ \langle\hat{a}_{i_3}^\dagger\hat{a}_{j_2}\rangle\langle\hat{a}_{i_2}^\dagger\hat{a}_{j_1}\rangle\langle\hat{a}_{i_1}^\dagger\hat{a}_{j_3}\rangle - \langle\hat{a}_{i_3}^\dagger\hat{a}_{j_2}\rangle\langle\hat{a}_{i_2}^\dagger\hat{a}_{j_3}\rangle\langle\hat{a}_{i_1}^\dagger\hat{a}_{j_1}\rangle\\ &+ \langle\hat{a}_{i_3}^\dagger\hat{a}_{j_1}\rangle\langle\hat{a}_{i_2}^\dagger\hat{a}_{j_3}\rangle\langle\hat{a}_{i_1}^\dagger\hat{a}_{j_2}\rangle - \langle\hat{a}_{i_3}^\dagger\hat{a}_{j_1}\rangle\langle\hat{a}_{i_2}^\dagger\hat{a}_{j_2}\rangle\langle\hat{a}_{i_1}^\dagger\hat{a}_{j_3}\rangle\\ &+ \langle\hat{a}_{i_3}^\dagger\hat{a}_{j_3}\rangle\Delta\langle\hat{a}_{i_2}^\dagger\hat{a}_{i_1}^\dagger\hat{a}_{j_1}\hat{a}_{j_2}\rangle - \langle\hat{a}_{i_3}^\dagger\hat{a}_{j_2}\rangle\Delta\langle\hat{a}_{i_2}^\dagger\hat{a}_{i_1}^\dagger\hat{a}_{j_1}\hat{a}_{j_3}\rangle\\ &+ \langle\hat{a}_{i_3}^\dagger\hat{a}_{j_1}\rangle\Delta\langle\hat{a}_{i_2}^\dagger\hat{a}_{i_1}^\dagger\hat{a}_{j_2}\hat{a}_{j_3}\rangle - \langle\hat{a}_{i_2}^\dagger\hat{a}_{j_3}\rangle\Delta\langle\hat{a}_{i_3}^\dagger\hat{a}_{i_1}^\dagger\hat{a}_{j_1}\hat{a}_{j_2}\rangle\\ &+ \langle\hat{a}_{i_2}^\dagger\hat{a}_{j_2}\rangle\Delta\langle\hat{a}_{i_3}^\dagger\hat{a}_{i_1}^\dagger\hat{a}_{j_1}\hat{a}_{j_3}\rangle - \langle\hat{a}_{i_2}^\dagger\hat{a}_{j_1}\rangle\Delta\langle\hat{a}_{i_3}^\dagger\hat{a}_{i_1}^\dagger\hat{a}_{j_2}\hat{a}_{j_3}\rangle\\ &+ \langle\hat{a}_{i_1}^\dagger\hat{a}_{j_3}\rangle\Delta\langle\hat{a}_{i_3}^\dagger\hat{a}_{i_2}^\dagger\hat{a}_{j_1}\hat{a}_{j_2}\rangle - \langle\hat{a}_{i_1}^\dagger\hat{a}_{j_2}\rangle\Delta\langle\hat{a}_{i_3}^\dagger\hat{a}_{i_2}^\dagger\hat{a}_{j_1}\hat{a}_{j_3}\rangle\\ &+ \langle\hat{a}_{i_1}^\dagger\hat{a}_{j_1}\rangle\Delta\langle\hat{a}_{i_3}^\dagger\hat{a}_{i_2}^\dagger\hat{a}_{j_2}\hat{a}_{j_3}\rangle\\ &+ \Delta\langle\hat{a}_{i_3}^\dagger\hat{a}_{i_2}^\dagger\hat{a}_{i_1}^\dagger\hat{a}_{j_1}\hat{a}_{j_2}\hat{a}_{j_3}\rangle.\end{aligned}\tag{2.110}$$

Within this scheme, $\hat{a}_{i_m}^{\dagger}\hat{a}_{j_n}$ either corresponds to a pair of fermion operators or to a single boson operator.[4] Carrier-carrier, carrier-phonon, and carrier-photon correlations can thus be treated consistently on the same level of approximation.

One advantage of the cluster expansion is that the factorization often allows a direct physical interpretation. For instance, when there is no classical light field, the singlet part of any expectation value that involves photon operators vanishes. The remaining correlated parts may thus be interpreted as the quantum-mechanical corrections to the light-matter coupling. To give just one further example, the exciton operators $\hat{X}_{\nu,\mathbf{Q}}$, $\hat{X}_{\nu,\mathbf{Q}}^{\dagger}$ defined in Appendix A do not fulfill bosonic commutation relations due to the fermionic substructure of an exciton. Consequently, $\hat{X}_{\nu,\mathbf{Q}}^{\dagger}\hat{X}_{\nu,\mathbf{Q}}$ does not have the properties of a number operator. However, one can show that the correlated part $\Delta\langle\hat{X}_{\nu,\mathbf{Q}}^{\dagger}\hat{X}_{\nu,\mathbf{Q}}\rangle$ of the expectation value $\langle\hat{X}_{\nu,\mathbf{Q}}^{\dagger}\hat{X}_{\nu,\mathbf{Q}}\rangle$ may be interpreted as population of the exciton state $(\nu,\mathbf{Q})$ with quantum number ν and center-of-mass momentum $\hbar\mathbf{Q}$ provided that a dominant amount of excitons have formed in the carrier system.

---

[4]When the expansion scheme is applied to a operator combination $\hat{O}_N$ that contains a bosonic operator $\hat{A}_{\mathbf{q}}$, we formally replace that operator by $\hat{a}_i^{\dagger}\hat{a}_j$ and omit all terms where $\hat{a}_i^{\dagger}$ and $\hat{a}_j$ are distributed among different factors.

3 Optics with semiconductor quantum dots

This chapter is organized as follows. In Sec. 3.1, we define the model system that we use for our studies and relate it to the properties of realistic semiconductor quantum dots. The semiconductor Bloch equations (SBE) are presented in Sec. 3.2. We use the exciton basis for the quantum dot to derive an analytical formula for the linear absorption spectrum. The incoherent regime is considered in Sec. 3.3. We explore the generic phase space for the excited states of the dot by means of a phenomenological pumping model. Semiconductor luminescence equations (SLE) are derived and solved in the stationary limit to calculate steady-state emission from stable dot states. In Sec. 3.4, the SBE are extended to describe coupling of the carrier system to a bath of lattice vibrations. The electron-phonon scattering leads to dephasing of polarization and build-up of excitonic populations after coherent optical pumping of the carrier system. Finally, we sketch a possible technical application of semiconductor quantum dots in Sec. 3.5. We propose a device design for the field of Zeno-based optoelectronics that enables conditional absorption of a signal field at the exciton-to-biexciton transition in a dot.

The majority of the material in Secs. 3.1, 3.2.1–3.2.3, and 3.3 has been published in Ref. [I] of the author's publications list.

3.1 Model system

Semiconductor quantum dots can be produced in a number of fundamentally different ways. Colloidal synthesis yields very small dots with diameters of a few nanometers that are evenly dispersed in a liquid medium [96]. Individual or periodically arranged dots with lateral extensions of about 100 nm can be fabricated through lithographic methods [97]. In this work, we consider so-called *self-assembled dots* (SAD) that form automatically under suitable conditions during the epitaxial growth of thin films on a substrate [98–100]. When the adsorbate is deposited from the vapor phase, the resulting film geometry follows from the force balance of surface tensions and contact angles and thus critically depends on the interaction strength between the adatoms and the substrate surface [101]. Strong interaction favors the build-up of atomically smooth epilayers (Frank-van der Merwe growth) while in the opposite case, three-dimensional adatom clusters form on the substrate surface (Volmer-Weber growth). SAD emerge from an intermediary process where nanoscale islands nucleate on the wetting layer (Stranski-Krastanov growth) [102]. For hetero structures, the lattice constants of substrate and adsorbate do not match such that a misfit strain is induced at the interface. When the wetting layer has reached a critical thickness, lattice defects and surface undulations can occur that increase the dislocation and elastic deformation energy, respectively, at the expense of the strain energy. In the latter case, dislocation-free so called coherent islands are created that can subsequently be buried under a cap layer to form the quantum dots. The shapes and the sizes of the SAD depend on both the material parameters and the growth conditions. Usual dot diameters lie in the range of 10 nm to 50 nm. The Stranski-Krastanov growth often yields lens-shaped islands that can roughly be described as spherical caps sitting on on a planar wet-
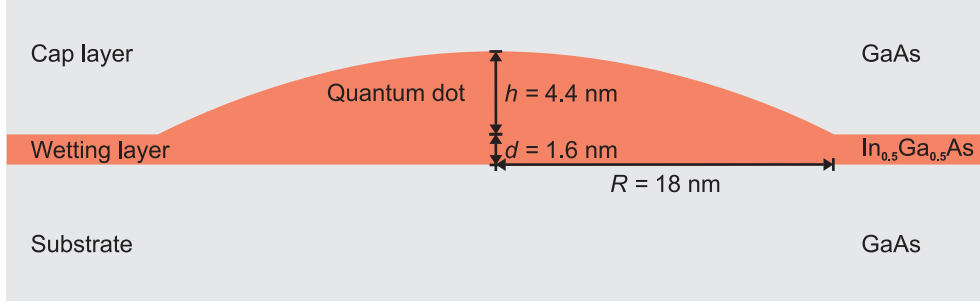
Figure 3: Geometry of a lens-shaped InGaAs/GaAs self-assembled quantum dot. Typical values for the wetting-layer thickness d, the dot height h, and the dot radius R are taken from Ref. [103].

ting layer. Individual samples are characterized by a fixed aspect ratio $h : R$ of cap height h and cap radius R and sharp distributions of the dot size with standard deviations below 10% of the average size. Typical dot densities are of the order of $10^{10} \, \text{cm}^{-2}$.

For the following analysis, we assume that the substrate and the film material are GaAs and $\text{In}_x\text{Ga}_{1-x}\text{As}$, respectively. A representative dot geometry for an Indium concentration of $x = 0.5$ is shown in Fig. 3. The narrow wetting layer with diameter $d \simeq 1.6 \, \text{nm}$ acts as a quantum well that confines the electrons and holes to the well plane. Due to the increased layer thickness, the charge carriers are further localized inside the dot. The single-particle energies of the confined carriers can be calculated within the effective-mass approximation. The electronic energy spectrum as function of the lens radius is shown in Fig. 4 where for the numerical evaluation, a conduction-band offset of $\Delta V_{\text{c}} = 350 \, \text{meV}$ and an aspect ratio of $h : R = 0.24$ as in Fig. 3 have been assumed. One observes that with increasing dot size, one discrete level after another steps out of the continuum of the wetting-layer states. A closer inspection reveals that for smaller dots, neighboring discrete energies are equally spaced and the k-th energy from below is k-fold degenerate. This behavior can accurately be modeled by a parabolic in-plane confinement with a dissociation threshold where the discrete dot states merge into the wetting-layer continuum. Since strained InGaAs is characterized by a small mixing between light holes and heavy holes, the hole spectrum can be modeled analogously. In the following section, we explicitly define the phenomenological confinement potentials and corresponding envelope functions.

3.1.1 Single-particle wave functions

We choose the coordinate system such that the wetting-layer plane is defined by $z = 0$. Thus, the in-plane and perpendicular components of the position vector $\mathbf{r}$ are $\mathbf{r}_{\parallel} = (x, y)$ and $r_{\perp} = z$, respectively. The dots lie in the half space $z > 0$. We consider an individual dot that is symmetric with respect to the z axis. The parabolic in-plane confinement potentials for electrons and holes can then be written as

$$V_{\text{QD}}^{\lambda}(\mathbf{r}_{\parallel}) = \frac{1}{2} m_{\lambda} \omega_{\lambda}^2 |\mathbf{r}_{\parallel}|^2 \qquad (\lambda = \text{e}, \text{h}), \tag{3.1}$$

where m_{e} and m_{h} denote the effective electron and hole mass, respectively. The interlevel spacings are given by $\hbar\omega_{\lambda}$. For the z-confinement perpendicular to the quantum well, we
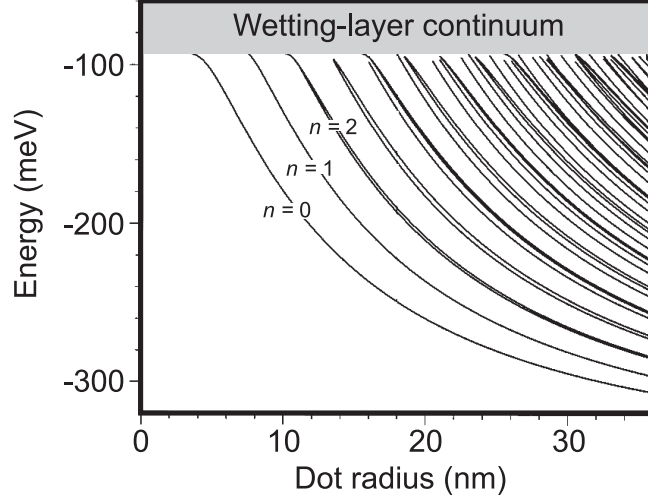
Figure 4: Dependence of the electronic energy spectrum of a lens-shaped InGaAs/GaAs self-assembled quantum dot on the dot radius R. The results are taken from Ref. [104] where the single-particle energies are calculated through numerical diagonalization for a conduction-band offset of 350 meV and an aspect ratio $h : R = 0.24$ of dot height and dot radius. The labeling of the energy levels refers to the principal quantum numbers introduced in Sec. 3.1.1.

assume an infinite potential well

$$V_{\text{QW}}(z) = \begin{cases} 0 & \text{for } |z| < \frac{L}{2}, \\ \infty & \text{for } |z| \geq \frac{L}{2}. \end{cases} \tag{3.2}$$

In envelope-function approximation (see Sec. 2.1), the single-particle wavefunctions take the form

$$\psi_{\lambda,\beta}(\mathbf{r}) = \zeta_{\lambda,\beta}(\mathbf{r})u_{\lambda,\mathbf{k}\simeq\mathbf{0}}(\mathbf{r}) \tag{3.3}$$

where $u_{\lambda,\mathbf{k}}(\mathbf{r})$ is the bulk Bloch function with band index $\lambda = \text{e}, \text{h}$ and crystal momentum $\hbar\mathbf{k}$ while the subband index β includes all quantum numbers that originate from the confinement. The envelope function $\zeta_{\lambda,\beta}(\mathbf{r})$ follows from the Schrödinger equation for a single particle exposed to the confinement potential,

$$\left[-\frac{\hbar^2\nabla^2}{2m_\lambda} + V_{\text{QD}}^\lambda(\mathbf{r}_\parallel) + V_{\text{QW}}(z) \right] \zeta_{\lambda,\beta}(\mathbf{r}) = E_{\lambda,\beta}\zeta_{\lambda,\beta}(\mathbf{r}). \tag{3.4}$$

Separation of variables decomposes $\zeta_{\lambda,\beta}(\mathbf{r}) = \xi(z)\phi(\mathbf{r}_\parallel)$ into eigenfunctions $\xi(z)$ and $\phi(\mathbf{r}_\parallel)$ of the z-confinement and the in-plane confinement, respectively, that means

$$\left[-\frac{\hbar^2}{2m_\lambda}\frac{\partial^2}{\partial z^2} + V_{\text{QW}}(z) \right] \xi(z) = E^{\text{QW}}\xi(z), \tag{3.5}$$

$$\left[-\frac{\hbar^2}{2m_\lambda}\left(\frac{\partial^2}{\partial x^2} + \frac{\partial^2}{\partial y^2} \right) + V_{\text{QD}}^\lambda(\mathbf{r}_\parallel) \right] \phi(\mathbf{r}_\parallel) = E^{\text{QD}}\phi(\mathbf{r}_\parallel). \tag{3.6}$$

Both eigenvalue problems are standard textbook examples. The well confinement is solved by

$$E^{\mathrm{QW}} = E^{\mathrm{QW}}_{\lambda,j} = \frac{\hbar^2 \pi^2 j^2}{2 m_\lambda L^2}, \tag{3.7}$$

$$\xi(z) = \xi_j(z) = \Theta\left(\frac{L}{2} - |z|\right) \begin{cases} \sqrt{\frac{2}{L}} \cos \frac{\pi}{L}(2j+1)z & \text{if } j \text{ is even,} \\ \sqrt{\frac{2}{L}} \sin \frac{\pi}{L} 2jz & \text{if } j \text{ is odd,} \end{cases} \tag{3.8}$$

with quantum numbers $j = 0, 1, 2, \ldots$ where

$$\Theta(x) = \begin{cases} 0 & \text{for } x < 0, \\ 1 & \text{for } x \geq 0 \end{cases} \tag{3.9}$$

denotes the Heaviside step function. For an infinite potential well, the wave functions $\xi_j(z)$ do not depend on the band index λ. Since the spacing $E^{\mathrm{QW}}_{\lambda,j=1} - E^{\mathrm{QW}}_{\lambda,j=0}$ between the first two eigenenergies is of the order of $100\,\mathrm{meV}$ for both bands, the carriers are strongly confined to the lowest subband $j = 0$. Equation (3.6) describes a two-dimensional harmonic oscillator. Due to the azimuthal symmetry of the parabolic confinement potential $V^\lambda_{\mathrm{QD}}(\mathbf{r}_\parallel)$, the wave functions $\phi(\mathbf{r}_\parallel)$ can be chosen as eigenfunctions of the angular momentum in z direction $\hat{L}_z = -\mathrm{i}\hbar \frac{\partial}{\partial \varphi}$. In polar coordinates (ρ, φ), this choice leads to

$$\phi(\mathbf{r}_\parallel) = \phi_{\lambda,n,m}(\rho, \varphi) = c_0 \mathrm{e}^{\mathrm{i}m\varphi} \mathrm{e}^{-\eta\rho^2} \rho^{|m|} L_{l^-}^{|m|}\left(2\eta\rho^2\right), \tag{3.10}$$

where $l^\pm \equiv (n \pm |m|)/2$, $c_0 \equiv \sqrt{l^-!/l^+!}\,(2\eta)^{\frac{1}{2}(1+|m|)}/\sqrt{\pi}$, $\eta \equiv m_\lambda \omega_\lambda / 2\hbar$, and $L_{l^-}^{|m|}$ denotes the generalized Laguerre polynomial [105]. By the choice $m_\mathrm{e}\omega_\mathrm{e} = m_\mathrm{h}\omega_\mathrm{h}$, we obtain identical wavefunctions for electrons and holes. This characterizes the so-called *symmetric case* that is often employed in the literature. The principal quantum number n and the angular-momentum quantum number m can assume the values $n = 0, 1, 2, \ldots$ and $m = -n, -n+2, \ldots, n-2, n$, respectively. The corresponding eigen energies are

$$E^{\mathrm{QD}}_{\lambda,n,m} = \hbar\omega_\lambda (n+1). \tag{3.11}$$

The level scheme of the quantum dot is shown schematically in Fig. 5. For a principal quantum number $n > n_{\max}$, the corresponding energy level lies in the wetting-layer continuum. Analogously to the atomic case, the shells are often labeled as s, p, d, ... with increasing n. Maximal principal quantum numbers $n_{\max} = 0, 1, 2, \ldots$ characterize an s dot, s-p dot, s-p-d dot, and so on.

3.1.2 System Hamiltonian

Having defined the single-particle basis for the quantum dot, we can now determine the explicit form of the system Hamiltonian in second quantization. To simplify the notation, we include the electron-spin quantum number σ in the subband index β. For the time being, we restrict the analysis to the carrier-photon system that is described by the quantum-electrodynamical Hamiltonian

$$\hat{H}_{\mathrm{QED}} = \hat{H}_{\mathrm{el}} + \hat{H}_{\mathrm{el-el}} + \hat{H}_{\mathrm{em}} + \hat{H}_{\mathrm{el-em}}. \tag{3.12}$$

Electron-phonon interaction will be considered in Sec. 3.4.2. After the preparatory work performed in Sec. 2.3, it merely remains to evaluate the matrix elements.
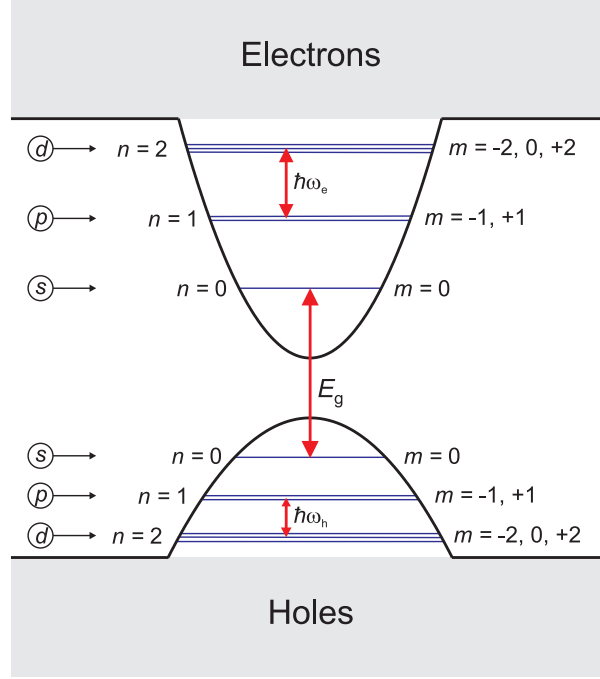
Figure 5: Energy-level scheme of the *s-p-d* quantum dot. The principal quantum number and the angular-momentum quantum number are denoted as n and m, respectively. States with different m but same n are degenerate. The sketch is not to scale—the gap energy is of the order of $1\,\mathrm{eV}$ while the interlevel spacings $\hbar\omega_{\mathrm{e/h}}$ are of the order of $10\,\mathrm{meV}$. The gray shaded areas indicate the continua of wetting-layer states.

The pure carrier part of the Hamiltonian can be written as

$$\hat{H}_{\mathrm{el}} = \sum_{\lambda,\beta} \varepsilon_{\lambda,\beta}\hat{a}^{\dagger}_{\lambda,\beta}\hat{a}_{\lambda,\beta}, \tag{3.13}$$

$$\hat{H}_{\mathrm{el-el}} = \sum_{\lambda,\lambda'} \sum_{\beta,\beta',\beta'',\beta'''} V^{\,\beta\,\,\beta'}_{\,\beta''\beta'''}\hat{a}^{\dagger}_{\lambda,\beta}\hat{a}^{\dagger}_{\lambda',\beta'}\hat{a}_{\lambda',\beta''}\hat{a}_{\lambda,\beta'''} \tag{3.14}$$

with $\lambda, \lambda' = \mathrm{c}, \mathrm{v}$ and the single-particle energies $\varepsilon_{\mathrm{c},\beta} = E_{\mathrm{g}} + E^{\mathrm{QD}}_{\mathrm{e},\beta}$, $\varepsilon_{\mathrm{v},\beta} = -E^{\mathrm{QD}}_{\mathrm{h},\beta}$. The real-valued Coulomb matrix elements $V^{\,\beta\,\,\beta'}_{\,\beta''\beta'''}$ are calculated in Appendix C.1.1. For the following derivations, only the selection rules

$$V^{\,\beta\,\,\beta'}_{\,\beta''\beta'''} = \delta_{m+m',m''+m'''}\delta_{\sigma,\sigma'''}\delta_{\sigma',\sigma''}V^{\,\beta\,\,\beta'}_{\,\beta''\beta'''} \tag{3.15}$$

and the symmetry relations

$$V^{\,\beta\,\,\beta'}_{\,\beta''\beta'''} = V^{\,\beta''\beta'''}_{\,\beta\,\,\beta'}, \qquad V^{\,\beta\,\,\beta'}_{\,\beta''\beta'''} = V^{\,\beta'\,\,\beta}_{\,\beta'''\beta''} \tag{3.16}$$

are explicitly needed. We notice that the matrix elements are not band-dependent in the symmetric case but do depend on the electron spins now that σ is absorbed by the label β.

The Hamiltonian $\hat{H}_{\mathrm{em}}$ of the free radiation field is defined in Eq. (2.86). When evaluating the matrix element in the dipole Hamiltonian $\hat{H}_{\mathrm{el-em}}$ from Eq. (2.100), we use that the diameters

of the considered quantum dots are more than one order of magnitude smaller than optical wave lengths. It is therefore justified to replace the mode function in the overlap integral (2.101) by its value at the position of the dot $\mathbf{r} = \mathbf{0}$. This approximation leads to

$$\hat{H}_{\mathrm{el-em}} = -\sum_{\beta,\mathbf{q}} \mathrm{i} \mathscr{E}_{\mathbf{q}} \mathbf{U}_{\mathbf{q}}(\mathbf{0}) \cdot \left(\mathbf{d}_{\mathrm{c,v}} \hat{a}_{\mathrm{c},\beta}^{\dagger} \hat{a}_{\mathrm{v},\beta} + \mathbf{d}_{\mathrm{c,v}}^{*} \hat{a}_{\mathrm{v},\beta}^{\dagger} \hat{a}_{\mathrm{c},\beta} \right) \hat{B}_{\mathbf{q}} + \mathrm{H.C.} \tag{3.17}$$

which can be rewritten as $\hat{H}_{\mathrm{el-em}} = -\hat{\mathbf{P}} \cdot \hat{\mathbf{E}}_{\mathrm{T}}(\mathbf{0})$ where

$$\hat{\mathbf{P}} = \sum_{\beta} \left(\mathbf{d}_{\mathrm{c,v}}^{*} \hat{a}_{\mathrm{v},\beta}^{\dagger} \hat{a}_{\mathrm{c},\beta} + \mathrm{H.C.} \right) \tag{3.18}$$

denotes the polarization operator of the dot. In the following, the subscript T will be omitted since $\mathbf{E}$ will always denote the transverse light field.

We observe that the system Hamiltonian exclusively contains operator combinations where the total angular momentum of the involved carriers remains unchanged. Consequently, all factorization terms in the equation of motion for an "anisotropic" N-particle expectation value, that is $\langle \hat{a}_{\lambda_N,\beta_N}^{\dagger} \cdots \hat{a}_{\lambda_1,\beta_1}^{\dagger} \hat{a}_{\lambda_1',\beta_1'} \cdots \hat{a}_{\lambda_N',\beta_N'} \rangle$ with $m_1 + \cdots + m_N \neq m_1' + \cdots + m_N'$, contain at least one "anisotropic" factor. If all "anisotropic" quantities vanish initially, they thus remain zero during the evolution of the system. This condition considerably reduces the number of equations of motion to be solved.

3.2 Singlet properties

Many basic features of the coherent excitation dynamics with a classical light field can already be described on the singlet level of cluster expansion, i.e. in Hartree-Fock approximation. The central equations of motion in this regime are the semiconductor Bloch equations (SBE) derived in Sec. 3.2.1. The eigen solutions of the homogeneous parts of the SBE define the exciton basis introduced explicitly in Sec. 3.2.2. As shown in Sec. 3.2.3, this basis can be used to solve the SBE analytically, which yields the Elliott formula for the linear absorption spectrum. The calculated optical spectra contain only a subset of the excitonic resonances that arise from the diagonalization procedure. The symmetries and density dependencies of the "bright" and "dark" excitons are analyzed numerically in Sec. 3.2.4.

3.2.1 Semiconductor Bloch equations

The proper single-particle quantities can be distinguished into interband expectation values

$$p_{\beta'}^{\beta} \equiv \langle \hat{a}_{\mathrm{v},\beta}^{\dagger} \hat{a}_{\mathrm{c},\beta'} \rangle \tag{3.19}$$

and intraband expectation values

$$f_{\mathrm{e}\,\beta'}^{\ \beta} \equiv \langle \hat{a}_{\mathrm{c},\beta}^{\dagger} \hat{a}_{\mathrm{c},\beta'} \rangle, \quad f_{\mathrm{h}\,\beta'}^{\ \beta} \equiv \delta_{\beta,\beta'} - \langle \hat{a}_{\mathrm{v},\beta}^{\dagger} \hat{a}_{\mathrm{v},\beta'} \rangle. \tag{3.20}$$

Since the expectation value $\mathbf{P} = \langle \hat{\mathbf{P}} \rangle$ of the polarization operator (3.18) can be written as

$$\mathbf{P} = \sum_{\beta} \left[\mathbf{d}_{\mathrm{c,v}}^{*} p_{\beta}^{\beta} + \mathbf{d}_{\mathrm{c,v}} \left(p_{\beta}^{\beta} \right)^{*} \right], \tag{3.21}$$

the diagonal interband quantities p^{β}_{β} can be interpreted as the *microscopic polarizations* of the quantum dot. For convenience, we also call the off-diagonal $p^{\beta}_{\beta'}$ with $\beta \neq \beta'$ "polarizations". Similarly, we always refer to $f_{\mathrm{e}}{}^{\beta}_{\beta'}$ and $f_{\mathrm{h}}{}^{\beta}_{\beta'}$ as *electron* and *hole densities*, respectively, although only the diagonal expectation values $f^{\mathrm{e}}_{\beta} \equiv f_{\mathrm{e}}{}^{\beta}_{\beta}$ and $f^{\mathrm{h}}_{\beta} \equiv f_{\mathrm{h}}{}^{\beta}_{\beta}$ are proper occupation numbers.

The coupled equations of motion for polarizations and densities form the *semiconductor Bloch equations* (SBE) of the quantum dot:

$$i\hbar \frac{\mathrm{d}}{\mathrm{d}t} p^{\beta}_{\beta'} = \sum_{\beta_1} \left(E^{\mathrm{e}}_{\beta',\beta_1} p^{\beta}_{\beta_1} + E^{\mathrm{h}}_{\beta_1,\beta} p^{\beta_1}_{\beta'} \right)$$
$$- \sum_{\beta_1,\beta_2} \Omega^{\mathrm{R}}_{\beta_1,\beta_2} \left(\delta_{\beta,\beta_2} \delta_{\beta_1,\beta'} - \delta_{\beta,\beta_2} f_{\mathrm{e}}{}^{\beta_1}_{\beta'} - \delta_{\beta_1,\beta'} f_{\mathrm{h}}{}^{\beta}_{\beta_2} \right) + D_p{}^{\beta}_{\beta'}, \tag{3.22}$$

$$i\hbar \frac{\mathrm{d}}{\mathrm{d}t} f_{\mathrm{e}}{}^{\beta}_{\beta'} = \sum_{\beta_1} \left(E^{\mathrm{e}}_{\beta',\beta_1} f_{\mathrm{e}}{}^{\beta}_{\beta_1} - E^{\mathrm{e}}_{\beta_1,\beta} f_{\mathrm{e}}{}^{\beta_1}_{\beta'} \right)$$
$$+ \sum_{\beta_1} \left[\left(\Omega^{\mathrm{R}}_{\beta,\beta_1} \right)^* p^{\beta_1}_{\beta'} - \Omega^{\mathrm{R}}_{\beta',\beta_1} \left(p^{\beta_1}_{\beta} \right)^* \right] + D_{\mathrm{e}}{}^{\beta}_{\beta'}, \tag{3.23}$$

$$i\hbar \frac{\mathrm{d}}{\mathrm{d}t} f_{\mathrm{h}}{}^{\beta}_{\beta'} = -\sum_{\beta_1} \left(E^{\mathrm{h}}_{\beta',\beta_1} f_{\mathrm{h}}{}^{\beta}_{\beta_1} - E^{\mathrm{h}}_{\beta_1,\beta} f_{\mathrm{h}}{}^{\beta_1}_{\beta'} \right)$$
$$+ \sum_{\beta_1} \left[\left(\Omega^{\mathrm{R}}_{\beta_1,\beta'} \right)^* p^{\beta}_{\beta_1} - \Omega^{\mathrm{R}}_{\beta_1,\beta} \left(p^{\beta'}_{\beta_1} \right)^* \right] + D_{\mathrm{h}}{}^{\beta}_{\beta'}. \tag{3.24}$$

The first terms on the right-hand sides of these equations always contain the *mean-field energies*

$$E^{\mathrm{e}}_{\beta,\beta'} \equiv \delta_{\beta,\beta'} \varepsilon_{\mathrm{c},\beta} - \sum_{\beta_1,\beta_2} V^{\beta\,\beta_1}_{\beta'\beta_2} f_{\mathrm{e}}{}^{\beta_1}_{\beta_2} + \sum_{\beta_1,\beta_2} V^{\beta\,\beta_1}_{\beta_2\beta'} (f_{\mathrm{e}}{}^{\beta_1}_{\beta_2} - f_{\mathrm{h}}{}^{\beta_1}_{\beta_2}), \tag{3.25a}$$

$$E^{\mathrm{h}}_{\beta,\beta'} \equiv -\delta_{\beta,\beta'} \varepsilon_{\mathrm{v},\beta} - \sum_{\beta_1,\beta_2} V^{\beta\,\beta_1}_{\beta'\beta_2} f_{\mathrm{h}}{}^{\beta_1}_{\beta_2} - \sum_{\beta_1\beta_2} V^{\beta\,\beta_1}_{\beta_2\beta'} (f_{\mathrm{e}}{}^{\beta_1}_{\beta_2} - f_{\mathrm{h}}{}^{\beta_1}_{\beta_2}). \tag{3.25b}$$

Formally, $E^{\mathrm{e(h)}}_{\beta,\beta'}$ also includes terms such as $U^{\beta}_{\beta'} \equiv \sum_{\beta_1} V^{\beta\,\beta_1}_{\beta'\beta_1}$ which lead to a divergence when the summation over β_1 runs over all states of the system including the extended wetting layer states. However, the completeness relation of the envelope functions and the explicit form of $V^{\beta\,\beta_1}_{\beta'\beta_1}$ shown in Eq. (C.12) provide $U^{\beta}_{\beta'} = \delta_{\beta,\beta'} U$ where U does not depend on β. These formally infinite terms can thus be included in the band-gap energy so that they do not appear in Eqs. (3.25a), (3.25b). The second terms on the right-hand sides of Eqs. (3.22)–(3.24) contain the classical electric field $\mathbf{E} = \langle \hat{\mathbf{E}} \rangle$ that drives the polarization and thus contributes to the creation of electron and hole densities. Often, $\mathbf{d}_{\mathrm{c,v}} \cdot \mathbf{E}/\hbar$ is referred to as *Rabi frequency*. The Coulomb interaction leads to the renormalized Rabi frequencies

$$\Omega^{\mathrm{R}}_{\beta,\beta'} \equiv \delta_{\beta,\beta'} \mathbf{d}_{\mathrm{c,v}} \cdot \mathbf{E} + \sum_{\beta_1,\beta_2} V^{\beta\,\beta_1}_{\beta'\beta_2} p^{\beta_1}_{\beta_2}. \tag{3.26}$$

For a quantum-dot system, these renormalizations are somewhat more complicated than the corresponding terms for quantum wells [61]. We observe that the proper polarizations p^{β}_{β} have a driving term $\mathbf{d}_{\mathrm{c,v}} \cdot \mathbf{E}(1 - f^{\mathrm{e}}_{\beta} - f^{\mathrm{h}}_{\beta})$ that is always present even for the unexcited dot. On the contrary, the densities are only driven after the system has been polarized. In optical

experiments with a semiconductor material, the relevant photons have an energy $\hbar\omega_{\mathbf{q}}$ that is close to the band gap. Consequently, the phase of $\langle \hat{B}_{\mathbf{q}} \rangle$ roughly rotates like that of a microscopic polarization. We can thus replace $\mathbf{E}$ in the SBE by its co-rotating part

$$\mathbf{E}^{(+)} \equiv \mathrm{i} \sum_{\mathbf{q}} \mathscr{E}_{\mathbf{q}} \mathbf{U}_{\mathbf{q}}(\mathbf{0}) \langle \hat{B}_{\mathbf{q}} \rangle \tag{3.27}$$

because the counter-rotating part $\mathbf{E}^{(-)} = \left[\mathbf{E}^{(+)}\right]^{*}$ leads to fast rotating source terms that do not contribute to the build-up of polarizations and densities. This approach is often called *rotating-wave approximation* (RWA) in the literature. When we introduce the effective coupling constant $\mathcal{F}_{\mathbf{q}} \equiv \mathscr{E}_{\mathbf{q}} \mathbf{U}_{\mathbf{q}}(\mathbf{0}) \cdot \mathbf{d}_{\mathrm{c,v}}$ and the collective photon operator $\hat{B}_{\Sigma} \equiv \sum_{\mathbf{q}} \mathcal{F}_{\mathbf{q}} \hat{B}_{\mathbf{q}}$, we can write the Rabi frequency in RWA as $\mathbf{d}_{\mathrm{c,v}} \cdot \mathbf{E}^{(+)} = \mathrm{i}\langle \hat{B}_{\Sigma} \rangle$.

We see from the SBE that the singlet dynamics couples to pure doublet terms indicated by $D_{p}{}^{\beta}_{\beta'}$, $D_{\mathrm{e}}{}^{\beta}_{\beta'}$, and $D_{\mathrm{h}}{}^{\beta}_{\beta'}$. They originate from Coulombic and quantum-optical correlations. Explicitly, these terms can be written as

$$D_{p}{}^{\beta}_{\beta'} = - \sum_{\beta_1,\beta_2,\beta_3} \left[V^{\beta'\beta_1}_{\beta_2\beta_3} \sum_{\lambda} C\!\left({}^{\mathrm{v}\,\lambda}_{\lambda\mathrm{c}} \Big| {}^{\beta\ \beta_1}_{\beta_2\beta_3} \right) - V^{\beta\ \beta_1}_{\beta_2\beta_3} \sum_{\lambda} C\!\left({}^{\mathrm{v}\,\lambda}_{\lambda\mathrm{c}} \Big| {}^{\beta_3\beta_2}_{\beta_1\beta'} \right) \right]$$
$$+ \mathrm{i} \left[\Delta\langle \hat{B}_{\Sigma} \hat{a}^{\dagger}_{\mathrm{c},\beta} \hat{a}_{\mathrm{c},\beta'} \rangle - \Delta\langle \hat{B}_{\Sigma} \hat{a}^{\dagger}_{\mathrm{v},\beta} \hat{a}_{\mathrm{v},\beta'} \rangle \right], \tag{3.28}$$

$$D_{\mathrm{e}}{}^{\beta}_{\beta'} = - \sum_{\beta_1,\beta_2,\beta_3} \left[V^{\beta'\beta_1}_{\beta_2\beta_3} \sum_{\lambda} C\!\left({}^{\mathrm{c}\,\lambda}_{\lambda\mathrm{c}} \Big| {}^{\beta\ \beta_1}_{\beta_2\beta_3} \right) - V^{\beta\ \beta_1}_{\beta_2\beta_3} \sum_{\lambda} C\!\left({}^{\mathrm{c}\,\lambda}_{\lambda\mathrm{c}} \Big| {}^{\beta_3\beta_2}_{\beta_1\beta'} \right) \right]$$
$$+ \mathrm{i} \left[\Delta\langle \hat{B}^{\dagger}_{\Sigma} \hat{a}^{\dagger}_{\mathrm{v},\beta} \hat{a}_{\mathrm{c},\beta'} \rangle + \Delta\langle \hat{B}^{\dagger}_{\Sigma} \hat{a}^{\dagger}_{\mathrm{v},\beta'} \hat{a}_{\mathrm{c},\beta} \rangle^{*} \right], \tag{3.29}$$

$$D_{\mathrm{h}}{}^{\beta}_{\beta'} = \sum_{\beta_1,\beta_2,\beta_3} \left[V^{\beta'\beta_1}_{\beta_2\beta_3} \sum_{\lambda} C\!\left({}^{\lambda\mathrm{v}}_{\mathrm{v}\lambda} \Big| {}^{\beta_1\beta}_{\beta_3\beta_2} \right) - V^{\beta\ \beta_1}_{\beta_2\beta_3} \sum_{\lambda} C\!\left({}^{\lambda\mathrm{v}}_{\mathrm{v}\lambda} \Big| {}^{\beta_2\beta_3}_{\beta'\beta_1} \right) \right]$$
$$+ \mathrm{i} \left[\Delta\langle \hat{B}^{\dagger}_{\Sigma} \hat{a}^{\dagger}_{\mathrm{v},\beta} \hat{a}_{\mathrm{c},\beta'} \rangle + \Delta\langle \hat{B}^{\dagger}_{\Sigma} \hat{a}^{\dagger}_{\mathrm{v},\beta'} \hat{a}_{\mathrm{c},\beta} \rangle^{*} \right] \tag{3.30}$$

where we have identified the genuine two-particle correlations

$$C\!\left({}^{\lambda\ \lambda'}_{\lambda''\lambda'''} \Big| {}^{\beta\ \beta'}_{\beta''\beta'''} \right) \equiv \Delta\langle \hat{a}^{\dagger}_{\lambda\beta} \hat{a}^{\dagger}_{\lambda'\beta'} \hat{a}_{\lambda'''\beta'''} \hat{a}_{\lambda''\beta''} \rangle. \tag{3.31}$$

The Coulomb correlations describe a variety of phenomena such as dephasing, energy renormalization, and scattering contributions that are well known from the quantum-well case [7]. Our numerical calculations show that the dephasing is much smaller in isolated quantum dots than in spatially homogeneous systems. The two-particle correlations that include photon operators provide quantum-optical corrections to the SBE. For example, D_{e} and D_{h} lead to spontaneous recombination of electron-hole pairs which is observed as reduction of carrier densities. A more detailed discussion will be given in Sec. 3.3. In RWA, the photon correlation terms can also be expressed with the help of the collective operator $\hat{B}_{\Sigma}$ defined above that describes the operator form of the Rabi frequency.

For further analytical considerations, it will prove useful to rewrite Eq. (3.22) such that the homogeneous contributions are isolated. This procedure yields

$$\mathrm{i}\hbar \frac{\mathrm{d}}{\mathrm{d}t} p^{\beta}_{\beta'} = \sum_{\beta_1,\beta_2} A_{(\beta,\beta'),(\beta_1,\beta_2)} p^{\beta_1}_{\beta_2} - \mathbf{d}_{\mathrm{c,v}} \cdot \mathbf{E}^{(+)} \left(\delta_{\beta,\beta'} - f_{\mathrm{e}}{}^{\beta}_{\beta'} - f_{\mathrm{h}}{}^{\beta}_{\beta'} \right) + D_{p}{}^{\beta}_{\beta'} \tag{3.32}$$

with the matrix

$$A_{(\beta,\beta'),(\beta'',\beta''')} \equiv \delta_{\beta,\beta''} E^{\mathrm{e}}_{\beta',\beta'''} + \delta_{\beta',\beta'''} E^{\mathrm{h}}_{\beta'',\beta}$$
$$- \sum_{\beta_1,\beta_2} V^{\beta_1\beta''}_{\beta_2\beta'''} \left(\delta_{\beta,\beta_2}\delta_{\beta_1,\beta'} - \delta_{\beta,\beta_2} f_{\mathrm{e}\,\beta'}^{\,\beta_1} - \delta_{\beta_1,\beta'} f_{\mathrm{h}\,\beta_2}^{\,\beta} \right). \tag{3.33}$$

The homogeneous part of the equation of motion for the polarizations can be diagonalized by means of the generalized exciton basis introduced in the next section.

3.2.2 Exciton basis

Because electrons and holes are oppositely charged, they can form bound states that are called *excitons*. As discussed in Appendix A, the relative motion of electron and hole is described by *excitonic wave functions*. These wave functions are solutions of the *Wannier equation* that corresponds to the Schrödinger equation for the hydrogen problem where the electron and proton masses are replaced by the effective electron and hole masses, respectively, and a dielectric background constant is introduced. As a consequence, excitons have much larger Bohr radii a_{B} and much smaller binding energies $\mathcal{E}_{\mathrm{B}}$ than a hydrogen atom. So long as the lateral extensions of a hetero structure exceed a_{B}, the electron-hole pair states of the confined system do not deviate much from the bulk case but their center-of-mass movement is restricted. With the material parameters for strained InGaAs, we find $\mathcal{E}_{\mathrm{B}} = 3.4\,\mathrm{meV}$ and $a_{\mathrm{B}} = 15.4\,\mathrm{nm}$. The considered quantum-dot confinement is therefore strong in the sense that bulk excitons cannot exist anymore. Hence, the concept of an exciton must be adjusted to describe electron-hole pair states in the dot system. We show in this section how the more formal definition of the excitonic wave functions as eigen solutions of the homogeneous Bloch equations for the microscopic polarizations (cf. Appendix A) can be adopted for the quantum-dot case.

To avoid cumbersome index book-keeping, we employ a bra-ket notation for double-indexed quantities such as $p_{\beta'}^{\,\beta}$ or $\phi_{\beta,\beta'}$. The column vector with components $x_{\beta,\beta'}$ is written as "ket" $|x\rangle = (x_{\beta,\beta'})$. Accordingly, the "bra" $\langle x| = (x^*_{\beta,\beta'})^{\mathrm{T}}$ denotes the row vector with components $x^*_{\beta,\beta'}$. Here, we use bold delimiters $|x\rangle$ instead of $|x\rangle$ to prevent confusion with quantum-mechanical state vectors. A scalar product can be defined as $\langle x|y\rangle = \sum_{\beta,\beta'} x^*_{\beta,\beta'} y_{\beta,\beta'}$. The entries of a matrix $\boldsymbol{M} = \left(M_{(\beta,\beta'),(\beta'',\beta''')} \right)$ are labeled by pairs of double indices. The product of a matrix $\boldsymbol{M}$ and a column vector $|x\rangle$ yields a new column vector $|y\rangle = \boldsymbol{M}|x\rangle$ with components $y_{\beta,\beta'} = \sum_{\beta_1,\beta_2} M_{(\beta,\beta'),(\beta_1,\beta_2)} x_{\beta_1,\beta_2}$. Consistently, $\langle y| = \langle x|\boldsymbol{M}$ is a row vector with components $y^*_{\beta,\beta'} = \sum_{\beta_1,\beta_2} x^*_{\beta_1,\beta_2} M_{(\beta_1,\beta_2),(\beta,\beta')}$.

We notice that in case of vanishing densities $f_{\mathrm{e/h}\,\beta'}^{\,\beta} = 0$, the matrix $\boldsymbol{A}$ from Eq. (3.33) that defines the homogeneous part of the SBE is Hermitian and thus has a complete orthogonal set of eigen vectors with real eigen values $\mathcal{E}_i$. For non-vanishing $f_{\mathrm{e/h}\,\beta'}^{\,\beta}$, however, $\boldsymbol{A}$ becomes non-Hermitian such that eigen vectors with different eigenvalues are not necessarily orthogonal anymore. Then, it is useful to introduce right- and left-handed eigen vectors that obey generalized orthogonality and completeness relations. More explicitly, the *right-handed* solutions $|\phi^{i,\mathrm{R}}\rangle$ of the excitonic eigenvalue problem for the quantum dot are defined by

$$\boldsymbol{A}|\phi^{i,\mathrm{R}}\rangle = \mathcal{E}_i|\phi^{i,\mathrm{R}}\rangle. \tag{3.34}$$

It turns out that $\boldsymbol{A}$ remains diagonalizable and the excitonic eigenvalues $\mathcal{E}_i$ remain real-valued for finite densities. With respect to an arbitrary orthonormal basis $\{|\psi^i\rangle = (\psi^i_{\beta,\beta'})\}$, we define

the matrix[1] Φ by $\Phi_{i,j} \equiv \langle \psi^i | \phi^{j,\mathrm{R}} \rangle$. Since $\boldsymbol{A}$ can be diagonalized, Φ corresponds to a basis transformation and can be inverted. This allows us to define another basis $\{|\phi^{i,\mathrm{L}}\rangle\}$ via the condition $\langle \phi^{j,\mathrm{L}} | \psi^i \rangle \equiv (\Phi^{-1})_{j,i}$. It can easily be seen that $\{|\phi^{i,\mathrm{L}}\rangle\}$ and $\{|\phi^{i,\mathrm{R}}\rangle\}$ are reciprocal, that means they fulfill the *generalized orthogonality and completeness relations*

$$\langle \phi^{i,\mathrm{L}} | \phi^{j,\mathrm{R}} \rangle = \delta_{i,j}, \tag{3.35}$$

$$\sum_j |\phi^{j,\mathrm{R}}\rangle\langle\phi^{j,\mathrm{L}}| = \boldsymbol{I} \tag{3.36}$$

with the unity matrix $\boldsymbol{I}$. Consequently,

$$\langle \phi^{i,\mathrm{L}} | \boldsymbol{A} = \sum_j \langle \phi^{i,\mathrm{L}} | \boldsymbol{A} | \phi^{j,\mathrm{R}} \rangle\langle\phi^{j,\mathrm{L}}| = \sum_j \mathcal{E}_j \langle \phi^{i,\mathrm{L}} | \phi^{j,\mathrm{R}} \rangle\langle\phi^{j,\mathrm{L}}| = \mathcal{E}_i \langle \phi^{i,\mathrm{L}} |, \tag{3.37}$$

which shows that the $|\phi^{i,\mathrm{L}}\rangle$ are nothing else but the *left-handed* eigen vectors of $\boldsymbol{A}$. In components, Eqs. (3.36), (3.35) take the forms

$$\sum_{\beta,\beta'} \phi^{i,\mathrm{L}}_{\beta,\beta'} \phi^{j,\mathrm{R}}_{\beta,\beta'} = \delta_{i,j}, \tag{3.38}$$

$$\sum_i \phi^{i,\mathrm{R}}_{\beta,\beta'} \left(\phi^{i,\mathrm{L}}_{\beta'',\beta'''} \right)^* = \delta_{\beta,\beta''} \delta_{\beta',\beta'''}. \tag{3.39}$$

In view of the generalized orthogonality and completeness relations, we can introduce *excitonic creation and annihilation operators*

$$\hat{X}_i^\dagger = \sum_{\beta\beta'} \phi^{i,\mathrm{L}}_{\beta\beta'} \hat{a}^\dagger_{\mathrm{c},\beta'} \hat{a}_{\mathrm{v},\beta}, \tag{3.40a}$$

$$\hat{X}_i = \sum_{\beta\beta'} \left(\phi^{i,\mathrm{L}}_{\beta\beta'} \right)^* \hat{a}^\dagger_{\mathrm{v},\beta} \hat{a}_{\mathrm{c},\beta'} \tag{3.40b}$$

The inverse relations read

$$\hat{a}^\dagger_{\mathrm{c},\beta'} \hat{a}_{\mathrm{v},\beta} = \sum_i \left(\phi^{i,\mathrm{R}}_{\beta\beta'} \right)^* \hat{X}_i^\dagger, \tag{3.41a}$$

$$\hat{a}^\dagger_{\mathrm{v},\beta} \hat{a}_{\mathrm{c},\beta'} = \sum_i \phi^{i,\mathrm{R}}_{\beta\beta'} \hat{X}_i. \tag{3.41b}$$

Equations (3.40), (3.41) enable us to transform back and forth between the exciton basis and the single-particle (Bloch) basis.

In analogy to higher-dimensional systems (cf. Appendix A), we refer to the two-particle correlation

$$\Delta N_i \equiv \Delta\langle \hat{X}_i^\dagger \hat{X}_i \rangle \tag{3.42}$$

as *population* of the i-th exciton state. Moreover, we call configurations of the carrier system with finite densities but vanishing excitonic correlations $\Delta\langle \hat{X}_i^\dagger \hat{X}_j \rangle$ *uncorrelated electron-hole plasma*. The physical meaning of such a distinction will be analyzed in the following sections.

---

[1] This is not a matrix in the same sense as $\boldsymbol{A}$—it cannot act on a ket vector $|x\rangle$, and its rows and columns are denoted by integer indices i, j instead of double indices $(\beta, \beta'), (\beta'', \beta''')$.

3.2.3 Elliott formula for the linear absorption spectrum

The semiconductor Bloch equations (3.22)–(3.24) can be solved numerically to describe the coherent and classical excitation dynamics of the quantum dot. It turns out that the precise inclusion of the two-particle correlations (3.28)–(3.30) is computationally rather demanding. The analysis becomes particularly involved when also the scattering from the wetting layer is fully included [34–37]. To gain some fundamental insight into the excitation dynamics, we first simplify these contributions by including only their generic properties. The full singlet-doublet analysis is then performed later in Secs. 3.3 and 3.4.

If we assume that the two-particle correlations D_p, D_e, and D_h only lead to dephasing for the polarization when dot states are considered, we may replace $D_p{}^{\beta}_{\beta'}$ in Eq. (3.22) by a phenomenological dephasing term $-\mathrm{i}\gamma p^{\beta}_{\beta'}$. If we further assume that the densities are quasi-stationary, Eqs. (3.23), (3.24) can adiabatically be decoupled from Eq. (3.22). As a result, we find the frequency-domain version of Eq. (3.32),

$$(\hbar\omega + \mathrm{i}\gamma)\, p^{\beta}_{\beta'}(\omega) = \sum_{\beta_1,\beta_2} A_{(\beta,\beta'),(\beta_1,\beta_2)} p^{\beta_1}_{\beta_2}(\omega) - \mathbf{d}_{\mathrm{c,v}}\mathbf{E}(\omega)\left(\delta_{\beta,\beta'} - f_{\mathrm{e}}{}^{\beta}_{\beta'} - f_{\mathrm{h}}{}^{\beta}_{\beta'}\right), \quad (3.43)$$

with the matrix $\boldsymbol{A}$ as defined in Eq. (3.33). This linear system of equations can be solved analytically such that $p^{\beta}_{\beta'}$ is expressed in terms of the exciting light field. This result then yields the macroscopic polarization of the quantum dot

$$\mathbf{P}(\omega) = \sum_{\beta} \left\{ \mathbf{d}^*_{\mathrm{c,v}} p^{\beta}_{\beta}(\omega) + \mathbf{d}_{\mathrm{c,v}} \left[p^{\beta}_{\beta}(-\omega) \right]^* \right\} \tag{3.44}$$

in the frequency domain as material response to an external, transverse electric field $\mathbf{E}(\omega)$. For weak probe fields, the relation between $\mathbf{P}$ and $\mathbf{E}$ is linear and can be written as

$$\mathbf{P}(\omega) = \chi(\omega)\mathbf{E}(\omega) \tag{3.45}$$

with the *linear susceptibility* $\chi(\omega)$ that is a tensorial quantity in general. We assume for simplicity that $\mathbf{E}$ is parallel to the dipole matrix-element $\mathbf{d}_{\mathrm{c,v}}$ such that the susceptibility becomes a scalar function

$$\chi(\omega) = \frac{P(\omega)}{E(\omega)}. \tag{3.46}$$

By using the exciton basis introduced in the previous section, we can diagonalize and invert Eq. (3.43). This procedure finally leads to the *Elliott formula* [106]

$$\chi(\omega) = |\mathbf{d}_{\mathrm{c,v}}|^2 \sum_i \frac{\langle 1|\phi^{i,\mathrm{R}}\rangle\langle \phi^{i,\mathrm{L}}|1 - f_{\mathrm{e}} - f_{\mathrm{h}}\rangle}{\mathcal{E}_i - \hbar\omega - \mathrm{i}\gamma} \tag{3.47}$$

where $|1\rangle$ and $|f_{\mathrm{e/h}}\rangle$ denote the vectors with components $\delta_{\beta,\beta'}$ and $f_{\mathrm{e/h}}{}^{\beta}_{\beta'}$, respectively, and $|1 - f_{\mathrm{e}} - f_{\mathrm{h}}\rangle = |1\rangle - |f_{\mathrm{e}}\rangle - |f_{\mathrm{h}}\rangle$. In components, the scalar products appearing in the nominator thus read

$$\langle 1|\phi^{i,\mathrm{R}}\rangle = \sum_{\beta} \phi^{i,\mathrm{R}}_{\beta,\beta}, \tag{3.48}$$

$$\langle \phi^{i,\mathrm{L}}|1 - f_{\mathrm{e}} - f_{\mathrm{h}}\rangle = \sum_{\beta,\beta'} \left(\phi^{i,\mathrm{L}}_{\beta'\beta}\right)^* \left(\delta_{\beta,\beta'} - f_{\mathrm{e}}{}^{\beta}_{\beta'} - f_{\mathrm{h}}{}^{\beta}_{\beta'}\right). \tag{3.49}$$
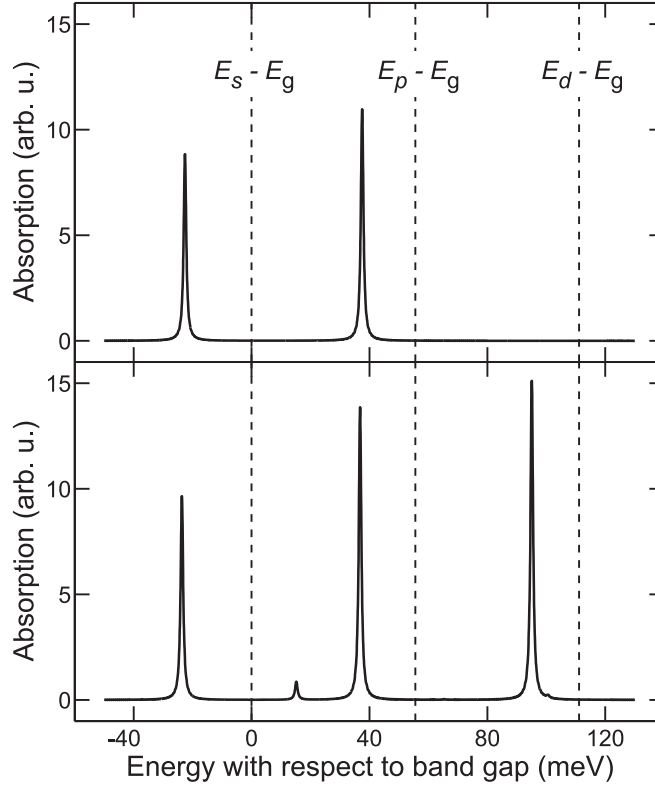
Figure 6: Linear absorption spectra for initially unexcited dots with maximum principal quantum numbers $n_{max} = 1$ (a) and $n_{max} = 2$ (b).

In Eq. (3.47), we have omitted the non-resonant terms proportional to $(\mathcal{E}_i + \hbar\omega + i\gamma)^{-1}$ that have a negligible contribution for positive frequencies ω and a small dephasing constant γ.

Owing to the oscillating macroscopic polarization of the dot, the material systems radiates classical light. The wave equation for **E** must thus be solved simultaneously with the SBE when the material response is to be calculated self-consistently. Such an approach introduces additional broadening of the optical spectra since the emission leads to decay of the polarization.[2] However, for a single dot or a wetting layer with a small dot density, the radiative broadening can often be neglected. The *linear absorption spectrum* $\alpha(\omega)$ is then proportional to $\omega \mathrm{Im}\chi(\omega)$ [7]. The excitonic eigenenergies $\mathcal{E}_i$ appearing in the denominator of the Elliott formula clearly define the spectral positions of the absorption resonances. When the Coulomb correlations are fully included in the analysis, they provide density-dependent energy renormalizations as well as excitation induced dephasing [34,35,37] which also varies with the resonance index i. All these effects are well known from quasi two-dimensional systems [51,107].

---

[2]This point will be discussed in more detail in Sec. 3.5.
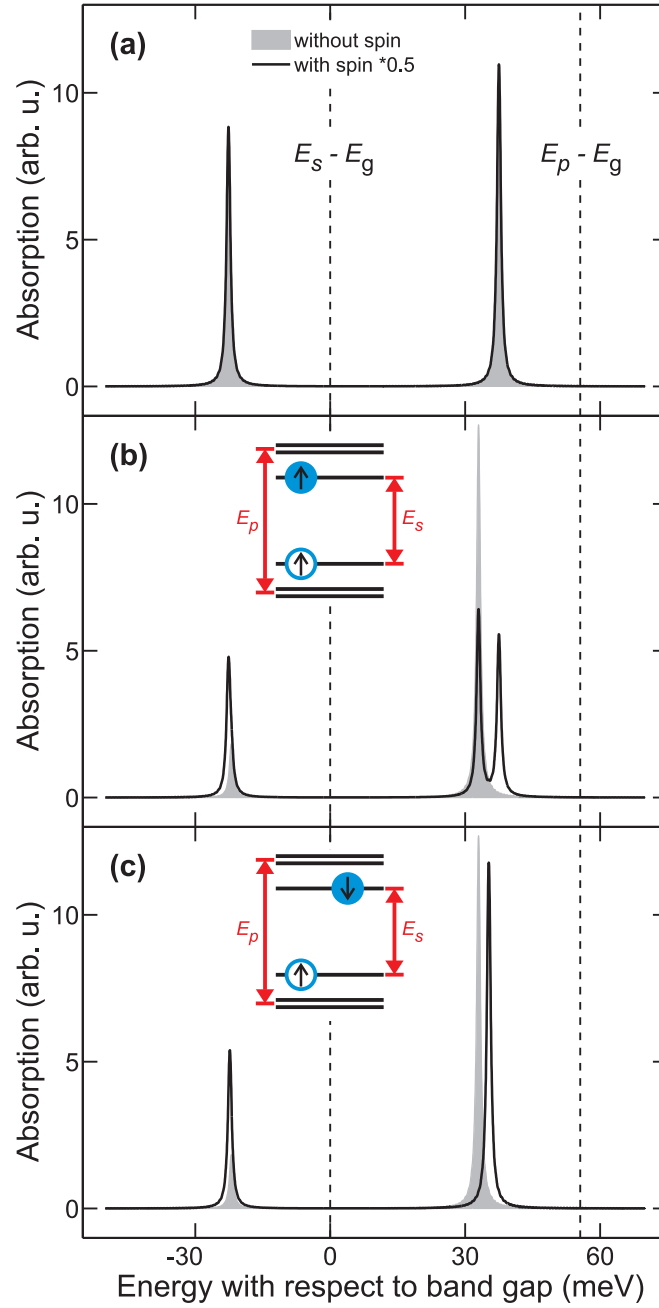
Figure 7: Influence of the electron spin on the optical resonances of the quantum dot. The shaded areas represent the absorption spectra for spinless carriers. When the spin is included (solid lines), the spectra are multiplied by 0.5 to compensate for the larger phase space. Frame (a) shows the results for the unexcited dot, frame (b) for initial densities $f^{e}_{(0,0,\uparrow)} = f^{h}_{(0,0,\uparrow)} = 0.4$ (otherwise zero), and frame (c) for $f^{e}_{(0,0,\downarrow)} = f^{h}_{(0,0,\uparrow)} = 0.4$ (otherwise zero).

Elliott absorption spectra for the unexcited dot are shown in Fig. 6. We use material parameters for InGaAs/GaAs systems and truncate the discrete spectrum of single-particle states at principal quantum numbers $n_{max} = 1$ (a) or $n_{max} = 2$ (b). In the absence of Coulomb interaction, the optical resonances would coincide with the unrenormalized vertical transition energies $E_s = E_g$, $E_p = E_g + \hbar(\omega_e + \omega_h)$, $E_d = E_g + 2\hbar(\omega_e + \omega_h)$, and so on. Contrary to the quantum-well case, the lowest resonance does not dominate the spectrum. The discussion of the energy spectra of lens-shaped quantum dots in Sec. 3.1.1 has shown that the interlevel spacings $\hbar\omega_{e/h}$ and the dissociation threshold n_{max} cannot be varied independently since all these quantities depend on the dot size. However, we conclude from a comparison of the absorption spectra in Fig. 6 that decreasing n_{max} basically restricts the spectrum to a subset of the original resonances where the remaining peaks do not change significantly. For the numerical examples in the remainder of this chapter, we will always assume an s-p dot, i.e. $n_{max} = 1$.

We can also analyze the influence of the electron spin on the optical resonances. In Fig. 7, Elliott spectra for electrons with spin (solid lines) and hypothetical electrons without spin (shaded areas) are compared. For the unexcited dot (a), inclusion of the spin just enhances the absorption by a factor of two owing to the larger phase space. The situation is more complicated when electrons and holes are initially present in the dot. For an elementary discussion, we neglect that the excitons always mix s- and p-shell densities to a certain degree as shown in the following section. In frame (b) and frame (c) of Fig. 7, an initial s-shell density of 0.4 is assumed for both electrons and holes. The conduction-band electron and the missing valence-band electron have equal spins in the former case. When further electron-hole pairs are excited in the p shells, they can have either the same or the opposite spin as the s-shell carriers. Because exchange interaction only occurs between carriers with equal spin, the degeneracy of the second resonance is lifted when the electron spin is included in the calculation. This effect cannot be observed for the first resonance since the build-up of further s-shell density with the same spin as the initial carriers is inhibited by the Pauli exclusion principle. For frame (c), the carriers are assumed to have opposite spin. Such a dot state cannot be achieved by optical excitation but may result from carrier capture from the wetting layer. Here, the absorbed amount of energy is identical if electron-hole pairs with spin up or spin down are created. Consequently, the degeneracy of the second resonance is not lifted in this case. Having identified the role of the electron spin, we will restrict the following analysis to the spin-selective case where only one of the spin species is considered such that the dot states in each band are uniquely specified by the principal quantum number n and the angular-momentum quantum number m.

3.2.4 Bright and dark excitons

We have found in the previous section that only two resonances are visible in the optical spectra of an s-p quantum dot although the corresponding excitonic eigenvalue problem is nine-dimensional. To shed some light on the underlying symmetries and their physical consequences, we now have a closer look on the exciton spectrum for $n_{max} = 1$. In this case, there are only six different excitonic eigenenergies $\mathcal{E}_i$ out of which three are two-fold degenerate. We label the exciton states such that for the unexcited dot,

$$\mathcal{E}_1 < \mathcal{E}_2 = \mathcal{E}_3 < \mathcal{E}_4 = \mathcal{E}_5 < \mathcal{E}_6 < \mathcal{E}_7 = \mathcal{E}_8 < \mathcal{E}_9. \tag{3.50}$$

i	s,s	p_+,p_+	p_-,p_-	s,p_+	s,p_-	p_+,s	p_-,s	p_+,p_-	p_-,p_+
1	●	○	○						
2				○	○	●	●		
3				○	○	●	●		
4				●	●	○	○		
5				●	●	○	○		
6	○	●	●						
7								●	
8									●
9		●	●						

Table 1: Components $\phi^{i,\mathrm{R/L}}_{\beta,\beta'}$ of the excitonic eigen functions $|\phi^{i,\mathrm{R/L}}\rangle$. Circles indicate the non-vanishing components where the dominant ones are marked by filled circles.

The explicit analysis shows that all six eigenenergies are continuous functions of the carrier densities. When $f^{\mathrm{e}}_{p_\pm} = f^{\mathrm{h}}_{p_\pm} > \frac{1}{2}$, the order becomes

$$\mathcal{E}_1 < \mathcal{E}_2 = \mathcal{E}_3 < \mathcal{E}_4 = \mathcal{E}_5 < \mathcal{E}_9 < \mathcal{E}_7 = \mathcal{E}_8 < \mathcal{E}_6. \tag{3.51}$$

Here and in the following, we label the individual dot states in each band by $s \equiv (n = 0, m = 0)$ and $p_\pm \equiv (n = 1, m = \pm 1)$. As discussed at the end of Sec. 3.1.2, only proper densities $f^{\mathrm{e/h}}_\beta = f_{\mathrm{e/h}}{}^\beta_\beta$ have to be considered for the s-p dot.

Table 1 gives an overview over the components of the excitonic eigenfunctions. For the degenerate exciton states $i = 2, 3, 4, 5, 7, 8$, the "diagonal" components $\phi^{i,\mathrm{R/L}}_{\beta,\beta}$ are zero. Consequently, the factor $\langle 1|\phi^{i,\mathrm{R}}\rangle = \sum_\beta \phi^{i,\mathrm{R}}_{\beta,\beta}$ that appears in the nominators of both the absorption formula (3.47) and the luminescence formula (3.72) vanishes for those i such that the corresponding eigen energies do not show up in the optical spectra. The degenerate states thus represent *dark excitons*. On the other hand, the "off-diagonal" components $\phi^{i,\mathrm{R/L}}_{\beta,\beta'}$ with $\beta \neq \beta'$ vanish for the non-degenerate exciton states $i = 1, 6, 9$ where

$$\phi^{i,\mathrm{R/L}}_{\beta,\beta'} \equiv \delta_{\beta,\beta'} \phi^{i,\mathrm{R/L}}_\beta. \tag{3.52}$$

The first and the sixth exciton are the *bright excitons* that define the optical resonances of the quantum dot. *In the following, we will refer to the first and the second bright exciton as A and B exciton, respectively.* Finally, the ninth exciton is dark since $\phi^{9,\mathrm{R/L}}_{p_+} = -\phi^{9,\mathrm{R/L}}_{p_-}$.

The excitonic eigen functions $|\phi^{i,\mathrm{R/L}}\rangle$ do not depend on the carrier densities for $i = 7, 8, 9$. For the remaining quantum numbers, the dominant components are plotted in Fig. 8 as function of s- and p-shell densities. The analysis is restricted to symmetrical excitations where $f^{\mathrm{e}}_s = f^{\mathrm{h}}_s \equiv f_s$ and $f^{\mathrm{e}}_{p_\pm} = f^{\mathrm{h}}_{p_\pm} \equiv f_{p_\pm}$. We define the quantities

$$\varrho^i_{\beta,\beta'} \equiv \left(\phi^{i,\mathrm{L}}_{\beta,\beta'}\right)^* \phi^{i,\mathrm{R}}_{\beta,\beta'} \tag{3.53}$$

that can be interpreted as probability distributions when the dot is unexcited. In the non-Hermitian case for finite densities, $\varrho^i_{\beta,\beta'}$ is not necessarily restricted to the interval $[0, 1]$ anymore. However, we always find $\sum_{\beta,\beta'} \varrho^i_{\beta,\beta'} = 1$ due to the generalized orthogonality relation (3.39). In view of the symmetries

$$\varrho^1_{s,s} = \varrho^6_{p_+,p_+} + \varrho^6_{p_-,p_-} \equiv \varrho_{\mathrm{bright}}, \tag{3.54}$$

$$\varrho^{2/3}_{p_+,s} + \varrho^{2/3}_{p_-,s} = \varrho^{4/5}_{s,p_+} + \varrho^{4/5}_{s,p_-} \equiv \varrho_{\mathrm{dark}}, \tag{3.55}$$
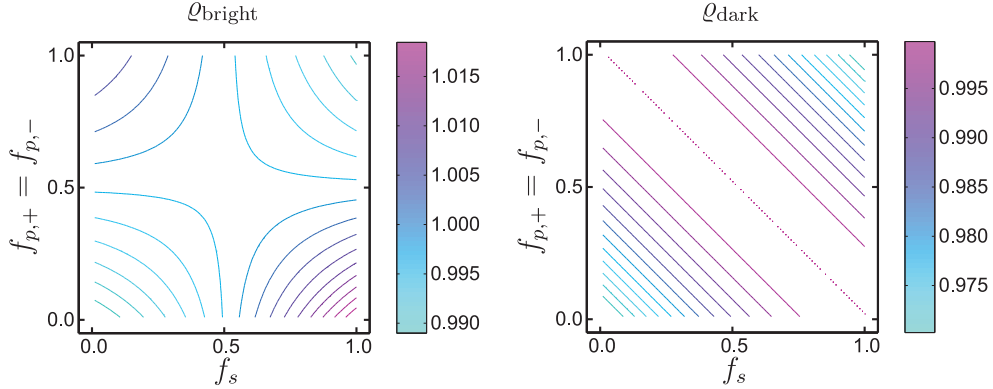
Figure 8: Density dependence of the excitonic eigen functions. See the text for the definitions of $\varrho_{\mathrm{bright}}$ and ϱ_{dark}.

it is sufficient to scan the functional dependence of $\varrho_{\mathrm{bright}}$ for the bright and ϱ_{dark} for the dark excitons. We see from Fig. 8 that both quantities remain close to unity and barely change with the carrier densities. The lines of constant ϱ_{dark} are defined by $f_s + f_{p_\pm} = \mathrm{const}$, which implies that ϱ_{dark} only depends on the sum of the s-shell density and half the p-shell density. The fact that $\varrho_{\mathrm{bright}}$ is not exactly 1 proves that both the A and the B exciton mix s- and p-shell carriers to a certain degree. However, the mixing is so weak that the A and B exciton mainly involve electron-hole pairs in the s and in the p shell, respectively.

Figure 9 shows the functional dependence of the the excitonic eigen energies on the carrier densities. We find that the eigen energies corresponding to dark excitons can roughly be written as function of $f_s + f_{p_\pm}$ such that they redshift whenever the s- or p-shell density increases. On the contrary, the position of the first (second) optical resonance shifts only moderately for s-shell (p-shell) pumping while it redshifts for p-shell (s-shell) pumping. This observation indicates that no higher-order correlations are needed to obtain a spectrally stable peak position when the dot is excited resonantly with one of the bright excitons. Apparently, this result does not hold for the off-resonant case where the exciton energies may well be influenced by higher-order clusters where also wetting-layer states have to be considered. We will therefore concentrate in Secs. 3.3 and 3.4 on situations where either the A or the B exciton is predominantly excited. The singlet-doublet analysis can then be expected to provide sufficient accuracy.

As a general result, pronounced excitonic effects turn out to be present even for high densities where the Pauli blocking becomes considerably strong. This feature clearly distinguishes the quantum dot from the quantum-well case [8]. We will therefore investigate in Sec. 3.3 how electron-hole pairs become correlated or uncorrelated when the density is increased. While quantum-well excitons eventually become ionized [108], quantum-dot excitons may still show large correlations even for elevated densities.

3.3 Incoherent regime

In typical experimental situations, the electron-electron and the electron-phonon scattering lead to dephasing of the polarization such that the quantum dot reaches the so-called *incoherent regime* on a picosecond time scale after excitation. In this regime, all singlets, except densities,
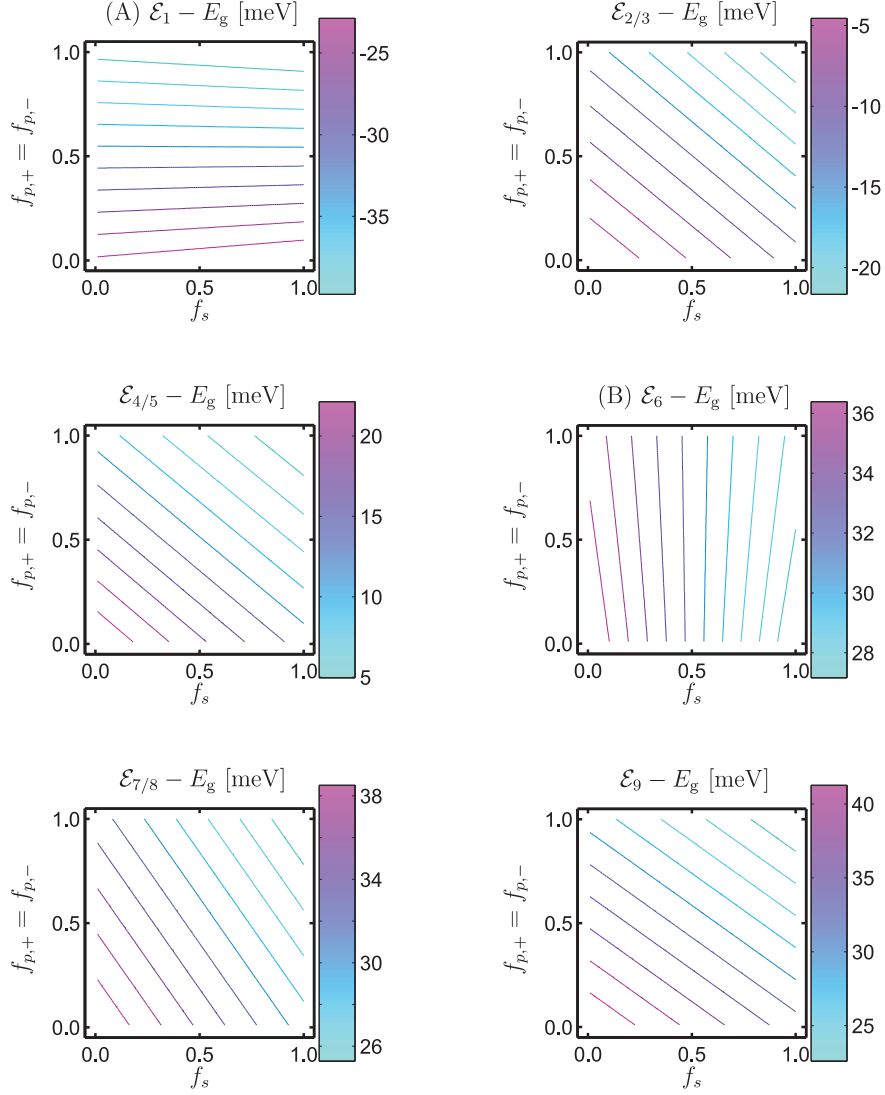
Figure 9: Density dependence of the excitonic eigen energies $\mathcal{E}_i$ that are given relative to the band gap E_{g}. The bright excitons are marked by "A" and "B".

remain zero during the evolution of the system. Furthermore, the quantum corrections and the Coulomb correlations in the equations of motion (3.23), (3.24) for the densities become dominant once the coherent quantities disappear. Hence, it is crucial to consider the full set of equations of motion at the singlet-doublet level.

Under incoherent conditions, the equations of motion for the densities reduce to

$$
i\hbar \frac{\mathrm{d}}{\mathrm{d}t} f_\mathrm{e}{}^{\beta}_{\beta'} = \sum_{\beta_1} \left(E^\mathrm{e}_{\beta',\beta_1} f_\mathrm{e}{}^{\beta}_{\beta_1} - E^\mathrm{e}_{\beta_1,\beta} f_\mathrm{e}{}^{\beta_1}_{\beta'} \right)
$$
$$
- \sum_{\beta_1,\beta_2,\beta_3} \left[V^{\beta'\beta_1}_{\beta_2\beta_3} \sum_\lambda C\left({}^{\mathrm{c}\,\lambda}_{\lambda\mathrm{c}} \Big|{}^{\beta\ \beta_1}_{\beta_2\beta_3}\right) - V^{\beta\ \beta_1}_{\beta_2\beta_3} \sum_\lambda C\left({}^{\mathrm{c}\,\lambda}_{\lambda\mathrm{c}} \Big|{}^{\beta_3\beta_2}_{\beta_1\beta'}\right) \right]
$$
$$
+ i\Delta \langle \hat{B}^\dagger_\Sigma \hat{a}^\dagger_{\mathrm{v},\beta} \hat{a}_{\mathrm{c},\beta'} \rangle + i\Delta \langle \hat{B}^\dagger_\Sigma \hat{a}^\dagger_{\mathrm{v},\beta'} \hat{a}_{\mathrm{c},\beta} \rangle^*, \tag{3.56}
$$
$$
i\hbar \frac{\mathrm{d}}{\mathrm{d}t} f_\mathrm{h}{}^{\beta}_{\beta'} = - \sum_{\beta_1} \left(E^\mathrm{h}_{\beta',\beta_1} f_\mathrm{h}{}^{\beta}_{\beta_1} - E^\mathrm{h}_{\beta_1,\beta} f_\mathrm{h}{}^{\beta_1}_{\beta'} \right)
$$
$$
+ \sum_{\beta_1,\beta_2,\beta_3} \left[V^{\beta'\beta_1}_{\beta_2\beta_3} \sum_\lambda C\left({}^{\lambda\mathrm{v}}_{\mathrm{v}\lambda} \Big|{}^{\beta_1\beta}_{\beta_3\beta_2}\right) - V^{\beta\ \beta_1}_{\beta_2\beta_3} \sum_\lambda C\left({}^{\lambda\mathrm{v}}_{\mathrm{v}\lambda} \Big|{}^{\beta_2\beta_3}_{\beta'\beta_1}\right) \right]
$$
$$
+ i\Delta \langle \hat{B}^\dagger_\Sigma \hat{a}^\dagger_{\mathrm{v},\beta} \hat{a}_{\mathrm{c},\beta'} \rangle + i\Delta \langle \hat{B}^\dagger_\Sigma \hat{a}^\dagger_{\mathrm{v},\beta'} \hat{a}_{\mathrm{c},\beta} \rangle^*. \tag{3.57}
$$

For the *excitonic correlations*

$$
C_\mathrm{X}{}^{\beta\ \beta'}_{\beta''\beta'''} \equiv C\left({}^{\mathrm{cv}}_{\mathrm{vc}} \Big|{}^{\beta\ \beta'}_{\beta''\beta'''}\right), \tag{3.58}
$$

we obtain

$$
i\hbar \frac{\mathrm{d}}{\mathrm{d}t} C_\mathrm{X}{}^{\beta\ \beta'}_{\beta''\beta'''} = - \sum_{\beta_1,\beta_2} A_{(\beta,\beta''),(\beta_1,\beta_2)} C_\mathrm{X}{}^{\beta_1\beta'}_{\beta_2\beta'''} + \sum_{\beta_1,\beta_2} A_{(\beta',\beta'''),(\beta_1,\beta_2)} C_\mathrm{X}{}^{\beta\ \beta_1}_{\beta''\beta_2}
$$
$$
+ \sum_{\beta_1,\beta_2,\beta_3,\beta_4} V^{\beta_2\beta_3}_{\beta_1\beta_4} \Big[(\delta_{\beta,\beta_1} - f_\mathrm{e}{}^{\beta}_{\beta_1})(\delta_{\beta_2,\beta''} - f_\mathrm{h}{}^{\beta_2}_{\beta''}) f_\mathrm{e}{}^{\beta_3}_{\beta'''} f_\mathrm{h}{}^{\beta'}_{\beta_4}
$$
$$
- (\delta_{\beta_3,\beta'''} - f_\mathrm{e}{}^{\beta_3}_{\beta'''})(\delta_{\beta',\beta_4} - f_\mathrm{h}{}^{\beta'}_{\beta_4}) f_\mathrm{e}{}^{\beta}_{\beta_1} f_\mathrm{h}{}^{\beta_2}_{\beta''} \Big]
$$
$$
+ D_\mathrm{X}^{\mathrm{exc}\,\beta\ \beta'}_{\ \ \ \beta''\beta'''} + T_\mathrm{X}{}^{\beta\ \beta'}_{\beta''\beta'''}
$$
$$
- i(\delta_{\beta\beta''} - f_\mathrm{h}{}^{\beta}_{\beta''} - f_\mathrm{e}{}^{\beta}_{\beta''}) \Delta \langle \hat{B}^\dagger_\Sigma \hat{a}^\dagger_{\mathrm{v},\beta'} \hat{a}_{\mathrm{c},\beta'''} \rangle
$$
$$
- i(\delta_{\beta'\beta'''} - f_\mathrm{h}{}^{\beta'}_{\beta'''} - f_\mathrm{e}{}^{\beta'}_{\beta'''}) \Delta \langle \hat{B}^\dagger_\Sigma \hat{a}^\dagger_{\mathrm{v},\beta''} \hat{a}_{\mathrm{c},\beta} \rangle^*. \tag{3.59}
$$

Although quite complicated, this equation can be interpreted straightforwardly. The first line on the right-hand side would be diagonal in the exciton basis, which characterizes C_X as an "excitonic" correlation. The Coulomb sum beginning in the second line constitutes the singlet source term that has the form of a generalized Boltzmann equation. The last two lines are responsible for the radiative decay of the excitonic correlations. Finally, $D_\mathrm{X}^{\mathrm{exc}\,\beta\ \beta'}_{\ \ \ \beta''\beta'''}$ denotes all terms originating from the fermionic exchange which are explicitly given in Appendix C.2 where also the correlated triplets $T_\mathrm{X}{}^{\beta\ \beta'}_{\beta''\beta'''}$ can be found. The latter are omitted within the pure singlet-doublet analysis performed in this section. The equations of motion for the *electron-electron* and *hole-hole correlations*

$$
C_\mathrm{ee}{}^{\beta\ \beta'}_{\beta''\beta'''} \equiv C\left({}^{\mathrm{cc}}_{\mathrm{cc}} \Big|{}^{\beta\ \beta'}_{\beta''\beta'''}\right), \tag{3.60}
$$
$$
C_\mathrm{hh}{}^{\beta\ \beta'}_{\beta''\beta'''} \equiv C\left({}^{\mathrm{vv}}_{\mathrm{vv}} \Big|{}^{\beta\ \beta'}_{\beta''\beta'''}\right) \tag{3.61}
$$

have similar structures. For the explicit forms, see Appendix C.2.

In Sec. 3.3.1, we investigate the stable configurations of the dot system in the incoherent regime which are defined by the stationary solutions of the above set of equations. Inclusion of quantum-optical correlations leads to the semiconductor luminescence equations presented in Sec. 3.3.2. With the help of these equations, we calculate the quantum emission from stable dot states in Sec. 3.3.3.

3.3.1 Stable quantum-dot states

A quantum dot can be excited in several different ways. One possibility involves pumping by means of an optically resonant coherent light field. Other methods include non-resonant optical excitation as well as optical or electronic pumping of the wetting-layer where the last two cases imply carrier-capture dynamics between wetting-layer and quantum-dot states [36]. For all indirect excitations, one can anticipate a significant Coulomb- and phonon-induced relaxation. To define the form of the excitation, one must, in principle, describe the dynamics of all relevant quantities microscopically. We will outline in Sec. 3.4 how this can be performed for coherent optical excitation in the presence of electron-phonon coupling. Here, we simplify the discussion by using a phenomenological description of the excitation process. For this purpose, we assume a generic form for the pumping of singlets and doublets, demanding that a steady-state configuration is reached after excitation. As additional constraint, the fermionic levels may only be excited to values between 0 and 1. These conditions define the generic phase space of possible excitations.

Explicitly, we model the pumping by adding a term

$$i\hbar \frac{\mathrm{d}}{\mathrm{d}t}\bigg|_{\mathrm{pump}} Y = Y_0 \dot{\mathcal{S}}_Y(t) , \quad (3.62)$$

with Y_0 as the pumping amplitude, to the dynamics of the quantity Y that can either be a density or a genuine two-particle correlation. Pumping the exciton and plasma densities separately will later allow us us to study the influence of the different population contributions on the emission characteristics. The switch-on function $\mathcal{S}_Y(t)$ vanishes in the beginning and approaches unity for large t while its derivative approaches zero. For all examples throughout this section, we have chosen a common func-

Figure 10: Pumping of the s-shell density for different switch-on times τ.

tion $\mathcal{S}_Y(t) \equiv 1/(1 + \mathrm{e}^{-t/\tau})$ for all Y. So long as the the switch-on time τ is not too short, the final value of Y does not depend on τ. In order to estimate the shortest admissible τ, we consider the simplest case, where only the s-shell densities $f_s^{\mathrm{e/h}} = f_{\mathrm{e/h}\,(0,0)}^{(0,0)}$ are pumped with amplitude $Y_0 = 1$. The results for three different switch-on times are shown in Fig. 10. Pumping with τ larger than 30 fs leads to a well-defined final density while $\tau = 10$ fs constitutes a too fast switch-on such that no stable configuration is reached. As a consequence, all expectation values exhibit periodic oscillations which is most pronounced for an immediate switch on, i.e., $\tau \to 0$.

Moreover, we observe that for a reasonably slow switch-on, the density terminates a little below the value of the pumping amplitude, which expresses the fact that during the excitation, a certain amount of density is transferred to the p-shell. This effect can be traced back to the Coulomb correlations between the shells and is related to the non-vanishing $\phi_{p,p}^{1,\mathrm{R}}$ component of the first excitonic wave function (see Fig. 8). Since the comparatively slow radiative decay analyzed below is the only process in our model that changes the number of carriers per band, the density transfer from s- to p-shell does not change the total density. Because we will exclusively consider situations where electrons and holes are pumped symmetrically, the total number of electron-hole pairs N_{eh} will be a well-defined quantity in the following.

Next, we analyze how the reached steady state depends on the pumping amplitude. Here, we exclusively treat excitation of the s-shell density. To be assured that the switch-on process is sufficiently slow in all cases, we choose a large switch-on time $\tau = 270\,\mathrm{fs}$. As a well-defined way to quantify what kind of excitation is present in the quantum dot, we consider the energy per particle. The total energy of the carrier system

$$\langle \hat{H}_{\mathrm{el}}^{\mathrm{tot}} \rangle \equiv \langle \hat{H}_{\mathrm{el}} \rangle + \langle \hat{H}_{\mathrm{el-el}} \rangle \tag{3.63}$$

decomposes into the singlet contribution

$$\langle \hat{H}_{\mathrm{el}}^{\mathrm{tot}} \rangle_{\mathrm{S}} = \sum_{\beta} \left(E_{\beta}^{\mathrm{e}} f_{\mathrm{e}}{}_{\beta}^{\beta} - E_{\beta}^{\mathrm{h}} f_{\mathrm{h}}{}_{\beta}^{\beta} \right)$$
$$+ \frac{1}{2} \sum_{\beta_1,\ldots,\beta_4} V_{\beta_3\beta_4}^{\beta_1\beta_2} \left(f_{\mathrm{h}}{}_{\beta_4}^{\beta_1} f_{\mathrm{h}}{}_{\beta_3}^{\beta_2} - f_{\mathrm{h}}{}_{\beta_3}^{\beta_1} f_{\mathrm{h}}{}_{\beta_4}^{\beta_2} + f_{\mathrm{e}}{}_{\beta_4}^{\beta_1} f_{\mathrm{e}}{}_{\beta_3}^{\beta_2} - f_{\mathrm{e}}{}_{\beta_3}^{\beta_1} f_{\mathrm{e}}{}_{\beta_4}^{\beta_2} - 2 f_{\mathrm{e}}{}_{\beta_4}^{\beta_1} f_{\mathrm{h}}{}_{\beta_3}^{\beta_2} \right) \tag{3.64}$$

where for the Coulomb part, we have taken into account the renormalizations discussed in Sec. 3.2.1 directly after Eqs. (3.25a)–(3.25b), and the contribution of the two-particle correlations

$$\Delta \langle \hat{H}_{\mathrm{el}}^{\mathrm{tot}} \rangle = \frac{1}{2} \sum_{\beta_1,\ldots,\beta_4} V_{\beta_3\beta_4}^{\beta_1\beta_2} \left(C_{\mathrm{hh}}{}_{\beta_4\beta_3}^{\beta_1\beta_2} + C_{\mathrm{ee}}{}_{\beta_4\beta_3}^{\beta_1\beta_2} - 2 C_{\mathrm{X}}{}_{\beta_3\beta_4}^{\beta_1\beta_2} \right). \tag{3.65}$$

In frame (a) of Fig. 11, both the total energy (thick solid line) and its singlet contribution (thin solid line), each normalized with respect to the number N_{eh} of excited electron-hole pairs, are plotted as function of N_{eh}. For low densities, the energy per particle is close to the gap which means that the system is in an electron-hole plasma state where electrons and holes are independent and uncorrelated entities such that the density matrix ρ of the carrier system approximately has the product form $\rho = \rho_{\mathrm{e}} \otimes \rho_{\mathrm{h}}$. For elevated densities, however, the total energy per particle approaches the lowest resonance, i.e., the excitonic eigen energy $\mathcal{E}_1$ (dashed line). Moreover, the absolute value of the doublet contribution to the energy per particle becomes larger, indicating that the stable electron-hole states become truly correlated.

In the next step, we additionally allow for pumping of the A-exciton population $\Delta N_1 \equiv \Delta \langle \hat{X}_1^\dagger \hat{X}_1 \rangle$. It turns out that stable excitation states are thus reached for an almost arbitrary pumping amplitude where as a general tendency, the energy per particle decreases with increasing strength of the population pumping. Physically, however, the phenomenological excitation of the lowest exciton population has to be limited such that the total energy per particle does not go below the excitonic eigen energy $\mathcal{E}_1$ of the unexcited dot because this is the minimal energy that a single-pair state of the system can assume, see Appendix A. Hence, the shaded area in Fig. 11 (a) designates the physically allowed stable states. From below, it is limited by the excitonic eigen energy that defines the *population-saturation line* of the system, and the upper limit is given by the *plasma line* that yields the total energy per particle in the
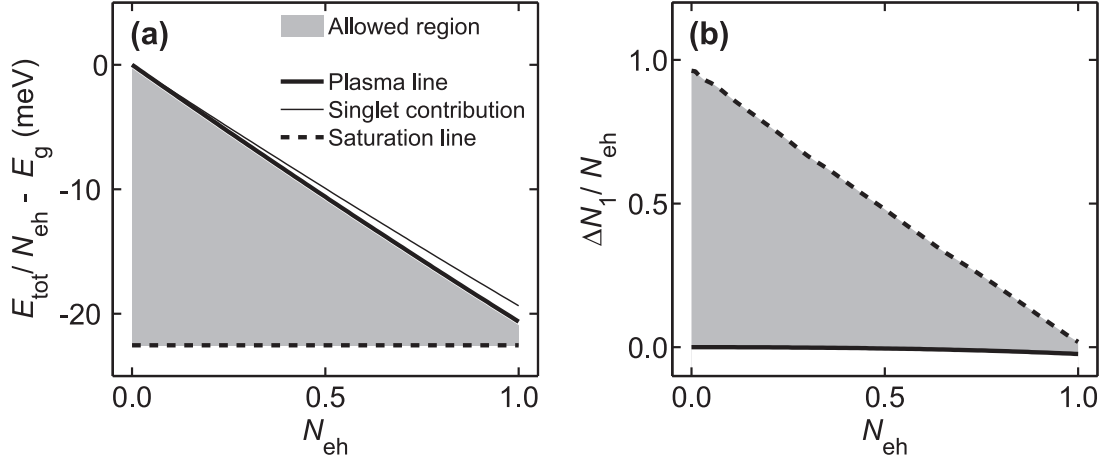
Figure 11: (a) Total energy $E_{\text{tot}} = \langle \hat{H}_{\text{el}}^{\text{tot}} \rangle$ per electron-hole pair reached by pumping of the s-shell density as function of the number of pairs N_{eh} (thick solid line). The thin solid line gives the singlet contribution to the total energy, while the saturation line is defined by the first excitonic resonance. **(b)** First-exciton population ΔN_1 per electron-hole pair reached for density pumping alone (solid line) and maximum allowed exciton-population pumping (dashed line).

absence of population pumping. Frame (b) of Fig. 11 shows the amount of generated excitonic population per particle for both the saturation regime (dashed line) and the plasma regime (solid line). The shaded area in between indicates the physically allowed phase space for the exciton pumping. We notice that the population per particle assumes values between 0 to 1 and is largest for dilute densities. We conclude that, depending on the excitation conditions, a quantum dot in the low-density regime can have a stable many-body configuration ranging from pure plasma ($\Delta N / N_{\text{eh}} \simeq 0$) up to fully correlated electron-hole pairs ($\Delta N / N_{\text{eh}} \simeq 1$).

3.3.2 Semiconductor luminescence equations

Under quasi-stationary conditions, the photoluminescence spectrum follows from the photon flux [61]

$$I_{\text{PL}}(\omega_{\mathbf{q}}) \equiv \frac{\mathrm{d}}{\mathrm{d}t} \langle \hat{B}_{\mathbf{q}}^{\dagger} \hat{B}_{\mathbf{q}} \rangle . \tag{3.66}$$

The equations of motion for the photon-number-like expectation values in the incoherent regime are given by

$$\left[\mathrm{i}\hbar \frac{\mathrm{d}}{\mathrm{d}t} + \hbar(\omega_{\mathbf{q}} - \omega_{\mathbf{q}'}) \right] \Delta \langle \hat{B}_{\mathbf{q}}^{\dagger} \hat{B}_{\mathbf{q}'} \rangle = \mathrm{i} \sum_{\beta} \left\{ \mathcal{F}_{\mathbf{q}'}^{*} \Pi_{\beta}^{\beta}(\mathbf{q}) + \mathcal{F}_{\mathbf{q}} \left[\Pi_{\beta}^{\beta}(\mathbf{q}') \right]^{*} \right\} \tag{3.67}$$

where we have defined the *photon-assisted polarization*

$$\Pi_{\beta'}^{\beta}(\mathbf{q}) \equiv \Delta \langle \hat{B}_{\mathbf{q}}^{\dagger} \hat{a}_{\text{v},\beta}^{\dagger} \hat{a}_{\text{c},\beta'} \rangle \tag{3.68}$$

that contains the correlated part of the process where a photon is emitted via the recombination of an electron-hole pair. The corresponding dynamics follows from

$$\left(\mathrm{i}\hbar\frac{\mathrm{d}}{\mathrm{d}t}+\hbar\omega_{\mathbf{q}}\right)\Pi_{\beta'}^{\beta}(\mathbf{q})=\sum_{\beta_1,\beta_2}A_{(\beta,\beta'),(\beta_1,\beta_2)}\Pi_{\beta_2}^{\beta_1}(\mathbf{q})+T_{\beta'}^{\beta}(\mathbf{q})$$
$$+\mathrm{i}S_{\beta'}^{\beta}(\mathbf{q})-\mathrm{i}\left(\delta_{\beta\beta'}-f_{\mathrm{h}}{}_{\beta'}^{\beta}-f_{\mathrm{e}}{}_{\beta'}^{\beta}\right)\Delta\langle\hat{B}_{\mathbf{q}}^{\dagger}\hat{B}_{\Sigma}\rangle, \tag{3.69}$$

with the matrix $\boldsymbol{A}$ as defined in Eq. (3.33). In the following, we will approximate the full three-particle scattering term $T_{\beta'}^{\beta}(\mathbf{q})$ by a phenomenological dephasing term $-\mathrm{i}\gamma\Pi_{\beta'}^{\beta}(\mathbf{q})$. The last line of Eq. (3.69) contains the source terms, of which the second one gives the contribution by the stimulated emission which would only be important if the system were positioned inside a cavity. Hence, we will completely neglect this effect, thus decoupling Eq. (3.69) from Eq. (3.67). The source term

$$S_{\beta'}^{\beta}(\mathbf{q})\equiv\mathcal{F}_{\mathbf{q}}\sum_{\beta_1}\left(f_{\mathrm{h}}{}_{\beta_1}^{\beta}f_{\mathrm{e}}{}_{\beta'}^{\beta_1}+C_{\mathrm{X}}{}_{\beta_1\beta'}^{\beta_1\beta}\right) \tag{3.70}$$

is due to spontaneous emission from either the plasma or correlated electron-hole pairs. Equations (3.67) and (3.69) constitute the *semiconductor luminescence equations* (SLE) for the quantum dot.

3.3.3 Steady-state luminescence

Now that we have the SLE at our disposal, we can calculate the luminescence spectra for some exemplary stable states out of the allowed phase space determined in Sec. 3.3.1. The justification to concentrate on stable states of the material system is provided by the fact that radiative decay of excitation typically takes place on a comparatively large time scale—radiative lifetimes of less than 1 ns are usually only reached when the spontaneous emission of the dot is drastically enhanced with help of a microcavity [109] or a photonic-crystal environment [110]. We may thus assume that the quantum-dot carrier system remains stationary sufficiently long such that steady-state luminescence can be determined. Under these conditions, the carrier system acts as a constant source for the photoemission, and the recombination correlations, the densities, and the excitonic correlations are quasi-stationary quantities. In this case, Eq. (3.69) leads to

$$(\hbar\omega_{\mathbf{q}}+\mathrm{i}\gamma)\,\Pi_{\beta'}^{\beta}(\mathbf{q})=\sum_{\beta_1,\beta_2}A_{(\beta,\beta'),(\beta_1,\beta_2)}\Pi_{\beta_2}^{\beta_1}(\mathbf{q})+\mathrm{i}S_{\beta'}^{\beta}(\mathbf{q}). \tag{3.71}$$

This equation has the same structure as the Bloch equation (3.43) for the microscopic polarization $p_{\beta'}^{\beta}$ in the frequency domain. Hence, we can again diagonalize the problem by means of the exciton basis from Sec. 3.2.2. This procedure finally leads to

$$I_{\mathrm{PL}}(\omega_{\mathbf{q}})=\frac{2\left|\mathcal{F}_{\mathbf{q}}\right|^2}{\hbar}\,\mathrm{Im}\sum_{i,j}\frac{\langle\phi^{i,\mathrm{R}}|1\rangle\langle\hat{X}_i^{\dagger}\hat{X}_j\rangle\langle1|\phi^{j,\mathrm{R}}\rangle}{\mathcal{E}_j-\hbar\omega_{\mathbf{q}}-\mathrm{i}\gamma} \tag{3.72}$$

with the scalar products $\langle\phi^{i,\mathrm{R}}|1\rangle$ as given explicitly in Eq. (3.48). The doublet part $\Delta\langle\hat{X}_i^{\dagger}\hat{X}_j\rangle$ of the expectation value $\langle\hat{X}_i^{\dagger}\hat{X}_j\rangle$ describes excitonic correlations while the singlet part $\langle\hat{X}_i^{\dagger}\hat{X}_j\rangle_{\mathrm{S}}$
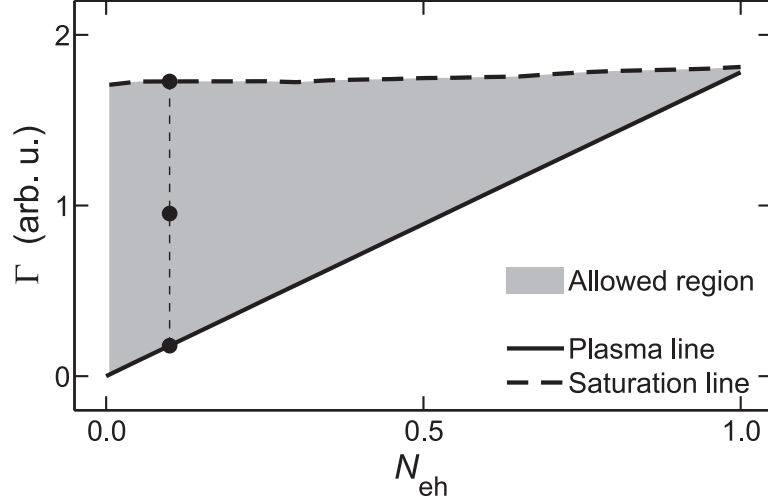
Figure 12: Recombination rate Γ as function of the number of electron-hole pairs N_{eh} for plasma (solid line) and population-saturation (dashed line) regime. The bold dots mark the three cases shown in frame (a) of Fig. 13.

is also present for an uncorrelated electron-hole plasma. We thus find that, similarly to higher-dimensional semiconductor structures, both sources provide contributions to the spectrum that cannot be distinguished by a standard photoluminescence experiment [111].

From Eq. (3.67) and Eqs. (3.56), (3.57), it follows that the total number of recombined electron-hole pairs per unit time,

$$-\frac{\mathrm{d}N_{\mathrm{eh}}}{\mathrm{d}t} = -\left.\frac{\mathrm{d}}{\mathrm{d}t}\right|_{\hat{H}_{\mathrm{el-em}}} \sum_{\beta} f_{\mathrm{e/h}}{}_{\beta}^{\beta}, \tag{3.73}$$

equals the total number of emitted photons per unit time,

$$\frac{\mathrm{d}}{\mathrm{d}t} \sum_{\mathbf{q}} \Delta\langle \hat{B}_{\mathbf{q}}^{\dagger}\hat{B}_{\mathbf{q}}\rangle = 2\mathrm{i}\frac{\mathrm{d}}{\mathrm{d}t} \mathrm{Re} \sum_{\beta} \Delta\langle \hat{B}_{\Sigma}^{\dagger} p_{\beta}^{\beta}\rangle. \tag{3.74}$$

In frame (b) of Fig. 12, the recombination rate

$$\Gamma \equiv -\frac{1}{N_{\mathrm{eh}}}\frac{\mathrm{d}N_{\mathrm{eh}}}{\mathrm{d}t} \tag{3.75}$$

is plotted for both the plasma (solid line) and the population-saturation (dashed line) regime. While Γ has a high constant value along the saturation line, it decreases linearly along the plasma line as the density is decreased. This behavior can be understood in view of the density dependencies of the different source terms contributing to the steady-state luminescence. Plasma versus exciton luminescence can thus be distinguished via their respective decay dynamics. In general, the system can decay along any curve through the shaded area in Fig. 12. The dynamics then allows one to draw conclusions about the nature of the decaying quasi-stationary states. Microscopically, this is determined by a number of effects such as relaxation, carrier capture, phonon coupling, etc. Only for constant Γ, Eq. (3.75) describes an exponential decay. Our analysis indicates that the radiative decay in a quantum dot does not necessarily show an exponential behavior.
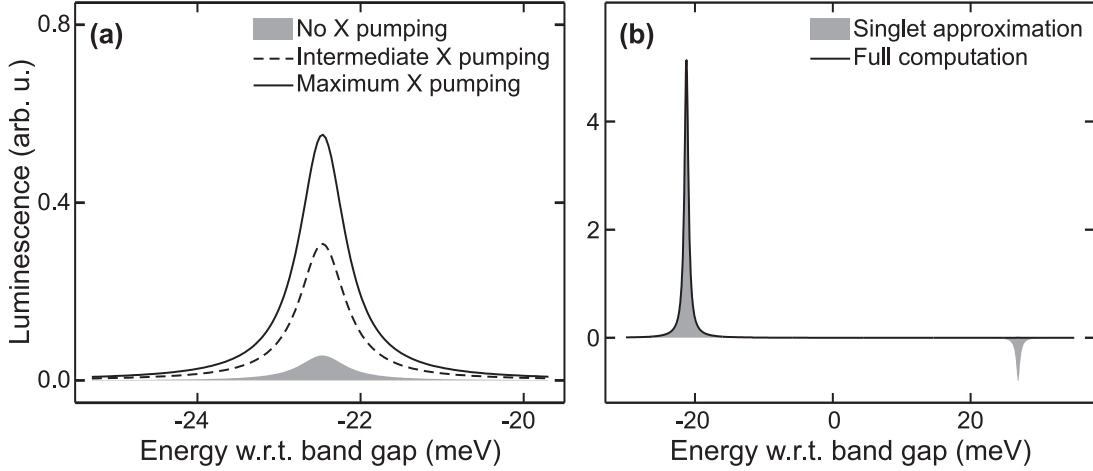
Figure 13: **(a)** First luminescence peak in case of weak density pumping ($N_{eh} = 0.1$) for maximum ΔN_1 pumping (solid line), half-as-strong ΔN_1 pumping (dashed line), and no ΔN_1 pumping at all (shaded area). **(b)** Luminescence spectrum for a high density of $N_{eh} = 0.95$. For the singlet approximation, only the $f_e f_h$ source term has been considered.

Representative emission spectra are shown in Fig. 13. Frame (a) displays the luminescence at the first excitonic resonance when the s-shell density is weakly pumped with the amplitude 0.1. The dashed and solid curves are obtained by additional pumping of the A exciton. We find that the magnitude of the luminescence increases strongly for higher exciton densities. However, its spectral shape and position are not affected by the population, i.e., luminescence is observed at the excitonic resonance regardless of whether the system is in the plasma or in the population-saturation regime. This behavior can directly be deduced from the explicit form of the steady-state luminescence formula (3.72) which shows that the emission frequencies are independent of the population source. For the luminescence spectrum in frame (b), we have pumped the s-shell density with a high amplitude of 0.95 without any exciton-population pumping. The solid line gives the result of the full computation. We find that even with a high excitation, light is still emitted at the excitonic resonance. While the spectral position of the peak remains almost unchanged compared with the low-density spectra in frame (a), the height of the peak is enlarged by more than one order of magnitude. The shaded area is calculated from the steady-state formula (3.72) within a singlet approximation where only the $f_e f_h$ source term from Eq. (3.70) is considered in the luminescence equation (3.69). Formally, this corresponds to describing the carrier system by single-particle densities alone, assuming that this would constitute a stable state of the system. This case has already been studied in Fig. 10 with the immediate switch-on. From that analysis, we see that such a state can actually not be stationary, since the densities are strongly oscillating. Nevertheless, it turns out that the singlet source term alone produces the luminescence at the first resonance rather accurately. On the other hand, an artifact of negative emission is observed at the second excitonic resonance which is a consequence of the instability of the corresponding singlet state. This clearly demonstrates that doublets are necessary to provide a stable state of the system with a physically meaningful steady-state luminescence spectrum. For the given pumping conditions, the singlet approximation underestimates the recombination rate Γ from the full computation by a factor of about 0.74.

A close inspection of the second optical resonance shows that for every s-shell-pumping

amplitude from 0 to 1, one can find a pumping strength of the A exciton such that the luminescence at the B-exciton resonance turns negative. Although for all physically allowed ΔN_1-pumping amplitudes the absolute height of the negative peak remains several orders of magnitude smaller than for the artifact from the singlet approximation discussed above, this would definitely be an unphysical feature of a steady-state luminescence spectrum. To understand the origin of this, we remember the comment to Fig. 10 that pumping of the s-shell density always affects the p-shell densities, too. This was traced back to the Coulomb correlations between the shells. In a similar manner, pumping of the A exciton is always accompanied by a change of the population of the B-exciton state. The fact that this influence can lead to negative luminescence is a clear evidence that in certain cases, population of the A exciton without population of the B exciton constitutes an unphysical situation. However, it turns out that this can easily be cured by exciting the second bright excitonic state very weakly. Within the phase space determined in Fig. 11, the ΔN_6-pumping amplitude that is required for the luminescence at the second resonance to become positive is always smaller than 10^{-3}. This additional constraint upon the physically accessible phase space has practically no effect on the emission of light at the first excitonic resonance and on the recombination rate. The fully microscopic study in the following section will reveal which processes give rise to such a B-exciton pumping when the system is excited optically at the first optical resonance. In order to prepare for that discussion, we now identify the source terms that can formally lead to negative luminescence.

The steady-state luminescence formula

$$I_{\mathrm{PL}}(\omega_{\mathbf{q}}) = \frac{2|\mathcal{F}_{\mathbf{q}}|^2}{\hbar} \mathrm{Im} \sum_j \frac{\Theta_{\mathrm{dia}}(j) + \Theta_{\mathrm{off}}(j)}{\mathcal{E}_j - \hbar\omega_{\mathbf{q}} - \mathrm{i}\gamma} \tag{3.76}$$

contains contributions

$$\Theta_{\mathrm{dia}}(j) \equiv \left|\langle\phi^{j,\mathrm{R}}|1\rangle\right|^2 \langle \hat{X}_j^\dagger \hat{X}_j \rangle, \tag{3.77a}$$

$$\Theta_{\mathrm{off}}(j) \equiv \sum_{i \neq j} \langle\phi^{i,\mathrm{R}}|1\rangle \langle \hat{X}_i^\dagger \hat{X}_j \rangle \langle 1|\phi^{j,\mathrm{R}}\rangle \tag{3.77b}$$

from diagonal and off-diagonal excitonic correlations, respectively. Obviously, $\Theta_{\mathrm{dia}}(j)$ cannot be negative. To determine the off-diagonal parts, we transform Eq. (3.59) for the C_{X} into the exciton basis,

$$\mathrm{i}\hbar\frac{\mathrm{d}}{\mathrm{d}t}\Delta\langle\hat{X}_i^\dagger\hat{X}_j\rangle = (\mathcal{E}_j - \mathcal{E}_i - \mathrm{i}\gamma_{\mathrm{X}})\left(\Delta\langle\hat{X}_i^\dagger\hat{X}_j\rangle + \langle\hat{X}_i^\dagger\hat{X}_j\rangle_{\mathrm{S}}\right) + D_{i,j}^{\mathrm{exc}} + \xi_{i,j}. \tag{3.78}$$

Because we consider the luminescence source terms on a time scale that is small compared to the radiative decay times, we have neglected the quantum-optical correlations from the last two lines of Eq. (3.59). The triplet-scattering contributions are replaced by a phenomenological damping term with constant $\gamma_{\mathrm{X}} > 0$. The contributions

$$D_{i,j}^{\mathrm{exc}} \equiv \sum_{\beta,\beta',\beta'',\beta'''} \phi_{\beta'',\beta}^{i,\mathrm{L}} \left(\phi_{\beta',\beta'''}^{j,\mathrm{L}}\right)^* D^{\mathrm{exc}\,\beta\,\beta'}_{\phantom{\mathrm{exc}}\beta''\beta'''} \tag{3.79}$$

originate from the exchange terms $D_{\mathrm{X}}^{\mathrm{exc}}$ in the C_{X} equations while

$$\xi_{i,j} \equiv \sum_{\beta,\beta',\beta'',\beta'''} C_{\mathrm{X}\,\beta''\beta'''}^{\phantom{\mathrm{X}}\beta\,\beta'} \mathrm{i}\hbar\frac{\mathrm{d}}{\mathrm{d}t}\left[\phi_{\beta'',\beta}^{i,\mathrm{L}}\left(\phi_{\beta',\beta'''}^{j,\mathrm{L}}\right)^*\right] \tag{3.80}$$

is due to the dynamics of the excitonic eigen functions which are implicitly time-dependent via the densities appearing in the generalized eigen-value equations (3.34), (3.37). For $i \neq j$, we find the steady-state solution

$$\langle \hat{X}_i^\dagger \hat{X}_j \rangle = \langle \hat{X}_i^\dagger \hat{X}_j \rangle_\mathrm{s} + \Delta \langle \hat{X}_i^\dagger \hat{X}_j \rangle = -\frac{D_{i,j}^\mathrm{xch}}{\mathcal{E}_j - \mathcal{E}_i - \mathrm{i}\gamma_\mathrm{X}}. \tag{3.81}$$

Without the exchange terms, the off-diagonal contributions would vanish in the stationary limit such that no negative luminescence could occur. However, the numerical results discussed in the following section show that $\Theta_\mathrm{off}(j)$ can become negative when the system is pumped at the other optical resonance $j' \neq j$. This observation shows that we must describe the dynamics of the exchange terms carefully to ensure that our theory always yields non-negative steady-state luminescence.

3.4 Optical excitation

Having defined the generic phase space of the stable quantum-dot states, we now investigate resonant optical pumping as a concrete example for the excitation process. In order to describe the build-up of excitonic correlations consistently, the doublets have to be included. This leads to the extension of the SBE presented in Sec. 3.4.1. Which parts of the phase space can actually be reached via optical excitation depends on the dephasing scheme for the coherent quantities. We must therefore improve the simple phenomenological damping model used so far to find the microscopically correct symmetries. To this end, we consider the effect of the electron-phonon coupling in Sec. 3.4.2. It turns out that the interaction with lattice vibrations does not only yield dephasing of coherent quantities but also thermalization of the carrier system as well as strictly positive steady-state luminescence.

3.4.1 Dynamics of the two-particle correlations

Except for the phonon-related terms derived in the following section, the dynamics of the singlets is completely described by the equations of motion (3.22)–(3.24). However, in order to close the SBE, the dynamics of the two-particle correlations must be solved simultaneously. When coherent excitation with a classical light field is considered, a number of coherent contributions have to be added to the equation of motion (3.59) for the excitonic correlations in

the incoherent regime. These terms explicitly read

$$
\begin{aligned}
i\hbar \frac{d}{dt} C_{\mathrm{X}}{}^{\beta\ \beta'}_{\beta''\beta'''}\Big|_{\mathrm{coh.}} &= \sum_{\beta_1} \Big[\left(\Omega^{\mathrm{R}}_{\beta,\beta_1}\right)^* C_{\mathrm{hp}}{}^{\beta_1\beta'}_{\beta''\beta'''} + \Omega^{\mathrm{R}}_{\beta_1,\beta'} \left(C_{\mathrm{ep}}{}^{\beta'''\beta''}_{\beta_1\ \beta}\right)^* \\
&\quad - \left(\Omega^{\mathrm{R}}_{\beta_1,\beta''}\right)^* C_{\mathrm{ep}}{}^{\beta\ \beta'}_{\beta_1\beta'''} - \Omega^{\mathrm{R}}_{\beta''',\beta_1} \left(C_{\mathrm{hp}}{}^{\beta_1\beta''}_{\beta'\ \beta}\right)^* \Big] \\
&\quad + \sum_{\beta_1,\beta_2,\beta_3,\beta_4} V\,{}^{\beta_1\beta_3}_{\beta_4\beta_2} \Big\{ \Big[\left(p\,{}^{\beta_2}_{\beta}\right)^* \delta_{\beta_1,\beta''} - \delta_{\beta,\beta_2} \left(p\,{}^{\beta''}_{\beta_1}\right)^* \Big] \left(C_{\mathrm{ep}}{}^{\beta_3\beta'}_{\beta_4\beta'''} + C_{\mathrm{hp}}{}^{\beta_3\beta'}_{\beta_4\beta'''} \right) \\
&\quad + \Big[p\,{}^{\beta'}_{\beta_2}\delta_{\beta_1,\beta'''} - \delta_{\beta',\beta_2} p\,{}^{\beta_1}_{\beta'''} \Big] \left(C_{\mathrm{ep}}{}^{\beta_4\beta''}_{\beta_3\beta} + C_{\mathrm{hp}}{}^{\beta_4\beta''}_{\beta_3\beta} \right)^* \Big\} \\
&\quad - \sum_{\beta_1,\beta_3,\beta_2,\beta_4} V\,{}^{\beta_1\beta_2}_{\beta_4\beta_3} \Big[\left(p\,{}^{\beta_2}_{\beta}\right)^* \delta_{\beta_1,\beta'''} C_{\mathrm{hp}}{}^{\beta_3\beta'}_{\beta''\beta_4} - \delta_{\beta,\beta_2} p\,{}^{\beta_1}_{\beta'''} \left(C_{\mathrm{hp}}{}^{\beta_4\beta''}_{\beta'\beta_3} \right)^* \\
&\quad - \left(p\,{}^{\beta''}_{\beta_1}\right)^* \delta_{\beta',\beta_2} C_{\mathrm{ep}}{}^{\beta\ \beta_3}_{\beta_4\beta'''} + \delta_{\beta_1,\beta''} p\,{}^{\beta'}_{\beta_2} \left(C_{\mathrm{ep}}{}^{\beta'''\beta_4}_{\beta_3\ \beta} \right)^* \\
&\quad + \left(p\,{}^{\beta_2}_{\beta}\right)^* \delta_{\beta_1,\beta''} C_{\mathrm{hp}}{}^{\beta_3\beta'}_{\beta_4\beta'''} - \delta_{\beta,\beta_2} \left(p\,{}^{\beta''}_{\beta_1}\right)^* C_{\mathrm{ep}}{}^{\beta_3\beta'}_{\beta_4\beta'''} \\
&\quad - p\,{}^{\beta_1}_{\beta'''}\delta_{\beta',\beta_2} \left(C_{\mathrm{hp}}{}^{\beta_4\beta''}_{\beta_3\beta} \right)^* + \delta_{\beta_1,\beta''} p\,{}^{\beta'}_{\beta_2} \left(C_{\mathrm{ep}}{}^{\beta_4\beta''}_{\beta_3\beta} \right)^* \Big] \\
&\quad + \sum_{\beta_1,\beta_2,\beta_3,\beta_4} V\,{}^{\beta_1\beta_2}_{\beta_4\beta_3} \Big[\left(p\,{}^{\beta_1}_{\beta}\right)^* \delta_{\beta',\beta_2} C_{\mathrm{hp}}{}^{\beta_3\beta_4}_{\beta''\beta'''} + \delta_{\beta,\beta_1} p\,{}^{\beta'}_{\beta_2} \left(C_{\mathrm{ep}}{}^{\beta'''\beta''}_{\beta_4\ \beta_3} \right)^* \\
&\quad - \left(p\,{}^{\beta''}_{\beta_1}\right)^* \delta_{\beta_2,\beta'''} C_{\mathrm{ep}}{}^{\beta\ \beta'}_{\beta_3\beta_4} - \delta_{\beta_1,\beta''} p\,{}^{\beta_2}_{\beta'''} \left(C_{\mathrm{hp}}{}^{\beta_4\beta_3}_{\beta'\beta} \right)^* \Big] \\
&\quad + \sum_{\beta_1,\beta_2,\beta_3,\beta_4} V\,{}^{\beta_1\beta_2}_{\beta_4\beta_3} \Big[\left(p\,{}^{\beta_1}_{\beta}\right)^* p\,{}^{\beta'}_{\beta_2} \left(f_{\mathrm{h}}\,{}^{\beta_3}_{\beta''}\delta_{\beta_4,\beta'''} - \delta_{\beta_3,\beta''} f_{\mathrm{e}}\,{}^{\beta_4}_{\beta'''} \right) \\
&\quad + \left(p\,{}^{\beta'}_{\beta_3}\right)^* p\,{}^{\beta_4}_{\beta'''} \left(f_{\mathrm{e}}\,{}^{\beta}_{\beta_1}\delta_{\beta',\beta_2} - \delta_{\beta,\beta_1} f_{\mathrm{h}}\,{}^{\beta'}_{\beta_2} \right) \Big] \\
&\quad + \sum_{\beta_1,\beta_2,\beta_3,\beta_4} \left(V\,{}^{\beta_1\beta_2}_{\beta_4\beta_3} - V\,{}^{\beta_1\beta_2}_{\beta_3\beta_4} \right) \Big[p\,{}^{\beta'}_{\beta_2} \left(p\,{}^{\beta''}_{\beta_3}\right)^* \left(f_{\mathrm{e}}\,{}^{\beta_4}_{\beta'''}\delta_{\beta,\beta_1} - \delta_{\beta_4,\beta'''} f_{\mathrm{e}}\,{}^{\beta}_{\beta_1} \right) \\
&\quad + p\,{}^{\beta_4}_{\beta'''} \left(p\,{}^{\beta_1}_{\beta}\right)^* \left(f_{\mathrm{h}}\,{}^{\beta'}_{\beta_2}\delta_{\beta_3,\beta''} - \delta_{\beta',\beta_2} f_{\mathrm{h}}\,{}^{\beta_3}_{\beta''} \right) \Big].
\end{aligned}
\tag{3.82}
$$

Thus, $C_{\mathrm{X}}{}^{\beta\ \beta'}_{\beta''\beta'''}$ also couples to the electric field $\mathbf{E}$ via the renormalized Rabi frequencies $\Omega^{\mathrm{R}}_{\beta,\beta'}$ defined in Eq. (3.26) and to the microscopic polarizations $p\,{}^{\beta}_{\beta'}$. The two-particle correlations

$$
C_{\mathrm{ep}}{}^{\beta\ \beta'}_{\beta''\beta'''} \equiv C\left({}^{\mathrm{cv}}_{\mathrm{cc}} \Big| {}^{\beta\ \beta'}_{\beta''\beta'''} \right) = \Delta \langle \hat{a}^{\dagger}_{\mathrm{c},\beta} \hat{a}^{\dagger}_{\mathrm{v},\beta'} \hat{a}_{\mathrm{c},\beta'''} \hat{a}_{\mathrm{c},\beta''} \rangle,
\tag{3.83}
$$

$$
C_{\mathrm{hp}}{}^{\beta\ \beta'}_{\beta''\beta'''} \equiv C\left({}^{\mathrm{vv}}_{\mathrm{vc}} \Big| {}^{\beta\ \beta'}_{\beta''\beta'''} \right) = \Delta \langle \hat{a}^{\dagger}_{\mathrm{v},\beta} \hat{a}^{\dagger}_{\mathrm{v},\beta'} \hat{a}_{\mathrm{c},\beta'''} \hat{a}_{\mathrm{v},\beta''} \rangle
\tag{3.84}
$$

are coherent quantities in the sense that their phases rotate with roughly the gap frequency, similarly to the microscopic polarizations. Both $C_{\mathrm{ep}}{}^{\beta\ \beta'}_{\beta''\beta'''}$ and $C_{\mathrm{hp}}{}^{\beta\ \beta'}_{\beta''\beta'''}$ couple to biexcitonic correlations

$$
C_{\mathrm{biX}}{}^{\beta\ \beta'}_{\beta''\beta'''} \equiv C\left({}^{\mathrm{vv}}_{\mathrm{cc}} \Big| {}^{\beta\ \beta'}_{\beta''\beta'''} \right) = \Delta \langle \hat{a}^{\dagger}_{\mathrm{v},\beta} \hat{a}^{\dagger}_{\mathrm{v},\beta'} \hat{a}_{\mathrm{c},\beta'''} \hat{a}_{\mathrm{c},\beta''} \rangle
\tag{3.85}
$$

that roughly oscillate with twice the gap frequency. The equations of motions for $C_{\mathrm{ee}}{}^{\beta\ \beta'}_{\beta''\beta'''}$, $C_{\mathrm{hh}}{}^{\beta\ \beta'}_{\beta''\beta'''}$, $C_{\mathrm{ep}}{}^{\beta\ \beta'}_{\beta''\beta'''}$, $C_{\mathrm{hp}}{}^{\beta\ \beta'}_{\beta''\beta'''}$, and $C_{\mathrm{biX}}{}^{\beta\ \beta'}_{\beta''\beta'''}$ can be found in Appendix C.2. Quantum-optical corrections can usually be neglected on the time scale where the optical excitation

takes place since they describe the comparatively slow radiative decay due to spontaneous emission. The electric field $\mathbf{E}$ can be treated as an external field so long as individual dots or small dot densities are considered.[3] With these approximations, the singlet-doublet dynamics for polarizations, densities, and the two-particle correlations C_X, C_{ee}, C_{hh}, C_{ep}, C_{hp}, and C_{biX} form a closed set of equations of motion.

For the following numerical examples, we assume that the light-field is resonant with the A exciton such that its co-rotating part (3.27) can be written as

$$E^{(+)}(t) = E_0(t)\mathrm{e}^{-\mathrm{i}\mathcal{E}_1 t/\hbar}. \tag{3.86}$$

We consider excitation with a Gaussian pulse of width $\Delta t = 0.5\,\mathrm{ps}$ that arrives at $t_0 = 2\,\mathrm{ps}$. The envelope $E_0(t)$ of the light pulse then takes the form

$$E_0(t) = E_{\max} \exp\left(-\frac{1}{2}\left[\frac{t - t_0}{\Delta t}\right]^2\right). \tag{3.87}$$

Before we calculate the full singlet-doublet dynamics in the next section, we solve the singlet equations alone to analyze how the total excited density depends on the amplitude $E_{\max}$ of the light pulse. As shown in Fig. 14, the quantum dot features *Rabi flopping* [112, 113] when $E_{\max}$ is increased because the system periodically absorbs light energy and re-emits it through stimulated emission. Without Coulomb interaction and without polarization dephasing (gray shaded area), the total density oscillates between 0 and 1, which corresponds to the behavior of a simple two-level system [114, 115]. As is well-known from quantum-well systems [116, 117], the oscillation period decreases and no full population inversion is reached anymore when the Coulomb interaction is switched on (dashed line). Moreover, the Rabi flopping does not fully lead the system back to the ground state some if polarization dephasing is included (solid line).

3.4.2 Physical relevance of electron-phonon scattering

The SBE also yield polarization dephasing due to electron-electron scattering via the Coulomb correlations from Eq. (3.28) that enter Eq. (3.22). However, the *excitation-induced dephasing* is very weak in an isolated dot owing to the small number of degrees of freedom of the carrier system. Efficient dephasing of polarizations and thermalization of densities is found when scattering with delocalized electrons is included such that energy can be transferred between the quantum dot and the wetting layer [36]. For low carrier densities in the layer, the electron-phonon interaction becomes the dominant scattering mechanism. When optical phonons are considered, Fermi's golden rule predicts vanishing scattering rates for the case that the phonon energy does not match the transition energies of the carrier system [118]. By contrast, it has been shown experimentally [38] that the Fröhlich interaction enables coherent coupling of localized electrons and LO phonons, which can be described in terms of so-called exciton-polarons and leads to considerable carrier-phonon scattering at elevated temperatures [40, 41, 119]. Moreover, the interlevel spacing $\hbar\omega_e = 40.2\,\mathrm{meV}$ in the conduction band of the considered quantum dot is close to the optical phonon energy $\hbar\Omega \simeq 37\,\mathrm{meV}$ in GaAs. Second-order processes involving a combination of an optical and an acoustic phonon become important in that case [120–122]. Since a microscopic theory of these processes would be beyond the scope of this work, we restrict the analysis to deformation-potential scattering with longitudinal acoustic phonons. As derived in Sec. 2.2.4.2, the corresponding interaction Hamiltonian can

---

[3]The self-consistent calculation of $\mathbf{E}$ is outlined in Sec. 3.5.1.
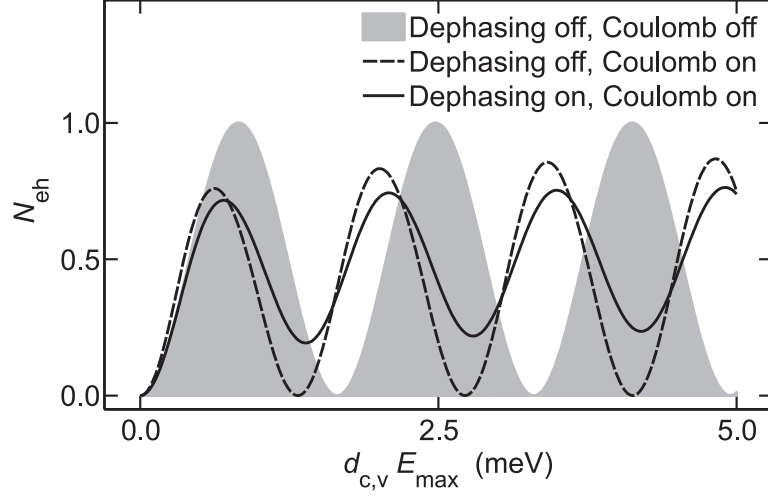
Figure 14: Rabi flopping for the quantum dot. The number N_{eh} of excited electron-hole pairs is plotted as function of the electric field amplitude for non-interacting carriers without polarization dephasing (shaded area), interacting carriers without polarization dephasing (dashed line), and a full solution of the Bloch equations on the singlet level (solid line).

be written as

$$\hat{H}_{\mathrm{el-vib}} = \sum_{\lambda,\beta,\beta',\mathbf{p}} G_{\lambda,\beta,\beta',\mathbf{p}} \left(\hat{D}^\dagger_{-\mathbf{p}} + \hat{D}_{\mathbf{p}} \right) \hat{a}^\dagger_{\lambda,\beta} \hat{a}_{\lambda,\beta'} \tag{3.88}$$

where the $\mathbf{p}$ sum only extends over the LA modes. The explicit form of the matrix elements $G_{\lambda,\beta,\beta',\mathbf{p}}$ is given in Appendix C.1.2. Neglecting the mixing with LO phonons will generally produce too long dephasing times. Additionally, the calculated thermalization rates will be too low since the interaction matrix elements are already very small at phonon momenta for which the phonon energy $\hbar\Omega_{\mathbf{p}} = c_{\mathrm{LA}}|\mathbf{p}|$ is of the order of the interlevel spacing. Still, our approach defines a consistent dephasing model with the physically correct symmetries. One can then study phenomena such as dephasing, thermalization, and phonon-induced build-up of excitonic population by adjusting the model parameters to experimental data.

We treat the phonon subsystem as a reservoir in thermal equilibrium that is described by the reduced density operator

$$\hat{\rho}_{\mathrm{phon}} = \prod_{\mathbf{p}} \left[1 - \exp\left(-\frac{\hbar\Omega_{\mathbf{p}}}{k_{\mathrm{B}} T_{\mathrm{phon}}} \right) \right] \exp\left(-\frac{\hbar\Omega_{\mathbf{p}} \hat{D}^\dagger_{\mathbf{p}} \hat{D}_{\mathbf{p}}}{k_{\mathrm{B}} T_{\mathrm{phon}}} \right) \tag{3.89}$$

where k_{B} denotes the Boltzmann constant and T_{phon} the lattice temperature. Expectation values of pure phonon-operator combinations $\hat{O}$ can be calculated from $\langle \hat{O} \rangle = \mathrm{tr}(\hat{\rho}_{\mathrm{phon}} \hat{O})$. In particular, we find

$$\langle \hat{D}_{\mathbf{p}} \rangle = 0 = \langle \hat{D}^\dagger_{\mathbf{p}} \rangle, \tag{3.90a}$$

$$\Delta\langle \hat{D}_{\mathbf{p}} \hat{D}_{\mathbf{p}'} \rangle = 0 = \Delta\langle \hat{D}^\dagger_{\mathbf{p}} \hat{D}^\dagger_{\mathbf{p}'} \rangle, \tag{3.90b}$$

$$\Delta\langle \hat{D}^\dagger_{\mathbf{p}} \hat{D}_{\mathbf{p}'} \rangle = \delta_{\mathbf{p},\mathbf{p}'} n^{\mathrm{phon}}_{\mathbf{p}}, \tag{3.90c}$$

$$\Delta\langle \hat{D}_{\mathbf{p}} \hat{D}^\dagger_{\mathbf{p}'} \rangle = \delta_{\mathbf{p},\mathbf{p}'} \left(n^{\mathrm{phon}}_{\mathbf{p}} + 1 \right) \tag{3.90d}$$

with the Bose-Einstein distribution for the phonon numbers

$$n_{\mathbf{p}}^{\mathrm{phon}} = \frac{1}{e^{\hbar\Omega_{\mathbf{p}}/k_{\mathrm{B}}T_{\mathrm{phon}}} - 1}. \tag{3.91}$$

The electron-phonon interaction produces additional terms in the SBE. For the phonon-related dynamics of densities and polarizations, we obtain

$$i\hbar \frac{\mathrm{d}}{\mathrm{d}t} \langle \hat{a}_{\lambda,\beta}^{\dagger} \hat{a}_{\lambda',\beta'} \rangle \Big|_{\hat{H}_{\mathrm{el-vib}}} = \sum_{\beta_1} \left(\Delta\langle D_{\Sigma}^{\lambda',\beta',\beta_1} \hat{a}_{\lambda,\beta}^{\dagger} \hat{a}_{\lambda',\beta_1} \rangle - \Delta\langle D_{\Sigma}^{\lambda,\beta_1,\beta} \hat{a}_{\lambda,\beta_1}^{\dagger} \hat{a}_{\lambda',\beta'} \rangle \right) \tag{3.92}$$

where we have used Eq. (3.90a) and introduced the collective phonon operator

$$D_{\Sigma}^{\lambda,\beta,\beta'} = \sum_{\mathbf{p}} G_{\lambda,\beta,\beta',\mathbf{p}} \left(\hat{D}_{-\mathbf{p}}^{\dagger} + \hat{D}_{\mathbf{p}} \right). \tag{3.93}$$

The equations of motion for the carrier-carrier correlations

$$i\hbar \frac{\mathrm{d}}{\mathrm{d}t} C\left({\lambda\ \lambda' \atop \lambda''\lambda'''} \Big| {\beta\ \beta' \atop \beta''\beta'''} \right) \Big|_{\hat{H}_{\mathrm{el-vib}}} =$$

$$\sum_{\beta_1} \left(\langle \hat{a}_{\lambda,\beta}^{\dagger} \hat{a}_{\lambda'',\beta_1} \rangle \Delta\langle D_{\Sigma}^{\lambda'',\beta'',\beta_1} \hat{a}_{\lambda',\beta'}^{\dagger} \hat{a}_{\lambda''',\beta'''} \rangle - \langle \hat{a}_{\lambda,\beta}^{\dagger} \hat{a}_{\lambda''',\beta_1} \rangle \Delta\langle D_{\Sigma}^{\lambda''',\beta''',\beta_1} \hat{a}_{\lambda',\beta'}^{\dagger} \hat{a}_{\lambda'',\beta''} \rangle \right.$$

$$+ \langle \hat{a}_{\lambda',\beta'}^{\dagger} \hat{a}_{\lambda''',\beta_1} \rangle \Delta\langle D_{\Sigma}^{\lambda''',\beta''',\beta_1} \hat{a}_{\lambda,\beta}^{\dagger} \hat{a}_{\lambda'',\beta''} \rangle - \langle \hat{a}_{\lambda',\beta'}^{\dagger} \hat{a}_{\lambda'',\beta_1} \rangle \Delta\langle D_{\Sigma}^{\lambda'',\beta'',\beta_1} \hat{a}_{\lambda,\beta}^{\dagger} \hat{a}_{\lambda''',\beta'''} \rangle$$

$$+ \langle \hat{a}_{\lambda',\beta_1}^{\dagger} \hat{a}_{\lambda'',\beta''} \rangle \Delta\langle D_{\Sigma}^{\lambda',\beta_1,\beta'} \hat{a}_{\lambda,\beta}^{\dagger} \hat{a}_{\lambda''',\beta'''} \rangle - \langle \hat{a}_{\lambda,\beta_1}^{\dagger} \hat{a}_{\lambda'',\beta''} \rangle \Delta\langle D_{\Sigma}^{\lambda,\beta_1,\beta} \hat{a}_{\lambda',\beta'}^{\dagger} \hat{a}_{\lambda''',\beta'''} \rangle$$

$$+ \langle \hat{a}_{\lambda,\beta_1}^{\dagger} \hat{a}_{\lambda''',\beta'''} \rangle \Delta\langle D_{\Sigma}^{\lambda,\beta_1,\beta} \hat{a}_{\lambda',\beta'}^{\dagger} \hat{a}_{\lambda'',\beta''} \rangle - \langle \hat{a}_{\lambda',\beta_1}^{\dagger} \hat{a}_{\lambda''',\beta'''} \rangle \Delta\langle D_{\Sigma}^{\lambda',\beta_1,\beta'} \hat{a}_{\lambda,\beta}^{\dagger} \hat{a}_{\lambda'',\beta''} \rangle \right)$$

$$+ T_{\mathrm{phon}} \left({\lambda\ \lambda' \atop \lambda''\lambda'''} \Big| {\beta\ \beta' \atop \beta''\beta'''} \right) \tag{3.94}$$

contain both phonon-assisted two-particle correlations $\Delta\langle \hat{D}_{\Sigma} \hat{a}^{\dagger} \hat{a} \rangle$ and triplet contributions

$$T_{\mathrm{phon}} \left({\lambda\ \lambda' \atop \lambda''\lambda'''} \Big| {\beta\ \beta' \atop \beta''\beta'''} \right) \equiv \sum_{\beta_1} \left(-\Delta\langle D_{\Sigma}^{\lambda,\beta_1,\beta} \hat{a}_{\lambda,\beta_1}^{\dagger} \hat{a}_{\lambda',\beta'}^{\dagger} \hat{a}_{\lambda''',\beta'''} \hat{a}_{\lambda'',\beta''} \rangle \right.$$

$$- \Delta\langle D_{\Sigma}^{\lambda',\beta_1,\beta'} \hat{a}_{\lambda,\beta}^{\dagger} \hat{a}_{\lambda',\beta_1}^{\dagger} \hat{a}_{\lambda''',\beta'''} \hat{a}_{\lambda'',\beta''} \rangle$$

$$+ \Delta\langle D_{\Sigma}^{\lambda'',\beta'',\beta_1} \hat{a}_{\lambda,\beta}^{\dagger} \hat{a}_{\lambda',\beta'}^{\dagger} \hat{a}_{\lambda''',\beta'''} \hat{a}_{\lambda'',\beta_1} \rangle$$

$$+ \Delta\langle D_{\Sigma}^{\lambda''',\beta''',\beta_1} \hat{a}_{\lambda,\beta}^{\dagger} \hat{a}_{\lambda',\beta'}^{\dagger} \hat{a}_{\lambda''',\beta_1} \hat{a}_{\lambda'',\beta''} \rangle \right) \tag{3.95}$$

The dynamics of $\Delta\langle \hat{D}\hat{a}^{\dagger}\hat{a} \rangle$ and $\Delta\langle \hat{D}\hat{a}^{\dagger}\hat{a}^{\dagger}\hat{a}\hat{a} \rangle$ is solved in Markov approximation as defined in Appendix B where we only consider kinetic terms and true source terms in the equations of motion. For the correlations between phonons and single carriers, we thus get

$$\Delta\langle \hat{D}_{\mathbf{p}} \hat{a}_{\lambda,\beta}^{\dagger} \hat{a}_{\lambda',\beta'} \rangle \simeq n_{\mathbf{p}}^{\mathrm{phon}} \sum_{\beta_1} G_{\lambda,\beta,\beta_1,\mathbf{p}}^{*} \langle \hat{a}_{\lambda,\beta_1}^{\dagger} \hat{a}_{\lambda',\beta'} \rangle g_{\eta_1} \left(\hbar\Omega_{\mathbf{p}} - \varepsilon_{\lambda,\beta} + \varepsilon_{\lambda,\beta_1} \right)$$

$$- \left(n_{\mathbf{p}}^{\mathrm{phon}} + 1 \right) \sum_{\beta_1} G_{\lambda',\beta_1,\beta',\mathbf{p}}^{*} \langle \hat{a}_{\lambda,\beta}^{\dagger} \hat{a}_{\lambda',\beta_1} \rangle g_{\eta_1} \left(\hbar\Omega_{\mathbf{p}} - \varepsilon_{\lambda',\beta_1} + \varepsilon_{\lambda',\beta'} \right)$$

$$+ \sum_{\lambda_1,\beta_1,\beta_2} G_{\lambda_1,\beta_2,\beta_1,\mathbf{p}}^{*} \left[\langle \hat{a}_{\lambda,\beta}^{\dagger} \hat{a}_{\lambda_1,\beta_2} \rangle \langle \hat{a}_{\lambda_1,\beta_1}^{\dagger} \hat{a}_{\lambda',\beta'} \rangle + C\left({\lambda_1\lambda \atop \lambda'\lambda_1} \Big| {\beta_1\beta \atop \beta'\beta_2} \right) \right]$$

$$\times g_{\eta_1} \left(\hbar\Omega_{\mathbf{p}} - \varepsilon_{\lambda_1,\beta_2} + \varepsilon_{\lambda_1,\beta_1} \right) \tag{3.96}$$

with $g_\eta(E) \equiv 1/(E - \mathrm{i}\eta)$ where η_1 is a phenomenological dephasing constant for $\Delta\langle\hat{D}\hat{a}^\dagger\hat{a}\rangle$. The energy denominators fulfill the Dirac identity $\lim_{\eta\to 0} g_\eta(E) = \mathscr{P}(1/E) + \mathrm{i}\pi\delta(E)$ where $\mathscr{P}$ denotes the principal value. Instead of considering the full singlet-doublet-triplet equations for $\Delta\langle\hat{D}\hat{a}^\dagger\hat{a}^\dagger\hat{a}\hat{a}\rangle$, we only expand the occurring four-particle expectation values up to the singlet-doublet level. With this approach, we concentrate on the scattering processes involving singlets and two-particle correlations while we neglect the coupling to genuine three-particle correlations. The Markov approximation then results in

$$
\begin{aligned}
&\Delta\langle\hat{D}_\mathbf{p}\hat{a}^\dagger_{\lambda,\beta}\hat{a}^\dagger_{\lambda',\beta'}\hat{a}_{\lambda''',\beta'''}\hat{a}_{\lambda'',\beta''}\rangle \simeq \\
&\quad n^{\mathrm{phon}}_\mathbf{p}\sum_{\beta_1} G^*_{\lambda,\beta,\beta_1,\mathbf{p}} C\begin{pmatrix}\lambda\ \lambda' & \big|\beta_1\ \beta' \\ \lambda''\lambda''' & \big|\beta''\beta'''\end{pmatrix} g_{\eta_2}\big(\hbar\Omega_\mathbf{p} - \varepsilon_{\lambda,\beta} + \varepsilon_{\lambda,\beta_1}\big) \\
&\quad + n^{\mathrm{phon}}_\mathbf{p}\sum_{\beta_1} G^*_{\lambda',\beta',\beta_1,\mathbf{p}} C\begin{pmatrix}\lambda\ \lambda' & \big|\beta\ \beta_1 \\ \lambda''\lambda''' & \big|\beta''\beta'''\end{pmatrix} g_{\eta_2}\big(\hbar\Omega_\mathbf{p} - \varepsilon_{\lambda',\beta'} + \varepsilon_{\lambda',\beta_1}\big) \\
&\quad - \big(n^{\mathrm{phon}}_\mathbf{p}+1\big)\sum_{\beta_1} G^*_{\lambda'',\beta_1,\beta'',\mathbf{p}} C\begin{pmatrix}\lambda\ \lambda' & \big|\beta\ \beta' \\ \lambda''\lambda''' & \big|\beta_1\beta'''\end{pmatrix} g_{\eta_2}\big(\hbar\Omega_\mathbf{p} - \varepsilon_{\lambda'',\beta_1} + \varepsilon_{\lambda'',\beta''}\big) \\
&\quad - \big(n^{\mathrm{phon}}_\mathbf{p}+1\big)\sum_{\beta_1} G^*_{\lambda''',\beta_1,\beta''',\mathbf{p}} C\begin{pmatrix}\lambda\ \lambda' & \big|\beta\ \beta' \\ \lambda''\lambda''' & \big|\beta''\beta_1\end{pmatrix} g_{\eta_2}\big(\hbar\Omega_\mathbf{p} - \varepsilon_{\lambda''',\beta_1} + \varepsilon_{\lambda''',\beta'''}\big) \\
&\quad + \sum_{\lambda_1,\beta_1,\beta_2} G^*_{\lambda_1,\beta_2,\beta_1,\mathbf{p}} \Bigg[\langle\hat{a}^\dagger_{\lambda,\beta}\hat{a}_{\lambda_1,\beta_2}\rangle C\begin{pmatrix}\lambda_1\lambda' & \big|\beta_1\ \beta' \\ \lambda''\lambda''' & \big|\beta''\beta'''\end{pmatrix} + \langle\hat{a}^\dagger_{\lambda',\beta'}\hat{a}_{\lambda_1,\beta_2}\rangle C\begin{pmatrix}\lambda\ \lambda_1 & \big|\beta\ \beta_1 \\ \lambda''\lambda''' & \big|\beta''\beta'''\end{pmatrix} \\
&\qquad\qquad + \langle\hat{a}^\dagger_{\lambda_1,\beta_1}\hat{a}_{\lambda'',\beta''}\rangle C\begin{pmatrix}\lambda\ \lambda' & \big|\beta\ \beta' \\ \lambda_1\lambda''' & \big|\beta_2\beta'''\end{pmatrix} + \langle\hat{a}^\dagger_{\lambda_1,\beta_1}\hat{a}_{\lambda''',\beta'''}\rangle C\begin{pmatrix}\lambda\ \lambda' & \big|\beta\ \beta' \\ \lambda''\lambda_1 & \big|\beta''\beta_2\end{pmatrix} \Bigg] \\
&\quad \times g_{\eta_2}\big(\hbar\Omega_\mathbf{p} - \varepsilon_{\lambda_1,\beta_2} + \varepsilon_{\lambda_1,\beta_1}\big)
\end{aligned}
\tag{3.97}
$$

where η_2 is a phenomenological dephasing constant for $\Delta\langle\hat{D}\hat{a}^\dagger\hat{a}^\dagger\hat{a}\hat{a}\rangle$.

When inserting the Markov solutions into Eqs. (3.92), (3.94), we can distinguish two physically different classes of contributions. *Class I* contains all terms proportional to $g_\eta(\hbar\Omega_\mathbf{p})$ while the terms proportional to $g_\eta(\hbar\Omega_\mathbf{p}\pm\Delta E)$ with $\Delta E > 0$ define *class II*. The former contributions originate from microscopic processes where no energy is transferred between the electrons and the phonons. Hence, these terms can only describe dephasing of coherent quantities where the total energy of the interacting electrons is conserved. On the other hand, the terms from class II can lead to thermalization of the carrier subsystem where the phonon bath acts as a heat reservoir. We will exclusively consider the dissipative terms that are proportional to the imaginary part of $g_\eta(E)$ because our numerical results do not change qualitatively when the real part of $g_\eta(E)$ is also included. In the following, the different phonon-induced phenomena are discussed in separate subsections.

3.4.2.1 Dephasing and build-up of excitonic population

The class-I terms in the equations of motion for the coherent quantities can be written as

$$
\left.\frac{\mathrm{d}}{\mathrm{d}t}p^{\beta}_{\beta'}\right|_{\mathrm{I}} = -\frac{1}{\hbar}\sum_{\beta_1}\left[\left(\gamma_{\mathrm{c,c}} - \gamma_{\mathrm{c,v}}\right)p^{\beta}_{\beta_1} + \left(\gamma_{\mathrm{v,v}} - \gamma_{\mathrm{v,c}}\right)p^{\beta_1}_{\beta'}\right],
\tag{3.98}
$$

$$
\begin{aligned}
\left.\frac{\mathrm{d}}{\mathrm{d}t}C_{\mathrm{ep}}{}^{\beta\ \beta'}_{\beta''\beta'''}\right|_{\mathrm{I}} = -\sum_{\beta_1}\Bigg[&\left(\gamma_{\mathrm{c,v}} - \gamma_{\mathrm{c,c}}\right)C_{\mathrm{ep}}{}^{\beta_1\beta'}_{\beta''\beta'''} + \left(\gamma_{\mathrm{v,v}} - \gamma_{\mathrm{v,c}}\right)C_{\mathrm{ep}}{}^{\beta\ \beta_1}_{\beta''\beta'''} \\
&+ \left(\gamma_{\mathrm{c,c}} - \gamma_{\mathrm{c,v}}\right)C_{\mathrm{ep}}{}^{\beta\ \beta'}_{\beta_1\beta'''} + \left(\gamma_{\mathrm{c,c}} - \gamma_{\mathrm{c,v}}\right)C_{\mathrm{ep}}{}^{\beta\ \beta'}_{\beta''\beta_1}\Bigg],
\end{aligned}
\tag{3.99}
$$

$$\frac{\mathrm{d}}{\mathrm{d}t} C_{\mathrm{hp}}{}_{\beta''\beta'''}^{\beta\ \beta'}\bigg|_{\mathrm{I}} = -\sum_{\beta_1}\Big[(\gamma_{\mathrm{v,v}}-\gamma_{\mathrm{v,c}})\,C_{\mathrm{hp}}{}_{\beta''\beta'''}^{\beta_1\,\beta'} + (\gamma_{\mathrm{v,v}}-\gamma_{\mathrm{v,c}})\,C_{\mathrm{hp}}{}_{\beta''\beta'''}^{\beta\ \beta_1}$$

$$+ (\gamma_{\mathrm{v,c}}-\gamma_{\mathrm{v,v}})\,C_{\mathrm{hp}}{}_{\beta_1\beta'''}^{\beta\ \beta'} + (\gamma_{\mathrm{c,c}}-\gamma_{\mathrm{c,v}})\,C_{\mathrm{hp}}{}_{\beta''\beta_1}^{\beta\ \beta'}\Big], \tag{3.100}$$

$$\frac{\mathrm{d}}{\mathrm{d}t} C_{\mathrm{biX}}{}_{\beta''\beta'''}^{\beta\ \beta'}\bigg|_{\mathrm{I}} = -2\sum_{\beta_1}\Big[(\gamma_{\mathrm{v,v}}-\gamma_{\mathrm{v,c}})\,C_{\mathrm{biX}}{}_{\beta''\beta'''}^{\beta_1\,\beta'} + (\gamma_{\mathrm{v,v}}-\gamma_{\mathrm{v,c}})\,C_{\mathrm{biX}}{}_{\beta''\beta'''}^{\beta\ \beta_1}$$

$$+ (\gamma_{\mathrm{c,c}}-\gamma_{\mathrm{c,v}})\,C_{\mathrm{biX}}{}_{\beta_1\beta'''}^{\beta\ \beta'} + (\gamma_{\mathrm{c,c}}-\gamma_{\mathrm{c,v}})\,C_{\mathrm{biX}}{}_{\beta''\beta_1}^{\beta\ \beta'}\Big]. \tag{3.101}$$

Because the occurring momentum sums

$$\Gamma\,{}_{\lambda'\beta_1'\beta_2'}^{\lambda\ \beta_1\beta_2} \equiv \sum_{\mathbf{p}}(2n_{\mathbf{p}}^{\mathrm{phon}}+1)G_{\lambda,\beta_1,\beta_2,\mathbf{p}}^{*}G_{\lambda',\beta_1',\beta_2',\mathbf{p}}\,\mathrm{Im}g_{\eta_1}\big(\hbar\Omega_{\mathbf{p}}\big) > 0 \tag{3.102}$$

change by no more than a few percent when only the subband indices β_1, β_2, β_1', β_2' are varied, we have replaced these quantities by constants $\gamma_{\lambda,\lambda'}$ that only depend on the band indices. Because the conduction band has a one order of magnitude larger deformation potential than the valence band, the dominant contributions are provided by $\gamma_{\mathrm{c,c}}$. Hence, the diagonal terms in Eqs. (3.98)–(3.101) lead to exponential decay of the polarization and the coherent two-particle correlations. The densities f_{e}, f_{h} and the intraband correlations C_{ee}, C_{hh} are not subject to dephasing while for the excitonic correlations C_{X}, we find

$$\frac{\mathrm{d}}{\mathrm{d}t} C_{\mathrm{X}}{}_{\beta''\beta'''}^{\beta\ \beta'}\bigg|_{\mathrm{I}} = \frac{1}{\hbar}\sum_{\beta_1}\Big\{\big(p\,{}_{\beta}^{\beta''}\big)^{*}\Big[p\,{}_{\beta_1}^{\beta'}(\gamma_{\mathrm{c,c}}-\gamma_{\mathrm{c,v}}) + p\,{}_{\beta'''}^{\beta_1}(\gamma_{\mathrm{v,v}}-\gamma_{\mathrm{v,c}})\Big]$$

$$+ p\,{}_{\beta'''}^{\beta'}\Big[\big(p\,{}_{\beta}^{\beta_1}\big)^{*}(\gamma_{\mathrm{v,v}}-\gamma_{\mathrm{v,c}}) + \big(p\,{}_{\beta_1}^{\beta''}\big)^{*}(\gamma_{\mathrm{c,c}}-\gamma_{\mathrm{c,v}})\Big]\Big\}. \tag{3.103}$$

The energy $\langle\hat{H}_{\mathrm{el}}^{\mathrm{tot}}\rangle = \langle\hat{H}_{\mathrm{el}}\rangle + \langle\hat{H}_{\mathrm{el-el}}\rangle$ of the interacting carrier system can be expressed in terms of singlets and incoherent correlations. In the general case where the polarization does not vanish, Eqs. (3.64), (3.65) must be generalized to

$$\langle\hat{H}_{\mathrm{el}}^{\mathrm{tot}}\rangle = \sum_{\beta}\Big(\varepsilon_{\beta}^{\mathrm{e}}f_{\mathrm{e}}{}_{\beta}^{\beta} + \varepsilon_{\beta}^{\mathrm{h}}f_{\mathrm{h}}{}_{\beta}^{\beta}\Big)$$

$$+ \frac{1}{2}\sum_{\beta_1,\dots,\beta_4}V\,{}_{\beta_3\beta_4}^{\beta_1\beta_2}\Big[f_{\mathrm{h}}{}_{\beta_4}^{\beta_1}f_{\mathrm{h}}{}_{\beta_3}^{\beta_2} - f_{\mathrm{h}}{}_{\beta_3}^{\beta_1}f_{\mathrm{h}}{}_{\beta_4}^{\beta_2} + f_{\mathrm{e}}{}_{\beta_4}^{\beta_1}f_{\mathrm{e}}{}_{\beta_3}^{\beta_2} - f_{\mathrm{e}}{}_{\beta_3}^{\beta_1}f_{\mathrm{e}}{}_{\beta_4}^{\beta_2} - 2f_{\mathrm{e}}{}_{\beta_4}^{\beta_1}f_{\mathrm{h}}{}_{\beta_3}^{\beta_2}$$

$$- p\,{}_{\beta_3}^{\beta_1}\big(p\,{}_{\beta_2}^{\beta_4}\big)^{*} - C_{\mathrm{ee}}{}_{\beta_3\beta_4}^{\beta_1\beta_2} - C_{\mathrm{hh}}{}_{\beta_3\beta_4}^{\beta_1\beta_2} - 2C_{\mathrm{X}}{}_{\beta_3\beta_4}^{\beta_1\beta_2}\Big]. \tag{3.104}$$

It is straightforward to prove that the dynamics due to class-I terms conserves $\langle\hat{H}_{\mathrm{el}}^{\mathrm{tot}}\rangle$. We conclude that Eqs. (3.98), (3.103) describe energy transfer from coherent polarizations to incoherent excitonic correlations. The analogous process is well-known from the quantum-well case [7].

For the *s-p* dot, the above equations simplify considerably because then, $p\,{}_{\beta'}^{\beta} = \delta_{\beta,\beta}$, and all correlations $C\big({}_{\lambda''\lambda'''}^{\lambda\ \lambda'}\big|{}_{\beta''\beta'''}^{\beta\ \beta'}\big)$ either have the form $C\big({}_{\lambda''\lambda'''}^{\lambda\ \lambda'}\big|{}_{\beta\beta'}^{\beta\beta'}\big)$ (*type a*) or $C\big({}_{\lambda''\lambda'''}^{\lambda\ \lambda'}\big|{}_{\beta'\beta}^{\beta\ \beta'}\big)$ with $\beta \neq \beta'$ (*type b*), as follows from the discussion at the end of Sec. 3.1.2.[4] We then have

---

[4] In principle, correlations of the form $C\big({}_{\lambda''\lambda'''}^{\lambda\ \lambda'}\big|{}_{p_{\pm}p_{\mp}}^{s\ s}\big)$ (*type c*) do not have to vanish, either. However, the explicit solution of the SBE leads to configurations of the carrier system where type-c correlations are several orders of magnitude smaller than type-a or type-b correlations.

$$\frac{\mathrm{d}}{\mathrm{d}t}p_\beta\bigg|_{\text{deph}} = -\frac{\gamma}{\hbar}p_\beta, \tag{3.105}$$

$$\frac{\mathrm{d}}{\mathrm{d}t}C_{\mathrm{X}\,\beta\beta'}^{\ \ \beta\beta'}\bigg|_{\text{deph}} = \frac{2\gamma}{\hbar}p_\beta p_{\beta'}^*, \qquad\qquad \frac{\mathrm{d}}{\mathrm{d}t}C_{\mathrm{X}\,\beta'\beta}^{\ \ \beta\,\beta'}\bigg|_{\text{deph}} = 0, \tag{3.106}$$

$$\frac{\mathrm{d}}{\mathrm{d}t}C_{\mathrm{ee}\,\beta''\beta'''}^{\ \ \beta\,\beta'}\bigg|_{\text{deph}} = 0, \qquad\qquad \frac{\mathrm{d}}{\mathrm{d}t}C_{\mathrm{hh}\,\beta''\beta'''}^{\ \ \beta\,\beta'}\bigg|_{\text{deph}} = 0, \tag{3.107}$$

$$\frac{\mathrm{d}}{\mathrm{d}t}C_{\mathrm{ep}\,\beta''\beta'''}^{\ \ \beta\,\beta'}\bigg|_{\text{deph}} = -\frac{\gamma}{\hbar}C_{\mathrm{ep}\,\beta''\beta'''}^{\ \ \beta\,\beta'}, \qquad\qquad \frac{\mathrm{d}}{\mathrm{d}t}C_{\mathrm{hp}\,\beta''\beta'''}^{\ \ \beta\,\beta'}\bigg|_{\text{deph}} = -\frac{\gamma}{\hbar}C_{\mathrm{hp}\,\beta''\beta'''}^{\ \ \beta\,\beta'}, \tag{3.108}$$

$$\frac{\mathrm{d}}{\mathrm{d}t}C_{\mathrm{biX}\,\beta''\beta'''}^{\ \ \beta\,\beta'}\bigg|_{\text{deph}} = -\frac{4\gamma}{\hbar}C_{\mathrm{biX}\,\beta''\beta'''}^{\ \ \beta\,\beta'}, \tag{3.109}$$

i.e., the dephasing model can be defined by specifying a single, positive dephasing constant $\gamma \equiv \gamma_{\mathrm{c,c}} + \gamma_{\mathrm{v,v}} - \gamma_{\mathrm{v,c}} - \gamma_{\mathrm{c,v}}$. For the reason mentioned in the introduction to this section, the parameter γ should be fitted to the experiment rather than calculated from the deformation-potential matrix elements $G_{\lambda,\beta,\beta',\mathbf{p}}$.

Type-a and type-b excitonic correlations can be related to the bright and dark excitons, respectively. In view of the symmetries of the excitonic wave functions as discussed in Sec. 3.2.4, we find that

$$\Delta\langle \hat{X}_i^\dagger \hat{X}_{i'}\rangle = \sum_{\beta\neq\beta'}\phi_{\beta'\beta}^{i,\mathrm{L}}\left(\phi_{\beta'\beta}^{i,\mathrm{L}}\right)^* C_{\mathrm{X}\,\beta'\beta}^{\ \ \beta\,\beta'}, \tag{3.110}$$

$$\Delta\langle \hat{X}_j^\dagger \hat{X}_{j'}\rangle = \sum_{\beta\beta'}\phi_\beta^{j,\mathrm{L}}\left(\phi_{\beta'}^{j',\mathrm{L}}\right)^* C_{\mathrm{X}\,\beta\beta'}^{\ \ \beta\beta'}, \tag{3.111}$$

$$\Delta\langle \hat{X}_i^\dagger \hat{X}_j\rangle = 0 \tag{3.112}$$

if $i, i' \in \{2, 3, 4, 5, 7, 8\}$ label degenerate and $j, j' \in \{1, 6, 9\}$ non-degenerate excitonic eigen energies. It turns out that type-a correlations correspond to non-degenerate and type-b correlations to degenerate excitons. According to Eq. (3.106), degenerate excitons are not build up via phonon-induced dephasing. The case $j = 9$ plays a special role as the type-a contributions to $\Delta N_9 = \Delta\langle \hat{X}_9^\dagger \hat{X}_9\rangle$ nearly cancel each other since $\phi_{p_+}^{9,\mathrm{L}} = -\phi_{p_-}^{9,\mathrm{L}}$. We conclude that the phonon-induced energy transfer from coherent to incoherent quantities leads to configurations of the carrier system where the bright exciton states A ($j = 1$) and B ($j = 6$) are much stronger populated than the dark exciton states.

Having derived the dephasing model, we can now analyze numerically how efficiently the bright excitons are actually build up during the excitation process. We assume optical pumping where the light field is resonant with the A exciton as in the Rabi-flopping analysis performed above. Figure 15 shows the final values of the energy per electron-hole pair (a) and the population ΔN_1 of the A exciton (b) as function of the number of electron-hole pairs N_{eh}. The shaded areas indicate the generic phase space for the stable quantum-dot states as defined in Sec. 3.3.1. A simple phenomenological dephasing for the coherent singlets and two-particle correlations where Eq. (3.106) is not implemented (solid lines) produces no significant amount of excitonic population such that the system remains close to the plasma line of the allowed region where electrons and holes are basically uncorrelated. On the other hand, the full inclusion of the microscopically consistent dephasing model (3.105)–(3.109) (dashed lines) leads the system close to the maximally correlated case that defines the saturation line of the phase space. Here,
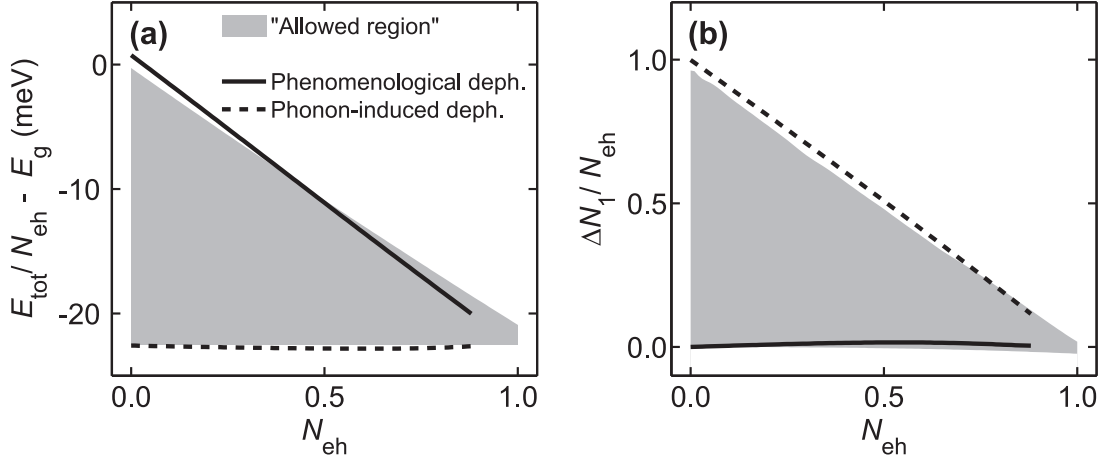
Figure 15: **(a)** Total energy $E_{\text{tot}} = \langle \hat{H}_{\text{el}}^{\text{tot}} \rangle$ per electron-hole pair as function of the number of pairs N_{eh} (thick solid line). The thin solid line gives the singlet contribution to the total energy, while the saturation line is defined by the first excitonic resonance. **(b)** First-exciton population ΔN_1 per electron-hole pair reached for density pumping alone (solid line) and maximum allowed exciton-population pumping (dashed line).

the amplitude of the constant γ determines the time scale on which the polarization decays but does not influence the final configuration of the carrier system after the incoherent regime has been reached. A closer look at frame (a) shows that for low densities, the energy per particle can even exceed the gap energy when no excitonic correlations are build up. We conclude that the actual coherent excitation dynamics yields a slightly higher amount of p-shell population than the phenomenological pumping studied in Sec. 3.3. As a consequence, the coherent optical pumping can lead to a slightly higher A-exciton population before the energy per particle reaches the lowest excitonic eigen energy. Aside from these minor modifications, we find that resonant optical excitation in the presence of phonon-induced dephasing reproduces the population-saturation limit of our generic phase-space analysis.

3.4.2.2 Thermalization

Thermalization of the excited carrier system can only be due to the class-II terms that describe electron-phonon scattering processes where the energy of the involved electron changes. In order to gain some analytical insight how the thermalization works, we explicitly write down the phonon-induced dynamics of the proper densities $f_{\beta}^{\text{e/h}} = f_{\text{e/h}}{}_{\beta}^{\beta}$. By neglecting the correlated terms in the Markov solution (3.96), we find

$$
\frac{\mathrm{d}}{\mathrm{d}t} f_{\beta}^{\lambda} \bigg|_{\hat{H}_{\text{el-vib}}} = -\frac{2\pi}{\hbar} \sum_{\mathbf{p}} \sum_{\beta_1} \sum_{\pm} |G_{\lambda,\beta,\beta_1,\mathbf{p}}|^2 \delta(\varepsilon_{\beta}^{\lambda} - \varepsilon_{\beta_1}^{\lambda} \mp \hbar\Omega_{\mathbf{p}})
$$
$$
\times \left[f_{\beta}^{\lambda}(1 - f_{\beta_1}^{\lambda})\left(n_{\mathbf{p}}^{\text{phon}} + \frac{1 \pm 1}{2}\right) - (1 - f_{\beta}^{\lambda})f_{\beta_1}^{\lambda}\left(n_{\mathbf{p}}^{\text{phon}} + \frac{1 \mp 1}{2}\right) \right]. \quad (3.113)
$$

This result agrees with the Boltzmann limit of the quantum-kinetical *collision integral* [1,123]

and can be interpreted straightforwardly. The density $f_\beta^{e/h}$ changes whenever an electron is scattered from another state β_1 into β or from β into another state β_1 under the emission or absorption of a phonon. The probability of scattering from a state β into a state β' is proportional to $f_\beta^{e/h}(1 - f_{\beta'}^{e/h})$, and the probability that a phonon is annihilated or created is proportional to $n_{\mathbf{p}}^{phon}$ and $n_{\mathbf{p}}^{phon} + 1$, respectively. In the limit $\eta \to 0$ where $\text{Im}g(E)$ approaches the delta function $\pi\delta(E)$, the collision integral vanishes if $f_\beta^{e/h}$ and $n_{\mathbf{p}}^{phon}$ obey Fermi and Bose distributions, respectively, at a common temperature T_{phon}. This result is independent of the concrete form of the interaction matrix element $G_{\lambda,\beta,\beta',\mathbf{p}}$ and thus remains valid when the delocalized wetting-layer states are included in the analysis. We notice that the acoustic deformation-potential matrix elements $G_{\lambda,\beta,\beta',\mathbf{p}}$ as calculated in Appendix C.1.2 have almost completely decayed when the phonon energy $\hbar\Omega_{\mathbf{p}} = c_{LA}|\mathbf{p}|$ comes close to the interlevel spacings. This observation emphasizes that in general, the scattering with acoustic phonons does not yield the main contribution to the thermalization. As for the dephasing, the physically correct time scale for the intraband relaxation must thus be determined by a theory-experiment comparison. When Coulomb interaction and two-particle correlations are included, the steady-state densities do not obey the Fermi-Dirac statistics anymore. Relaxation of the excitonic populations is described by the three-particle correlations $\Delta\langle\hat{D}^\dagger\hat{a}^\dagger\hat{a}^\dagger\hat{a}\hat{a}\rangle$. The complicated thermalization dynamics of an interacting, highly correlated carrier system will be solved numerically as part of the switch-on analysis that concludes Sec. 3.4.2.

3.4.2.3 Strictly positive steady-state luminescence

The generic phase-space analysis from Sec. 3.3 has shown that resonant pumping of the A exciton can produce an artifact of negative steady-state luminescence at the B resonance. At the end of Sec. 3.3.3, we have related this unphysical possibility to the non-vanishing exchange terms in the equations of motion for excitonic correlations. The dephasing model Eqs. (3.106), (3.107) leads to steady-state configurations of the dot where $C_X{}_{sp\pm}^{sp\pm}$ provides the dominant contribution to the off-diagonal contributions $\Theta_{off}(j = 2)$ defined in Eq. (3.77b). Dephasing of $C_X{}_{sp\pm}^{sp\pm}$ can thus be expected to turn the luminescence at the second excitonic resonance positive. When we neglect the subband dependence of the dephasing constants $\Gamma_{\lambda'\beta_1'\beta_2'}^{\lambda\beta_1\beta_2}$ from Eq. (3.102), the class-I contributions to the triplet scattering terms $\Delta\langle\hat{D}^\dagger\hat{a}^\dagger\hat{a}^\dagger\hat{a}\hat{a}\rangle$ in the equations of motion for the excitonic correlations cancel each other. However, when the subband dependence is evaluated accurately, we find that all type-a excitonic correlations with non-vanishing kinetic terms in their equations of motion, i.e. all $C_X{}_{\beta\beta'}^{\beta\beta'}$ with $\beta \neq \beta'$, are very weakly damped. With the matrix elements $G_{\lambda,\beta,\beta'\mathbf{p}}$ from Appendix C.1.2, these correlations would decay on a time scale that is three orders of magnitude larger than for the coherent quantities. Our numerical calculations indicate that this is sufficient to turn the marginally negative luminescence at the B resonance positive while barely changing the luminescence at the A resonance. This result shows that only a fully consistent dephasing scheme ensures strictly positive steady-state luminescence.
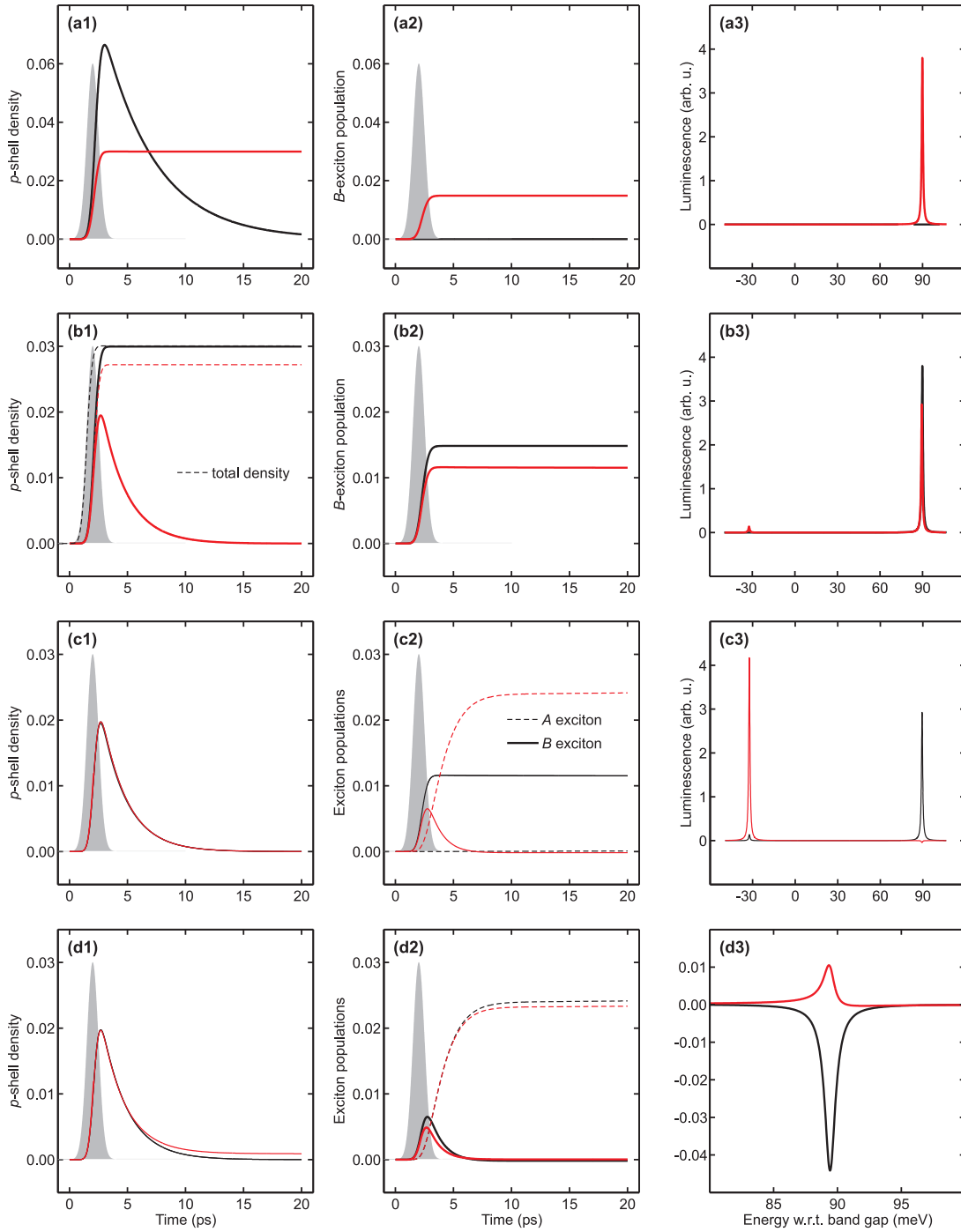
Figure 16: Switch-on analysis for the phonon-related processes in a quantum dot. The shaded areas indicate the envelope of the exciting light pulse. See the text at the end of Sec. 3.4.2 for a detailed discussion.

We conclude the discussion with a numerical switch-on analysis that clearly demonstrates the influence of the different phonon-related phenomena on the excitation level of the quantum-dot system. Deviating from the previous examples, we now assume optical pumping of the initially unexcited dot resonantly with the B exciton. Starting from the phonon-free case, we successively implement (a) the phonon-induced build-up of excitonic population, (b) the thermalization of densities, (c) the thermalization of excitonic populations, and (d) the damping of the exchange terms by switching on the corresponding terms in the equations of motion as identified above. In each row of Fig. 16, black and red curves represent the situation before and after the switch-on, respectively. The time scales for dephasing and thermalization are chosen so as to emphasize the considered phenomena. Without electron-phonon coupling, the excited polarization is only subject to dipole radiation but not to dephasing (except for the very weak excitation-induced dephasing). As a result, the energy that the light pulse has pumped into the carrier system is completely emitted again such that the system returns to its ground state. For the present analysis, we have added the classical radiative decay phenomenologically. The wave equation for the **E** field would have to be solved simultaneously with the SBE to calculate the dipole emission self-consistently.[5] When the dephasing model (3.105)–(3.109) is included, there is an additional decay channel for the polarization such that incoherent quantities do not decay completely anymore, see frame (a1). The energy transfer from the coherent polarization leads to a considerable build-up of B-exciton population (a2). Luminescence is observed at the B resonance (a3). After switching on the collision integral (3.113), the densities (b1) but not the excitonic populations (b2) thermalize. Some luminescence at the first excitonic resonance is observed while the emission at the B resonance slightly decreases (b3). With the class-II contributions to the triplet scattering terms $\Delta\langle\hat{D}\hat{a}^\dagger\hat{a}^\dagger\hat{a}\hat{a}\rangle$ (row (c)), also the excitonic populations thermalize (c2). This results in a strong luminescence signal at the A resonance while the emission at the B resonance becomes slightly negative (c3). Finally, the damping of excitonic correlations with non-vanishing kinetic terms leads to a certain redistribution of densities (d1) and populations (d2) from the major to the minor resonance. Consequently, the luminescence at the B resonance becomes positive again (d3).

The full inclusion of the electron-phonon scattering is computationally rather demanding. As a general tendency, the small number of degrees of freedom in a dot system makes the cluster-expansion analysis more sensitive to numerical errors and analytical approximations. For the examples in Fig. 16, we have chosen equal electron and hole masses to achieve better convergence of the numerical solutions.

3.5 Exciton-biexciton pumping

Conceptually, the exciton can be introduced as a single-pair state with minimum energy. For two electron-hole pairs, such an approach defines the *biexciton* that can roughly be interpreted as an exciton molecule. The energy of a biexciton is reduced with respect to the sum of the two exciton energies by the biexciton binding energy $\Delta\mathcal{E}$. In this section, we present a possible technical application of that energy mismatch. The aim is to develop a practical material system where the presence of a control field at a certain wavelength induces strong absorption of a signal field at another wavelength. Such a system could be used as basic component of a wide range of all-optical devices that are covered by the term *Zeno-based optoelectronics* [124]. We propose a design where the signal field is resonant with the exciton-to-biexciton transition while the control field is resonant with the transition from the ground state to the exciton state of a semiconductor quantum dot. Provided that the spectral overlap between the two fields is

---

[5]A simplified treatment of this coupled system of differential equations will be outlined in Sec. 3.5.1.

small, we expect that the signal field can only be absorbed efficiently if also the control field is switched on.

To model the properties of our device, we use a slightly different theoretical approach than in the previous sections. We assume that the dot contains at most two electron-hole pairs. One can then employ a matrix-diagonalization method [20, 125] to express the quantum-dot Hamiltonian in terms of projection operators on the ground state, the exciton states, and the biexciton states. In that basis, the semi-classical optical Bloch equations are closed on the singlet level. The model system is introduced explicitly in Sec. 3.5.1. We then define a figure of merit for the operation of the device and calculate how it depends on the system parameters in Sec. 3.5.2.

3.5.1 Physical realization

We consider an ensemble of identical quantum dots with sheet density n_{QD} on a planar wetting layer. For simplicity, we restrict the analysis to the lowest exciton and biexciton states. In other words, each dot is treated as a three-level system with ground state $|0\rangle$, exciton state $|1\rangle$, and biexciton state $|2\rangle$ that are normalized and pairwise orthogonal. The total Hamiltonian [20,125] has the form

$$\hat{H} = \hat{H}_0 + \hat{H}_{\mathrm{D}}. \tag{3.114}$$

The material Hamiltonian reads

$$\hat{H}_0 = \sum_{\nu=0}^{2} \varepsilon_\nu |\nu\rangle\langle\nu| \tag{3.115}$$

where $\varepsilon_0 = 0$ while the exciton and biexciton energies are $\varepsilon_1 = \mathcal{E}_1$ and $\varepsilon_2 = 2\mathcal{E}_1 - \Delta\mathcal{E}$, respectively. Coupling to the classical light field is described by the dipole Hamiltonian $\hat{H}_{\mathrm{D}} = -\hat{P}E$ with the total polarization operator[6]

$$\hat{P} = n_{\mathrm{QD}}\big(d_1|0\rangle\langle1| + d_2|1\rangle\langle2| + \mathrm{H.C.}\big). \tag{3.116}$$

The classical light field

$$E(t) = E_{\mathrm{S}}(t) + E_{\mathrm{C}}(t) + E_{\mathrm{mat}}(t) \tag{3.117}$$

contains the signal field $E_{\mathrm{S}}(t) \propto \cos(\varepsilon_2 - \varepsilon_1)t/\hbar$, the control field $E_{\mathrm{C}}(t) \propto \cos\varepsilon_1 t/\hbar$, and the material response $E_{\mathrm{mat}}(t)$. If the analysis is not restricted to low dot densities, E_{mat} has to be included. For a self-consistent calculation, the equations of motion for the dot system must be solved simultaneously with the wave equation for the electric field. Under the simplifying assumption of a constant background refractive index n, one can show [126] that

$$E_{\mathrm{mat}}(t) = -\frac{\mu_0 c}{2n}\dot{P}(t) \tag{3.118}$$

with the expectation value of the total polarization $P(t) = \langle\hat{P}(t)\rangle$.

To determine the dynamics of the three-level system, we derive the Heisenberg equations of motion for the single-particle operators

$$\hat{p}_{\nu,\nu'} \equiv |\nu\rangle\langle\nu'|. \tag{3.119}$$

---

[6]Contrary to Eq. (3.116), the polarization operator (3.18) does not contain the dot density because such a definition makes no sense for a single dot.

The corresponding expectation values are densities $f_\nu \equiv \langle \hat{p}_{\nu,\nu} \rangle$ for $\nu = \nu'$ and microscopic polarizations $p_{\nu,\nu'} \equiv \langle \hat{p}_{\nu,\nu'} \rangle$ for $\nu \neq \nu'$. The optical Bloch equations take the form

$$i\hbar \frac{\mathrm{d}}{\mathrm{d}t} f_0 = -2\mathrm{i} \operatorname{Im}\left[d_1 E^{(+)} p_{1,0}^* \right], \tag{3.120}$$

$$i\hbar \frac{\mathrm{d}}{\mathrm{d}t} f_1 = 2\mathrm{i} \operatorname{Im}\left[d_1 E^{(+)} p_{1,0}^* - d_2 E^{(+)} p_{2,1}^* \right], \tag{3.121}$$

$$i\hbar \frac{\mathrm{d}}{\mathrm{d}t} f_2 = 2\mathrm{i} \operatorname{Im}\left[d_2 E^{(+)} p_{2,1}^* \right], \tag{3.122}$$

$$i\hbar \frac{\mathrm{d}}{\mathrm{d}t} p_{1,0} = -\left(\varepsilon_1 + \mathrm{i}\gamma_{1,0}\right) p_{1,0} - d_1 E^{(+)} \left(f_1 - f_0 \right) + d_2 \left[E^{(+)} \right]^* p_{2,0}, \tag{3.123}$$

$$i\hbar \frac{\mathrm{d}}{\mathrm{d}t} p_{2,1} = -\left(\varepsilon_2 - \varepsilon_1 + \mathrm{i}\gamma_{2,1}\right) p_{2,1} - d_2 E^{(+)} \left(f_2 - f_1 \right) - d_1 \left[E^{(+)} \right]^* p_{2,0}, \tag{3.124}$$

$$i\hbar \frac{\mathrm{d}}{\mathrm{d}t} p_{2,0} = -\left(\varepsilon_2 + \mathrm{i}\gamma_{2,0}\right) p_{2,0} - d_1 E^{(+)} p_{2,1} + d_2 E^{(+)} p_{1,0} \tag{3.125}$$

where we have added phenomenological dephasing terms with positive constants $\gamma_{\nu,\nu'}$. In rotating-wave approximation, only the co-rotating part $E^{(+)}$ of the electric field enters the equations of motion, see Sec. 3.2.1. More explicitly, $E^{(+)} = E_\mathrm{S}^{(+)} + E_\mathrm{C}^{(+)} + E_\mathrm{mat}^{(+)}$ where $E_\mathrm{S}^{(+)} \propto \mathrm{e}^{\mathrm{i}(\varepsilon_2 - \varepsilon_1)t/\hbar}$, $E_\mathrm{C}^{(+)} \propto \mathrm{e}^{\mathrm{i}\varepsilon_1 t/\hbar}$, and $E_\mathrm{mat}^{(+)} \propto \dot{P}^{(+)}$. The macroscopic polarization P can be expressed in terms of the microscopic polarizations $p_{\nu,\nu'}$ via

$$P^{(+)}(t) = 2 n_\mathrm{QD} \left[d_1^* p_{1,0}(t) + d_2^* p_{2,1}(t) \right]. \tag{3.126}$$

As a further simplification, we replace $\dot{p}_{1,0}$ by $\mathrm{i}\varepsilon_1 p_{1,0}/\hbar$ and $\dot{p}_{2,1}$ by and $\mathrm{i}(\varepsilon_2 - \varepsilon_1) p_{2,1}/\hbar$ when evaluating the time derivative $\dot{P}^{(+)}$.

3.5.2 Figure of merit

The proposed scheme is tested using a quasi continuous-wave signal that is switched on adiabatically and a Gaussian pulsed control with a 1 MHz repetition rate. The spectral width of the control pulses is four orders of magnitudes smaller than the detuning between control and signal such that there is practically no spectral overlap between the two pump fields. We use material parameters that are typical for CdSe-based quantum dots, see Tab. 2. Frame (a) of Fig. 17 shows the dynamics of the generated biexciton population f_2 for a signal intensity of $4.1\,\mu\mathrm{W}/\mu\mathrm{m}^2$ and a cycle-averaged control intensity of $0.038\,\mu\mathrm{W}/\mu\mathrm{m}^2$. These values are within the specifications given in Ref. [124]. The bright and the dark shaded areas represent the envelopes of signal and control, respectively. We find that the signal field alone does not lead to an appreciable excitation level (dashed line). Signal and control together produce large biexciton population (solid line).

As a figure of merit for the device, we suggest to use the signal contrast, i.e. the ratio of the material absorption at the exciton-to-biexciton transition with and without control pulse. We show in the following how this quantity can be calculated from the numerical solution of the equations of motion. In the wetting-layer plane, the reflected and transmitted fields are given by

$$E_\mathrm{R}(t) = E_\mathrm{mat}(t), \tag{3.127}$$

$$E_\mathrm{T}(t) = E_\mathrm{S}(t) + E_\mathrm{C}(t) + E_\mathrm{mat}(t), \tag{3.128}$$

Quantity	Symbol	Value	Source
Dipole moments	d_1	$5.6\,\text{Å}e$	[127]
	d_2	$5.6\,\text{Å}e$	[127]
Dephasing constants	$\gamma_{1,0}$	$1.0\,\text{meV}$	[128]
	$\gamma_{2,1}$	$1.0\,\text{meV}$	[128]
	$\gamma_{2,0}$	$2.0\,\text{meV}$	[128]
Exciton energy	$\mathcal{E}_1$	$2.3\,\text{eV}$	[129]
Biexciton binding energy	$\Delta\mathcal{E}$	$20.0\,\text{meV}$	[129]
Dot density	n_{QD}	$10^{12}\,\text{cm}^{-2}$	

Table 2: Material parameters for CdSe-based quantum dots
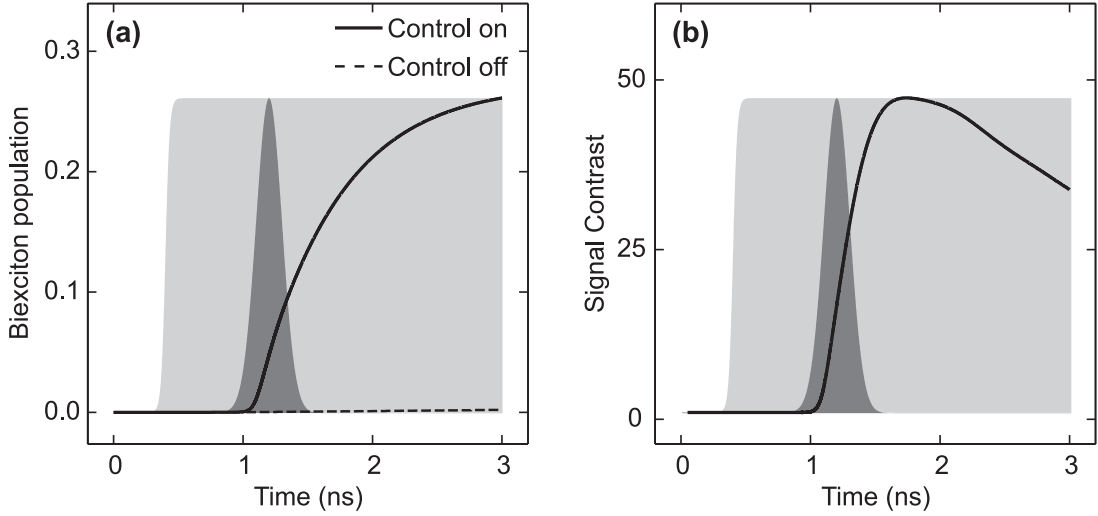
Figure 17: Operation of the Zeno device. Frame (a) shows the dynamics of the biexciton population f_2 with (solid line) and without (dashed line) control pulse. The signal contrast $C(t)$ is plotted in frame (b) (solid line). The bright and dark shaded areas indicate the envelopes of signal and control, respectively.
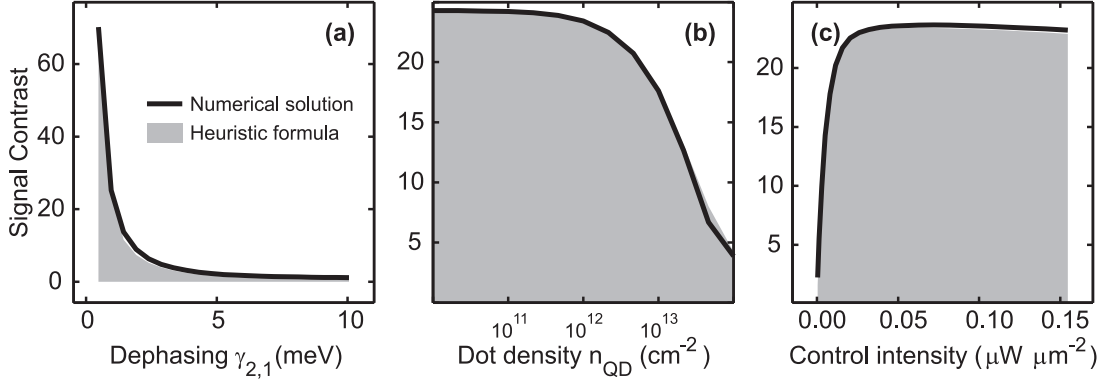
Figure 18: Dependence of the maximal signal contrast of the Zeno device on (a) the dephasing constant for the exciton-biexciton transition, (b) the dot density, and (c) the control-pulse intensity. The solid lines represent the results from the full numerical calculation. For the shaded areas, we have used the heuristic formula (3.139) with a constant correction factor.

respectively. We use the incomplete Fourier transform

$$F(\omega, t) \equiv \int_{-\infty}^{t} F(t') e^{-i\omega t'} \, dt' \tag{3.129}$$

to define time-dependent reflection, transmission, and absorption coefficients

$$R(\omega, t) \equiv \frac{E_R(\omega, t)}{E_0(\omega, t)}, \tag{3.130}$$

$$T(\omega, t) \equiv \frac{E_T(\omega, t)}{E_0(\omega, t)}, \tag{3.131}$$

$$\alpha(\omega, t) \equiv 1 - |R(\omega, t)|^2 - |T(\omega, t)|^2, \tag{3.132}$$

respectively. In order to quantify the absorption at the exciton-biexciton transition, we introduce $\tilde{\alpha}(t) \equiv \alpha(\omega = \omega_S, t)$ where $\omega_S \equiv (E_2 - E_1)/\hbar$ denotes the central frequency of the signal pulse. We can now define the signal contrast as

$$C(t) \equiv \frac{\tilde{\alpha}_{\mathrm{on}}(t)}{\tilde{\alpha}_{\mathrm{off}}(t)} \tag{3.133}$$

where $\tilde{\alpha}_{\mathrm{on}}(t)$ and $\tilde{\alpha}_{\mathrm{off}}(t)$ are the absorption coefficients in the presence and in the absence of the control pulse, respectively. For the parameters given above, the dynamics of $C(t)$ is shown in the right frame of Fig. 17. The signal contrast reaches a maximum value C_{max} of roughly 50. We can use C_{max} to characterize the operation of the device by a single figure of merit. Fig. 18 shows how the maximum signal contrast depends on the system parameters (solid lines). For each frame, one of the parameters is swept while the others are kept constant as given in Tab. 2. Based on these results, we propose the following device design: The dephasing constant for the exciton-to-biexciton transition should be smaller than $1 \, \mathrm{meV}$ (a). The dot density should be below $10^{12} \, \mathrm{cm}^{-2}$ (b). The control-field intensity should exceed $0.02 \, \mu\mathrm{W}/\mu\mathrm{m}^2$ (c). Moreover, we find that the device should work equally well for a large range of control-pulse durations.

We conclude the analysis by deriving a simple analytical result that relates the signal contrast to the population inversion at the exciton-to-biexciton transition. We start by observing that

$|p_{2,0}| \ll |p_{1,0}|, |p_{2,1}|$ during the optical excitation. When $p_{2,0}$ is neglected completely, the optical Bloch equations for $p_{1,0}$ and $p_{2,1}$ can easily be solved analytically in the frequency domain under the assumption that the densities are stationary. Analogously to Sec. 3.2.1, this procedure finally yields the linear susceptibility of the dot ensemble

$$\chi(\omega) \equiv \frac{P(\omega)}{\epsilon_0 E(\omega)} = \frac{n_{\mathrm{QD}}}{\epsilon_0} \left[\frac{(f_0 - f_1)|d_1|^2}{\mathcal{E}_1 - \hbar\omega - \mathrm{i}\gamma_{1,0}} + \frac{(f_1 - f_2)|d_2|^2}{\mathcal{E}_2 - \mathcal{E}_1 - \hbar\omega - \mathrm{i}\gamma_{2,1}} \right]. \tag{3.134}$$

As mentioned in Sec. 3.2.3, $\alpha(\omega) \propto \omega \mathrm{Im}\chi(\omega)$ when the radiative polarization dephasing can be neglected. In the present analysis, however, the material response and thus the dipole radiation are evaluated self-consistently. The absorption spectrum can then be calculated from [7]

$$\alpha(\omega) = \frac{2\mathrm{Im}\xi(\omega)}{1 + |\xi(\omega)|^2 + 2\mathrm{Im}\xi(\omega)} \tag{3.135}$$

where $\xi(\omega) \equiv \omega\chi(\omega)/2nc$. Before the control pulse arrives, we have $f_0 \simeq 1$ and $f_1 \simeq 0 \simeq f_2$ such that the absorption at the signal frequency is given by

$$\alpha_{\mathrm{off}}(\omega_{\mathrm{S}}) \simeq \frac{2\gamma_{1,0}\Gamma_{\mathrm{rad}}}{(\mathcal{E}_1 - \hbar\omega_{\mathrm{S}})^2 + (\gamma_{1,0} + \Gamma_{\mathrm{rad}})^2} \tag{3.136}$$

with the radiative coupling constant

$$\Gamma_{\mathrm{rad}} \equiv \frac{1}{2} \frac{|d_1|^2}{\epsilon_0} \frac{\omega_{\mathrm{S}}}{nc} n_{\mathrm{QD}}. \tag{3.137}$$

In the presence of the control, the phase-space filling factor $f_1 - f_2$ becomes considerable. Here, we can neglect the first term in Eq. (3.134) because the biexcitonic binding energy $\Delta\mathcal{E} = \mathcal{E}_1 - \hbar\omega_{\mathrm{S}}$ exceeds the dephasing constants $\gamma_{1,0}$, $\gamma_{2,1}$ by one order of magnitude. Thus, the absorption at $\omega = \omega_{\mathrm{S}}$ becomes

$$\alpha_{\mathrm{on}}(\omega_{\mathrm{S}}) \simeq \frac{2\gamma_{2,1}\Gamma_{\mathrm{rad}} \left| \frac{d_2}{d_1} \right|^2 (f_1 - f_2)}{\left[\gamma_{2,1} + \Gamma_{\mathrm{rad}} \left| \frac{d_2}{d_1} \right|^2 (f_1 - f_2) \right]^2}. \tag{3.138}$$

Combining these two results, we obtain

$$\tilde{C} \equiv \frac{\alpha_{\mathrm{on}}(\omega_{\mathrm{S}})}{\alpha_{\mathrm{off}}(\omega_{\mathrm{S}})} \simeq \frac{\Delta\mathcal{E}^2 + (\gamma_{1,0} + \Gamma_{\mathrm{rad}})^2}{(\gamma_{1,0} + Q\Gamma_{\mathrm{rad}})^2} Q \tag{3.139}$$

with

$$Q \equiv \frac{\gamma_{1,0}}{\gamma_{2,1}} \left| \frac{d_2}{d_1} \right|^2 (f_1 - f_2) \tag{3.140}$$

where f_1 and f_2 are the exciton and biexciton population, respectively, after the control pulse has been absorbed.

This simplified analysis treats the densities after the arrival of the control pulse as stationary quantities, which is not confirmed by the full numerical solution. It turns out, however, that we can compensate for this fact by introducing a correction factor η between the actual figure of merit C_{max} and the heuristic signal contrast $\tilde{C}$ such that $C_{\mathrm{max}} = \eta\tilde{C}$. As demonstrated by the shaded areas in Fig. 18, we achieve quantitative agreement with the numerical results throughout the entire parameter space for the choice $\eta = 0.66$ if we take f_1 and f_2 at the time when $C(t)$ reaches C_{max}.

4 Phonon sidebands in the luminescence spectrum

This chapter is organized as follows. In Sec. 4.1, we qualitatively discuss the microscopic processes that lead to phonon-assisted photoemission. The existing theory is briefly reviewed in Sec. 4.2. We present our cluster-expansion analysis of the first replicum in Sec. 4.3. Finally, higher-order sidebands are considered in Sec. 4.4.

The majority of the material in Secs. 4.3.3.3, 4.4.2, 4.4.3.2, and 4.4.3.3 has been published in Refs. [II] and [III] of the author's publications list.

4.1 Generic features of sideband emission

Phonon-assisted luminescence is based on microscopic processes where electron-hole pairs recombine under the emission of a photon and the simultaneous emission or absorption of a number of phonons. The participation of long-wavelength optical phonons that have constant dispersion gives rise to a series of additional resonances in the luminescence spectrum that are detuned from the excitonic resonance by an integer multiple of the optical phonon energy $\hbar\Omega$. When the electron-phonon interaction is sufficiently strong, these resonances can be observed as replica of the exciton peak that are commonly referred to as *phonon sidebands* while the exciton peak is called *zero-phonon line* in this context. More explicitly, it follows from the energy conservation that recombination processes involving the creation of n and the annihilation of m optical phonons contribute to the replicum at detuning $\Delta\omega = (m - n)\Omega$ from the zero-phonon line. In the minimal-order processes that yield the main contribution to the n-th sideband on the low-(high-)energy side of the exciton peak, exactly n phonons are emitted (absorbed). Because $\hbar\Omega$ is usually large on the scale of thermal energies, only few optical phonons will be present even at higher temperatures. Hence, pronounced phonon sidebands can only be found on the low-frequency side of the zero-phonon line in most luminescence experiments. This situation is illustrated in Fig. 19 where a blue and a gray ball represent an electron-hole pair and yellow and magenta lines indicate photon and phonon energies, respectively. The acronyms ZPL for the zero-phonon line and PSB_n for the n-th phonon sideband are commonly used in the literature. Typically, the intensity decreases rapidly with increasing sideband index n although a non-monotonous behavior might occur for very strong electron-phonon coupling as considered, e.g., in Sec. 4.4.3.3. The zero-phonon line mainly involves processes without phonons such that the photons receive directly the center-of-mass momenta of the electron-hole pairs. When a photon has energy $\hbar\omega_{\mathbf{q}}$, the absolute value of its wave vector $\mathbf{q}$ is also fixed via the dispersion relation $\omega_{\mathbf{q}} = c_0|\mathbf{q}|$. For photon energies of the order of the band gap, $|\mathbf{q}|$ is very small. Consequently, only electron-hole pairs with nearly vanishing center-of-mass momenta contribute to the zero-phonon line. On the other hand, the phonons may carry arbitrary momenta. The center-of-mass energy of the electron-hole pairs can thus vary considerably when they contribute to the sideband luminescence. This can be observed as asymmetric broadening of sideband peaks for elevated temperatures, as indicated by the yellow shaded peaks in Fig. 19. We will discuss in the following sections how these generic features of sideband luminescence
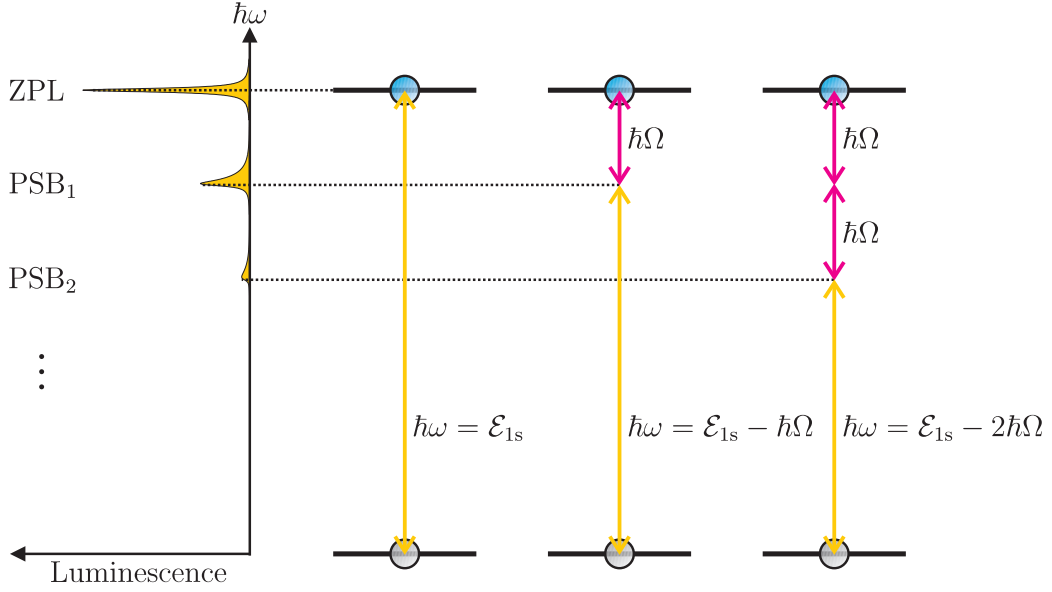
Figure 19: Schematic picture of LO-phonon assisted luminescence. The zero-phonon line (ZPL) is located at the excitonic resonance $\mathcal{E}_{1s}$. Participation of n LO phonons with energy $\hbar\Omega$ each leads to emission at photon energy $\hbar\omega = \mathcal{E}_{1s} - n\hbar\Omega$ when an electron-hole pair with vanishing center-of-mass momentum $\hbar\mathbf{Q}$ recombines. In case $\mathbf{Q} \neq \mathbf{0}$, the recombination process contributes to the high-energy tail of the n-th phonon sideband (PSB$_n$).

emerge from the microscopic description of LO-phonon assisted luminescence.

4.2 Perturbational approach to the phonon-sideband problem

There exists a well-established perturbational treatment of the phonon-sideband problem that was already developed in the 1970s [49] and is widely used in the literature till the present day. This theory describes the excited states of the carrier system purely in terms of excitons.[1] Emission processes contributing to the n-th sideband are viewed as series of n consecutive exciton-phonon scattering processes followed by recombination from inside the radiative cone. With this approach, the n-th term of the perturbation series yields the n-th replicum.

When we translate the results from Ref. [49] into our notation, the luminescence intensity of the n-th sideband of the excitonic resonance ν takes the form

$$I_{\text{PL},\nu}^{(n)}(\omega) \propto \sum_{\mathbf{Q}} W_\nu^{(n)}(\mathbf{Q}) \Delta N_\nu(\mathbf{Q}) \delta\big(E_\nu(\mathbf{Q}) - n\hbar\Omega - \hbar\omega\big). \tag{4.1}$$

Here, $E_\nu(\mathbf{Q})$ and $\Delta N_\nu(\mathbf{Q})$ denote the energy and the population, respectively, of the exciton state $(\nu, \mathbf{Q})$ with quantum number ν and center-of-mass momentum $\hbar\mathbf{Q}$ while $W_\nu^{(n)}(\mathbf{Q})$ stands for the probability that such an exciton recombines radiatively under the assistance of n phonons. More explicitly, the perturbational approach assumes that the exciton $(\nu, \mathbf{Q})$ is phonon-scattered through a series of intermediate states $(\nu_1, \mathbf{Q}_1), \ldots, (\nu_{n-1}, \mathbf{Q}_{n-1})$ until it

---

[1]We will introduce the corresponding Hamiltonian later in Sec. 4.4.1.

reaches a state $(\nu_n, \mathbf{Q}_n \simeq \mathbf{0})$ within the radiative cone from which it recombines. The probability $W_\nu^{(n)}(\mathbf{Q})$ thus follows from the scattering cross-section

$$W_\nu^{(n)}(\mathbf{Q}) = \sum_{\mathbf{Q}_1,\ldots,\mathbf{Q}_{n-1}} |A_\nu^{(n)}(\mathbf{Q}_1,\ldots,\mathbf{Q}_{n-1};\mathbf{Q})|^2 \tag{4.2}$$

where

$$A_\nu^{(n)}(\mathbf{Q}_1,\ldots,\mathbf{Q}_{n-1};\mathbf{Q}) = \sum_{\nu_1,\ldots,\nu_{n-1},\nu_n} f_{\nu_n} \frac{G_{\mathbf{Q}-\mathbf{Q}_1}^{\nu,\nu_1}}{E_\nu(\mathbf{Q}) - \hbar\Omega - E_{\nu_1}(\mathbf{Q}_1)}$$

$$\times \cdots \times \frac{G_{\mathbf{Q}_{n-2}-\mathbf{Q}_{n-1}}^{\nu_{n-2},\nu_{n-1}}}{E_\nu(\mathbf{Q}) - (n-1)\hbar\Omega - E_{\nu_{n-1}}(\mathbf{Q}_{n-1})} \frac{G_{\mathbf{Q}_{n-1}}^{\nu_{n-1},\nu_n}}{E_\nu(\mathbf{Q}) - n\hbar\Omega - E_{\nu_n}(\mathbf{0})}. \tag{4.3}$$

In this formula, $|f_\nu|^2$ denotes the oscillator strength for the radiative annihilation of exciton $(\nu, \mathbf{Q} \simeq \mathbf{0})$, that is $|f_\nu|^2 = |\mathcal{F}\phi_\nu(\mathbf{r} = \mathbf{0})|^2$ with the excitonic wave function $\phi_\nu(\mathbf{r})$ and the light-matter interaction matrix element $\mathcal{F}$ defined below. The scattering matrix elements $G_\mathbf{Q}^{\nu,\nu'}$ determine the strength of the electron-phonon coupling. They are related to the electron-phonon coupling parameters $G_{\mathrm{c},\mathbf{Q}}$, $G_{\mathrm{v},\mathbf{Q}}$ via [130]

$$G_\mathbf{Q}^{\nu,\nu'} = \frac{1}{\mathscr{L}^3} \int \phi_\nu^*(\mathbf{r})\phi_{\nu'}(\mathbf{r}) \left(G_{\mathrm{c},\mathbf{Q}} e^{-i\mathbf{Q}_\mathrm{h}\cdot\mathbf{r}} - G_{\mathrm{v},\mathbf{Q}} e^{i\mathbf{Q}_\mathrm{e}\cdot\mathbf{r}} \right) d^3r \tag{4.4}$$

where $\mathbf{Q}_{\mathrm{e/h}} \equiv m_{\mathrm{e/h}}\mathbf{Q}/M$ with the exciton mass $M \equiv m_\mathrm{e} + m_\mathrm{h}$.[2] Usually, only the Fröhlich part of $G_{\lambda,\mathbf{Q}}$ is taken into account. In typical photoluminescence experiments, only the replica of the lowest excitonic resonance $\nu = 1\mathrm{s}$ can be detected. Due to the high oscillator strength $|f_{1\mathrm{s}}|^2$, the excitons $(1\mathrm{s}, \mathbf{Q})$ mainly recombine through the final exciton state $(1\mathrm{s}, \mathbf{0})$ such that the ν_n sum in Eq. (4.3) can often be restricted to $\nu_n = 1\mathrm{s}$.

In this work, we will reconsider and generalize the existing theory in several aspects, as already mentioned in the introductory chapter. In particular, we will analyze whether also uncorrelated electron-hole plasma can participate in LO-phonon-assisted luminescence, we will have a closer look at the carrier-phonon interaction, and we will discuss a practical way to evaluate arbitrary-order phonon sidebands.

4.3 First phonon sideband

Interacting electrons, photons, and phonons in a semiconductor material can be treated fully quantum mechanically with the general system Hamiltonian

$$\hat{H} = \hat{H}_\mathrm{el} + \hat{H}_\mathrm{vib} + \hat{H}_\mathrm{em} + \hat{H}_{\mathrm{el}-\mathrm{el}} + \hat{H}_{\mathrm{el}-\mathrm{vib}} + \hat{H}_{\mathrm{el}-\mathrm{em}} \tag{4.5}$$

as derived in Secs. 2.2 and 2.3. For notational convenience, we first restrict the analysis to the bulk case. The corresponding results for confined systems will then be given in Appendix F.4. The contributions $\hat{H}_\mathrm{el}$, $\hat{H}_\mathrm{vib}$, and $\hat{H}_\mathrm{em}$ from free Bloch electrons, phonons, and photons are defined in Eqs. (2.89), (2.32), and (2.86), respectively. Coulomb interaction, electron-phonon interaction and light-matter coupling follow from the Hamiltonians $\hat{H}_{\mathrm{el}-\mathrm{el}}$, $\hat{H}_{\mathrm{el}-\mathrm{vib}}$, and $\hat{H}_{\mathrm{el}-\mathrm{em}}$, respectively, as defined in Eqs. (2.92), (2.66)+(2.71), and (2.104). We exclusively

---

[2]These matrix elements will be explicitly evaluated in Sec. 4.4.1.2 and Appendix E.3.

consider optical phonons since acoustic modes can lead to broadening of the exciton peak but do not create well-defined phonon replica. It will prove useful to introduce dimensionless matrix elements $g_{\lambda,\mathbf{p}} \equiv G_{\lambda,\mathbf{p}}/\hbar\Omega$. The interaction Hamiltonian then takes the form

$$\hat{H}_{\mathrm{el-phon}} = \sum_{\lambda,\mathbf{k},\mathbf{p}} \hbar\Omega g_{\lambda,\mathbf{p}} \hat{a}_{\lambda,\mathbf{k}-\mathbf{p}}^{\dagger} \hat{a}_{\lambda,\mathbf{k}} \left(\hat{D}_{-\mathbf{p}} + \hat{D}_{\mathbf{p}}^{\dagger} \right) \tag{4.6}$$

where the $\mathbf{p}$ sum extends over all LO modes and $g_{\lambda,\mathbf{p}}$ can follow from both Fröhlich and optical deformation-potential coupling. Here and in the following, we use an implicit notation where the phonon branch α, the photon polarization κ, and the electron spin σ are absorbed in the phonon wave-vector $\mathbf{p}$, the photon wave-vector $\mathbf{q}$, and the band index λ, respectively.

As discussed in Sec. 4.1, luminescence at the excitonic resonance is mainly due to radiative recombination of electron-hole pairs without phonon participation. Such processes are related to photon-assisted polarizations, that is to two-particle correlations of the form $\Delta\langle \hat{B}^{\dagger} \hat{a}_{\mathrm{v}}^{\dagger} \hat{a}_{\mathrm{c}} \rangle$. In order to evaluate these quantities, it is sufficient to perform the cluster expansion up to the singlet-doublet level. A full numerical solution is feasible in this case for semiconductor hetero structures of reduced spatial dimensionality [7]. However, in order to calculate the emission at the n-th phonon replicum on the low-energy side of the zero-phonon line, at least the $(n+2)$-particle correlations $\Delta\langle \hat{B}^{\dagger} \hat{D}^{\dagger} \cdots \hat{D}^{\dagger} \hat{a}_{\mathrm{v}}^{\dagger} \hat{a}_{\mathrm{c}} \rangle$ including n phonon creators have to be evaluated. Already for the first phonon sideband, clusters up to the triplet level are thus required. The inclusion of all terms emerging from the cluster-expansion scheme would then exceed the resources of current supercomputers when realistic model systems are considered. We therefore have to simplify our approach by additional approximations. In this section, we include only a physically relevant subset of the factorization terms. Truncation on the triplet level then allows to calculate the first replicum. Higher-order sidebands will be considered in Sec. 4.4.

4.3.1 Phonon-assisted semiconductor luminescence equations

The luminescence spectrum in the incoherent regime has already been defined in Sec. 3.3.2 as

$$I_{\mathrm{PL}}(\omega_{\mathbf{q}}) = \frac{\mathrm{d}}{\mathrm{d}t} \Delta\langle \hat{B}_{\mathbf{q}}^{\dagger} \hat{B}_{\mathbf{q}} \rangle. \tag{4.7}$$

In the bulk case, the photon flux follows from

$$\frac{\mathrm{d}}{\mathrm{d}t} \Delta\langle \hat{B}_{\mathbf{q}}^{\dagger} \hat{B}_{\mathbf{q}} \rangle = \frac{2}{\hbar} \operatorname{Re}\Big[\mathcal{F}_{\mathbf{q}}^{*} \sum_{\mathbf{k}} \Pi^{(0)}(\mathbf{k};\mathbf{q}) \Big] \tag{4.8}$$

where we have introduced the abbreviation $\mathcal{F}_{\mathbf{q}} \equiv \mathcal{E}_{\mathbf{q}} \boldsymbol{\varepsilon}_{\mathbf{q}} \cdot \mathbf{d}_{\mathrm{c,v}}/\sqrt{\mathscr{L}^3}$. The equations of motion for the photon-assisted polarizations $\Pi^{(0)}(\mathbf{k};\mathbf{q}) \equiv \Delta\langle \hat{B}_{\mathbf{q}}^{\dagger} \hat{a}_{\mathrm{v},\mathbf{k}-\mathbf{q_h}}^{\dagger} \hat{a}_{\mathrm{c},\mathbf{k}+\mathbf{q_e}} \rangle$ read

$$\left(\mathrm{i}\hbar \frac{\mathrm{d}}{\mathrm{d}t} + \hbar\omega_{\mathbf{q}} \right) \Pi^{(0)}(\mathbf{k};\mathbf{q}) = \sum_{\mathbf{k}'} A_{\mathbf{k},\mathbf{k}'}(\mathbf{q}) \Pi^{(0)}(\mathbf{k}';\mathbf{q})$$

$$+ \mathrm{i}\mathcal{F}_{\mathbf{q}} \Big(f_{\mathbf{k}+\mathbf{q_e}}^{\mathrm{e}} f_{\mathbf{k}-\mathbf{q_h}}^{\mathrm{h}} + \sum_{\mathbf{k}'} \Delta\langle \hat{a}_{\mathrm{c},\mathbf{k}'+\mathbf{q_e}}^{\dagger} \hat{a}_{\mathrm{v},\mathbf{k}-\mathbf{q_h}}^{\dagger} \hat{a}_{\mathrm{c},\mathbf{k}+\mathbf{q_e}} \hat{a}_{\mathrm{v},\mathbf{k}'-\mathbf{q_h}} \rangle \Big)$$

$$+ \hbar\Omega \sum_{\mathbf{p}} \Big[g_{\mathrm{c},\mathbf{p}} \Delta\langle \hat{B}_{\mathbf{q}}^{\dagger} (\hat{D}_{-\mathbf{p}} + \hat{D}_{\mathbf{p}}^{\dagger}) \hat{a}_{\mathrm{v},(\mathbf{k}+\mathbf{p_h})-(\mathbf{q}+\mathbf{p})_{\mathrm{h}}}^{\dagger} \hat{a}_{\mathrm{c},(\mathbf{k}+\mathbf{p_h})+(\mathbf{q}+\mathbf{p})_{\mathrm{e}}} \rangle$$

$$- g_{\mathrm{v},\mathbf{p}} \Delta \langle \hat{B}_{\mathbf{q}}^{\dagger} (\hat{D}_{-\mathbf{p}} + \hat{D}_{\mathbf{p}}^{\dagger}) \hat{a}_{\mathrm{v},(\mathbf{k}-\mathbf{p}_{\mathrm{e}})-(\mathbf{q}+\mathbf{p})_{\mathrm{h}}}^{\dagger} \hat{a}_{\mathrm{c},(\mathbf{k}-\mathbf{p}_{\mathrm{e}})+(\mathbf{q}+\mathbf{p})_{\mathrm{e}}} \rangle \Big]$$

$$+ \Theta_{\mathrm{st}}^{(0)}(\mathbf{k};\mathbf{q}) + \Theta_{\mathrm{sc}}^{(0)}(\mathbf{k};\mathbf{q}) \tag{4.9}$$

with electron densities $f_{\mathbf{k}}^{\mathrm{e}} \equiv \langle \hat{a}_{\mathrm{c},\mathbf{k}}^{\dagger} \hat{a}_{\mathrm{c},\mathbf{k}} \rangle$ and hole densities $f_{\mathbf{k}}^{\mathrm{h}} \equiv 1 - \langle \hat{a}_{\mathrm{v},\mathbf{k}}^{\dagger} \hat{a}_{\mathrm{v},\mathbf{k}} \rangle$. The matrix

$$A_{\mathbf{k},\mathbf{k}'}(\mathbf{q}) \equiv \delta_{\mathbf{k},\mathbf{k}'} \left(\tilde{\varepsilon}_{\mathbf{k}+\mathbf{q}_{\mathrm{e}}}^{\mathrm{e}} + \tilde{\varepsilon}_{\mathbf{k}-\mathbf{q}_{\mathrm{h}}}^{\mathrm{h}} \right) - \left(1 - f_{\mathbf{k}+\mathbf{q}_{\mathrm{e}}}^{\mathrm{e}} - f_{\mathbf{k}-\mathbf{q}_{\mathrm{h}}}^{\mathrm{h}} \right) V_{\mathbf{k}-\mathbf{k}'} \tag{4.10}$$

contains kinetic terms with mean-field energies $\tilde{\varepsilon}_{\mathbf{k}}^{\mathrm{e}} = \varepsilon_{\mathrm{c},\mathbf{k}} - \sum_{\mathbf{k}'} V_{\mathbf{k}-\mathbf{k}'} f_{\mathbf{k}'}^{\mathrm{e}}$ and $\tilde{\varepsilon}_{\mathbf{k}}^{\mathrm{h}} = -\varepsilon_{\mathrm{v},\mathbf{k}} - \sum_{\mathbf{k}'} V_{\mathbf{k}-\mathbf{k}'} f_{\mathbf{k}'}^{\mathrm{h}}$ as well as excitonic signatures due to Coulomb interaction. The terms in the second line of Eq. (4.9) give rise to spontaneous emission from both uncorrelated plasma and excitonic correlations. Stimulated emission due to re-absorbed photons is described by terms of the form $\Theta_{\mathrm{st}}^{(0)} = -(1 - f^{\mathrm{e}} - f^{\mathrm{h}}) \mathrm{i} \sum \mathcal{F} \Delta \langle \hat{B}^{\dagger} \hat{B} \rangle + \mathrm{i} \sum \mathcal{F} \Delta \langle \hat{B}^{\dagger} \hat{B} \hat{a}_{\lambda}^{\dagger} \hat{a}_{\lambda} \rangle$ where pairs of photon operators are involved. Typically, these contributions can be neglected so long as the sample is not placed inside a microcavity. Coulomb scattering for photon-assisted polarizations is mainly described by terms of the form $\Theta_{\mathrm{sc}}^{(0)} = \sum V \Delta \langle \hat{B}^{\dagger} \hat{a}_{\mathrm{v}}^{\dagger} \hat{a}_{\lambda}^{\dagger} \hat{a}_{\lambda} \hat{a}_{\mathrm{c}} \rangle$. Since a microscopic evaluation of these contributions would go beyond the scope of the present work, we replace the scattering terms by a phenomenological damping term $\Theta_{\mathrm{sc}}^{(0)}(\mathbf{k};\mathbf{q}) = -\mathrm{i}\gamma_0 \Pi^{(0)}(\mathbf{k};\mathbf{q})$. When the calculated spectra are to be compared to the experiment, the parameter γ_0 has to be fitted to the measured line width of the exciton peak. Without the phonon degrees of freedom, Eq. (4.9) would agree with the usual semiconductor luminescence equations [50, 54]. The third and fourth line of Eq. (4.9), however, contain the coupling to three-particle correlations that describe radiative recombination assisted by a single phonon. Phonon absorption (emission) processes correspond to correlations of the form $\Delta \langle \hat{B} \hat{D} \hat{a}_{\mathrm{v}}^{\dagger} \hat{a}_{\mathrm{c}} \rangle$ ($\Delta \langle \hat{B} \hat{D}^{\dagger} \hat{a}_{\mathrm{v}}^{\dagger} \hat{a}_{\mathrm{c}} \rangle$) and create additional resonances in the luminescence spectrum on the high-(low-)energy side of the exciton peak. Since the optical-phonon energies in most semiconductor materials are of the order of 10 to $100\,\mathrm{meV}$, very few optical phonons are excited in typical experimental situations such that phonon absorption can be neglected. We will therefore exclusively consider phonon-emission contributions $\Pi^{(1)}(\mathbf{k};\mathbf{q};\mathbf{p}) \equiv \Delta \langle \hat{B}_{\mathbf{q}}^{\dagger} \hat{D}_{\mathbf{p}}^{\dagger} \hat{a}_{\mathrm{v},\mathbf{k}-(\mathbf{q}+\mathbf{p})_{\mathrm{h}}}^{\dagger} \hat{a}_{\mathrm{c},\mathbf{k}+(\mathbf{q}+\mathbf{p})_{\mathrm{e}}} \rangle$ that lead to the first sideband below the zero-phonon line. The corresponding equations of motion read

$$\left(\mathrm{i}\hbar \frac{\mathrm{d}}{\mathrm{d}t} + \hbar\omega_{\mathbf{q}} + \hbar\Omega \right) \Pi^{(1)}(\mathbf{k};\mathbf{q};\mathbf{p}) = \sum_{\mathbf{k}'} A_{\mathbf{k},\mathbf{k}'}(\mathbf{q}+\mathbf{p}) \Pi^{(1)}(\mathbf{k}';\mathbf{q};\mathbf{p})$$

$$+ \mathrm{i}\mathcal{F}_{\mathbf{q}} \Big[f_{\mathbf{k}-(\mathbf{q}+\mathbf{p})_{\mathrm{h}}}^{\mathrm{h}} \Delta \langle \hat{D}_{\mathbf{p}}^{\dagger} \hat{a}_{\mathrm{c},(\mathbf{k}+\mathbf{q}_{\mathrm{e}})-\mathbf{p}_{\mathrm{h}}}^{\dagger} \hat{a}_{\mathrm{c},(\mathbf{k}+\mathbf{q}_{\mathrm{e}})+\mathbf{p}_{\mathrm{e}}} \rangle$$

$$- f_{\mathbf{k}+(\mathbf{q}+\mathbf{p})_{\mathrm{e}}}^{\mathrm{e}} \Delta \langle \hat{D}_{\mathbf{p}}^{\dagger} \hat{a}_{\mathrm{v},(\mathbf{k}-\mathbf{q}_{\mathrm{h}})-\mathbf{p}_{\mathrm{h}}}^{\dagger} \hat{a}_{\mathrm{v},(\mathbf{k}-\mathbf{q}_{\mathrm{h}})+\mathbf{p}_{\mathrm{e}}} \rangle$$

$$+ \sum_{\mathbf{k}'} \Delta \langle \hat{D}_{\mathbf{p}}^{\dagger} \hat{a}_{\mathrm{c},\mathbf{k}'+\mathbf{q}_{\mathrm{e}}}^{\dagger} \hat{a}_{\mathrm{v},\mathbf{k}-(\mathbf{q}+\mathbf{p})_{\mathrm{h}}}^{\dagger} \hat{a}_{\mathrm{c},\mathbf{k}+(\mathbf{q}+\mathbf{p})_{\mathrm{e}}} \hat{a}_{\mathrm{v},\mathbf{k}'-\mathbf{q}_{\mathrm{h}}} \rangle \Big]$$

$$+ \Theta_{\mathrm{st}}^{(1)}(\mathbf{k};\mathbf{q};\mathbf{p}) + \Theta_{\mathrm{sc}}^{(1)}(\mathbf{k};\mathbf{q};\mathbf{p}) + \Theta_{\mathrm{nu}}^{(1)}(\mathbf{k};\mathbf{q};\mathbf{p}) + \Theta_{0}^{(1)}(\mathbf{k};\mathbf{q};\mathbf{p}) + \Theta_{\mathrm{co}}^{(1)}(\mathbf{k};\mathbf{q};\mathbf{p}). \tag{4.11}$$

The structure of all contributions that follow from the carrier-photon part of the total Hamiltonian is very similar to Eq. (4.9) for the photon-assisted polarizations. In detail, we again have kinetic terms and excitonic correlations in the first line on the right-hand side, spontaneous-emission terms in the next three lines, stimulated-emission terms of the form $\Theta_{\mathrm{st}}^{(1)} = -(1 - f^{\mathrm{e}} - f^{\mathrm{h}}) \mathrm{i} \sum \mathcal{F} \Delta \langle \hat{B}^{\dagger} \hat{B} \hat{D}^{\dagger} \rangle + \mathrm{i} \sum \mathcal{F} \Delta \langle \hat{B}^{\dagger} \hat{B} \hat{D}^{\dagger} \hat{a}_{\lambda}^{\dagger} \hat{a}_{\lambda} \rangle$, and Coulomb-scattering terms of the form $\Theta_{\mathrm{sc}}^{(1)} = \sum V \Delta \langle \hat{B}^{\dagger} \hat{D}^{\dagger} \hat{a}_{\mathrm{v}}^{\dagger} \hat{a}_{\lambda}^{\dagger} \hat{a}_{\lambda} \hat{a}_{\mathrm{c}} \rangle$. Analogously to Eq. (4.9), we account for the scat-

tering contributions by a phenomenological damping term $\Theta_{\text{sc}}^{(1)}(\mathbf{k};\mathbf{q};\mathbf{p}) = -\mathrm{i}\gamma_1\Pi^{(1)}(\mathbf{k};\mathbf{q};\mathbf{p})$ where γ_1 is fitted to the line shape of the first phonon sideband. Terms of the form $\Theta_{\text{nu}}^{(1)} = \hbar\Omega\sum g\,n^{\text{phon}}\Pi^{(0)}$ will be neglected in the following because they contain phonon numbers. Since the numerical evaluation of the full set of singlet-doublet-triplet equations for a realistic semiconductor system would exceed the available computer resources, we make use of an additional truncation criterion. From the leading source terms in the corresponding equations of motion, one finds how each source term in Eq. (4.11) scales with the carrier densities. We assume sufficiently low densities such that only contributions up to second order in f^{e} and f^{h} need to be considered. Thus, we neglect all terms contained in $\Theta_0^{(1)} = \sum V\Delta\langle\hat{D}^\dagger\hat{a}_\lambda^\dagger\hat{a}_\lambda\rangle\Pi^{(0)} + \hbar\Omega\sum g_\lambda f^\lambda\Pi^{(0)} + \hbar\Omega\sum g_\lambda\Delta\langle\hat{B}^\dagger\hat{a}_\lambda^\dagger\hat{a}_\lambda\hat{a}_{\text{c}}\rangle$ in the further analysis. Finally, terms of the form $\Theta_{\text{co}}^{(1)} = \hbar\Omega\sum g(\Delta\langle\hat{B}^\dagger\hat{D}^\dagger\hat{D}^\dagger\hat{a}_\lambda^\dagger\hat{a}_{\text{c}}\rangle + \Delta\langle\hat{B}^\dagger\hat{D}^\dagger\hat{D}\hat{a}_{\text{v}}^\dagger\hat{a}_{\text{c}}\rangle)$ describe coupling to four-particle correlations that are related to radiative recombination assisted by two phonons. While the $\Delta\langle\hat{B}^\dagger\hat{D}^\dagger\hat{D}\hat{a}_{\text{v}}^\dagger\hat{a}_{\text{c}}\rangle$ terms yield corrections to the zero-phonon line, the $\Delta\langle\hat{B}^\dagger\hat{D}^\dagger\hat{D}^\dagger\hat{a}_{\text{v}}^\dagger\hat{a}_{\text{c}}\rangle$ terms produce the second phonon replicum. Here, we truncate the equation hierarchy at the triplet level such that only the first sideband can be evaluated. This procedure is consistent with a perturbative treatment of the electron-phonon interaction as the main contributions to the second sideband are of second order in $|g_{\text{c}}|^2$ and $|g_{\text{v}}|^2$ while the present analysis only includes first-order terms. Higher-order sidebands will be discussed in Sec. 4.4.

4.3.2 Steady-state luminescence formula for the first sideband

In typical experimental situations, the spontaneous-emission sources become quasi-stationary shortly after excitation when they are only subject to the relatively slow radiative decay. Luminescence in this regime can be calculated from a steady-state solution of Eqs. (4.9), (4.11). More explicitly, we assume thermal distributions for densities and excitonic correlations and insert steady-state solutions for the phonon-assisted carrier correlations into the spontaneous-emission source terms in Eq. (4.11). Details of this procedure are given in Appendix D. The matrix (4.10) can be diagonalized with the help of the exciton basis introduced explicitly in Appendix A. Because the analysis is restricted to weak excitation levels, we may use the low-density version ϕ_ν of the excitonic wave functions in the definition (A.9) of the exciton operators $\hat{X}_{\nu,\mathbf{Q}}$, $\hat{X}_{\nu,\mathbf{Q}}^\dagger$. The exciton energy $E_\nu(\mathbf{Q}) = \mathcal{E}_\nu + \hbar^2|\mathbf{Q}|^2/2M$ decomposes into the excitonic eigen energy $\mathcal{E}_\nu$ and the center-of-mass energy of the electron-hole pair. See Appendix A for further properties of the exciton basis.

After diagonalization of the homogeneous parts of the phonon-assisted semiconductor luminescence equations (4.9), (4.11), the steady-state luminescence can be calculated analytically. We exclusively consider the dominant exciton peak for $\nu = 1\text{s}$ and its replicum. Off-diagonal expectation values $\langle\hat{X}_{1\text{s},\mathbf{Q}}^\dagger\hat{X}_{\nu,\mathbf{Q}}\rangle$ with $\nu \neq 1\text{s}$ are neglected with respect to diagonal ones $\langle X_{1\text{s},\mathbf{Q}}^\dagger X_{1\text{s},\mathbf{Q}}\rangle$ [7]. Moreover, we set the small photon momenta to zero in the following calculations and neglect the weak momentum dependence of the light-matter interaction matrix elements by writing $\mathcal{F}$ instead of $\mathcal{F}_{\mathbf{q}}$. Thus, we finally obtain the luminescence formula

$$I_{\text{PL}}(\omega) = I_{\text{PL}}^{(0)}(\omega) + I_{\text{PL}}^{(1)}(\omega) \tag{4.12}$$

where the contributions to the zero-phonon line and to the first phonon sideband can be written as

$$I_{\text{PL}}^{(0)}(\omega) = \frac{2}{\hbar}|\mathcal{F}\phi_{1\text{s}}(\mathbf{r} = \mathbf{0})|^2\text{Im}\left[\frac{N_{1\text{s}}^{(0)}(\mathbf{0}) - \sum_{\mathbf{Q}}N_{1\text{s}}^{(1)}(\mathbf{Q})}{E_{1\text{s}}(\mathbf{0}) - \hbar\omega - \mathrm{i}\gamma_0}\right], \tag{4.13}$$

$$I_{\text{PL}}^{(1)}(\omega) = \frac{2}{\hbar} |\mathcal{F}\phi_{1s}(\mathbf{r}=\mathbf{0})|^2 \text{Im} \left[\sum_{\mathbf{Q}} \frac{N_{1s}^{(1)}(\mathbf{Q})}{E_{1s}(\mathbf{Q}) - \hbar\Omega - \hbar\omega - i\gamma_1} \right], \tag{4.14}$$

respectively. The source term $N_{1s}^{(n)}(\mathbf{Q})$ defines the luminescence from electron-hole pairs with center-of-mass momentum $\mathbf{Q}$. In accordance with the qualitative discussion from Sec. 4.1, we find that pairs with arbitrary center-of-mass momentum can contribute to the sideband emission. For both resonances in the luminescence spectrum,

$$N_{1s}^{(n)}(\mathbf{Q}) = \Delta N_{1s}^{(n)}(\mathbf{Q}) + N_{1s}^{\text{eh}(n)}(\mathbf{Q}) \tag{4.15}$$

decomposes into a correlated and a singlet contribution. The former contains true exciton populations,

$$\Delta N_{1s}^{(0)}(\mathbf{Q}) \equiv \Delta\langle \hat{X}_{1s,\mathbf{Q}}^{\dagger} \hat{X}_{1s,\mathbf{Q}} \rangle, \tag{4.16}$$

$$\Delta N_{1s}^{(1)}(\mathbf{Q}) \equiv \left| \frac{\hbar\Omega g_{\mathbf{Q}}^{1s,1s}}{\hbar\Omega - \frac{\hbar^2|\mathbf{Q}|^2}{2M}} \right|^2 \Delta\langle \hat{X}_{1s,\mathbf{Q}}^{\dagger} \hat{X}_{1s,\mathbf{Q}} \rangle, \tag{4.17}$$

where

$$g_{\mathbf{Q}}^{\nu,\nu'} = \sum_{\mathbf{k}} \phi_{\nu}^*(\mathbf{k}) \left[g_{c,\mathbf{Q}}\phi_{\nu'}(\mathbf{k}+\mathbf{Q}_{\text{h}}) - g_{v,\mathbf{Q}}\phi_{\nu'}(\mathbf{k}-\mathbf{Q}_{\text{e}}) \right] \tag{4.18}$$

is just another way of writing the exciton-phonon matrix element $G_{\mathbf{Q}}^{\nu,\nu'}/\hbar\Omega$ according to Eq. (4.4). The excitonic contribution (4.17) agrees with the perturbative treatment summarized in Sec. 4.2. Our work generalizes that approach to include the singlet contributions $N_{1s}^{\text{eh}(n)}(\mathbf{Q})$. Explicitly, we obtain

$$N_{1s}^{\text{eh}(0)}(\mathbf{Q}) \equiv \langle \hat{X}_{1s,\mathbf{Q}}^{\dagger} \hat{X}_{1s,\mathbf{Q}} \rangle_{\text{S}} = \sum_{\mathbf{k}} |\phi_{1s}(\mathbf{k})|^2 f_{\mathbf{k}+\mathbf{Q}_{\text{e}}}^{\text{e}} f_{\mathbf{k}-\mathbf{Q}_{\text{h}}}^{\text{h}}, \tag{4.19}$$

$$N_{1s}^{\text{eh}(1)}(\mathbf{Q}) \equiv \frac{\hbar\Omega g_{\mathbf{Q}}^{1s,1s}}{\hbar\Omega - \frac{\hbar^2|\mathbf{Q}|^2}{2M}} \sum_{\mathbf{k}} |\phi_{1s}(\mathbf{k})|^2 f_{\mathbf{k}+\mathbf{Q}_{\text{e}}}^{\text{e}} f_{\mathbf{k}-\mathbf{Q}_{\text{h}}}^{\text{h}}$$
$$\times \left(\frac{\hbar\Omega g_{c,\mathbf{Q}}^*}{\hbar\Omega - \varepsilon_{\mathbf{k}+\mathbf{Q}_{\text{e}}}^{\text{e}} + \varepsilon_{\mathbf{k}-\mathbf{Q}_{\text{h}}}^{\text{e}}} - \frac{\hbar\Omega g_{v,\mathbf{Q}}^*}{\hbar\Omega + \varepsilon_{\mathbf{k}+\mathbf{Q}_{\text{e}}}^{\text{h}} - \varepsilon_{\mathbf{k}-\mathbf{Q}_{\text{h}}}^{\text{h}}} \right). \tag{4.20}$$

This result indicates that for both the zero-phonon line and the phonon sideband, uncorrelated electron-hole plasma can lead to luminescence at the same resonances as the excitons. In Sec. 4.3.3.2, this statement will be verified numerically.

According to Eq. (4.13), the phonon-assisted recombination processes also affect the intensity of the zero-phonon line. In many materials, the first replicum is two or more orders of magnitude weaker than the exciton peak such that the correction to the ZPL can be neglected. For very strong electron-phonon coupling, the intensities of the sidebands can become considerable. In that case, we would also have to consider higher-order corrections to the ZPL and the PSB$_1$ that are not contained in the singlet-doublet-triplet analysis. The non-perturbative treatment of the carrier-phonon interaction presented in Sec. 4.4.2 indicates that the combined effect of all these corrections reduces to an overall renormalization of the luminescence spectrum.

For the analytical discussion of certain properties of the sideband emission, it will prove useful to consider the low-temperature limit where only exciton states with small center-of-mass momenta are populated. We may then use a small-$|\mathbf{Q}|$ approximation for the source terms $N_{1s}^{(1)}(\mathbf{Q})$ in Eq. (4.14). More explicitly, we take the limit $\mathbf{Q} \to \mathbf{0}$ in the energy denominators in Eqs. (4.17), (4.20) and neglect $\mathbf{Q}_e$, $\mathbf{Q}_h$ with respect to $\mathbf{k}$ in Eq. (4.18) such that the exciton-phonon matrix element becomes

$$g_{\mathbf{Q}}^{1s,1s} \simeq g_{c,\mathbf{Q}} - g_{v,\mathbf{Q}}. \qquad (4.21)$$

The luminescence formula (4.14) for the first phonon sideband thus reduces to

$$I_{\mathrm{PL}}^{(1)}(\omega) \simeq \frac{2}{\hbar} |\mathcal{F}\phi_{1s}(\mathbf{r}=0)|^2 \mathrm{Im} \sum_{\mathbf{Q}} \frac{|\Delta g_{\mathbf{Q}}|^2 \left[\Delta N_{1s}^{(0)}(\mathbf{Q}) + N_{1s}^{\mathrm{eh}(0)}(\mathbf{Q}) \right]}{\mathcal{E}_{1s}(\mathbf{Q}) - \hbar\Omega - \hbar\omega - \mathrm{i}\gamma_1} \qquad (4.22)$$

with $\Delta g_{\mathbf{Q}} \equiv g_{v,\mathbf{Q}} - g_{c,\mathbf{Q}}$. This approximate result suggests that the intensity of the replicum will be very weak in case of band-independent electron-phonon matrix elements $g_{v,\mathbf{Q}} = g_{c,\mathbf{Q}}$. Moreover, because excitonic populations $\Delta N_{1s}^{(0)}(\mathbf{Q})$ and electron-hole plasma $N_{1s}^{\mathrm{eh}(0)}(\mathbf{Q})$ enter the sideband-emission formula additively, it appears impossible to distinguish the different contributions in a standard luminescence experiment. In the following section, both these statements will be checked numerically with the help of the exact sideband formula (4.14).

4.3.3 Numerical case studies

Having derived the steady-state result (4.14), we can now study the properties of single-phonon assisted luminescence numerically. In Sec. 4.3.3.1, we compare sideband emission due to Fröhlich and optical deformation-potential coupling. Exciton and plasma luminescence are analyzed in Sec. 4.3.3.2. Finally, we discuss the generic differences between bulk and quantum-well emission in Sec. 4.3.3.3. Further case studies that involve higher-order sidebands can only be performed later in Sec. 4.4.3.

4.3.3.1 Fröhlich and optical deformation-potential coupling

In most polar crystals, the long-ranged Fröhlich coupling usually contributes much more strongly to the carrier-phonon scattering than the short-ranged optical deformation-potential coupling. Usually, the latter interaction mechanism only dominates in inter-valley scattering where zone-edge phonons are involved [131] or in situations where the Fröhlich coupling is symmetry-forbidden [89, 90]. Phonon replica in III-V and II-VI compound semiconductors are automatically assigned to Fröhlich interaction in the majority of publications. However, the low-temperature approximation (4.22) suggests that the intensity of the replicum not only depends on the overall amplitude but also on the difference $\Delta g_{\mathbf{p}} = g_{v,\mathbf{p}} - g_{c,\mathbf{p}}$ of the electron-phonon matrix elements $g_{v,\mathbf{p}}$ and $g_{c,\mathbf{p}}$. To quantify this statement, we assume artificial matrix elements where $g_{\lambda,\mathbf{p}}$ has the $\mathbf{p}$ dependence of the Fröhlich matrix element $g_{\mathbf{p}}^{\mathrm{Fr}}$, fix $|g_{v,\mathbf{p}}|^2 + |g_{c,\mathbf{p}}|^2 = 2|g_{\mathbf{p}}^{\mathrm{Fr}}|^2$, and sweep $\Delta g_{\mathbf{p}}$ from $-2g_{\mathbf{p}}^{\mathrm{Fr}}$ to $+2g_{\mathbf{p}}^{\mathrm{Fr}}$. The solid lines in Fig. 20 show the intensity ratio of PSB$_1$ and ZPL as function of $x(\mathbf{p}) \equiv \Delta g_{\mathbf{p}}/2g_{\mathbf{q}}^{\mathrm{Fr}}$ for GaN parameters at two different carrier temperatures T. In both cases, the strength of the replicum becomes maximal for $x(\mathbf{p}) = \pm 1$ where $g_{v,\mathbf{p}} = -g_{c,\mathbf{p}}$. For $T = 10\,\mathrm{K}$ (a), the sideband luminescence becomes minimal when $g_{c,\mathbf{p}}$ and $g_{v,\mathbf{p}}$ are the band-independent Fröhlich matrix elements, i.e. for $x(\mathbf{p}) = 0$. The relative intensity of the replicum is then three orders of magnitude smaller than for an opposite sign of the matrix elements. For $T = 50\,\mathrm{K}$, the position of the minimum
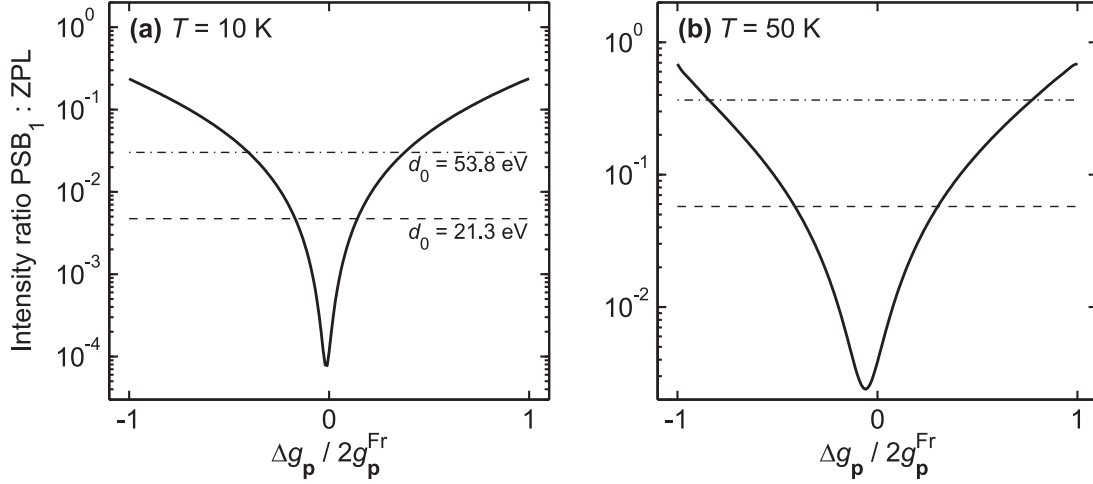
Figure 20: Dependence of the relative intensity of the first phonon sideband on the electron-phonon matrix elements $g_{v,\mathbf{p}}$, $g_{c,\mathbf{p}}$ for two different carrier temperatures. For the solid lines, we assume that $g_{\lambda,\mathbf{p}} \propto |\mathbf{p}|^{-1}$ as for the Fröhlich matrix element $g_{\mathbf{p}}^{\mathrm{Fr}}$ but sweep $\Delta g_{\mathbf{p}} = g_{v,\mathbf{p}} - g_{c,\mathbf{p}}$ while leaving $|g_{v,\mathbf{p}}|^2 + |g_{c,\mathbf{p}}|^2 = 2|g_{\mathbf{p}}^{\mathrm{Fr}}|^2$ unchanged. The dashed and the dash-dotted vertical lines represent the result for optical deformation-potential interaction with coupling constant $d_0 = 21.3\,\mathrm{eV}$ and $d_0 = 53.8\,\mathrm{eV}$, respectively.

is slightly shifted and the difference between the limiting cases is slightly less pronounced. Nevertheless, this analysis clearly shows that strong intraband electron-phonon scattering does not imply pronounced sideband luminescence.

The two horizontal lines in Fig. 20 represent results for optical deformation-potential interaction. The value $d_0 = 53.8\,\mathrm{eV}$ (dash-dotted line) of the coupling constant is taken from Ref. [91]. As discussed in Sec. 2.2.4.2, the optical deformation-potential constant is effectively reduced for polar optical modes. The choice $d_0 = 21.3\,\mathrm{eV}$ (dashed line) corresponds to the fit result presented later in Fig. 26. It turns out that for the given temperature and material parameters, the short-range part of the electron-phonon interaction actually provides the dominant contribution to the sideband luminescence, irrespective of the strongly polar nature of GaN. We will return to this point and examine it further in Sec. 4.4.3.1 where we will analyze the second phonon sideband.

4.3.3.2 Exciton and plasma contributions

Because not only excitonic populations but also uncorrelated plasma contribute to the source term $N_{1s}^{(0)}(\mathbf{Q})$ for the ZPL, luminescence at the excitonic resonance does not provide unique evidence that bound electron-hole pairs have formed in the material. This somewhat counter-intuitive result was first pointed out in Ref. [50] and was subsequently confirmed in a number of experiments [51–53]. However, the question whether plasma can also participate in phonon-assisted luminescence has not yet been addressed quantitatively in the literature. The perturbative treatment summarized in Sec. 4.2, for example, describes sideband emission as series of exciton-phonon scattering events followed by recombination from within the radiative cone. It is not obvious whether this kind of microscopic processes could also involve uncorrelated electron-hole pairs. In this section, we therefore analyze the effect of the plasma source term
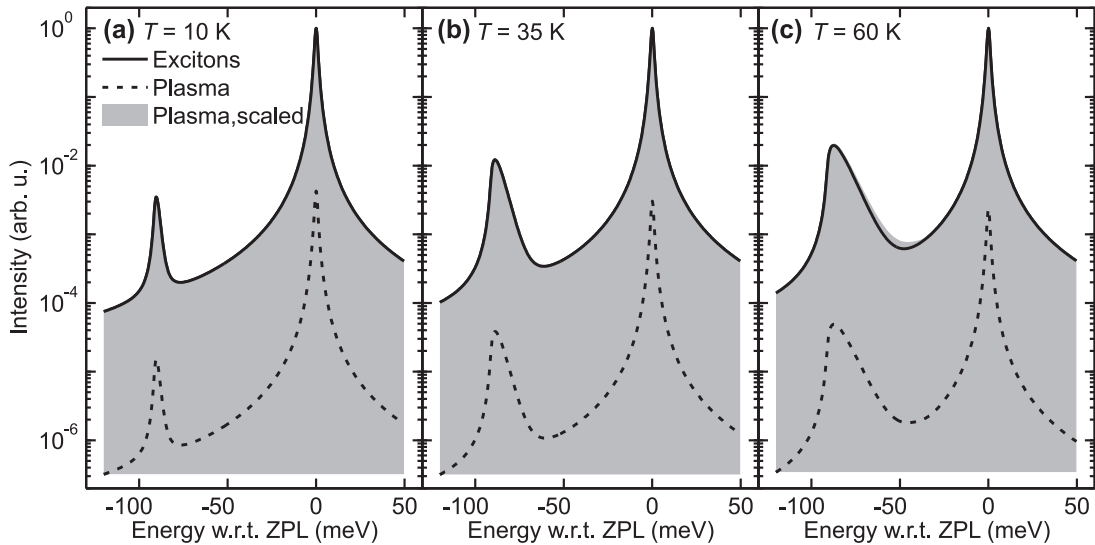
Figure 21: Calculated sideband emission from excitonic populations (solid lines) and uncorrelated plasma (dashed lines) for GaN parameters with an electron-hole pair density $n_{\mathrm{eh}} = 10^{12}\,\mathrm{cm}^{-3}$ at three different carrier temperatures. The same small homogeneous broadening was assumed for the exciton peak and its replicum. For the shaded areas, the plasma contribution has been scaled such that the zero-phonon lines coincide.

$N_{1\mathrm{s}}^{\mathrm{eh}(1)}(\mathbf{Q})$ on the sideband emission quantitatively.

Figure 21 shows the numerical results for GaN parameters with $d_0 = 21.3\,\mathrm{eV}$ and an electron-hole pair density $n_{\mathrm{eh}} = 10^{12}\,\mathrm{cm}^{-3}$ at three different carrier temperatures. The solid lines correspond to the fully correlated case where all electron-hole pairs form excitons while the dashed lines represent the fully uncorrelated case where only the plasma source term contributes to the sideband luminescence. For the given density, the exciton emission clearly dominates the plasma emission. However, the position of the exciton-phonon resonance is identical for both contributions, and the line shape of the sideband and its intensity relative to the zero-phonon line are very similar (shaded areas), as already indicated by the low-temperature approximation (4.22). Only at elevated temperatures (right frame), small deviations can be detected. We conclude that the correlated and the singlet sources of the sideband emission cannot be distinguished by means of a standard luminescence experiment.

As explained in Sec. 3.3.3 for the quantum-dot case, excitons and uncorrelated plasma have different radiative decay dynamics because the former source term is proportional to n_{eh} while the latter source term is proportional to n_{eh}^2. The corresponding transients are sketched schematically in frame (a) of Fig. 22. Strictly exponential decay is a signature of excitonic luminescence while the decay rate decreases in time for plasma emission. Experimental results [132] for the first three sidebands in ZnO bulk spectra at $T = 210\,\mathrm{K}$ are shown as dashed line in frame (b). For comparison, the solid line represents the dynamics of the exciton peak.[3] It was found that even at high excitation power and elevated temperatures, all transients retained their exponential behavior, where the small deviations that are visible in the figure can

---

[3]We will see in Sec. 4.4.3.2 that the sidebands can be assigned to free excitons while the zero-phonon line originates from impurity-bound excitons.
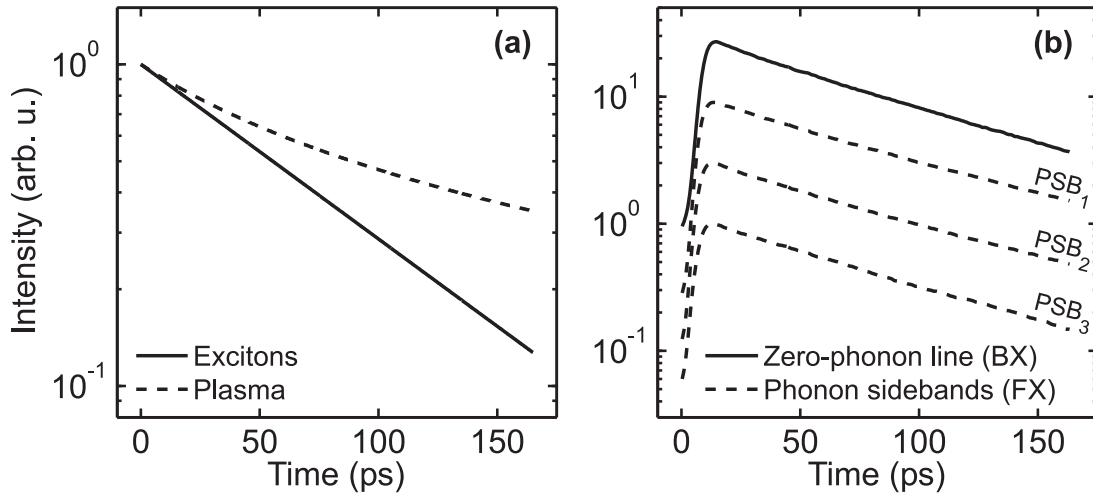
Figure 22: Radiative decay dynamics. Frame (a) shows schematically the generic difference between exciton and plasma emission. For a better comparison, identical decay rates are assumed at time $t = 0$. Frame (b) shows experimental results [132] for the zero-phonon line due to impurity-bound excitons (BX) and the first three sidebands due to free electron-hole pairs (FX) as measured with a ZnO bulk sample at temperature $T = 210\,\mathrm{K}$.

be ascribed to non-radiative decay channels that lead to multi-exponential transients even in the fully correlated case. To interpret this observation, we notice that prominent sideband emission requires strong electron-phonon coupling. At the same time, this strong electron-phonon interaction favors the formation of excitons [7]. Because the large exciton binding energy of about $60\,\mathrm{meV}$ inhibits thermal ionization of the excitons, one can expect a high amount of excitons in ZnO systems even after non-resonant excitation, in striking contrast to GaAs systems. Still, the singlet source term $N_{1s}^{\mathrm{eh}(1)}(\mathbf{Q})$ is always present even in the fully correlated case. At sufficiently high densities, the plasma emission should eventually become noticeable. However, no higher excitation levels could be reached in the above experiments without damaging the sample. Thus, sideband emission due to uncorrelated plasma has not yet been verified experimentally at the time of writing this thesis.

4.3.3.3 Sideband emission from quantum wells

In materials with strong electron-phonon interaction, phonon replica can appear in both bulk and quantum-well luminescence spectra. In order to discuss the generic differences between emission from three- and two-dimensional carrier systems, we now study the temperature dependence of the sideband intensities in both cases. It is shown in Appendix F.4 how the luminescence formula has to be modified for confined carrier systems. For the purposes of the present analysis, it is sufficient to consider the respective low-temperature approximations (4.22) and (F.38).[4] The integrated intensities $J(n) \equiv \int I_{\mathrm{PL}}^{(n)}(\omega)\,\mathrm{d}(\hbar\omega)$ for $n = 1$ thus take the

---

[4]Actually, Eq. (F.38) is derived within the polaron-picture analysis from Sec. 4.4.2. However, we will see that this approach reproduces the low-temperature approximation to the cluster-expansion formula for the first sideband.

forms

$$J^{\text{bulk}}(1) \propto \sum_{\mathbf{Q}} |\Delta g_{\mathbf{Q}}|^2 N_{1\text{s}}(\mathbf{Q}), \tag{4.23}$$

$$J^{\text{QW}}(1) \propto \sum_{\mathbf{Q}_{\|}} |\Delta \tilde{g}_{\mathbf{Q}_{\|}}|^2 N_{1\text{s}}(\mathbf{Q}_{\|}) \tag{4.24}$$

for bulk and well emission, respectively. For simplicity, we only consider optical deformation-potential interaction where the matrix elements in the long-wavelength limit have the form $g_{\text{c},\mathbf{Q}} = 0$ and $g_{\text{v},\mathbf{Q}} \simeq g = \text{const}$. Hence, the above relations reduce to

$$J^{\text{bulk}}(1) \propto |g|^2 \sum_{Q_z} \sum_{\mathbf{Q}_{\|}} N_{1\text{s}}(\mathbf{Q}_{\|}, Q_z), \tag{4.25}$$

$$J^{\text{QW}}(1) \propto |g|^2 \sum_{Q_z} |\gamma(Q_z)|^2 \sum_{\mathbf{Q}_{\|}} N_{1\text{s}}(\mathbf{Q}_{\|}) \tag{4.26}$$

with the form factor $\gamma(Q_z)$ as defined in Eq. (F.39) that originates from the carrier confinement. In the bulk case, the $\mathbf{Q}$-dependent integrand decays in all three directions like the thermal distribution function for the excitons while in the quantum-well case, the integrand decays like the form factor in Q_z direction. Since the exciton distribution broadens with increasing temperature, there is a critical temperature T_c below which the relative intensity of the first sideband is weaker in the bulk case than in the quantum-well case. Above T_c, the situation is reversed. This critical temperature obviously depends on both the material parameters and the confinement width L.
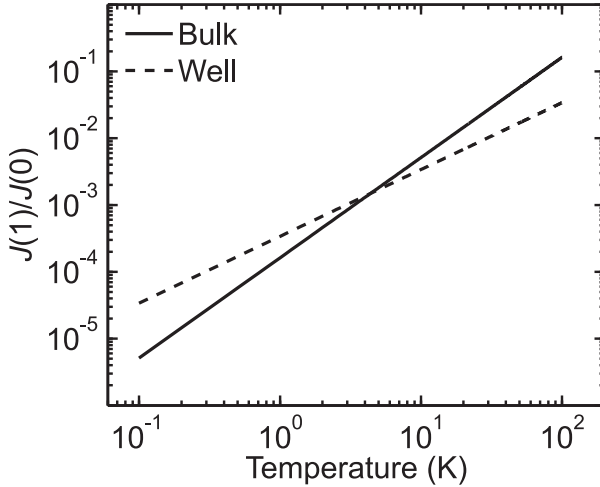
Figure 23: Integrated intensity of the first phonon sideband relative to the zero-phonon line as function of the carrier temperature for GaN bulk (solid line) and a GaN quantum well where the carriers are confined to a width of half a Bohr radius (dashed line).

A concrete numerical example for GaN parameters with $d_0 = 21.3\,\text{eV}$ and $L = 0.5a_{\text{B}}$ where a_{B} denotes the exciton Bohr radius is shown in Fig. 23. For both bulk and well, the integrated intensity of the first sideband relative to the zero-phonon line obeys a power-law dependence on the temperature, as discussed in more detail later in Sec. 4.4.3.1. The exponents are different, however, such that the curves cross at $T_c \simeq 4\,\text{K}$.

When theoretical results for confined systems are quantitatively compared to experimental data, the explicit form of $\gamma(Q_z)$ often plays a minor role, and the width L can be treated as a fitting parameter. Such an approach has to be refined when an accurate value for the critical temperature T_c is to be calculated. Nevertheless, the simplified analysis presented in this section already gives a hint why identical materials can feature very different sideband spectra in bulk and quantum-well experiments.

4.4 Higher-order sidebands

We have discussed at the beginning of Sec. 4.3 how phonon replica emerge within the cluster-expansion scheme. For the n-th sideband, at least $(n + 2)$-particle correlations of the form $\Delta\langle \hat{B}^\dagger \hat{D}^\dagger \cdots \hat{D}^\dagger \hat{a}_\mathrm{v}^\dagger \hat{a}_\mathrm{c} \rangle$ that involve n phonon creation operators have to be calculated. In general, the number of correlations grows exponentially with the level of cluster expansion. Physical insight often allows to drastically reduce the number of equations of motion that are to be solved. When only the correlated contribution to the sideband emission is to be evaluated, the analysis may be performed in the *exciton picture*. Here, the exciton basis defined in Appendix A diagonalizes the purely electronic part of the Hamiltonian such that the equation hierarchy due to Coulomb interaction is eliminated. We use this approximation in Sec. 4.4.1 to calculate arbitrary-order sidebands analytically. However, when the fermionic substructure of the electron-hole pairs is taken into account, the analysis becomes very involved already for the second phonon replicum. A different approach is preferred in Sec. 4.4.2 where the electron-electron interaction is fully included while the electron-phonon interaction is treated non-perturbatively by means of a unitary transformation. That way, we find a much more compact luminescence formula than with the exciton-picture analysis.

4.4.1 Exciton-picture analysis

When we restrict the analysis to sufficiently low excitation levels, the parts of the system Hamiltonian (4.5) that contain carrier operators can be expressed in terms of the low-density exciton operators $\hat{X}_{\nu,\mathbf{Q}}$, $\hat{X}_{\nu,\mathbf{Q}}^\dagger$. This procedure is explicitly performed in Appendix E.1 and casts the system Hamiltonian into form

$$\hat{H} = \hat{H}_\mathrm{X} + \hat{H}_\mathrm{vib} + \hat{H}_\mathrm{em} + \hat{H}_{\mathrm{X-vib}} + \hat{H}_{\mathrm{X-em}} \tag{4.27}$$

where

$$\hat{H}_\mathrm{X} = \sum_{\nu,\mathbf{Q}} E_\nu(\mathbf{Q}) \hat{X}_{\nu,\mathbf{Q}}^\dagger \hat{X}_{\nu,\mathbf{Q}} \tag{4.28}$$

gives the contribution from non-interacting excitons. The exciton-phonon and exciton-photon interaction are described by

$$\hat{H}_{\mathrm{X-vib}} = \sum_{\nu,\nu'} \sum_{\mathbf{Q},\mathbf{p}} \hbar\Omega g_\mathbf{p}^{\nu,\nu'} \hat{X}_{\nu,\mathbf{Q}-\mathbf{p}}^\dagger \hat{X}_{\nu',\mathbf{Q}} \left(\hat{D}_{-\mathbf{p}} + \hat{D}_\mathbf{p}^\dagger \right), \tag{4.29}$$

$$\hat{H}_{\mathrm{X-em}} = -\sum_{\nu,\mathbf{q}} \mathrm{i}\big[\mathcal{F}_\mathbf{q} \phi_\nu^*(\mathbf{r} = \mathbf{0}) \hat{X}_{\nu,\mathbf{q}}^\dagger + \mathcal{F}_\mathbf{q}^* \phi_\nu(\mathbf{r} = \mathbf{0}) \hat{X}_{\nu,\mathbf{q}} \big] \hat{B}_\mathbf{q} + \mathrm{H.C.}, \tag{4.30}$$

respectively, while the Hamiltonians $\hat{H}_\mathrm{vib}$ for the free lattice-vibration field and $\hat{H}_\mathrm{em}$ for the free electromagnetic fields remain unchanged. Generally, it does not facilitate the microscopic treatment of the interacting carrier system when the system Hamiltonian is transformed into the exciton basis. The downside of such an approach is that due to the fermionic substructure of the electron-hole pairs, the exciton operators have complicated commutation relations. For the purposes of the present analysis, however, it is justified to treat the excitons as proper bosons such that $\hat{X}_{\nu,\mathbf{Q}}$, $\hat{X}_{\nu,\mathbf{Q}}^\dagger$ fulfill bosonic commutation relations

$$[\hat{X}_{\nu,\mathbf{Q}}, \hat{X}_{\nu',\mathbf{Q}'}^\dagger]_- = \delta_{\nu,\nu'}\delta_{\mathbf{Q},\mathbf{Q}'}, \qquad [\hat{X}_{\nu,\mathbf{Q}}, \hat{X}_{\nu',\mathbf{Q}'}]_- = 0 = [\hat{X}_{\nu,\mathbf{Q}}^\dagger, \hat{X}_{\nu',\mathbf{Q}'}^\dagger]_-. \tag{4.31}$$

We motivate in Appendix E.2 why this approach should describe the sideband emission correctly in the low-density limit.

In Sec. 4.4.1.1, we present the phonon-assisted luminescence equations in the exciton picture and solve them analytically in steady state for arbitrary-order phonon replica. To identify the dominant contributions to the resulting luminescence formula, we have a closer look at the exciton-phonon matrix elements $g_{\mathbf{p}}^{\nu,\nu'}$ in Sec. 4.4.1.2.

4.4.1.1 Steady-state luminescence formula for arbitrary-order sidebands

In the exciton picture, the incoherent photon flux (4.7) follows from

$$\frac{\mathrm{d}}{\mathrm{d}t}\Delta\langle\hat{B}_{\mathbf{q}}^{\dagger}\hat{B}_{\mathbf{q}}\rangle = \frac{2}{\hbar}\mathrm{Re}\Big[\mathcal{F}_{\mathbf{q}}^{*}\sum_{\nu}\phi_{\nu}(\mathbf{r}=\mathbf{0})\Pi_{\nu}^{(0)}(\mathbf{q})\Big]. \tag{4.32}$$

Together with Eq. (4.32), the equations of motion for the photon-assisted polarization $\Pi_{\nu}^{(0)}(\mathbf{q}) \equiv \Delta\langle\hat{B}_{\mathbf{q}}^{\dagger}\hat{X}_{\nu,\mathbf{q}}\rangle$ and the phonon-assisted recombination correlations $\Pi_{\nu}^{(n)}(\mathbf{q};\mathbf{p}_{1},\ldots,\mathbf{p}_{n}) \equiv \Delta\langle\hat{D}_{\mathbf{p}_{n}}^{\dagger}\cdots\hat{D}_{\mathbf{p}_{1}}^{\dagger}\hat{B}_{\mathbf{q}}^{\dagger}\hat{X}_{\nu,\mathbf{q}+\mathbf{p}_{1}+\cdots+\mathbf{p}_{n}}\rangle$,

$$\begin{aligned}
\Big(\mathrm{i}\hbar\frac{\mathrm{d}}{\mathrm{d}t} + \hbar\omega_{\mathbf{q}} + n\hbar\Omega\Big)\Pi_{\nu}^{(n)}(\mathbf{q};\mathbf{p}_{1},\ldots,\mathbf{p}_{n}) &= E_{\nu}(\mathbf{q}+\mathbf{p}_{1}+\cdots+\mathbf{p}_{n})\Pi_{\nu}^{(n)}(\mathbf{q};\mathbf{p}_{1},\ldots,\mathbf{p}_{n}) \\
&+ \mathrm{i}\mathcal{F}_{\mathbf{q}}\sum_{\nu'}\phi_{\nu'}^{*}(\mathbf{r}=\mathbf{0})\Delta\langle\hat{D}_{\mathbf{p}_{n}}^{\dagger}\cdots\hat{D}_{\mathbf{p}_{1}}^{\dagger}\hat{X}_{\nu',\mathbf{q}}^{\dagger}\hat{X}_{\nu,\mathbf{q}+\mathbf{p}_{1}+\cdots+\mathbf{p}_{n}}\rangle \\
&+ \hbar\Omega\sum_{\nu',\mathbf{p}}g_{\mathbf{p}}^{\nu,\nu'}\Pi_{\nu'}^{(n+1)}(\mathbf{q};\mathbf{p},\mathbf{p}_{1},\ldots,\mathbf{p}_{n}) \\
&+ \Theta_{\mathrm{st},\nu}^{(n)}(\mathbf{q};\mathbf{p}_{1},\ldots,\mathbf{p}_{n}) + \Theta_{\mathrm{nu},\nu}^{(n)}(\mathbf{q};\mathbf{p}_{1},\ldots,\mathbf{p}_{n}),
\end{aligned} \tag{4.33}$$

constitute the *phonon-assisted semiconductor luminescence equations in the exciton picture*. We do not include the stimulated-emission source term $\Theta_{\mathrm{st},\nu}^{(n)} = \mathrm{i}\phi_{\nu}^{*}(\mathbf{r}=\mathbf{0})\mathcal{F}\langle(\hat{D}^{\dagger})^{n}\hat{B}^{\dagger}\hat{B}\rangle$ in the following analysis. Similarly to our approach in Sec. 4.3.1, we neglect in Eq. (4.33) all source terms that are of higher order in the exciton density than $\Pi_{\nu}^{(n)}$ as well as all terms that are proportional to phonon numbers. Because the factorization of $\Theta_{\mathrm{nu},\nu}^{(n)} = -\hbar\Omega\sum g\langle(\hat{D}^{\dagger})^{n-1}\hat{B}^{\dagger}\hat{X}^{\dagger}\hat{X}\hat{X}\rangle$ exclusively produces contributions with that properties, we omit $\Theta_{\mathrm{nu},\nu}^{(n)}$ altogether. The steady-state solutions for the spontaneous-emission source terms in the second line of Eq. (4.33) are derived in Appendix E.4. Analogously to Eqs. (4.9), (4.11), $\Pi_{\nu}^{(n)}$ is coupled to higher-order phonon-assisted quantities via the third line of Eq. (4.33). When the equation hierarchy is truncated on the $(n+2)$-th level of cluster expansion, the recombination correlations $\Pi_{\nu}^{(n)}$, $\Pi_{\nu}^{(n-1)}$, ..., $\Pi_{\nu}^{(0)}$ can be evaluated iteratively in steady state. Details of this procedure are presented in Appendix E.4. We only include those contributions to each replicum that are of lowest order in the absolute values squared of the exciton-phonon matrix elements $g_{\mathbf{p}}^{\nu,\nu'}$, cf. the discussion after Eq. (4.20). Thus, we finally obtain closed steady-state luminescence formulas for the zero-phonon line,

$$I_{\text{PL}}^{(0)}(\omega) = \frac{2}{\hbar} |\mathcal{F}\phi_{1\text{s}}(\mathbf{r} = \mathbf{0})|^2 \text{Im} \left[\frac{\Delta N_{1\text{s}}(\mathbf{0})}{E_{1\text{s}}(\mathbf{0}) - \hbar\omega - \mathrm{i}\gamma_0} \right], \qquad (4.34)$$

and arbitrary-order phonon sidebands,

$$
\begin{aligned}
I_{\text{PL}}^{(n)}(\omega) = {}& \frac{2}{\hbar} |\mathcal{F}\phi_{1\text{s}}(\mathbf{r} = \mathbf{0})|^2 \, \text{Im} \sum_{\substack{\nu_1,\ldots,\nu_{n-1} \\ \nu_1',\ldots,\nu_{n-1}'}} \sum_{\mathbf{p}_1,\ldots,\mathbf{p}_n} \frac{\Delta N_{1\text{s}}(\mathbf{p}_1 + \cdots + \mathbf{p}_n)}{E_{1\text{s}}(\mathbf{p}_1 + \cdots + \mathbf{p}_n) - n\hbar\Omega - \hbar\omega - \mathrm{i}\gamma_n} \\
& \times \sum_\pi \prod_{j=0}^{n-1} \left[\frac{\hbar\Omega g_{\mathbf{p}_{j+1}}^{\nu_j, \nu_{j+1}}}{(n-j)\hbar\Omega - E_{1\text{s}}(\mathbf{p}_1 + \cdots + \mathbf{p}_n) + E_{\nu_j}(\mathbf{p}_1 + \cdots + \mathbf{p}_j)} \right. \\
& \qquad\qquad \times \left. \frac{\hbar\Omega g_{\mathbf{p}_{\pi[j+1]}}^{\nu_j', \nu_{j+1}'}}{(n-j)\hbar\Omega - E_{1\text{s}}(\mathbf{p}_1 + \cdots + \mathbf{p}_n) + E_{\nu_j'}(\mathbf{p}_{\pi[1]} + \cdots + \mathbf{p}_{\pi[j]})} \right].
\end{aligned}
\qquad (4.35)
$$

As in Sec. 4.3.2, we restrict the analysis to the 1s peak and its replica and set the photon wave vector $\mathbf{q}$ to zero. The π sum in Eq. (4.35) extends over all permutations $j \mapsto \pi[j]$ of the set $\{1,\ldots,n\}$. For a compact notation, we have defined $\nu_0 = \nu_0' \equiv 1\text{s}$. For the zero-phonon line and the first phonon sideband, the exciton-picture analysis reproduces the correlated contributions to Eqs. (4.13), (4.14). Moreover, Eq. (4.35) can directly be compared to the perturbative result (4.2), (4.3). We find that the cluster-expansion approach in the exciton picture yields a slightly more complicated index structure than the perturbative approach. However, we will see in the following section that the exciton-phonon matrix elements $g_{\mathbf{p}}^{\nu,\nu'}$ decay rapidly with $|\mathbf{p}|$ such that only small phonon momenta contribute to the $\mathbf{p}_j$ sums and only small center-of-mass kinetic energies appear in the denominators. If the optical phonon energy $\hbar\Omega$ is large compared to the energetic distance between the relevant excitonic resonances, the energy denominators in both our and the perturbative result will only weakly depend on the phonon momenta, and both formulas will lead to very similar steady-state luminescence. We actually find numerically for the second phonon sidebands in ZnO and GaN that at temperatures from absolute zero to 60 K, the relative deviation remains below 1 % throughout the entire spectral range.

4.4.1.2 Exciton-phonon scattering

The perturbative approach summarized in Sec. 4.2 describes phonon-assisted luminescence as series of exciton-phonon scattering events followed by recombination from within the radiative cone. For the second and higher-order sidebands, these scattering sequences can contain arbitrary intermediate states such that each ν_j sum in Eq. (4.3) extends over the entire spectrum of excitonic quantum numbers. There is a one-to-one mapping between the different scattering contributions to the perturbative result and the corresponding terms in our exciton-picture formula (4.35). When all possible sequences are included, the evaluation of the n-th replicum becomes a formidable task already for $n = 2$. For practical computations, it is therefore necessary to identify the dominant contributions.

The relevant exciton-phonon matrix elements $g_{\mathbf{p}}^{\nu,\nu'}$ are calculated analytically in Appendix E.3, and the scattering probabilities $|g_{\mathbf{p}}^{\nu,\nu'}|^2$ are plotted in Fig. 24 for $\nu = 1\text{s}$ and $\nu' = 1\text{s}, 2\text{s}, 2\text{p}$. While $g_{\mathbf{p}}^{1\text{s},1\text{s}}$ and $g_{\mathbf{p}}^{1\text{s},2\text{s}}$ only depend on $|\mathbf{p}|$, the matrix element $g_{\mathbf{p}}^{1\text{s},2\text{p}}$ is proportional to the z component of $\mathbf{p}$ such that $|g_{\mathbf{p}}^{1\text{s},2\text{p}}|^2$ can assume any value inside the shaded area. A scattering
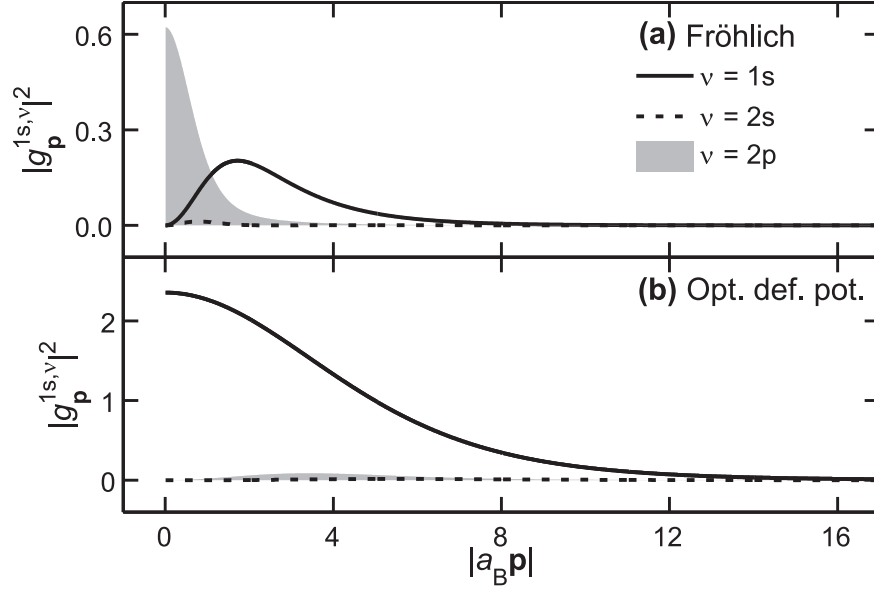
Figure 24: Absolute values squared of the relevant exciton-phonon matrix elements $g_{\mathbf{p}}^{\nu,\nu'}$ as function of the transferred crystal momentum $\hbar\mathbf{p}$ (measured in inverse exciton Bohr radii a_{B}^{-1}) for GaN parameters with Fröhlich coupling (a) and optical deformation-potential coupling (b).

process with momentum transfer $\mathbf{p}$ is often said to have *forbidden* (*allowed*) *character* if the corresponding matrix element vanishes (does not vanish) for $|\mathbf{p}| \to 0$. We find that in case of Fröhlich interaction (a), the phonon-induced scattering out of an exciton state ν into an exciton state ν' has allowed character if ν and ν' have opposite parities and forbidden character, otherwise, see Eq. (E.31). Based on this observation, the author of Ref. [49] argues that scattering sequences through intermediate states with alternating parity should give the main contribution to the total scattering probability (4.2). This assumption is often used in the literature when the line shape of the second replicum is analyzed [56–58]. However, our numerical calculations for GaN and ZnO systems show that even at low temperatures where the small-$|\mathbf{p}|$ behavior of the matrix elements becomes more important, the 1s → 1s → 1s scattering sequence still contributes more strongly to the second sideband than the 1s → 2p → 1s scattering sequence. Scattering through higher exciton states only provides small corrections [133]. For optical deformation-potential coupling (b), the situation is very different from the Fröhlich case. Here, $g_{\mathbf{p}}^{1s,1s}$ approaches $-\Delta g_{\mathbf{p}} = g_{\mathrm{c},\mathbf{p}} - g_{\mathrm{v},\mathbf{p}}$ for $\mathbf{p} \to \mathbf{0}$ while all other 1s → ν scattering processes have forbidden character and much lower transition probabilities throughout the entire phonon-momentum range, see Eq. (E.32). Hence, scattering sequences where the relative motion of the electron-hole pair remains in the ground state 1s clearly provide the dominant contributions to all phonon replica. We will use this property in Sec. 4.4.2.3 to simplify Eq. (4.35) to a much more compact luminescence formula for arbitrary-order sidebands due to optical deformation-potential interaction.

We further conclude from Fig. 24 that excitons interact more strongly with phonons via optical deformation-potential interaction than via Fröhlich interaction although the opposite is true for the electron-phonon scattering. The physical reason for this behavior is that an exciton is a neutral quasi-particle and thus interacts relatively weakly with the macroscopic

electric fields that are caused by LO phonons in a polar crystal.[5]

4.4.2 Polaron-picture analysis

The non-perturbative treatment of the electron-phonon interaction is based on the so-called *polaron picture*. Conceptually, a polaron is a quasi-particle composed of an electron and the lattice polarization accompanying it. Such a combination is also referred to as *dressed electron* in the literature. Starting from the Hamiltonian (4.5), the polaron picture is formally introduced via the unitary transformation $\hat{\bar{H}} = \hat{T}\hat{H}\hat{T}^\dagger$ with

$$\hat{T} \equiv \exp \sum_{\lambda,\mathbf{k},\mathbf{p}} g_{\lambda,\mathbf{p}} \hat{a}^\dagger_{\lambda,\mathbf{k}-\mathbf{p}} a_{\lambda,\mathbf{k}} \left(\hat{D}^\dagger_{\mathbf{p}} - \hat{D}_{-\mathbf{p}} \right). \tag{4.36}$$

This transformation generalizes the textbook treatment of the shifted harmonic oscillator [82] and was previously used, e.g., in Ref. [59] to calculate phonon-assisted resonances in semiconductor absorption spectra. The explicit transformation rules are given in Appendix F.1. It is important to note that in the Coulomb Hamiltonian $\hat{H}_{\mathrm{el-el}}$, we have to replace the matrix element $V_{\mathbf{q}} = e^2/\epsilon_0\epsilon(0)\mathscr{L}^3|\mathbf{q}|^2$ by $e^2/\epsilon_0\epsilon(\infty)\mathscr{L}^3|\mathbf{q}|^2$ before the transformation. After all, as discussed in Sec. 2.2.4.2, the high-frequency permittivity $\epsilon(\infty)$ equals the static permittivity $\tilde{\epsilon}(0)$ of a fictitious system without lattice vibrations. The non-perturbative treatment of the electron-phonon coupling includes the phonon-induced screening of the carrier-carrier interaction fully microscopically. Consequently, this screening contribution must not be taken into account via the macroscopic dielectric constant.

In the following, we use a compact matrix notation for quantities $(M)_{\mathbf{k},\mathbf{k}'}$ that depend on a pair of crystal momenta. Powers $(M^n)_{\mathbf{k},\mathbf{k}'}$ and exponential series $(\mathrm{e}^M)_{\mathbf{k},\mathbf{k}'} \equiv \sum_{n=0}^\infty (M^n)_{\mathbf{k},\mathbf{k}'}/n!$ are defined by means of the matrix-multiplication rule $(MN)_{\mathbf{k},\mathbf{k}'} \equiv \sum_{\mathbf{k}_1} (M)_{\mathbf{k},\mathbf{k}_1} (N)_{\mathbf{k}_1,\mathbf{k}'}$. We apply this matrix notation to both numbers and operator quantities. The polaron transformation casts the original Hamiltonian into form

$$\hat{\bar{H}} = \hat{\bar{H}}_{\mathrm{pol}} + \hat{\bar{H}}_{\mathrm{em}} + \hat{\bar{H}}_{\mathrm{latt}} + \hat{\bar{H}}_{\mathrm{pol-pol}} + \hat{\bar{H}}_{\mathrm{pol-em}} \tag{4.37}$$

where the different contributions can be written as

$$\hat{\bar{H}}_{\mathrm{pol}} = \sum_{\lambda,\mathbf{k},\mathbf{q}} \left[(\mathrm{e}^{-\hat{C}_\lambda} \mathcal{E}_\lambda \mathrm{e}^{\hat{C}_\lambda})_{\mathbf{0},\mathbf{q}} \hat{a}^\dagger_{\lambda,\mathbf{k}} \hat{a}_{\lambda,\mathbf{k}+\mathbf{q}} - \hbar\Omega|g_{\lambda,\mathbf{q}}|^2 \hat{a}^\dagger_{\lambda,\mathbf{k}} \hat{a}_{\lambda,\mathbf{k}} \right] \tag{4.38}$$

$$\hat{\bar{H}}_{\mathrm{latt}} = \sum_{\mathbf{p}} \hbar\Omega \left(\hat{D}^\dagger_{\mathbf{p}} \hat{D}_{\mathbf{p}} + \frac{1}{2} \right), \tag{4.39}$$

$$\hat{\bar{H}}_{\mathrm{em}} = \sum_{\mathbf{q}} \hbar\omega_{\mathbf{q}} \left(\hat{B}^\dagger_{\mathbf{q}} \hat{B}_{\mathbf{q}} + \frac{1}{2} \right), \tag{4.40}$$

$$\hat{\bar{H}}_{\mathrm{pol-pol}} = \frac{1}{2} \sum_{\substack{\lambda,\lambda' \\ \mathbf{k},\mathbf{k}',\mathbf{q}}} V^{\lambda,\lambda'}_{\mathbf{q}} \hat{a}^\dagger_{\lambda,\mathbf{k}} \hat{a}^\dagger_{\lambda',\mathbf{k}'} \hat{a}_{\lambda',\mathbf{k}'+\mathbf{q}} \hat{a}_{\lambda,\mathbf{k}-\mathbf{q}}, \tag{4.41}$$

$$\hat{\bar{H}}_{\mathrm{pol-em}} = -\sum_{\mathbf{k},\mathbf{k}',\mathbf{q}} \mathrm{i} \left[\mathcal{F}_{\mathbf{q}}(\mathrm{e}^{\hat{C}})_{\mathbf{k},\mathbf{k}'} \hat{a}^\dagger_{\mathrm{c},\mathbf{k}+\mathbf{q}} \hat{a}_{\mathrm{v},\mathbf{k}'} + \mathcal{F}^*_{\mathbf{q}}(\mathrm{e}^{\hat{C}})_{\mathbf{k},\mathbf{k}'} \hat{a}^\dagger_{\mathrm{v},\mathbf{k}} \hat{a}_{\mathrm{c},\mathbf{k}'-\mathbf{q}} \right] \hat{B}_{\mathbf{q}} + \mathrm{H.C.} \tag{4.42}$$

---

[5]As shown in Ref. [134], the fermionic substructure of an exciton allows for strong Fröhlich-like exciton-phonon coupling in semiconductor quantum dots, which can be described in terms of excitonic polarons. It remains an open question whether a similar effect might also occur in bulk systems.

Here, we have defined the matrices $(\mathcal{E}_\lambda)_{\mathbf{k},\mathbf{k}'} \equiv \delta_{\mathbf{k},\mathbf{k}'}\varepsilon_{\lambda,\mathbf{k}}$, $(\hat{C}_\lambda)_{\mathbf{k},\mathbf{k}'} \equiv g_{\lambda,\mathbf{k}'-\mathbf{k}}(\hat{D}_{\mathbf{k}-\mathbf{k}'} - \hat{D}^\dagger_{\mathbf{k}'-\mathbf{k}})$, and $(\hat{C})_{\mathbf{k},\mathbf{k}'} \equiv (\hat{C}_{\mathrm{v}})_{\mathbf{k},\mathbf{k}'} - (\hat{C}_{\mathrm{c}})_{\mathbf{k},\mathbf{k}'}$. Details of the calculation can be found in Appendix F.1.

Following the spirit of Ref. [59] and earlier works on the polaron problem [82], we replace all phonon-operator combinations appearing in Eq. (4.38) by their thermal averages. This procedure yields

$$\hat{\tilde{H}}_{\mathrm{pol}} = \sum_{\lambda,\mathbf{k}} e_{\lambda,\mathbf{k}} \hat{a}^\dagger_{\lambda,\mathbf{k}} \hat{a}_{\lambda,\mathbf{k}}. \tag{4.43}$$

In view of this structure, $\hat{\tilde{H}}_{\mathrm{pol}}$ can be interpreted as energy of free polarons. The polaron dispersion $e_{\lambda\mathbf{k}}$ is explicitly evaluated in Appendix F.2 for a phonon bath at temperature $T_{\mathrm{phon}} = 0$. The resulting band structure is characterized by a smaller band gap and larger effective masses compared with the bare valence and conduction-band electrons. Moreover, as announced above, the incorporation of the lattice distortion into the carrier dynamics leads to screening of the Coulomb interaction. The renormalized Coulomb matrix elements $V^{\lambda,\lambda'}_{\mathbf{q}} = V_{\mathbf{q}} - 2\hbar\Omega g^*_{\lambda,\mathbf{q}} g_{\lambda',\mathbf{q}}$ can only become band-dependent when $g_{\mathrm{c},\mathbf{q}}$ and $g_{\mathrm{v},\mathbf{q}}$ are different. For the Fröhlich part of the electron-phonon matrix elements $g_{\lambda,\mathbf{q}}$ that is band-independent and proportional to $|\mathbf{q}|^{-1}$, this renormalization reduces to an enhancement of the dielectric constant. We have used this observation in Sec. 2.2.4.2 to determine the amplitude of the Fröhlich matrix elements. In the literature, the optical deformation-potential interaction is usually completely neglected when the polaron band structure and the polaron-polaron interaction are evaluated. Our numerical calculations indeed confirm that the Fröhlich coupling provides clearly the main contribution to the modifications imposed by the unitary transformation. This result constitutes just another example of how phonon-related phenomena in polar semiconductors are usually dominated by the long-range part of the electron-phonon interaction. In this respect, the phonon-assisted luminescence appears to be a very special case.

The main advantage of the polaron transformation with bath approximation is that in the absence of a light field, polaron and phonon degrees of freedom are not coupled anymore. However, the light-matter interaction Hamiltonian $\hat{\tilde{H}}_{\mathrm{pol-em}}$ contains phonon-operator combinations of arbitrary order, provided that $g_{\mathrm{c},\mathbf{p}} \neq g_{\mathrm{v},\mathbf{p}}$. We will see in the following how these terms give rise to arbitrary-order sideband emission. In Sec. 4.4.2.1, we apply the cluster-expansion scheme to derive semiconductor luminescence equations in the polaron picture. We solve these equations in Sec. 4.4.2.2 for arbitrary-order phonon replica and compare the result in Sec. 4.4.2.3 to the exciton-picture analysis.

4.4.2.1 Semiconductor luminescence equations in the polaron picture

In the polaron picture, the luminescence spectrum in the incoherent regime follows from

$$i\hbar \frac{\mathrm{d}}{\mathrm{d}t} \Delta\langle \hat{B}^\dagger_{\mathbf{q}} \hat{B}_{\mathbf{q}} \rangle = 2i\,\mathrm{Re}\Big[\mathcal{F}^*_{\mathbf{q}} \sum_{\mathbf{k},\mathbf{p}} \Delta\langle \hat{B}^\dagger_{\mathbf{q}} \hat{a}^\dagger_{\mathrm{v},\mathbf{k}} \hat{a}_{\mathrm{c},\mathbf{k}+\mathbf{q}+\mathbf{p}} (\mathrm{e}^{\hat{C}})_{\mathbf{0},\mathbf{p}} \rangle\Big]. \tag{4.44}$$

Normal ordering of the exponential matrix $\mathrm{e}^{\hat{C}}$ as performed in Sec. F.2 decomposes the expectation value on the right-hand side into the $(\alpha + \beta + 2)$-particle correlations

$$\Pi^\alpha_\beta(\mathbf{k};\mathbf{q};\mathbf{p}) \equiv \Delta\langle \hat{B}^\dagger_{\mathbf{q}} \hat{a}^\dagger_{\mathrm{v},\mathbf{k}-\mathbf{q}_{\mathrm{h}}-\mathbf{p}_{\mathrm{h}}} \hat{a}_{\mathrm{c},\mathbf{k}+\mathbf{q}_{\mathrm{e}}+\mathbf{p}_{\mathrm{e}}} ([\hat{d}^\dagger]^\alpha \hat{d}^\beta)_{\mathbf{0},\mathbf{p}} \rangle \tag{4.45}$$

with $(\hat{d})_{\mathbf{k},\mathbf{k}'} \equiv \Delta g^*_{\mathbf{k}-\mathbf{k}'} \hat{D}_{\mathbf{k}-\mathbf{k}'}$ and $(\hat{d}^\dagger)_{\mathbf{k},\mathbf{k}'} \equiv [(d)_{\mathbf{k}',\mathbf{k}}]^\dagger$. The quantity $\Pi^\alpha_\beta(\mathbf{k};\mathbf{q};\mathbf{p})$ describes radiative recombination of an electron-hole pair under the assistance of $\alpha + \beta$ phonons out of

which α are emitted and β are absorbed. According to the general discussion in Sec. 4.1 such processes contribute to the $(\alpha - \beta)^{\text{th}}$ phonon sideband if $\alpha \neq \beta$, and to the zero-phonon line if $\alpha = \beta$.

Since the full equation hierarchy on the $(\alpha+\beta+2)^{\text{th}}$ level of cluster expansion cannot be solved for arbitrary α and β, we need to restrict the analysis to a narrow subset of relevant correlations. When expanding the expectation values that appear in the equations of motion for the recombination correlations $\Pi_\beta^\alpha(\mathbf{k}; \mathbf{q}; \mathbf{p})$, we treat the photon-phonon part $\hat{O}_\beta^\alpha(\mathbf{q}, \mathbf{p}) \equiv \hat{B}_\mathbf{q}^\dagger([\hat{d}^\dagger]^\alpha \hat{d}^\beta)_{\mathbf{0},\mathbf{p}}$ as a single $(\alpha + \beta + 1)$-particle operator. In other words, we exclude factorization into terms that separate and distribute the photon operator and the phonon operators into products of lower-level correlations. After all, only those correlations produced by the factorization that include $\hat{O}_\beta^\alpha(\mathbf{q}, \mathbf{p})$ can describe processes involving one photon and $(\alpha + \beta)$ phonons. We therefore expect that the most significant aspects of phonon-assisted radiative recombination are included in such an analysis. The resulting luminescence equations in the polaron picture thus take the form

$$
\left[\mathrm{i}\hbar \frac{\mathrm{d}}{\mathrm{d}t} + \hbar\omega_\mathbf{q} + (\alpha - \beta)\hbar\Omega \right] \Pi_\beta^\alpha(\mathbf{k}; \mathbf{q}, \mathbf{p}) = \sum_{\mathbf{k}'} \bar{A}_{\mathbf{k},\mathbf{k}'}(\mathbf{q} + \mathbf{p}) \Pi_\beta^\alpha(\mathbf{k}'; \mathbf{q}, \mathbf{p})
$$

$$
+ \mathrm{i}\mathcal{F}_\mathbf{q} \sum_{\mathbf{k}',\mathbf{p}'} \langle \hat{a}_{\mathrm{c},\mathbf{k}'+\mathbf{q}_\mathrm{e}+\mathbf{p}_\mathrm{e}'}^\dagger \hat{a}_{\mathrm{v},\mathbf{k}'-\mathbf{q}_\mathrm{h}-\mathbf{p}_\mathrm{h}'} \hat{a}_{\mathrm{v},\mathbf{k}-\mathbf{q}_\mathrm{h}-\mathbf{p}_\mathrm{h}}^\dagger \hat{a}_{\mathrm{c},\mathbf{k}+\mathbf{q}_\mathrm{e}+\mathbf{p}_\mathrm{e}} (\mathrm{e}^{\hat{C}})_{\mathbf{p}',\mathbf{0}} [(\hat{d}^\dagger)^\alpha \hat{d}^\beta]_{\mathbf{0},\mathbf{p}} \rangle. \quad (4.46)
$$

Analogously to Eqs. (4.9), (4.11), the matrix

$$
\bar{A}_{\mathbf{k},\mathbf{k}'}(\mathbf{q}) = \delta_{\mathbf{k},\mathbf{k}'} \left(\tilde{e}_{\mathbf{k}+\mathbf{q}_\mathrm{e}}^\mathrm{e} + \tilde{e}_{\mathbf{k}-\mathbf{q}_\mathrm{h}}^\mathrm{h} \right) - \left(1 - f_{\mathbf{k}+\mathbf{q}_\mathrm{e}}^\mathrm{e} - f_{\mathbf{k}-\mathbf{q}_\mathrm{h}}^\mathrm{h} \right) V_{\mathbf{k}-\mathbf{k}'}^{\mathrm{v},\mathrm{c}} \quad (4.47)
$$

contains kinetic terms with mean-field energies $\tilde{e}_\mathbf{k}^\mathrm{e} = e_{\mathrm{c},\mathbf{k}} - \sum_{\mathbf{k}'} V_{\mathbf{k}-\mathbf{k}'}^{\mathrm{v},\mathrm{c}} f_{\mathbf{k}'}^\mathrm{e}$ and $\tilde{e}_\mathbf{k}^\mathrm{h} = -e_{\mathrm{v},\mathbf{k}} - \sum_{\mathbf{k}'} V_{\mathbf{k}-\mathbf{k}'}^{\mathrm{v},\mathrm{c}} f_{\mathbf{k}'}^\mathrm{h}$ as well as excitonic signatures due to Coulomb interaction. Stimulated-emission source terms are neglected again. The last term constitutes the spontaneous-emission sources that will be evaluated in the following section.

The coupled equations of motion (4.44), (4.46) constitute the *phonon-assisted semiconductor luminescence equations in the polaron picture.* In the absence of phonons, Eq. (4.46) would agree with the usual semiconductor luminescence equations [50, 54]. The crucial advantage of the polaron-picture analysis is that the general structure of the luminescence equations remains unchanged when carrier-phonon coupling is included. Contrary to the electron-picture analysis from Sec. 4.3 and the exciton-picture analysis from Sec. 4.4.1, recombination correlations containing different numbers of phonon operators are not coupled such that all phonon sidebands can be calculated separately.

4.4.2.2 Steady-state luminescence formula in the polaron picture

The phonon-assisted semiconductor luminescence equations can be solved analytically to calculate steady-state luminescence for arbitrary-order phonon sidebands. The spontaneous-emission source terms in Eq. (4.46) consist of multiple-phonon-assisted two-carrier correlations. In general, the cluster expansion of these contributions would produce a multitude of correlations containing different numbers of phonon creation and annihilation operators. Since the specific details of the phonon dynamics are unlikely to have a significant influence on the sideband luminescence, we evaluate the source terms by means of a bath approximation for the phonon subsystem. More explicitly, we factorize the phonon-assisted carrier correlations into expectation values over the carrier and over the phonon parts. When expanding the phonon

part, we neglect all correlations except for phonon numbers. In this work, we only consider materials where the optical-phonon energies $\hbar\Omega$ are considerable larger than the thermal energies k_BT. Then, it is justified to neglect thermal phonon populations, and the phonon correlations are evaluated as

$$\langle \text{vac}|\big(e^{\hat{C}}\big)_{\mathbf{p}',\mathbf{0}}\big[(\hat{d}^\dagger)^\alpha \hat{d}^\beta\big]_{\mathbf{0},\mathbf{p}}|\text{vac}\rangle = \delta_{\beta,0}\delta_{\mathbf{p},\mathbf{p}'}e^{-G/2}(Q^\alpha)_{\mathbf{p},\mathbf{0}} \tag{4.48}$$

with the matrix $(Q)_{\mathbf{k},\mathbf{k}'} \equiv |\Delta g_{\mathbf{k}-\mathbf{k}'}|^2$ and $G \equiv \sum_{\mathbf{p}}|\Delta g_{\mathbf{p}}|^2$ where $|\text{vac}\rangle$ denotes the phonon vacuum. This procedure is consistent with the calculation of the renormalized single-particle energies as presented in Appendix F.2 and reduces the source terms to densities and excitonic correlations. Because phonon-absorption processes are not included anymore in the analysis, the calculated luminescence spectrum will only have phonon replica on the low-energy side of the zero-phonon line, analogously to the results from Secs. 4.3 and 4.4.1.

In order to solve the luminescence equations analytically, we need to diagonalize the homogeneous part of Eq. (4.46). Again, this task can be achieved with the help of the exciton basis from Appendix A, we only have to replace the eigen-value equations (A.5), (A.6) by

$$E_\nu(\mathbf{Q})\phi^{\text{R}}_{\nu,\mathbf{Q}}(\mathbf{k}) = \sum_{\mathbf{k}'}\bar{A}_{\mathbf{k},\mathbf{k}'}(\mathbf{Q})\phi^{\text{R}}_{\nu,\mathbf{Q}}(\mathbf{k}'), \tag{4.49}$$

$$\big[\phi^{\text{L}}_{\nu,\mathbf{Q}}(\mathbf{k})\big]^* E_\nu(\mathbf{Q}) = \sum_{\mathbf{k}'}\big[\phi^{\text{L}}_{\nu,\mathbf{Q}}(\mathbf{k}')\big]^* \bar{A}_{\mathbf{k}',\mathbf{k}}(\mathbf{Q}). \tag{4.50}$$

Because the latter equations contain $\bar{A}_{\mathbf{k}',\mathbf{k}}(\mathbf{Q})$ instead of the matrix $A_{\mathbf{k}',\mathbf{k}}(\mathbf{Q})$ from Eq. (4.10), they lead to different excitonic eigen energies. The physical reason for this modification is that the non-perturbative treatment describes the phonon-induced shifts of the optical resonances fully consistently, including effects that would only follow from higher-order clusters in the electron-picture analysis.

When we assume stationary distributions for densities and electron-hole correlations, we can use the exciton basis to derive a compact steady-state formula for arbitrary-order sidebands,

$$I_{\text{PL}}(\omega) = \sum_{n=0}^{\infty}\sum_{\nu}I^{(n)}_{\text{PL},\nu}(\omega). \tag{4.51}$$

Luminescence at the zero-phonon line ($n = 0$) and the n-th replicum ($n = 1, 2, \ldots$) of the excitonic resonance ν follows from

$$I^{(n)}_{\text{PL},\nu}(\omega_{\mathbf{q}}) = \frac{2|\mathcal{F}_{\mathbf{q}}|^2}{\hbar}e^{-G}\frac{1}{n!}\sum_{\mathbf{Q}}|\phi^{\text{R}}_{\nu\mathbf{Q}}(\mathbf{r}=\mathbf{0})|^2\text{Im}\left[\frac{\mathcal{G}^{(n)}_{\mathbf{Q}-\mathbf{q}}N_\nu(\mathbf{Q})}{E_{\nu\mathbf{Q}} - n\hbar\Omega - \hbar\omega_{\mathbf{q}} - \mathrm{i}\gamma_n}\right]. \tag{4.52}$$

The source terms

$$N_\nu(\mathbf{Q}) = \Delta N_\nu(\mathbf{Q}) + N^{\text{eh}}_\nu(\mathbf{Q}) \tag{4.53}$$

contain contributions from both excitonic population and electron-hole plasma,

$$\Delta N_\nu(\mathbf{Q}) = \Delta\langle \hat{X}^\dagger_{\nu,\mathbf{Q}}\hat{X}_{\nu,\mathbf{Q}}\rangle, \tag{4.54}$$

$$N^{\text{eh}}_\nu(\mathbf{Q}) = \sum_{\mathbf{k}}|\phi^{\text{L}}_{\nu,\mathbf{Q}}(\mathbf{k})|^2 f^{\text{e}}_{\mathbf{k}+\mathbf{Q}_{\text{e}}}f^{\text{h}}_{\mathbf{k}-\mathbf{Q}_{\text{h}}}. \tag{4.55}$$

The weight factors $\mathcal{G}^{(n)}_{\mathbf{Q}-\mathbf{q}}$ are defined as iterated convolutions of the effective matrix element $\Delta g_{\mathbf{p}} = g_{v,\mathbf{p}} - g_{c,\mathbf{p}}$,

$$\mathcal{G}^{(0)}_{\mathbf{Q}-\mathbf{q}} \equiv \delta_{\mathbf{Q},\mathbf{q}}, \tag{4.56a}$$

$$\mathcal{G}^{(1)}_{\mathbf{Q}-\mathbf{q}} \equiv |\Delta g_{\mathbf{Q}-\mathbf{q}}|^2, \tag{4.56b}$$

$$\vdots$$

$$\mathcal{G}^{(n)}_{\mathbf{Q}-\mathbf{q}} \equiv \sum_{\mathbf{p}_1,\ldots,\mathbf{p}_{n-1}} |\Delta g_{\mathbf{Q}-\mathbf{p}_{n-1}}|^2 |\Delta g_{\mathbf{p}_{n-1}-\mathbf{p}_{n-2}}|^2 \cdots |\Delta g_{\mathbf{p}_2-\mathbf{p}_1}|^2 |\Delta g_{\mathbf{p}_1-\mathbf{q}}|^2. \tag{4.56c}$$

The factor e^{-G} with $G = \sum_{\mathbf{p}} |\Delta g_{\mathbf{p}}|^2$ renormalizes the whole spectrum. Thus, altering the amplitude of $\Delta g_{\mathbf{Q}}$ not only changes the relative strength of the sideband emission but also rescales the zero-phonon line, which generalizes the observation discussed after Eq. (4.20) to higher-order processes. The phenomenological constants γ_n account for higher-order scattering processes and can be fitted to the experimental line widths.

For comparison with the previous results, we consider the low-density limit, restrict the analysis to the ground state $\nu = 1s$, and neglect the photon momentum with respect to the phonon momenta. The luminescence formula can then be written in a more compact form $I_{\mathrm{PL}}(\omega) = \sum_{n=0}^{\infty} I^{(n)}_{\mathrm{PL}}(\omega)$ with

$$I^{(n)}_{\mathrm{PL}}(\omega) = \frac{2}{\hbar} |\mathcal{F}\phi_{1s}(\mathbf{r} = \mathbf{0})|^2 \, \mathrm{e}^{-G} \frac{1}{n!} \operatorname{Im} \sum_{\mathbf{Q}} \frac{\mathcal{G}^{(n)}_{\mathbf{Q}} N_{1s}(\mathbf{Q})}{E_{1s}(\mathbf{Q}) - n\hbar\Omega - \hbar\omega - \mathrm{i}\gamma_n}. \tag{4.57}$$

4.4.2.3 Relation to the exciton-picture analysis

At first glance, the steady-state luminescence formula (4.35) in the exciton picture appears to have a very different structure than the excitonic contribution to the polaron-picture formula (4.57). However, a close inspection reveals the conditions under which both approaches lead to comparable sideband spectra.

We notice that Eq. (4.57) predicts vanishing phonon replica in case of band-independent electron-phonon matrix elements $g_{c,\mathbf{p}} = g_{v,\mathbf{p}}$. The polaron-picture formula thus clearly underestimates the phonon-assisted luminescence due to Fröhlich coupling. This can directly be seen from the Hamiltonian in Eqs. (4.43), (4.39)–(4.42) that has the same form as the pure electron-photon Hamiltonian $\hat{H}_{\mathrm{el}} + \hat{H}_{\mathrm{em}} + \hat{H}_{\mathrm{el-el}} + \hat{H}_{\mathrm{el-em}}$ when $g_{c,\mathbf{p}} = g_{v,\mathbf{p}}$. Hence, the artifact of vanishing sidebands is a consequence of the bath approximation for the polaron Hamiltonian. If the phonon operators appearing in Eq. (4.38) were fully included, the photon-assisted polarizations $\Delta\langle \hat{B}^{\dagger} \hat{a}^{\dagger}_{v} \hat{a}_{c} \rangle$ would couple to all phonon-assisted recombination correlations $\Delta\langle \hat{B}^{\dagger} \hat{a}^{\dagger}_{v} \hat{a}_{c} (\hat{d}^{\dagger})^{\alpha} \hat{d}^{\beta} \rangle$. Even for $g_{c,\mathbf{p}} = g_{v,\mathbf{p}}$, arbitrary-order sideband emission would thus come into play via the coupled dynamics of all these quantities. Then, the polaron-picture analysis would not provide any advantage over the electron-picture analysis but would actually be even more complicated. However, the numerical examples from Secs. 4.3.3.1 and 4.4.1.2 suggest that in many experimental situations, the strongly band-dependent optical deformation-potential interaction yields the main contribution to the sideband luminescence. The explicit evaluation of the first replicum with the exact Hamiltonian (4.38) indicates that in that case, the bath approximation produces reasonable results.

As discussed in Sec. 4.4.1.2, only 1s-1s scattering has to be considered for optical deformation-potential coupling. In order to compare the exciton-picture and the polaron-picture results, we should therefore restrict all ν_j sums in the exciton-picture formula (4.35) to the ground

state $\nu_j = 1s$. Contrary to the electron-phonon matrix element $g_{\lambda,\mathbf{p}} = \text{const}$, the exciton-phonon matrix element $g_{\mathbf{p}}^{1s,1s}$ decays rapidly for large $|\mathbf{p}|$ as shown in Fig. 24. It follows that effectively, only small center-of-mass kinetic energies appear in the energy denominators in the last two lines of Eq. (4.35). When we neglect these energies with respect to the optical phonon energy $\hbar\Omega$, the sideband luminescence formula in the exciton picture simplifies considerably. Explicitly, we obtain

$$I_{\mathrm{PL}}^{(n)}(\omega) \simeq \frac{2}{\hbar}\,|\mathcal{F}\phi_{1s}(\mathbf{r}=\mathbf{0})|^2\,\frac{1}{n!}\,\mathrm{Im}\sum_{\mathbf{Q}}\frac{\mathcal{H}_{\mathbf{Q}}^{(n)}\Delta N_{1s}(\mathbf{Q})}{E_{1s}(\mathbf{Q})-n\hbar\Omega-\hbar\omega-\mathrm{i}\gamma_n} \tag{4.58}$$

with the iterated convolutions

$$\mathcal{H}_{\mathbf{Q}}^{(n)} \equiv \sum_{\mathbf{p}_1,\dots,\mathbf{p}_{n-1}}\left|g_{\mathbf{Q}-\mathbf{p}_{n-1}}^{1s,1s}\right|^2\left|g_{\mathbf{p}_{n-1}-\mathbf{p}_{n-2}}^{1s,1s}\right|^2\cdots\left|g_{\mathbf{p}_2-\mathbf{p}_1}^{1s,1s}\right|^2\left|g_{\mathbf{p}_1}^{1s,1s}\right|^2 \tag{4.59}$$

that are defined analogously to Eq. (4.56). Apart from the renormalization factor e^{-G}, the only difference between Eq. (4.57) and Eq. (4.58) is that the polaron-picture formula contains $|\Delta g_{\mathbf{p}}| = |g_{\mathrm{v},\mathbf{p}} - g_{\mathrm{c},\mathbf{p}}|$ instead of $|g_{\mathbf{p}}^{1s,1s}|$. As already noticed above, $\Delta g_{\mathbf{p}}$ is nothing else but the small-$\mathbf{p}$ limit of $g_{\mathbf{p}}^{1s,1s}$. We conclude that the polaron-picture analysis basically reproduces the results from the exciton-picture analysis so long as optical deformation-potential coupling is considered. The advantage of the non-perturbative treatment is that the analysis is not restricted to emission from excitonic populations. The numerical examples in Sec. 4.3.3.2 show that at least at low temperatures, uncorrelated plasma and excitonic populations contribute additively to the sideband luminescence. Because this observation is reproduced by Eq. (4.57), we expect that the polaron-picture approach also describes higher-order plasma emission correctly.

In spite of the formal elegance of the luminescence formula, the evaluation of higher-order sidebands with Eq. (4.58) is still rather involved. For the n-th replicum in a d-dimensional system, dn-dimensional integrals have to be computed. To make our theoretical results more practical, we replace the explicit form of $g_{\mathbf{p}}^{1s,1s}$ by an effective matrix element $g_{\mathbf{p}}^{\mathrm{eff}}$. At the Γ point, $g_{\mathbf{p}=\mathbf{0}}^{\mathrm{eff}} = \Delta g_{\mathbf{p}=\mathbf{0}} = g_{\mathbf{p}=\mathbf{0}}^{1s,1s}$, while for large $\mathbf{p}$, the coupling strength decays like $g_{\mathbf{p}}^{\mathrm{eff}} = \Delta g_{\mathbf{p}=\mathbf{0}}\varphi(|\mathbf{p}|)$ where $\varphi(0) = 1$ and $\varphi(|\mathbf{p}|)$ vanishes on a certain decay length σ. The parameter σ can be fitted such that very different explicit forms of $\varphi(p)$ yield very similar sideband spectra. This observation justifies our model for the matrix element in hindsight. For simplicity, we take $\varphi(p)$ as a Gaussian of width σ. This choice enables us to evaluate the luminescence formula analytically for arbitrary phonon replica. From Eq. (4.58), we obtain

$$I_{\mathrm{PL}}^{(n)}(\omega) \simeq \frac{2}{\hbar}|\mathcal{F}\phi_{1s}(\mathbf{r}=\mathbf{0})|^2 f_n(\omega)\frac{K^n}{n!} \tag{4.60}$$

where

$$K \equiv \left(\frac{\mathscr{L}}{2\pi}\right)^3|\Delta g_{\mathbf{p}=\mathbf{0}}|^2\left(\sigma\sqrt{2\pi}\right)^3 \tag{4.61}$$

with the quantization length $\mathscr{L}$ and

$$f_n(\omega) \equiv \int \Phi_{\sigma\sqrt{n}}(|\mathbf{Q}|)\,\mathrm{Im}\left[\frac{N_{1s}(\mathbf{Q})}{E_{1s}(\mathbf{Q})-n\hbar\Omega-\hbar\omega-\mathrm{i}\gamma_n}\right]\mathrm{d}^3Q \tag{4.62}$$
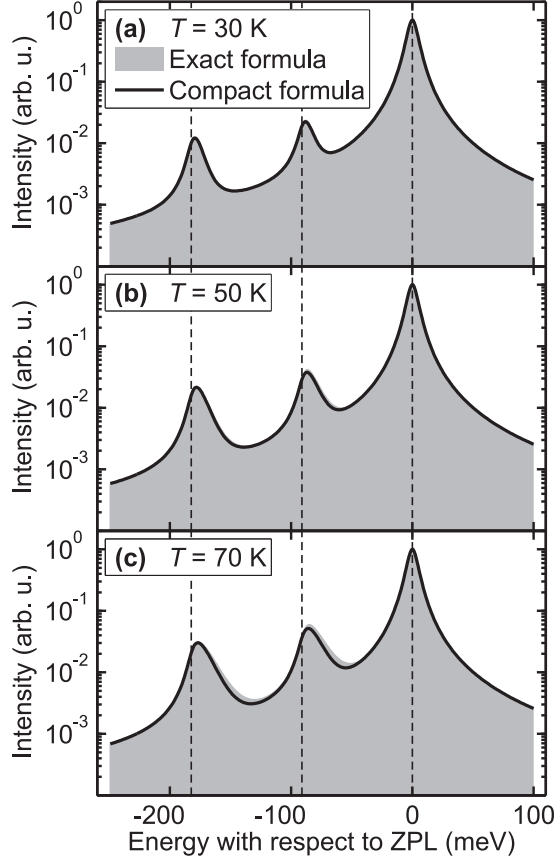
Figure 25: Sideband spectra calculated with the exact formula (4.35) (shaded areas) and with the compact formula (4.60) (solid lines) for GaN bulk at three different temperatures. We assume optical deformation-potential interaction with coupling constant $d_0 = 21.3\,\mathrm{eV}$. A reasonable fit is obtained by using a decay length $a_0\sigma = 2.8$ in the compact formula.

with the normalized Gaussian $\Phi_\sigma(Q) = (\sigma\sqrt{2\pi})^{-3}\exp(-Q^2/2\sigma^2)$. By comparison with the exact formula (4.35), we can define a unique procedure to determine the Gaussian width σ. It turns out that, as illustrated in Fig. 25, σ can generally be fitted such that Eqs. (4.35) and (4.60) yield very similar results for the first two sidebands in a wide temperature range. Having fixed σ, one can then use the much more compact formula (4.60) to compute higher-order sidebands.

4.4.3 Numerical case studies

Now that we have the luminescence formulas (4.35), (4.60) at our disposal, we can extend our numerical case studies to higher-order replica. In Sec. 4.4.3.1, we calculate how the relative sideband intensities depend on the carrier temperature. Phonon-assisted emission from free and impurity-bound excitons is compared in Sec. 4.4.3.2. Finally, we analyze phonon replica due to non-polar optical modes in Sec. 4.4.3.3.
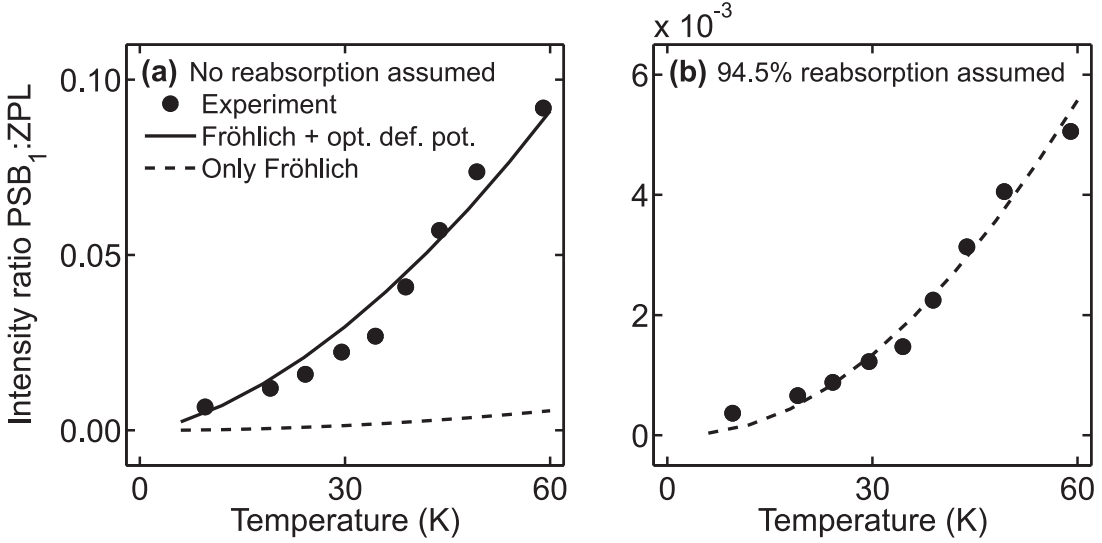
Figure 26: Relative intensity of the first phonon sideband as function of temperature for a GaN epilayer. The bold dots mark the experimental data [56]. Solid and dashed lines represent calculated results with and without inclusion of the optical deformation-potential interaction, respectively. For frame (a), we take the measured intensity ratios, while for frame (b), we compensate for an assumed amount of re-absorption of light emitted at the zero-phonon line.

4.4.3.1 Temperature dependence of the sideband emission

We have found in Sec. 4.3.3.1 that even in strongly polar semiconductors where the electron-phonon scattering rates are mainly determined by the Fröhlich coupling, the optical deformation-potential interaction might provide the dominant contribution to the sideband emission. Because this possibility is usually not considered in the literature, we need to identify clear-cut signatures in the sideband spectra that allow to distinguish between the two electron-phonon coupling mechanisms.

In view of Fig. 20, it appears that the intensity of the first replicum relative to the zero-phonon line would unambiguously show whether the phonon-assisted luminescence must be assigned to the long- or to the short-range part of the electron-phonon interaction. However, we have already mentioned in Sec. 2.2.4.2 that the optical deformation-potential constants d_0 for polar optical modes are generally less well defined than for non-polar optical modes. An even greater drawback is that prominent sideband emission is typically observed for bulk systems where re-absorption in the material due to polariton-propagation effects can strongly reduce the measured intensity of the zero-phonon line. The reduction factor is difficult to estimate because it also depends on the geometry of the sample. For quantum-well systems, on the other hand, the intensity ratio of PSB_1 and ZPL can only be calculated when the confinement potentials are known very accurately, see Sec. 4.3.3.3. Figure 26 illustrates these problems. The bold dots represent measured intensity ratios for a GaN epilayer as function of temperature [56] while the lines mark the calculated results. Quantitative agreement with the given experimental data is obtained when we combine Fröhlich interaction with optical deformation-potential interaction where we assume a coupling constant $d_0 = 21.3\,\mathrm{eV}$ that lies $60\,\%$ below the value for non-polar optical modes as found in the literature [91]. See the solid

line in frame (a). We see from the dashed line that Fröhlich coupling alone would yield much weaker sideband emission. However, the authors of Ref. [56] do not quantify the re-absorption in the epilayer. It is well possible that the polariton-propagation effects reduce the apparent intensity of the zero-phonon line to 5.5 % of the original intensity. In that case, we would achieve a reasonable fit by including only the Fröhlich contributions (b). Actually, any other combination of Fröhlich coupling and optical deformation-potential coupling between these two limiting cases would also come into consideration. We conclude that the overall amplitude of the sideband emission relative to the zero-phonon line is not a good criterion to distinguish the two electron-phonon interaction mechanisms.

In order to find a better criterion, we calculate the temperature dependence of the relative intensities of the first two sidebands. To this end, we use GaN parameters with $d_0 = 21.3\,\text{eV}$ and evaluate the accurate exciton-picture formula (4.35) where we consider 1s-1s and 1s-2p scattering for Fröhlich coupling and only 1s-1s scattering for optical deformation-potential interaction, as justified in Sec. 4.4.1.2. The results are shown as solid lines in Fig. 27 where for frame (a) and frame (b), respectively, only the short-range and the long-range part of the interaction are taken into account. The intensity ratios $F_{n,n'}$ are defined as

$$F_{n,n'} \equiv \frac{\displaystyle\int I_{\text{PL}}^{(n')}(\omega)\,\text{d}(\hbar\omega)}{\displaystyle\int I_{\text{PL}}^{(n)}(\omega)\,\text{d}(\hbar\omega)}. \tag{4.63}$$

It turns out that the intensities of the first two replica relatively to the zero-phonon line roughly follow power laws $F_{0,n}(T) \propto T^{\alpha_{0,n}}$ (shaded areas). In case $n = 2$, the exponents $\alpha_{0,2}^{\text{def}} \simeq 1.57$ for optical deformation-potential coupling and $\alpha_{0,2}^{\text{Fr}} \simeq 1.55$ for Fröhlich interaction are too close to be useful in a theory-experiment comparison. For the first sideband, we have $\alpha_{0,1}^{\text{def}} \simeq 1.55$ and $\alpha_{0,1}^{\text{Fr}} \simeq 2.20$. Figure 26 demonstrates that the difference between these two exponents can still be too small to draw a unique conclusion about the nature of the underlying coupling mechanism. Because $\alpha_{0,1}^{\text{def}}$ and $\alpha_{0,2}^{\text{def}}$ are similar, $F_{1,2} = F_{0,2} : F_{0,1}$ depends only weakly on the temperature for optical deformation-potential interaction. The situation is different for Fröhlich interaction where $F_{1,2}$ varies over more than one order of magnitude in the temperature range from absolute zero to 60 K. Since neither the first nor the second replicum is affected by re-absorption in the bulk material, we conclude that it should be possible to distinguish Fröhlich and optical deformation-potential coupling experimentally via both the amplitude and the temperature dependence of the intensity ratio of the first two sidebands.[6]

4.4.3.2 Free and bound excitons

Luminescence spectra can feature phonon sidebands due to both free excitons (FX) and impurity-bound excitons (BX). Actually, strong FX emission is only observed with high-purity samples. As a general rule, BX dominate at low and FX at elevated temperatures, which can be ascribed to thermal ionization of the bound excitons [135]. We show in this section how both FX and BX replica can be analyzed with our theory.

When evaluating steady-state luminescence, we may assume that the free excitons are thermally distributed. More explicitly, the free-exciton populations obey a Bose-Einstein distribution f_{BE},

$$\Delta N_{\text{FX}}(\mathbf{Q}) = \Delta\langle X_{1s,\mathbf{Q}}^\dagger X_{1s,\mathbf{Q}}\rangle = f_{\text{BE}}\big(E_{\text{com}}(\mathbf{Q})\big), \tag{4.64}$$

---

[6]In praxis, the analysis is often complicated by the fact that the carrier temperatures are not well known.
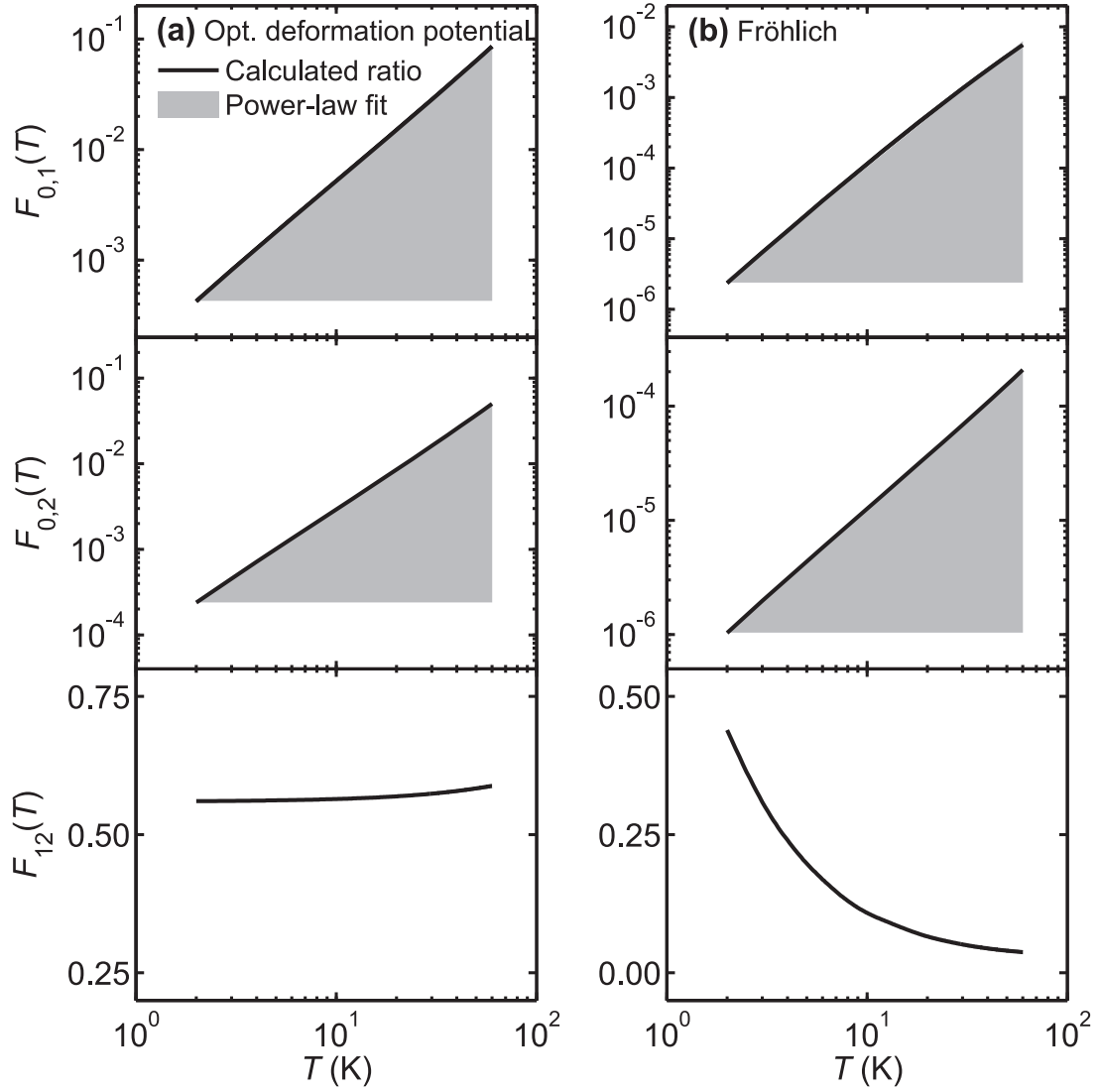
Figure 27: Calculated temperature dependences (solid lines) of the relative sideband intensities for GaN parameters with (a) optical deformation-potential interaction and (b) Fröhlich interaction. The ratios $F_{n,n'}$ are explicitly defined as $F_{n,n'} = J(n')/J(n)$ with the spectrally integrated intensities $J(n) = \int I_{\mathrm{PL}}^{(n)}(\omega)\, d(\hbar\omega)$. The shaded areas represent power-law fits $F_{0,n}(T) \propto T^{\alpha_{0,n}}$.
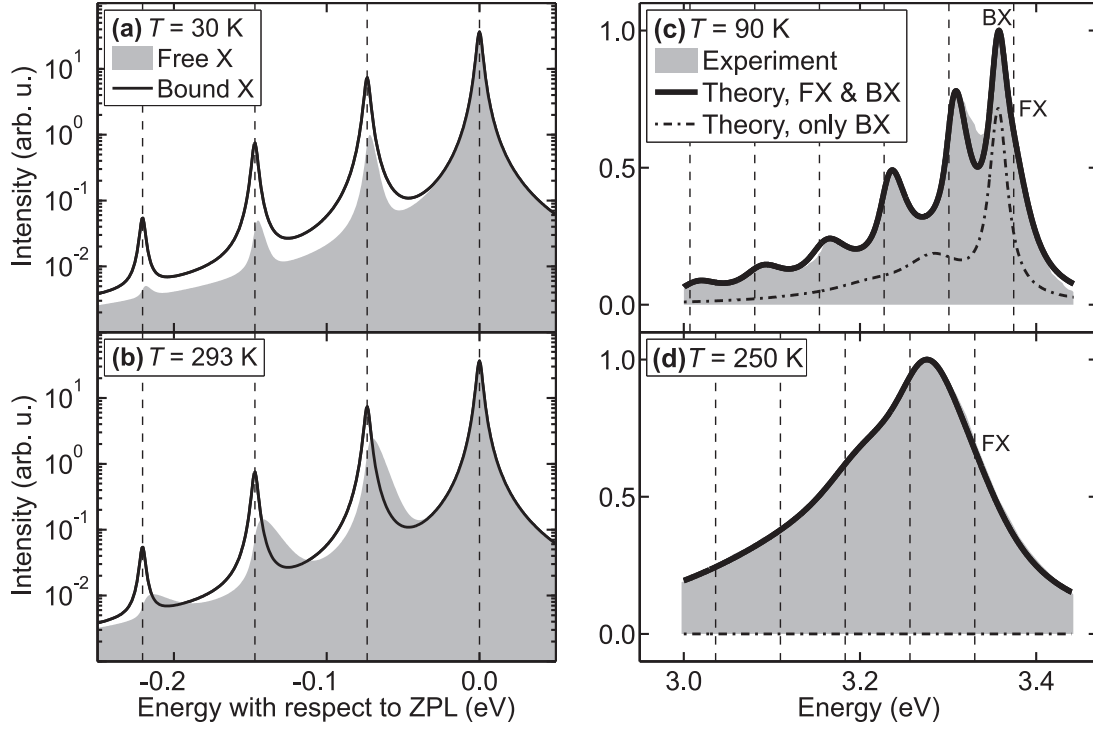
Figure 28: Sideband emission due to free and impurity-bound excitons.
Left frame: Calculated spectra for free (shaded areas) and bound (solid lines) excitons at low temperature (a) and room temperature (b). A constant homogeneous broadening $\gamma_n = 2\,\text{meV}$ is used for all resonances. The distance between neighboring vertical dashed lines corresponds to a LO-phonon energy of $73.5\,\text{meV}$ as in bulk ZnO. For a better comparison, the spectra are shifted and normalized such that the zero-phonon lines (ZPL) coincide.
Right frame: Measured (shaded areas) and calculated (solid lines) spectra for a ZnO bulk system at $90\,\text{K}$ (c) and $250\,\text{K}$ (d). The zero-phonon lines due to free and bound excitons are indicated by FX and BX, respectively. The dash-dotted lines represent the contribution from bound excitons. As in the left frame, vertical dashed lines mark the phonon-assisted resonances due to free excitons. The experimental data have been extracted from Ref. [48].

with respect to the center-of-mass kinetic energies $E_{\mathrm{com}}(\mathbf{Q}) = \hbar^2 |\mathbf{Q}|^2 / 2M$. Impurity-bound excitons can form in three genuinely different ways: The electron is bound to a donor while the hole is free, the hole is bound to an acceptor while the electron is free, or the whole exciton is trapped. While these three cases generally lead to different excitonic resonances, we can treat them identically by considering the limit $M \to \infty$ of infinite exciton mass. Then, the center-of-mass kinetic energy approaches zero and the excitons are uniformly distributed over all momenta in the Brillouin zone. The corresponding distributions become

$$\Delta N_{\mathrm{BX}}(\mathbf{Q}) = n_{\mathrm{BX}} V_{\mathrm{uc}} = \mathrm{const} \tag{4.65}$$

where n_{BX} denotes the density of bound excitons and V_{uc} the unit-cell volume.

The fact that bound excitons have constant occupation numbers becomes manifest in the line shapes of the phonon sidebands. This is demonstrated in the left frame of Fig. 28 where we assume identical homogeneous broadening γ_n for the zero-phonon line ($n = 0$) and all replica ($n \geq 1$) and neglect the temperature dependence of γ_n in order to emphasize the essential differences between the FX and the BX luminescence. Since electron-hole pairs with arbitrary center-of-mass momentum can contribute to the sideband emission, the FX replica feature extended high-energy tails at elevated temperatures (b) whereas the BX replica are much more symmetric. At low temperatures (a), the asymmetry of the FX sidebands is strongly reduced and, contrary to the bound case, the relative intensity of the phonon-assisted luminescence is weaker because only few electron-hole pairs with large center-of-mass momentum are available. One additionally observes that the maxima of the FX sidebands are blue-shifted with increasing carrier temperature [136] while the BX peaks do not change their positions.

In actual experimental spectra, the situation is more complicated than in our illustrative case study. The right frame of Fig. 28 shows experimental and numerical results for a ZnO bulk system at two different temperatures. The shaded areas present the measured spectra which have been extracted from Ref. [48] while the solid lines correspond to the calculated results. At $T = 90\,\mathrm{K}$ (c), both free and bound excitons contribute to the spectrum. Here, the dominant peaks are the BX zero-phonon line and the FX phonon replica. The FX zero-phonon line is strongly diminished and only appears as a small shoulder on the BX peak. This observation can be related to re-absorption in the bulk material due to polariton-propagation effects. Our theoretical results agree quantitatively with the measured spectra for an optical deformation potential of $d = 32.6$ which lies 18 % below the value for non-polar optical scattering as found in the literature [91]. The long-ranged Fröhlich interaction alone would yield a two orders of magnitude smaller intensity ratio of first and second replicum. The fact that doping locally changes the chemical composition of the crystal can be expected to influence the short-range part of the phonon coupling for an exciton that is bound to an impurity. We can fit the measured spectrum by assuming that the effective deformation potential for BX is reduced by about 60 % with respect to FX.[7] The corresponding BX contribution to the sideband spectrum is represented by the dash-dotted curve. The authors of Ref. [48] have found that at temperatures below 20 K, the replica of the BX peak are stronger than the FX sidebands. While 90 K lies in the intermediate regime where both FX and BX features can be detected, we do not need BX population anymore to reproduce the spectrum measured at $T = 250\,\mathrm{K}$ (d). Here, the FX phonon replica smear out completely because all spectral lines broaden with increasing temperature.

Phonon sidebands due to free and impurity-bound excitons are particularly easy to distinguish when the temperature dependence of the luminescence spectrum is analyzed. Because

---

[7]Calculations of the exciton-polaron dispersion [134, 137] indicate that also the Fröhlich interaction with BX is strongly reduced in ZnO [138].
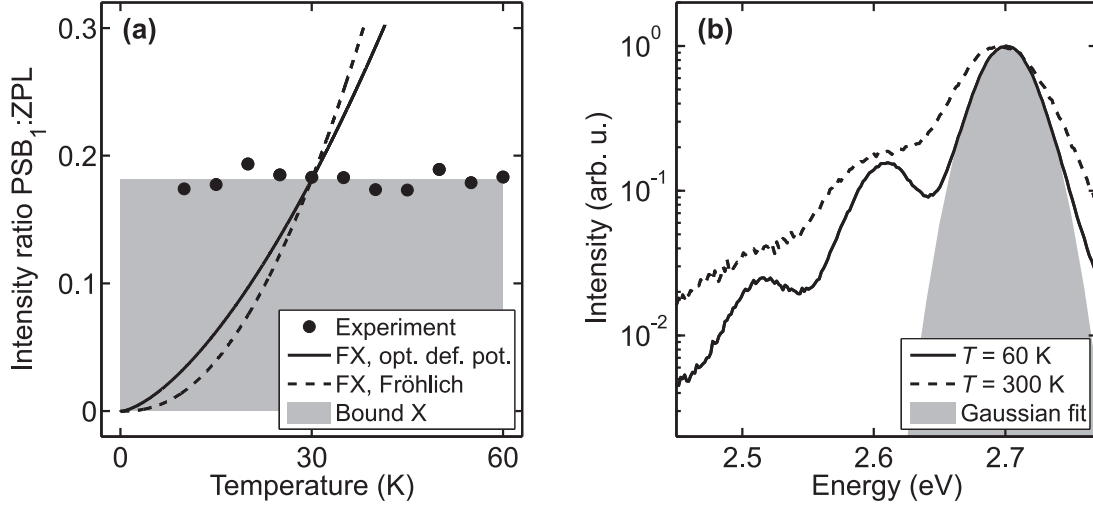
Figure 29: (a) Intensity of the first phonon sideband relative to the zero-phonon line for a InGaN quantum well as function of temperature. The bold dots represent the measured data [139], the lines show the calculated temperature dependencies for free excitons with optical deformation-potential (solid) and Fröhlich coupling (dashed). The shaded area gives the calculated results for impurity-bound excitons. **(b)** Measured photoluminescence spectra for the InGaN quantum well at two different temperatures. The almost Gaussian line shape (shaded area) of the zero-phonon line indicates strong inhomogeneous broadening.

BX have no center-of-mass dispersion and the zero-phonon line and all replica are equally affected by thermal ionization, the intensity ratios of any two of these peaks do not depend on the temperature, in striking contrast to the FX case considered in Sec. 4.4.3.1. For quantum-well systems, the spectral positions of the FX and BX resonances are usually not well known a priori. An experimental study of the sideband spectrum can therefore be a useful tool to draw a conclusion which kind of excitons are present in the material. This is illustrated in frame (a) of Fig. 29 where the ratio $F_{0,1}$ of the integrated intensities of PSB_1 and ZPL is plotted as function of temperature for a InGaN single quantum well with 20 % In content and a well width of about 3 nm [139]. The bold dots represent fit results for the measured photo-luminescence spectra. Based on the weak temperature dependence, the observed emission can unambiguously be assigned to BX (shaded area). For comparison, calculated ratios for FX with optical deformation-potential coupling (solid line) and Fröhlich coupling (dashed line) are also plotted where the overall amplitudes are chosen such that the calculated results coincide with the experimental result at $T = 30$ K. Frame (b) of Fig. 29 shows representative spectra at two different temperatures. In the InGaN quantum-well system, BX emission can still be detected at room temperature (dashed line) where the peaks have not yet smeared out. Moreover, we notice that the ZPL has an almost Gaussian line shape, as demonstrated by the shaded area for the spectrum at $T = 60$ K (solid line). This observation indicates strong inhomogeneous broadening due to disorder. Already for the ZnO spectrum presented in the right frame of Fig. 28, we had to account for a certain amount of inhomogeneous broadening in the calculations to achieve quantitative agreement with the measured data. An elementary discussion of sideband emission from disordered systems will be given in Appendix G.
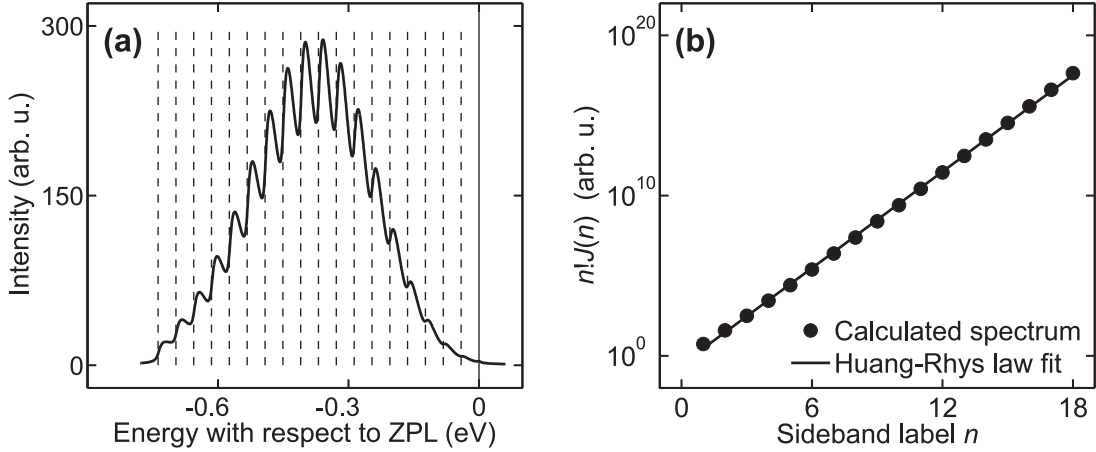
Figure 30: **(a)** Calculated ZnO nanorod spectrum at room temperature $T = 293\,\mathrm{K}$ for an optical deformation-potential constant $d_0 = 39.8\,\mathrm{eV}$. Vertical lines indicate the exciton-phonon resonances $\mathcal{E}_{1\mathrm{s}} - n\hbar\Omega$ with the phonon energy $\hbar\Omega = 41\,\mathrm{meV}$ of the non-polar $2\text{-}E_2$ mode according to Ref. [55]. The solid vertical line marks the position of the zero-phonon line ($n = 0$). **(b)** Integrated sideband intensities $J(n)$ as function of the sideband label n. The solid line gives the fit result based on a Huang-Rhys law $J(n) \propto S^n/n!$.

4.4.3.3 Phonon replica due to non-polar optical modes

In typical experimental luminescence spectra, the sideband intensities decrease rapidly with increasing order of the phonon replica. The spectrally integrated intensities $J(n) \equiv \int I_{\mathrm{PL}}^{(n)}(\omega)\,\mathrm{d}(\hbar\omega)$ are often found to obey the so-called *Huang-Rhys law* [140]

$$J(n) \propto \frac{S^n}{n!} \tag{4.66}$$

where only for very efficient electron-phonon coupling, the *Huang-Rhys factor* S exceeds unity. However, a recent publication [55] reports on exceptionally strong sidebands in ZnO nanorod spectra at room temperature that are remarkable in two different aspects: First, numerous phonon replica were observed with a strongly non-monotonous behavior of the sideband intensities. Moreover, the replica could unambiguously be assigned to non-polar optical modes in view of the energy spacing between the resonances. Consequently, the LO-phonon assisted luminescence in those samples can only be due to optical deformation-potential interaction. This makes the ZnO nanorods ideal systems to test our compact luminescence formula (4.60) that does not include Fröhlich contributions.

The diameters of the investigated nanorods were of the order of $100\,\mathrm{nm}$, which is much larger than the exciton Bohr radius in ZnO of $0.9\,\mathrm{nm}$. Therefore, the carrier system in those nanorods is essentially three-dimensional. In principle, the rod geometry can affect the phonon spectrum [141], but for the reasons discussed in Sec. 2.2.4.1, we may assume that the confinement has only a weak influence on the electron-phonon interaction. It is thus justified to apply the bulk formula (4.60) also to the nanorod case. For bound excitons, a spectral integration over the factor $f_n(\omega)$ defined in Eq. (4.62) yields $F_n \equiv \int f_n(\omega)\mathrm{d}(\hbar\omega) = \pi n_{\mathrm{BX}}V_{\mathrm{u.c.}}$ in view of Eq. (4.65) such that the integrated sideband intensities follow a Huang-Rhys law with $S = K$. The luminescence from Ref. [55] could be assigned to free excitons where the dependence of F_n on

the sideband label n leads to small deviations from the Huang-Rhys behavior.

Frame (a) of Fig. 30 shows the analytical result for an optical deformation-potential constant $d_0 = 39.8\,\mathrm{eV}$ [91] and a Gaussian width σ of 1.0 inverse Bohr radii as determined via the procedure described at the end of Sec. 4.4.2.3. With these parameters, we actually obtain a similar spectrum as in the above mentioned experiment. As can be seen in frame (b) of Fig. 30, the integrated intensities follow the Huang-Rhys law (4.66) very accurately. However, the Huang-Rhys factor $S = 10.1$ is remarkably strong. Since a Poisson distribution approaches a Gaussian distribution for large mean values, we can approximately rewrite the Huang-Rhys formula as

$$J(n) \propto \frac{\mathrm{e}^S}{\sqrt{2\pi S}} \exp\left(-\frac{[n-S]^2}{2S}\right), \tag{4.67}$$

which underlines that the intensity maximum is reached away from the zero-phonon line at the n-th replicum with $n \simeq S$.

It should be noted that in the majority of luminescence experiments with ZnO nanowires, similar spectra as in the right frame of Fig. 28 are measured where the phonon replica originate from polar optical modes [142, 143]. While our theory reproduces the extraordinary sideband emission observed for non-polar modes, we cannot identify the conditions that favor the participation of polar or non-polar optical phonons in the radiative recombination of electron-hole pairs. To answer this question, the theoretical approach would possibly have to go beyond the semi-phenomenological treatment of the electron-phonon coupling presented in Sec. 2.2.4.2 and to account, e.g., for the anisotropy of the optical deformation-potential interaction.

5 Conclusions and outlook

In this thesis, we have combined the Heisenberg equation-of-motion approach with a cluster expansion scheme to describe the coupled dynamics of electron-electron, electron-photon, and electron-phonon correlations in semiconductor materials. This general theoretical framework has been employed to compute the optical absorption and emission of quantum-dot systems and to analyze phonon sidebands in the luminescence spectra of polar semiconductors.

For a consistent microscopic treatment of interacting quantum-dot electrons coupled to a quantized light field, we have followed the spirit of earlier works on quantum-well and quantum-wire systems and have truncated the equation hierarchy on the singlet-doublet level of cluster expansion. In other words, our theory includes densities, polarizations, classical light fields, and all kinds of Coulombic and quantum-optical two-particle correlations. Regarding the internal degrees of freedom of the dot, our approach competes with diagonalization methods that can yield the exact energy spectrum of the interacting carriers if the dot contains only a small number of discrete single-particle states. We have therefore performed a generic phase-space analysis demonstrating that singlets and doublets are sufficient to characterize stable configurations of the dot system with well-defined optical resonances. As in higher-dimensional cases, bound electron-hole pairs, i.e. excitons, and electron-hole plasma can be identified by evaluating the carrier-carrier correlations in the system. We have found that a quantum dot in the low-density regime can have stable many-body configurations ranging from pure plasma up to fully correlated electron-hole pairs.

Depending on the physical phenomena that are to be studied, two different sets of equations of motion have to be solved. The semiconductor Bloch equations (SBE) describe the coherent excitation of the carrier system when it is driven by a classical light field. The quantum emission from the dot under incoherent conditions follows from the semiconductor luminescence equations (SLE). We have introduced an exciton basis that enables us to express analytical approximations for both the linear absorption and the stationary luminescence spectrum. Due to the symmetries of the excitonic eigen functions, only a small subset of the excitonic eigen energies can be observed as optical resonances. Analogously to higher-dimensional semiconductor structures, both excitonic correlations and uncorrelated plasma provide contributions to the steady-state luminescence that cannot be distinguished by a standard photoluminescence experiment.

The particular strength of the cluster-expansion approach lies in the fact that it can straightforwardly be generalized to describe the influence of the environment on the quantum dot. To this end, the existing theory does not need to be reformulated but the new coupling effects simply lead to additional terms in the equations of motion. As a concrete example, we have studied the interaction with a reservoir of acoustic lattice vibrations. After resonant optical excitation of the dot, phonon-assisted processes give rise to dephasing of coherent quantities such as the microscopic polarizations, to efficient build-up of excitonic population, and to thermalization of the carrier system. All these effects have been studied previously for quantum-well systems. However, recent theoretical and experimental results suggest that a quantitative analysis of phonon-related phenomena in quantum dots requires the inclusion of optical phonons where the strong-coupling regime must be considered to avoid the phonon-bottleneck problem.

The quantum-dot theory presented in this thesis may be extended into several directions. On the one hand, one could improve the treatment of the carrier-phonon interaction along the above mentioned lines and add the coupling between dot- and wetting-layer carriers to study all kinds of effects related to the solid-state environment of the quantum dot. On the other hand, one could compute higher-order correlation functions to analyze the quantum statistics of the emission. For example, in order to describe photon antibunching, conditional detection probabilities would have to be evaluated which are four-particle quantities in the language of the cluster expansion.

Besides the general microscopic theory of semiconductor quantum-dot systems, we have presented a possible technical application of quantum dots in the field of Zeno-based optoelectronics. More explicitly, we have proposed a device design that allows conditional absorption of a signal field depending on the presence of a control field. The former field is resonant with the exciton-to-biexciton transition while the latter field is resonant with the transition from the ground state to the exciton state in an ensemble of identical quantum dots. For a simple theoretical model, we have chosen an elementary approach where each dot is treated as a system of three non-interacting levels. The operation of the device can then be studied via a full numerical solution of the optical Bloch equations. For CdSe-based quantum dots, high contrasts between the absorption with and without control are obtained in a wide range of device parameters. In the future, our fully microscopic theory could be generalized to higher-order Coulomb correlations in order to analyze the influence of the different coupling effects on the function of the device.

When the cluster-expansion approach is applied to the phonon-sideband problem, one can clearly assign phonon-assisted processes of different orders to different levels of cluster expansion. For the main contribution to the n-th replicum on the low-energy side of the exciton peak in the luminescence spectrum, recombination correlations involving n phonon creation operators have to be evaluated. The dynamics of these $(n+2)$-particle correlations is described by the LO-phonon-assisted SLE. Using the exciton basis, steady-state luminescence at the first phonon sideband can be calculated analytically. Similarly to the zero-phonon line, both plasma and excitonic populations lead to emission at the same wave lengths. We have found that at least at low temperatures, the line shapes and relative sideband intensities are so similar that the different luminescence sources cannot be distinguished by a standard photoluminescence experiment.

For the analysis of higher-order sideband emission, we have derived phonon-assisted SLE in the polaron picture. Here, the electron-phonon interaction is treated non-perturbatively with the effect that the different phonon replica can be computed separately. This procedure yields a compact luminescence formula for arbitrary-order sidebands where plasma and excitons contribute additively. Because the polaron-picture analysis relies on a bath approximation where a phonon reservoir at zero temperature is assumed, it reproduces the low-temperature limit of the accurate formula for the first sideband.

In order to relate the cluster-expansion approach to existing perturbative treatments of LO-phonon assisted luminescence, we have also considered the exciton picture as used in those earlier works. Since the hierarchy problem arising from the Coulomb interaction is eliminated when the excited carrier system is purely described in terms of excitons, the phonon-assisted SLE in the exciton picture can be solved recursively to calculate steady-state luminescence for arbitrary-order replica. However, only the correlated emission sources are taken into account with such an approach. It turns out that the cluster-expansion analysis in the exciton picture yields very similar spectra as the well-established perturbational theory. By comparison with the polaron-picture formula, we have developed a practical way to investigate systems with

very strong electron-phonon coupling where the luminescence spectrum can feature numerous phonon sidebands.

The short-range part of the interaction between electrons and LO phonons can be modeled with the help of optical deformation potentials. In polar media, there is also the long-ranged Fröhlich coupling due to the oscillating macroscopic polarizations induced by longitudinal optical lattice vibrations. Usually, the intra-band scattering is clearly dominated by the Fröhlich part. By contrast, our calculations indicate that even in strongly polar semiconductors, the short-range part can provide the main contribution to the phonon replica. For bulk systems, sideband emission due to Fröhlich and optical deformation-potential interaction can be distinguished via both the amplitude and the temperature dependence of the intensity ratio of the first two replica.

In order to evaluate and test our theory of the phonon-sideband problem, we have performed a number of numerical case studies. We have found that above a certain critical temperature, a bulk sample should feature stronger sideband emission than a quantum-well sample with the same material parameters. Sidebands originating from free and impurity-bound excitons can be identified in view of their line shapes and temperature dependences. The exceptionally strong phonon replica due to non-polar optical modes that have been observed in recent experiments with ZnO nanorods can be interpreted in the light of our theory.

The theoretical analysis presented in this thesis raises a couple of questions that might be answered in future experiments. At the time of writing these lines, sideband emission from uncorrelated electron-hole plasma has not yet been verified experimentally. The influence of the optical deformation-potential interaction on phonon replica ascribed to polar modes is barely discussed in the literature. A possible practical application of phonon-assisted luminescence is the construction of a low-threshold laser that is pumped at the excitonic resonance but emits at the first sideband. For the theoretical description of such a set-up, the phonon-assisted luminescence equations have to be solved simultaneously with the semiconductor Bloch equations.

A Exciton basis

Excitons can be defined as electron-hole pair states with minimum energy. More explicitly, one starts from a general single-pair state with a well-defined center-of-mass momentum $\hbar\mathbf{Q}$,

$$|X_{\mathbf{Q}}\rangle = \sum_{\beta,\beta'} \phi(\mathbf{k})\hat{a}^{\dagger}_{\mathrm{c},\mathbf{k}+\mathbf{Q}_{\mathrm{e}}}\hat{a}_{\mathrm{v},\mathbf{k}-\mathbf{Q}\mathrm{h}}|\mathrm{G}\rangle, \tag{A.1}$$

where $\mathbf{Q}_{\mathrm{e/h}} = (m_{\mathrm{e/h}}/M)\mathbf{Q}$ with the total mass $M = m_{\mathrm{e}} + m_{\mathrm{h}}$ of an electron-hole pair while $|\mathrm{G}\rangle = \prod_{\mathbf{k}} \hat{a}^{\dagger}_{\mathrm{v},\mathbf{k}}|\mathrm{vac}\rangle$ denotes the ground state of the semiconductor that is characterized by a fully occupied valence band and an empty conduction band. The coefficients $\phi(\mathbf{k})$ are chosen so as to minimize the energy of the carrier system

$$E_{\mathrm{el}} \equiv \langle X_{\mathbf{Q}}|\hat{H}_{\mathrm{el}} + \hat{H}_{\mathrm{el-el}}|X_{\mathbf{Q}}\rangle \tag{A.2}$$

under the constraint that $|X_{\mathbf{Q}}\rangle$ is normalized. The variational principle leads to an Hermitian eigenvalue problem for the *excitonic wave functions* $\phi(\mathbf{k})$, the so-called *Wannier equation*

$$E_{\nu}(\mathbf{Q})\phi_{\nu}(\mathbf{k}) = \left(\varepsilon^{\mathrm{e}}_{\mathbf{k}+\mathbf{Q}_{\mathrm{e}}} + \varepsilon^{\mathrm{h}}_{\mathbf{k}-\mathbf{Q}_{\mathrm{h}}}\right)\phi_{\nu}(\mathbf{k}) - \sum_{\mathbf{k}'}V_{\mathbf{k}-\mathbf{k}'}\phi_{\nu}(\mathbf{k}') \tag{A.3}$$

where $E_{\nu}(\mathbf{Q}) = \mathcal{E}_{\nu} + \hbar^2|\mathbf{Q}|^2/2M$ decomposes into the *excitonic eigen energy* $\mathcal{E}_{\nu}$ and the center-of-mass energy of the electron-hole pair. For parabolic bands, the Wannier equation in direct space has the same mathematical form as the Schrödinger equation for the relative motion of a hydrogen atom, albeit with a different reduced mass and a different background permittivity. The energy E_{el} of the ν-th exciton state

$$|X_{\nu,\mathbf{Q}}\rangle = \sum_{\mathbf{k}} \phi_{\nu}(\mathbf{k})\hat{a}^{\dagger}_{\mathrm{c},\mathbf{k}+\mathbf{Q}_{\mathrm{e}}}\hat{a}_{\mathrm{v},\mathbf{k}-\mathbf{p}_{\mathrm{h}}}|\mathrm{G}\rangle \tag{A.4}$$

is then given by $E_{\nu}(\mathbf{Q})$.

In case of vanishing densities $f^{\mathrm{e/h}}_{\mathbf{k}} = 0$, the excitonic wave functions $\phi_{\nu}(\mathbf{k})$ are nothing else but the eigen solutions of the homogeneous part of the semiconductor Bloch equations. In order to retain this useful property for finite densities, the exciton problem has to be generalized. For non-vanishing $f^{\mathrm{e/h}}_{\mathbf{k}}$, the eigenvalue problem defined by the SBE becomes non-Hermitian such that eigen vectors with different eigenvalues are not necessarily orthogonal anymore. In this case, it is practical to introduce *right- and left-handed eigen functions* $\phi^{\mathrm{R}}_{\nu,\mathbf{Q}}$ and $\phi^{\mathrm{L}}_{\nu,\mathbf{Q}}$, respectively, that solve the eigenvalue equations

$$\begin{aligned} E_{\nu}(\mathbf{Q})\phi^{\mathrm{R}}_{\nu,\mathbf{Q}}(\mathbf{k}) &= \left(\tilde{\varepsilon}^{\mathrm{e}}_{\mathbf{k}+\mathbf{Q}_{\mathrm{e}}} + \tilde{\varepsilon}^{\mathrm{h}}_{\mathbf{k}-\mathbf{Q}_{\mathrm{h}}}\right)\phi^{\mathrm{R}}_{\nu,\mathbf{Q}}(\mathbf{k}) \\ &\quad - \left(1 - f^{\mathrm{e}}_{\mathbf{k}+\mathbf{Q}_{\mathrm{e}}} - f^{\mathrm{h}}_{\mathbf{k}-\mathbf{Q}\mathrm{h}}\right)\sum_{\mathbf{k}'}V_{\mathbf{k}-\mathbf{k}'}\phi^{\mathrm{R}}_{\nu,\mathbf{Q}}(\mathbf{k}'), \end{aligned} \tag{A.5}$$

$$\begin{aligned} \left[\phi^{\mathrm{L}}_{\nu,\mathbf{Q}}(\mathbf{k})\right]^{*}E_{\nu}(\mathbf{Q}) &= \left[\phi^{\mathrm{L}}_{\nu,\mathbf{Q}}(\mathbf{k})\right]^{*}\left(\tilde{\varepsilon}^{\mathrm{e}}_{\mathbf{k}+\mathbf{Q}_{\mathrm{e}}} + \tilde{\varepsilon}^{\mathrm{h}}_{\mathbf{k}-\mathbf{Q}_{\mathrm{h}}}\right) \\ &\quad - \sum_{\mathbf{k}'}\left[\phi^{\mathrm{L}}_{\nu,\mathbf{Q}}(\mathbf{k}')\right]^{*}\left(1 - f^{\mathrm{e}}_{\mathbf{k}'+\mathbf{Q}_{\mathrm{e}}} - f^{\mathrm{h}}_{\mathbf{k}'-\mathbf{Q}\mathrm{h}}\right)V_{\mathbf{k}-\mathbf{k}'} \end{aligned} \tag{A.6}$$

and can be shown to obey the *generalized orthogonality and completeness relations*

$$\sum_{\mathbf{k}} \left[\phi^{\mathrm{L}}_{\nu,\mathbf{Q}}(\mathbf{k})\right]^* \phi^{\mathrm{R}}_{\nu',\mathbf{Q}}(\mathbf{k}) = \delta_{\nu,\nu'}, \tag{A.7}$$

$$\sum_{\nu} \left[\phi^{\mathrm{L}}_{\nu,\mathbf{Q}}(\mathbf{k})\right]^* \phi^{\mathrm{R}}_{\nu,\mathbf{Q}}(\mathbf{k}') = \delta_{\mathbf{k},\mathbf{k}'}. \tag{A.8}$$

In view of Eqs. (A.7), (A.8), one can define *excitonic creation and annihilation operators*

$$\hat{X}^{\dagger}_{\nu,\mathbf{Q}} = \sum_{\mathbf{k}} \phi^{\mathrm{L}}_{\nu,\mathbf{Q}}(\mathbf{k}) \hat{a}^{\dagger}_{\mathrm{c},\mathbf{k}+\mathbf{Q}_{\mathrm{e}}} \hat{a}_{\mathrm{v},\mathbf{k}-\mathbf{Q}_{\mathrm{h}}}, \tag{A.9a}$$

$$\hat{X}_{\nu,\mathbf{Q}} = \sum_{\mathbf{k}} \left[\phi^{\mathrm{L}}_{\nu\mathbf{Q}}(\mathbf{k})\right]^* \hat{a}^{\dagger}_{\mathrm{v},\mathbf{k}-\mathbf{Q}_{\mathrm{h}}} \hat{a}_{\mathrm{c},\mathbf{k}+\mathbf{Q}_{\mathrm{e}}}, \tag{A.9b}$$

which can be inverted back into the single-particle basis via

$$\hat{a}^{\dagger}_{\mathrm{c},\mathbf{k}+\mathbf{Q}_{\mathrm{e}}} \hat{a}_{\mathrm{v},\mathbf{k}-\mathbf{Q}_{\mathrm{h}}} = \sum_{\nu} \left[\phi^{\mathrm{R}}_{\nu,\mathbf{Q}}(\mathbf{k})\right]^* \hat{X}^{\dagger}_{\nu,\mathbf{Q}}, \tag{A.10}$$

$$\hat{a}^{\dagger}_{\mathrm{v},\mathbf{k}-\mathbf{Q}_{\mathrm{h}}} \hat{a}_{\mathrm{c},\mathbf{k}+\mathbf{Q}_{\mathrm{e}}} = \sum_{\nu} \phi^{\mathrm{R}}_{\nu,\mathbf{Q}}(\mathbf{k}) \hat{X}_{\nu,\mathbf{Q}}. \tag{A.11}$$

In the low-density regime, it is often justified to replace $\phi^{\mathrm{L/R}}_{\nu,\mathbf{Q}}(k)$ by $\phi_{\nu}(\mathbf{k})$ and to use the relations

$$\sum_{\mathbf{k}} \phi_{\nu}(\mathbf{k})^* \phi_{\nu'}(\mathbf{k}) = \delta_{\nu,\nu'}, \tag{A.12}$$

$$\sum_{\nu} \phi_{\nu}(\mathbf{k})^* \phi_{\nu}(\mathbf{k}') = \delta_{\mathbf{k},\mathbf{k}'}. \tag{A.13}$$

instead of Eqs. (A.7), (A.8).

Due to the fermionic substructure of the electron-hole pairs, the exciton operators do not fulfill bosonic commutation relations such that $\hat{X}^{\dagger}_{\nu,\mathbf{Q}} \hat{X}_{\nu,\mathbf{Q}}$ does not have the properties of a number operator. However, when a dominant amount of excitons has built in the carrier system, the correlated part

$$\Delta N_{\nu}(\mathbf{Q}) \equiv \Delta \langle \hat{X}^{\dagger}_{\nu,\mathbf{Q}} \hat{X}_{\nu,\mathbf{Q}} \rangle \tag{A.14}$$

may be interpreted as population of the exciton state with quantum number ν and center-of-mass momentum $\hbar\mathbf{Q}$ [7].

B Markov approximation

Because several slightly different kinds of approximations are covered by the term *Markov approximation* in the literature, we briefly define our approach in this appendix.

We consider a generic equation of motion

$$i\hbar \frac{\mathrm{d}}{\mathrm{d}t} X = (E_X - i\gamma)X + \sum_j S_j \tag{B.1}$$

where we assume that each source term S_j has a dominant oscillation frequency $E_j/\hbar$, i.e. $S_j(t) = S_j^0(t)e^{-iE_j t/\hbar}$ with a slowly varying envelope $S_j^0(t)$. By separation of time scales, the formal solution

$$X(t) = -\frac{i}{\hbar} \sum_j \int_{-\infty}^{t} S_j(t)e^{-i(E_X - i\gamma)(t-t')/\hbar} \, \mathrm{d}t' \tag{B.2}$$

of Eq. (B.1) can then be rewritten as

$$X(t) \simeq \sum_j \frac{S_j(t)}{E_j - E_X + i\gamma} = -\sum_j S_j(t)g_\gamma(E_X - E_j) \tag{B.3}$$

where

$$g_\gamma(E) \equiv \frac{1}{E - i\gamma} \xrightarrow{\gamma \to 0} \mathscr{P}(1/E) + i\pi\delta(E) \tag{B.4}$$

with the principal value $\mathscr{P}(1/E)$ and the Dirac delta function $\delta(E)$. We notice that the Markov approximation (B.3) reduces to the steady-state solution for X when all source terms are (quasi) stationary such that $E_j = 0$.

C Supplement to the quantum-dot analysis

Based on the general results from Chap. 2, the matrix elements for the lens-shaped self-assembled quantum dot are explicitly evaluated in Sec. C.1. In order to close the SBE on the singlet-doublet level of cluster expansion, we present the semi-classical dynamics of all possible two-particle correlations in Sec. C.2.

C.1 Matrix elements

C.1.1 Coulomb interaction

The explicit form of the Coulomb Hamiltonian for the quantum-dot carriers is found from Eqs. (2.94)–(2.96) by considering the case $d = 0$ where $r_\parallel = 0$ and $r_\perp = \mathbf{r}$. For the matrix element in Eq. (3.14), we thus obtain

$$V^{\,\beta_1\beta_2}_{\,\beta_3\beta_4} = \delta_{\sigma_1,\sigma_4}\delta_{\sigma_2,\sigma_3} V^{\text{eff}\,\beta_1\beta_2}_{\quad\ \beta_3\beta_4} \tag{C.1}$$

where

$$V^{\text{eff}\,\beta_1\beta_2}_{\quad\ \beta_3\beta_4} = \frac{e^2}{4\pi\epsilon_0\epsilon_{\mathrm{b}}} \iint \zeta^*_{\beta_1}(\mathbf{r})\zeta^*_{\beta_2}(\mathbf{r}')\frac{1}{|\mathbf{r}-\mathbf{r}'|}\zeta_{\beta_3}(\mathbf{r}')\zeta_{\beta_4}(\mathbf{r})\,\mathrm{d}^3 r\,\mathrm{d}^3 r' \tag{C.2}$$

with the confinement wave functions $\zeta_\beta(\mathbf{r})$ as defined in Sec. 3.1.1. In order to evaluate this integral, we need the Fourier transform of the Coulomb potential,

$$\frac{1}{|\mathbf{r}|} = \frac{1}{(2\pi)^3}\int \frac{4\pi}{|\mathbf{q}|^2}\,\mathrm{e}^{\mathrm{i}\mathbf{q}\cdot\mathbf{r}}\,\mathrm{d}^3 q. \tag{C.3}$$

Using the decompositions $\mathbf{r} = \boldsymbol{\rho}+z\mathbf{e}_z$ and $\mathbf{q} = \mathbf{q}_\rho+q_z\mathbf{e}_z$ where $\mathbf{e}_z$ is a unit vector in z-direction and $\boldsymbol{\rho},\mathbf{q}_\rho \perp \mathbf{e}_z$, we can apply the Cauchy theorem to perform the integration over q_z,

$$\frac{1}{|\mathbf{r}|} = \frac{4\pi}{(2\pi)^3}\int \frac{\mathrm{e}^{\mathrm{i}(\mathbf{q}_\rho\cdot\boldsymbol{\rho}+q_z z)}}{q_z^2 + |\mathbf{q}_\rho|^2}\,\mathrm{d}^2 q_\rho\,\mathrm{d}q_z = \frac{4\pi}{(2\pi)^3}\int \frac{\mathrm{e}^{\mathrm{i}(\mathbf{q}_\rho\cdot\boldsymbol{\rho}+q_z z)}}{(q_z + \mathrm{i}|\mathbf{q}_\rho|)(q_z - \mathrm{i}|\mathbf{q}_\rho|)}\,\mathrm{d}^2 q_\rho\,\mathrm{d}q_z$$
$$= \frac{1}{2\pi}\int \frac{\mathrm{e}^{\mathrm{i}\mathbf{q}_\rho\cdot\boldsymbol{\rho}}}{|\mathbf{q}_\rho|}\,\mathrm{e}^{-|z\mathbf{q}_\rho|}\,\mathrm{d}^2 q_\rho. \tag{C.4}$$

Inserting this result into Eq. (C.2) yields

$$V^{\text{eff}\,\beta_1\beta_2}_{\quad\ \beta_3\beta_4} = \frac{1}{2\pi}\frac{e^2}{4\pi\epsilon_0\epsilon_{\mathrm{b}}}\int \frac{1}{|\mathbf{q}_\rho|}\,I_0(|\mathbf{q}_\rho|)I_{\beta_1,\beta_4}(\mathbf{q}_\rho)I_{\beta_2,\beta_3}(-\mathbf{q}_\rho)\,\mathrm{d}^2 q_\rho \tag{C.5}$$

where we have defined

$$I_0(q_\rho) \equiv \iint |\xi(z)|^2\,|\xi(z')|^2\,\mathrm{e}^{-q_\rho|z-z'|}\,\mathrm{d}z\,\mathrm{d}z', \tag{C.6}$$

$$I_{\beta,\beta'}(\mathbf{q}_\rho) \equiv \int \psi^*_\beta(\boldsymbol{\rho})\psi_{\beta'}(\boldsymbol{\rho})\mathrm{e}^{\mathrm{i}\mathbf{q}_\rho\cdot\boldsymbol{\rho}}\,\mathrm{d}^2\rho. \tag{C.7}$$

The integral $I_0(q_\rho)$ that contains the contribution from the quantum-well confinement can be computed analytically,

$$I_0(q_\rho) = \left. \frac{32\left(\mathrm{e}^{-\pi\delta} - 1\right) + \pi\delta\left(32 + 20\delta^2 + 3\delta^4\right)}{4\delta^2\left(4 + \delta^2\right)^2} \right|_{\delta = q_\rho L/\pi}. \tag{C.8}$$

The integral $I_{\beta_1,\beta_2}(\mathbf{q}_\rho)$ that originates from the quantum-dot confinement can be written as

$$I_{\beta_1,\beta_2}(\mathbf{q}_\rho) = \mathrm{e}^{\mathrm{i}(m_2 - m_1)\phi(\mathbf{q}_\rho)} G_{\beta_1,\beta_2}(|\mathbf{q}_\rho|) \tag{C.9}$$

where $\phi(\mathbf{q}_\rho)$ denotes the azimuth angle of $\mathbf{q}_\rho$ and

$$G_{\beta_1,\beta_2}(q_\rho) \equiv 2\pi \mathrm{i}^{(m_2 - m_1)} c_0(\beta_1) c_0(\beta_2)$$
$$\int_0^\infty x \mathrm{e}^{-2x^2} x^{|m_1| + |m_2|} L_{l_1^-}^{|m_1|}(2x^2) L_{l_2^-}^{|m_2|}(2x^2) J_{m_2 - m_1}(q_\rho x/\sqrt{\eta}) \, \mathrm{d}x. \tag{C.10}$$

Here, we have used the integral representation for the Bessel function of the first kind

$$J_m(x) = \frac{1}{2\pi \mathrm{i}^m} \int_0^{2\pi} \mathrm{e}^{\mathrm{i}x\cos\alpha} \mathrm{e}^{\mathrm{i}m\alpha} \, \mathrm{d}\alpha. \tag{C.11}$$

The Coulomb matrix element thus takes the form

$$V_{\beta_3\beta_4}^{\beta_1\beta_2} = \delta_{\sigma_1,\sigma_4}\delta_{\sigma_2,\sigma_3}\delta_{m_1+m_2,m_3+m_4} \frac{e^2}{4\pi\epsilon_0\epsilon_\mathrm{b}} \int_0^\infty I_0(q_\rho) G_{\beta_1,\beta_4}(q_\rho) G_{\beta_2,\beta_3}(q_\rho) \, \mathrm{d}q_\rho. \tag{C.12}$$

C.1.2 Electron-phonon interaction

The explicit form of the acoustic deformation-potential matrix element in Eq. (3.88) follows from Eq. (2.63) together with Eq. (2.58). We find that

$$G_{\lambda,\beta,\beta',\mathbf{p}} = d_\mathrm{ac}^\lambda \sqrt{\frac{\hbar|\mathbf{p}|}{2\varrho\mathscr{L}^3 c_\mathrm{LA}}} \gamma_{\beta,\beta'}(\mathbf{p}) \tag{C.13}$$

with the form factor

$$\gamma_{\beta,\beta'}(\mathbf{p}) = \int \zeta_\beta^*(\mathbf{r}) \zeta_{\beta'}(\mathbf{r}) \mathrm{e}^{\mathrm{i}\mathbf{q}\cdot\mathbf{r}} \, \mathrm{d}^3 r = I_1(q_z) I_{\beta,\beta'}(\mathbf{q}_\rho). \tag{C.14}$$

The quantum-well confinement enters the integral

$$I_1(q_z) \equiv \int_{-\infty}^\infty |\xi(z)|^2 \mathrm{e}^{\mathrm{i}q_z z} \, \mathrm{d}z. \tag{C.15}$$

C.2 Dynamics of the two-particle correlations

Generic singlets, two-, and three-particle correlations are written as

$$S\left(\begin{smallmatrix}\lambda\\\lambda'\end{smallmatrix}\middle|\begin{smallmatrix}\beta\\\beta'\end{smallmatrix}\right) \equiv \langle \hat{a}_{\lambda,\beta}^\dagger \hat{a}_{\lambda',\beta'} \rangle, \tag{C.16}$$

$$C\left(\begin{smallmatrix}\lambda & \lambda'\\\lambda'' & \lambda'''\end{smallmatrix}\middle|\begin{smallmatrix}\beta & \beta'\\\beta'' & \beta'''\end{smallmatrix}\right) \equiv \Delta\langle \hat{a}_{\lambda,\beta}^\dagger \hat{a}_{\lambda',\beta'}^\dagger \hat{a}_{\lambda''',\beta'''} \hat{a}_{\lambda'',\beta''} \rangle, \tag{C.17}$$

$$C\left(\begin{smallmatrix}\lambda & \lambda' & \lambda''\\\lambda^{(3)} & \lambda^{(4)} & \lambda^{(5)}\end{smallmatrix}\middle|\begin{smallmatrix}\beta & \beta' & \beta''\\\beta^{(3)} & \beta^{(4)} & \beta^{(5)}\end{smallmatrix}\right) \equiv \Delta\langle \hat{a}_{\lambda,\beta}^\dagger \hat{a}_{\lambda',\beta'}^\dagger \hat{a}_{\lambda'',\beta''}^\dagger \hat{a}_{\lambda^{(5)},\beta^{(5)}} \hat{a}_{\lambda^{(4)},\beta^{(4)}} \hat{a}_{\lambda^{(3)},\beta^{(3)}} \rangle. \tag{C.18}$$

The mean-field energies $E^{\mathrm{c}}_{\beta,\beta'} = E^{\mathrm{e}}_{\beta,\beta'}$ and $E^{\mathrm{v}}_{\beta,\beta'} = -E^{\mathrm{h}}_{\beta,\beta'}$ are defined in Eq. (3.25). For the renormalized Rabi frequencies, we use a slightly more general notation than in Sec. 3.2.1,

$$\Omega^{\lambda}_{\beta,\beta'} \equiv \delta^{\beta}_{\beta'} \mathbf{d}_{\lambda,\overline{\lambda}} \cdot \mathbf{E} + \sum_{\beta_1,\beta_2} V^{\beta\,\beta_1}_{\beta'\beta_2} S\left(\begin{smallmatrix} \overline{\lambda} \\ \lambda \end{smallmatrix} \middle| \begin{smallmatrix} \beta_1 \\ \beta_2 \end{smallmatrix}\right) \tag{C.19}$$

where

$$\overline{\lambda} \equiv \begin{cases} \mathrm{v} & \text{for } \lambda = \mathrm{c}, \\ \mathrm{c} & \text{for } \lambda = \mathrm{v}. \end{cases} \tag{C.20}$$

Moreover, we introduce generalized phase-space filling and exchange factors

$$F_{\mathrm{I}}\left(\begin{smallmatrix} \lambda \\ \lambda' \end{smallmatrix} \middle| \begin{smallmatrix} \beta''\,\beta \\ \beta'\,\beta''' \end{smallmatrix}\right) \equiv \delta^{\beta''}_{\beta} S\left(\begin{smallmatrix} \lambda \\ \lambda' \end{smallmatrix} \middle| \begin{smallmatrix} \beta \\ \beta''' \end{smallmatrix}\right) - S\left(\begin{smallmatrix} \lambda \\ \lambda' \end{smallmatrix} \middle| \begin{smallmatrix} \beta'' \\ \beta' \end{smallmatrix}\right) \delta^{\beta}_{\beta'''}, \tag{C.21}$$

$$F_{\mathrm{II}}\left(\begin{smallmatrix} \lambda''\,\lambda \\ \lambda'\,\lambda''' \end{smallmatrix} \middle| \begin{smallmatrix} \beta''\,\beta \\ \beta'\,\beta''' \end{smallmatrix}\right) \equiv \delta^{\lambda''}_{\lambda'} \delta^{\beta''}_{\beta'} S\left(\begin{smallmatrix} \lambda \\ \lambda''' \end{smallmatrix} \middle| \begin{smallmatrix} \beta \\ \beta''' \end{smallmatrix}\right) - S\left(\begin{smallmatrix} \lambda'' \\ \lambda' \end{smallmatrix} \middle| \begin{smallmatrix} \beta'' \\ \beta' \end{smallmatrix}\right) \delta^{\lambda}_{\lambda'''} \delta^{\beta}_{\beta'''}, \tag{C.22}$$

$$F_{\mathrm{III}}\left(\begin{smallmatrix} \lambda\,\lambda' \\ \lambda''\lambda''' \end{smallmatrix} \middle| \begin{smallmatrix} \beta\,\beta' \\ \beta''\beta''' \end{smallmatrix}\right) \equiv \delta^{\lambda}_{\lambda''} \delta^{\beta}_{\beta''} \delta^{\lambda'}_{\lambda'''} \delta^{\beta'}_{\beta'''} - \delta^{\lambda}_{\lambda''} \delta^{\beta}_{\beta''} S\left(\begin{smallmatrix} \lambda' \\ \lambda''' \end{smallmatrix} \middle| \begin{smallmatrix} \beta' \\ \beta''' \end{smallmatrix}\right) - S\left(\begin{smallmatrix} \lambda \\ \lambda'' \end{smallmatrix} \middle| \begin{smallmatrix} \beta \\ \beta'' \end{smallmatrix}\right) \delta^{\lambda'}_{\lambda'''} \delta^{\beta'}_{\beta'''}. \tag{C.23}$$

With these notations, the dynamics of the incoherent two-particle correlations (3.58), (3.60), (3.61) and the coherent two-particle correlations (3.83), (3.84), (3.85) follows from

$$i\hbar \frac{\mathrm{d}}{\mathrm{d}t} C\left(\begin{smallmatrix} \lambda\,\lambda' \\ \lambda''\lambda''' \end{smallmatrix} \middle| \begin{smallmatrix} \beta\,\beta' \\ \beta''\beta''' \end{smallmatrix}\right) = \mathcal{M}\left(\begin{smallmatrix} \lambda\,\lambda' \\ \lambda''\lambda''' \end{smallmatrix} \middle| \begin{smallmatrix} \beta\,\beta' \\ \beta''\beta''' \end{smallmatrix}\right) + \mathcal{X}\left(\begin{smallmatrix} \lambda\,\lambda' \\ \lambda''\lambda''' \end{smallmatrix} \middle| \begin{smallmatrix} \beta\,\beta' \\ \beta''\beta''' \end{smallmatrix}\right) + \mathcal{S}\left(\begin{smallmatrix} \lambda\,\lambda' \\ \lambda''\lambda''' \end{smallmatrix} \middle| \begin{smallmatrix} \beta\,\beta' \\ \beta''\beta''' \end{smallmatrix}\right)$$
$$+ \mathcal{L}\left(\begin{smallmatrix} \lambda\,\lambda' \\ \lambda''\lambda''' \end{smallmatrix} \middle| \begin{smallmatrix} \beta\,\beta' \\ \beta''\beta''' \end{smallmatrix}\right) + \mathcal{T}\left(\begin{smallmatrix} \lambda\,\lambda' \\ \lambda''\lambda''' \end{smallmatrix} \middle| \begin{smallmatrix} \beta\,\beta' \\ \beta''\beta''' \end{smallmatrix}\right). \tag{C.24}$$

Here,

$$\mathcal{M}\left(\begin{smallmatrix} \lambda\,\lambda' \\ \lambda''\lambda''' \end{smallmatrix} \middle| \begin{smallmatrix} \beta\,\beta' \\ \beta''\beta''' \end{smallmatrix}\right) \equiv \sum_{\beta_1} \left[-E^{\lambda}_{\beta_1,\beta} C\left(\begin{smallmatrix} \lambda\,\lambda' \\ \lambda''\lambda''' \end{smallmatrix} \middle| \begin{smallmatrix} \beta_1\,\beta' \\ \beta''\beta''' \end{smallmatrix}\right) - E^{\lambda'}_{\beta_1,\beta'} C\left(\begin{smallmatrix} \lambda\,\lambda' \\ \lambda''\lambda''' \end{smallmatrix} \middle| \begin{smallmatrix} \beta\,\beta_1 \\ \beta''\beta''' \end{smallmatrix}\right) \right.$$
$$\left. + E^{\lambda''}_{\beta'',\beta_1} C\left(\begin{smallmatrix} \lambda\,\lambda' \\ \lambda''\lambda''' \end{smallmatrix} \middle| \begin{smallmatrix} \beta\,\beta' \\ \beta_1\beta''' \end{smallmatrix}\right) + E^{\lambda'''}_{\beta''',\beta_1} C\left(\begin{smallmatrix} \lambda\,\lambda' \\ \lambda''\lambda''' \end{smallmatrix} \middle| \begin{smallmatrix} \beta\,\beta' \\ \beta''\beta_1 \end{smallmatrix}\right) \right] \tag{C.25}$$

113

contains the mean-field terms,

$$\mathcal{X}\left(\begin{smallmatrix}\lambda & \lambda' \\ \lambda'' & \lambda'''\end{smallmatrix}\middle|\begin{smallmatrix}\beta & \beta' \\ \beta'' & \beta'''\end{smallmatrix}\right) \equiv \sum_{\beta_1,\beta_2,\beta_3,\beta_4}\sum_{\lambda_1,\lambda_2} V^{\beta_1\beta_2}_{\beta_4\beta_3}\left[F_{\text{III}}\left(\begin{smallmatrix}\lambda_1 & \lambda_2 \\ \lambda'' & \lambda'''\end{smallmatrix}\middle|\begin{smallmatrix}\beta_1 & \beta_2 \\ \beta'' & \beta'''\end{smallmatrix}\right)C\left(\begin{smallmatrix}\lambda & \lambda' \\ \lambda_1 & \lambda_2\end{smallmatrix}\middle|\begin{smallmatrix}\beta & \beta' \\ \beta_3 & \beta_4\end{smallmatrix}\right)\right.$$

$$\left.-F_{\text{III}}\left(\begin{smallmatrix}\lambda & \lambda' \\ \lambda_1 & \lambda_2\end{smallmatrix}\middle|\begin{smallmatrix}\beta & \beta' \\ \beta_1 & \beta_2\end{smallmatrix}\right)C\left(\begin{smallmatrix}\lambda_1 & \lambda_2 \\ \lambda'' & \lambda'''\end{smallmatrix}\middle|\begin{smallmatrix}\beta_3 & \beta_4 \\ \beta'' & \beta'''\end{smallmatrix}\right)\right]$$

$$+\sum_{\beta_1,\beta_2,\beta_3,\beta_4}\sum_{\lambda_1} V^{\beta_1\beta_3}_{\beta_4\beta_2}\left[F_{\text{I}}\left(\begin{smallmatrix}\lambda' \\ \lambda'''\end{smallmatrix}\middle|\begin{smallmatrix}\beta_1 & \beta' \\ \beta''' & \beta_2\end{smallmatrix}\right)C\left(\begin{smallmatrix}\lambda & \lambda_1 \\ \lambda'' & \lambda_1\end{smallmatrix}\middle|\begin{smallmatrix}\beta & \beta_3 \\ \beta'' & \beta_4\end{smallmatrix}\right)\right.$$

$$+F_{\text{I}}\left(\begin{smallmatrix}\lambda \\ \lambda''\end{smallmatrix}\middle|\begin{smallmatrix}\beta_1 & \beta \\ \beta'' & \beta_2\end{smallmatrix}\right)C\left(\begin{smallmatrix}\lambda_1 & \lambda' \\ \lambda_1 & \lambda'''\end{smallmatrix}\middle|\begin{smallmatrix}\beta_3 & \beta' \\ \beta_4 & \beta'''\end{smallmatrix}\right)$$

$$+F_{\text{I}}\left(\begin{smallmatrix}\lambda' \\ \lambda''\end{smallmatrix}\middle|\begin{smallmatrix}\beta_1 & \beta' \\ \beta'' & \beta_2\end{smallmatrix}\right)C\left(\begin{smallmatrix}\lambda & \lambda_1 \\ \lambda_1 & \lambda'''\end{smallmatrix}\middle|\begin{smallmatrix}\beta & \beta_3 \\ \beta_4 & \beta'''\end{smallmatrix}\right)$$

$$\left.+F_{\text{I}}\left(\begin{smallmatrix}\lambda \\ \lambda'''\end{smallmatrix}\middle|\begin{smallmatrix}\beta_1 & \beta \\ \beta''' & \beta_2\end{smallmatrix}\right)C\left(\begin{smallmatrix}\lambda_1 & \lambda' \\ \lambda'' & \lambda_1\end{smallmatrix}\middle|\begin{smallmatrix}\beta_3 & \beta' \\ \beta'' & \beta_4\end{smallmatrix}\right)\right]$$

$$-\sum_{\beta_1,\beta_2,\beta_3,\beta_4}\sum_{\lambda_1,\lambda_2} V^{\beta_1\beta_3}_{\beta_2\beta_4}\left[F_{\text{II}}\left(\begin{smallmatrix}\lambda_1 & \lambda' \\ \lambda''' & \lambda_2\end{smallmatrix}\middle|\begin{smallmatrix}\beta_1 & \beta' \\ \beta''' & \beta_2\end{smallmatrix}\right)C\left(\begin{smallmatrix}\lambda & \lambda_2 \\ \lambda'' & \lambda_1\end{smallmatrix}\middle|\begin{smallmatrix}\beta & \beta_3 \\ \beta'' & \beta_4\end{smallmatrix}\right)\right.$$

$$+F_{\text{II}}\left(\begin{smallmatrix}\lambda_1 & \lambda \\ \lambda'' & \lambda_2\end{smallmatrix}\middle|\begin{smallmatrix}\beta_1 & \beta \\ \beta'' & \beta_2\end{smallmatrix}\right)C\left(\begin{smallmatrix}\lambda_2 & \lambda' \\ \lambda_1 & \lambda'''\end{smallmatrix}\middle|\begin{smallmatrix}\beta_3 & \beta' \\ \beta_4 & \beta'''\end{smallmatrix}\right)$$

$$+F_{\text{II}}\left(\begin{smallmatrix}\lambda_1 & \lambda' \\ \lambda'' & \lambda_2\end{smallmatrix}\middle|\begin{smallmatrix}\beta_1 & \beta' \\ \beta'' & \beta_2\end{smallmatrix}\right)C\left(\begin{smallmatrix}\lambda & \lambda_2 \\ \lambda_1 & \lambda'''\end{smallmatrix}\middle|\begin{smallmatrix}\beta & \beta_3 \\ \beta_4 & \beta'''\end{smallmatrix}\right)$$

$$\left.+F_{\text{II}}\left(\begin{smallmatrix}\lambda_1 & \lambda \\ \lambda''' & \lambda_2\end{smallmatrix}\middle|\begin{smallmatrix}\beta_1 & \beta \\ \beta''' & \beta_2\end{smallmatrix}\right)C\left(\begin{smallmatrix}\lambda_2 & \lambda' \\ \lambda'' & \lambda_1\end{smallmatrix}\middle|\begin{smallmatrix}\beta_3 & \beta' \\ \beta'' & \beta_4\end{smallmatrix}\right)\right] \quad \text{(C.26)}$$

the exchange terms, excitonic signatures, and coupling to other two-particle correlations,

$$\mathcal{S}\left(\begin{smallmatrix}\lambda & \lambda' \\ \lambda'' & \lambda'''\end{smallmatrix}\middle|\begin{smallmatrix}\beta & \beta' \\ \beta'' & \beta'''\end{smallmatrix}\right) \equiv$$

$$\sum_{\beta_1,\beta_2,\beta_3,\beta_4}\sum_{\lambda_1,\lambda_2}\left(V^{\beta_1\beta_2}_{\beta_4\beta_3}\left\{S\left(\begin{smallmatrix}\lambda \\ \lambda_1\end{smallmatrix}\middle|\begin{smallmatrix}\beta \\ \beta_1\end{smallmatrix}\right)S\left(\begin{smallmatrix}\lambda' \\ \lambda_2\end{smallmatrix}\middle|\begin{smallmatrix}\beta' \\ \beta_2\end{smallmatrix}\right)\left[\delta^{\lambda_1}_{\lambda''}\delta^{\beta_3}_{\beta''}-S\left(\begin{smallmatrix}\lambda_1 \\ \lambda''\end{smallmatrix}\middle|\begin{smallmatrix}\beta_3 \\ \beta''\end{smallmatrix}\right)\right]\right.$$

$$\left[\delta^{\lambda_2}_{\lambda'''}\delta^{\beta_4}_{\beta'''}-S\left(\begin{smallmatrix}\lambda_2 \\ \lambda'''\end{smallmatrix}\middle|\begin{smallmatrix}\beta_4 \\ \beta'''\end{smallmatrix}\right)\right]$$

$$-S\left(\begin{smallmatrix}\lambda_1 \\ \lambda''\end{smallmatrix}\middle|\begin{smallmatrix}\beta_3 \\ \beta''\end{smallmatrix}\right)S\left(\begin{smallmatrix}\lambda_2 \\ \lambda'''\end{smallmatrix}\middle|\begin{smallmatrix}\beta_4 \\ \beta'''\end{smallmatrix}\right)\left[\delta^{\lambda}_{\lambda_1}\delta^{\beta}_{\beta_1}-S\left(\begin{smallmatrix}\lambda \\ \lambda_1\end{smallmatrix}\middle|\begin{smallmatrix}\beta \\ \beta_1\end{smallmatrix}\right)\right]$$

$$\left.\left[\delta^{\lambda'}_{\lambda_2}\delta^{\beta'}_{\beta_2}-S\left(\begin{smallmatrix}\lambda' \\ \lambda_2\end{smallmatrix}\middle|\begin{smallmatrix}\beta' \\ \beta_2\end{smallmatrix}\right)\right]\right\}$$

$$-V^{\beta_1\beta_2}_{\beta_3\beta_4}\left\{S\left(\begin{smallmatrix}\lambda \\ \lambda_1\end{smallmatrix}\middle|\begin{smallmatrix}\beta \\ \beta_1\end{smallmatrix}\right)S\left(\begin{smallmatrix}\lambda' \\ \lambda_2\end{smallmatrix}\middle|\begin{smallmatrix}\beta' \\ \beta_2\end{smallmatrix}\right)\left[\delta^{\lambda_2}_{\lambda''}\delta^{\beta_3}_{\beta''}-S\left(\begin{smallmatrix}\lambda_2 \\ \lambda''\end{smallmatrix}\middle|\begin{smallmatrix}\beta_3 \\ \beta''\end{smallmatrix}\right)\right]\right.$$

$$\left[\delta^{\lambda_1}_{\lambda'''}\delta^{\beta_4}_{\beta'''}-S\left(\begin{smallmatrix}\lambda_1 \\ \lambda'''\end{smallmatrix}\middle|\begin{smallmatrix}\beta_4 \\ \beta'''\end{smallmatrix}\right)\right]$$

$$-S\left(\begin{smallmatrix}\lambda_2 \\ \lambda''\end{smallmatrix}\middle|\begin{smallmatrix}\beta_3 \\ \beta''\end{smallmatrix}\right)S\left(\begin{smallmatrix}\lambda_1 \\ \lambda'''\end{smallmatrix}\middle|\begin{smallmatrix}\beta_4 \\ \beta'''\end{smallmatrix}\right)\left[\delta^{\lambda}_{\lambda_1}\delta^{\beta}_{\beta_1}-S\left(\begin{smallmatrix}\lambda \\ \lambda_1\end{smallmatrix}\middle|\begin{smallmatrix}\beta \\ \beta_1\end{smallmatrix}\right)\right]$$

$$\left.\left.\left[\delta^{\lambda'}_{\lambda_2}\delta^{\beta'}_{\beta_2}-S\left(\begin{smallmatrix}\lambda' \\ \lambda_2\end{smallmatrix}\middle|\begin{smallmatrix}\beta' \\ \beta_2\end{smallmatrix}\right)\right]\right\}\right) \quad \text{(C.27)}$$

the singlet source terms,

$$\mathcal{L}\left(\begin{smallmatrix}\lambda & \lambda' \\ \lambda'' & \lambda'''\end{smallmatrix}\middle|\begin{smallmatrix}\beta & \beta' \\ \beta'' & \beta'''\end{smallmatrix}\right) \equiv \sum_{\beta_1}\left[\left(\Omega^{\lambda}_{\beta,\beta_1}\right)^*C\left(\begin{smallmatrix}\overline{\lambda} & \lambda' \\ \lambda'' & \lambda'''\end{smallmatrix}\middle|\begin{smallmatrix}\beta_1 & \beta' \\ \beta'' & \beta'''\end{smallmatrix}\right) + \left(\Omega^{\lambda'}_{\beta',\beta_1}\right)^*C\left(\begin{smallmatrix}\lambda & \overline{\lambda'} \\ \lambda'' & \lambda'''\end{smallmatrix}\middle|\begin{smallmatrix}\beta & \beta_1 \\ \beta'' & \beta'\end{smallmatrix}\right)\right.$$

$$\left.-\Omega^{\lambda''}_{\beta'',\beta_1}C\left(\begin{smallmatrix}\lambda & \lambda' \\ \overline{\lambda''} & \lambda'''\end{smallmatrix}\middle|\begin{smallmatrix}\beta & \beta' \\ \beta_1 & \beta'''\end{smallmatrix}\right) - \Omega^{\lambda'''}_{\beta''',\beta_1}C\left(\begin{smallmatrix}\lambda & \lambda' \\ \lambda'' & \overline{\lambda'''}\end{smallmatrix}\middle|\begin{smallmatrix}\beta & \beta' \\ \beta'' & \beta_1\end{smallmatrix}\right)\right] \quad \text{(C.28)}$$

the coupling to the light field, and

$$
\mathcal{T}\left(\begin{smallmatrix} \lambda & \lambda' \\ \lambda'' & \lambda''' \end{smallmatrix} \Big| \begin{smallmatrix} \beta & \beta' \\ \beta'' & \beta''' \end{smallmatrix}\right) \equiv
$$

$$
\sum_{\beta_1,\beta_2,\beta_3} \sum_{\lambda_1} \Big[-V^{\,\beta\,\,\beta_2}_{\,\beta_3\beta_1} C\left(\begin{smallmatrix} \lambda & \lambda' & \lambda_1 \\ \lambda'' & \lambda''' & \lambda_1 \end{smallmatrix} \Big| \begin{smallmatrix} \beta_1 & \beta' & \beta_3 \\ \beta'' & \beta''' & \beta_2 \end{smallmatrix}\right) - V^{\,\beta_2\beta'}_{\,\beta_1\beta_3} C\left(\begin{smallmatrix} \lambda & \lambda' & \lambda_1 \\ \lambda'' & \lambda''' & \lambda_1 \end{smallmatrix} \Big| \begin{smallmatrix} \beta & \beta_1 & \beta_3 \\ \beta'' & \beta''' & \beta_2 \end{smallmatrix}\right)
$$

$$
+ V^{\,\beta_3\beta_1}_{\,\beta''\beta_2} C\left(\begin{smallmatrix} \lambda & \lambda' & \lambda_1 \\ \lambda'' & \lambda''' & \lambda_1 \end{smallmatrix} \Big| \begin{smallmatrix} \beta & \beta' & \beta_2 \\ \beta_1 & \beta''' & \beta_3 \end{smallmatrix}\right) + V^{\,\beta_1\beta_3}_{\,\beta_2\beta'''} C\left(\begin{smallmatrix} \lambda & \lambda' & \lambda_1 \\ \lambda'' & \lambda''' & \lambda_1 \end{smallmatrix} \Big| \begin{smallmatrix} \beta & \beta' & \beta_2 \\ \beta'' & \beta_1 & \beta_3 \end{smallmatrix}\right) \Big] \qquad (C.29)
$$

the coupling to three-particle correlations.

115

D Phonon-assisted carrier correlations

In the steady-state formula (4.14), the Markov solutions for the spontaneous-emission source terms in the phonon-assisted luminescence equation (4.11) appear in a sum over the phonon momenta. In situations like this, the final results do not depend critically on the basis that has been used for the Markov approximation. We may therefore restrict the equations of motion for the phonon-assisted intraband correlations to the kinetic terms and the true source terms. Thus, without Coulomb terms and quantum-optical correlations, we explicitly obtain

$$
\begin{aligned}
i\hbar \frac{d}{dt} \Delta \langle \hat{D}_{\mathbf{p}}^{\dagger} \hat{a}_{c,\mathbf{k}-\mathbf{p}_h}^{\dagger} \hat{a}_{c,\mathbf{k}+\mathbf{p}_e} \rangle ={}& \left(\varepsilon_{\mathbf{k}+\mathbf{p}_e}^{e} - \varepsilon_{\mathbf{k}-\mathbf{p}_h}^{e} - \hbar\Omega - i\eta_e \right) \Delta \langle \hat{D}_{\mathbf{p}}^{\dagger} \hat{a}_{c,\mathbf{k}-\mathbf{p}_h}^{\dagger} \hat{a}_{c,\mathbf{k}+\mathbf{p}_e} \rangle \\
&+ \hbar\Omega \sum_{\mathbf{k}'} \left(g_{v,\mathbf{p}}^{*} C_{X}^{\mathbf{k}-\mathbf{k}'+\mathbf{p}_e,\mathbf{k}',\mathbf{k}-\mathbf{p}_h} + g_{c,\mathbf{p}}^{*} C_{ee}^{\mathbf{k}-\mathbf{k}'+\mathbf{p}_e,\mathbf{k}',\mathbf{k}-\mathbf{p}_h} \right) \\
&- \hbar\Omega g_{c,\mathbf{p}}^{*} f_{\mathbf{k}+\mathbf{p}_e}^{e} \left(1 - f_{\mathbf{k}-\mathbf{p}_h}^{e} \right) \\
&+ \hbar\Omega g_{c,\mathbf{p}}^{*} n_{\mathbf{p}}^{phon} \left(f_{\mathbf{k}-\mathbf{p}_h}^{e} - f_{\mathbf{k}+\mathbf{p}_e}^{e} \right), &&\text{(D.1)} \\
i\hbar \frac{d}{dt} \Delta \langle \hat{D}_{\mathbf{p}}^{\dagger} \hat{a}_{v,\mathbf{k}-\mathbf{p}_h}^{\dagger} \hat{a}_{v,\mathbf{k}+\mathbf{p}_e} \rangle ={}& \left(\varepsilon_{\mathbf{k}-\mathbf{p}_h}^{h} - \varepsilon_{\mathbf{k}+\mathbf{p}_e}^{h} - \hbar\Omega - i\eta_h \right) \Delta \langle \hat{D}_{\mathbf{p}}^{\dagger} \hat{a}_{v,\mathbf{k}-\mathbf{p}_h}^{\dagger} \hat{a}_{v,\mathbf{k}+\mathbf{p}_e} \rangle \\
&+ \hbar\Omega \sum_{\mathbf{k}'} \left(g_{c,\mathbf{p}}^{*} C_{X}^{\mathbf{k}'-\mathbf{k}-\mathbf{p}_e,\mathbf{k}-\mathbf{p}_h,\mathbf{k}'} + g_{c,\mathbf{p}}^{*} C_{hh}^{\mathbf{k}'-\mathbf{k}-\mathbf{p}_e,\mathbf{k}-\mathbf{p}_h,\mathbf{k}'} \right) \\
&- \hbar\Omega g_{v,\mathbf{p}}^{*} f_{\mathbf{k}-\mathbf{p}_h}^{h} \left(1 - f_{\mathbf{k}+\mathbf{p}_e}^{h} \right) \\
&+ \hbar\Omega g_{v,\mathbf{p}}^{*} n_{\mathbf{p}}^{phon} \left(f_{\mathbf{k}+\mathbf{p}_e}^{h} - f_{\mathbf{k}-\mathbf{p}_h}^{h} \right) &&\text{(D.2)}
\end{aligned}
$$

with dephasing constants η_e, η_h where we have defined the incoherent two-particle correlations

$$
C_{X}^{\mathbf{q},\mathbf{k}',\mathbf{k}} \equiv \Delta \langle \hat{a}_{c,\mathbf{k}}^{\dagger} \hat{a}_{v,\mathbf{k}'}^{\dagger} \hat{a}_{c,\mathbf{k}'+\mathbf{q}} \hat{a}_{v,\mathbf{k}-\mathbf{q}} \rangle, \tag{D.3}
$$

$$
C_{ee}^{\mathbf{q},\mathbf{k}',\mathbf{k}} \equiv \Delta \langle \hat{a}_{c,\mathbf{k}}^{\dagger} \hat{a}_{c,\mathbf{k}'}^{\dagger} \hat{a}_{c,\mathbf{k}'+\mathbf{q}} \hat{a}_{c,\mathbf{k}-\mathbf{q}} \rangle, \tag{D.4}
$$

$$
C_{hh}^{\mathbf{q},\mathbf{k}',\mathbf{k}} \equiv \Delta \langle \hat{a}_{v,\mathbf{k}}^{\dagger} \hat{a}_{v,\mathbf{k}'}^{\dagger} \hat{a}_{v,\mathbf{k}'+\mathbf{q}} \hat{a}_{v,\mathbf{k}-\mathbf{q}} \rangle. \tag{D.5}
$$

The terms in the last lines of Eqs. (D.1), (D.2) can be neglected because they contain phonon numbers $n_{\mathbf{p}}^{phon}$. In accordance with the additional truncation criterion introduced in Sec. 4.3.1, we exclusively consider those source terms for the phonon-assisted correlations that are of first order in the carrier densities since all higher-order contributions would only lead to third-order source terms in Eq. (4.11). With this approach, the Markov solutions become

$$
\Delta \langle \hat{D}_{\mathbf{p}}^{\dagger} \hat{a}_{c,\mathbf{k}-\mathbf{p}_h}^{\dagger} \hat{a}_{c,\mathbf{k}+\mathbf{p}_e} \rangle \simeq \frac{\hbar\Omega g_{c,\mathbf{p}}^{*} f_{\mathbf{k}+\mathbf{p}_e}^{e}}{\varepsilon_{\mathbf{k}+\mathbf{p}_e}^{e} - \varepsilon_{\mathbf{k}-\mathbf{p}_h}^{e} - \hbar\Omega - i\eta_e}, \tag{D.6}
$$

$$
\Delta \langle \hat{D}_{\mathbf{p}}^{\dagger} \hat{a}_{v,\mathbf{k}-\mathbf{p}_h}^{\dagger} \hat{a}_{v,\mathbf{k}+\mathbf{p}_e} \rangle \simeq \frac{\hbar\Omega g_{v,\mathbf{p}}^{*} f_{\mathbf{k}-\mathbf{p}_h}^{h}}{\varepsilon_{\mathbf{k}-\mathbf{p}_h}^{h} - \varepsilon_{\mathbf{k}+\mathbf{p}_e}^{h} - \hbar\Omega - i\eta_h}. \tag{D.7}
$$

For small η_e, η_h, the final results are nearly independent of the dephasing constants because the real parts of the denominators are far from zero in the relevant momentum range.

For the phonon-assisted excitonic correlations $\Delta\langle \hat{D}^\dagger \hat{a}_c^\dagger \hat{a}_v^\dagger \hat{a}_c \hat{a}_v \rangle$, the inclusion of the Coulomb terms does not complicate the calculation because the equations of motion can be diagonalized with the help of the exciton basis. The corresponding Markov results are presented in the supplement to the exciton-picture analysis E.4. There, the excitons are treated as perfect bosons. However, it can easily be seen that any additional contribution in the equations of motion for the $\Delta\langle \hat{D}^\dagger \hat{a}_c^\dagger \hat{a}_v^\dagger \hat{a}_c \hat{a}_v \rangle$ that originate from the fermionic substructure of the excitons would only provide higher-order source terms that are neglected, anyway.

E Supplement to the exciton-picture analysis

We derive in Sec. E.1 how the system Hamiltonian (4.5) can be expressed in terms of phonon, photon, and exciton operators. The boson approximation for the exciton operators is justified in Sec. E.2. The relevant exciton-phonon matrix elements are evaluated analytically in Sec. E.3. Finally, we present the Markov solution for the phonon-assisted excitonic correlations in Sec. E.4.

E.1 Hamiltonian

For the following considerations, it is useful to introduce *electron operators* $\hat{e}_{\mathbf{k}} \equiv \hat{a}_{\mathrm{c},\mathbf{k}}$ and *hole operators* $\hat{h}_{\mathbf{k}} \equiv \hat{a}_{\mathrm{v},-\mathbf{k}}^{\dagger}$. After a renormalization of the band gap, the parts of the system Hamiltonian (4.5) that contain carrier operators thus take the form

$$\hat{H}_{\mathrm{el}} = \sum_{\mathbf{k}} \left(\varepsilon_{\mathbf{k}}^{\mathrm{e}} \hat{e}_{\mathbf{k}}^{\dagger} \hat{e}_{\mathbf{k}} + \varepsilon_{\mathbf{k}}^{\mathrm{h}} \hat{h}_{\mathbf{k}}^{\dagger} \hat{h}_{\mathbf{k}} \right), \tag{E.1}$$

$$\hat{H}_{\mathrm{el-el}} = \frac{1}{2} \sum_{\mathbf{k},\mathbf{k}',\mathbf{q}} V_{\mathbf{q}} \left(\hat{e}_{\mathbf{k}}^{\dagger} \hat{e}_{\mathbf{k}'}^{\dagger} \hat{e}_{\mathbf{k}'+\mathbf{q}} \hat{e}_{\mathbf{k}-\mathbf{q}} + \hat{h}_{\mathbf{k}}^{\dagger} \hat{h}_{\mathbf{k}'}^{\dagger} \hat{h}_{\mathbf{k}'+\mathbf{q}} \hat{h}_{\mathbf{k}-\mathbf{q}} - 2 \hat{e}_{\mathbf{k}}^{\dagger} \hat{h}_{\mathbf{k}'}^{\dagger} \hat{h}_{\mathbf{k}'+\mathbf{q}} \hat{e}_{\mathbf{k}-\mathbf{q}} \right), \tag{E.2}$$

$$\hat{H}_{\mathrm{el-vib}} = \sum_{\mathbf{k},\mathbf{p}} \hbar\Omega \left(g_{\mathrm{c},\mathbf{p}} \hat{e}_{\mathbf{k}-\mathbf{p}}^{\dagger} \hat{e}_{\mathbf{k}} - g_{\mathrm{v},\mathbf{p}} \hat{h}_{\mathbf{k}-\mathbf{p}}^{\dagger} \hat{h}_{\mathbf{k}} \right) \left(\hat{D}_{-\mathbf{p}} + \hat{D}_{\mathbf{p}}^{\dagger} \right), \tag{E.3}$$

$$\hat{H}_{\mathrm{el-em}} = -\sum_{\mathbf{k},\mathbf{q}} \mathrm{i} \left(\mathcal{F}_{\mathbf{q}} \hat{e}_{\mathbf{k}+\mathbf{q}}^{\dagger} \hat{h}_{-\mathbf{k}}^{\dagger} + \mathcal{F}_{\mathbf{q}}^{*} \hat{h}_{-\mathbf{k}} \hat{e}_{\mathbf{k}-\mathbf{q}} \right) \hat{B}_{\mathbf{q}} + \mathrm{H.C.} \tag{E.4}$$

With this Hamiltonian, the total electron and total hole density can only be changed via the creation or recombination of electron-hole pairs. We may therefore assume that the carrier system always contains as many electrons in the conduction band as it contains holes in the valence band. When they act on states with that property, the Hamiltonians (E.1), (E.3) can be rewritten as

$$\hat{H}_{\mathrm{el}} = \sum_{\mathbf{k}} \left[\varepsilon_{\mathbf{k}}^{\mathrm{e}} \hat{e}_{\mathbf{k}}^{\dagger} \sum_{\mathbf{k}'} \left(\hat{h}_{\mathbf{k}'}^{\dagger} \hat{h}_{\mathbf{k}'} - \hat{e}_{\mathbf{k}'}^{\dagger} \hat{e}_{\mathbf{k}'} \right) \hat{e}_{\mathbf{k}} + \varepsilon_{\mathbf{k}}^{\mathrm{h}} \hat{h}_{\mathbf{k}}^{\dagger} \sum_{\mathbf{k}'} \left(\hat{e}_{\mathbf{k}'}^{\dagger} \hat{e}_{\mathbf{k}'} - \hat{h}_{\mathbf{k}'}^{\dagger} \hat{h}_{\mathbf{k}'} \right) \hat{h}_{\mathbf{k}} \right], \tag{E.5}$$

$$\hat{H}_{\mathrm{el-vib}} = \sum_{\mathbf{k},\mathbf{p}} \hbar\Omega \left[g_{\mathrm{c},\mathbf{p}} \hat{e}_{\mathbf{k}-\mathbf{p}}^{\dagger} \sum_{\mathbf{k}'} \left(\hat{h}_{\mathbf{k}'}^{\dagger} \hat{h}_{\mathbf{k}'} - \hat{e}_{\mathbf{k}'}^{\dagger} \hat{e}_{\mathbf{k}'} \right) \hat{e}_{\mathbf{k}} \right.$$
$$\left. - g_{\mathrm{v},\mathbf{p}} \hat{h}_{\mathbf{k}-\mathbf{p}}^{\dagger} \sum_{\mathbf{k}'} \left(\hat{e}_{\mathbf{k}'}^{\dagger} \hat{e}_{\mathbf{k}'} - \hat{h}_{\mathbf{k}'}^{\dagger} \hat{h}_{\mathbf{k}'} \right) \hat{h}_{\mathbf{k}} \right] \left(\hat{D}_{-\mathbf{p}} + \hat{D}_{\mathbf{p}}^{\dagger} \right) \tag{E.6}$$

because $\hat{N}_{\mathrm{e}} = \sum_{\mathbf{k}} \hat{e}_{\mathbf{k}}^{\dagger} \hat{e}_{\mathbf{k}}$ and $\hat{N}_{\mathrm{h}} = \sum_{\mathbf{k}} \hat{h}_{\mathbf{k}}^{\dagger} \hat{h}_{\mathbf{k}}$ are the total number operators for electrons and holes, respectively. If we restrict the analysis to the low-density limit, we may neglect all terms

in the total Hamiltonian that include two electron or two hole annihilation operators in a row. Among others, we thus eliminate the intraband contributions to the Coulomb interaction. As a result of such an approximation on the operator level, the system Hamiltonian can be expressed in terms of e-h pair operators $\hat{p}_{\mathbf{k},\mathbf{k}'} \equiv \hat{h}_{\mathbf{k}}\hat{e}_{\mathbf{k}'}$,

$$\hat{H}_{\mathrm{el}} \simeq \sum_{\mathbf{k},\mathbf{k}'} \left(\varepsilon_{\mathbf{k}'}^{\mathrm{e}} + \varepsilon_{\mathbf{k}}^{\mathrm{h}}\right) \hat{p}_{\mathbf{k},\mathbf{k}'}^{\dagger} \hat{p}_{\mathbf{k},\mathbf{k}'}, \tag{E.7}$$

$$\hat{H}_{\mathrm{el-el}} \simeq \sum_{\mathbf{k},\mathbf{k}',\mathbf{q}} V_{\mathbf{q}} \hat{p}_{\mathbf{k},\mathbf{k}'}^{\dagger} \hat{p}_{\mathbf{k}+\mathbf{q},\mathbf{k}'-\mathbf{q}} \tag{E.8}$$

$$\hat{H}_{\mathrm{el-vib}} \simeq \sum_{\mathbf{k},\mathbf{k}',\mathbf{p}} \hbar\Omega \left(g_{\mathrm{c},\mathbf{p}} \hat{p}_{\mathbf{k},\mathbf{k}'-\mathbf{p}}^{\dagger} \hat{p}_{\mathbf{k},\mathbf{k}'} - g_{\mathrm{v},\mathbf{p}} \hat{p}_{\mathbf{k}-\mathbf{p},\mathbf{k}'}^{\dagger} \hat{p}_{\mathbf{k},\mathbf{k}'}\right) \left(\hat{D}_{-\mathbf{p}} + \hat{D}_{\mathbf{p}}^{\dagger}\right), \tag{E.9}$$

$$\hat{H}_{\mathrm{el-em}} = -\sum_{\mathbf{k},\mathbf{q}} \mathrm{i}\left(\mathcal{F}_{\mathbf{q}} \hat{p}_{-\mathbf{k},\mathbf{k}+\mathbf{q}}^{\dagger} + \mathcal{F}_{\mathbf{q}}^{*} \hat{p}_{-\mathbf{k},\mathbf{k}-\mathbf{q}}\right) \hat{B}_{\mathbf{q}} + \mathrm{H.C.} \tag{E.10}$$

We can now use the identity

$$\hat{p}_{\mathbf{k},\mathbf{k}'} = \sum_{\nu} \phi_{\nu}\left(\frac{m_{\mathrm{h}}\mathbf{k}' - m_{\mathrm{e}}\mathbf{k}}{m_{\mathrm{e}} + m_{\mathrm{h}}}\right) \hat{X}_{\nu,\mathbf{k}+\mathbf{k}'} \tag{E.11}$$

to transform the Hamiltonian into the low-density exciton basis. In view of the eigenvalue equation (A.3), we obtain

$$\hat{H}_{\mathrm{el}} + \hat{H}_{\mathrm{el-el}} \simeq \hat{H}_{\mathrm{X}} \equiv \sum_{\nu,\mathbf{Q}} E_{\nu}(\mathbf{Q}) \hat{X}_{\nu,\mathbf{Q}}^{\dagger} \hat{X}_{\nu,\mathbf{Q}} \tag{E.12}$$

while

$$\hat{H}_{\mathrm{el-vib}} \simeq \hat{H}_{\mathrm{X-phon}} \equiv \sum_{\nu,\nu'} \sum_{\mathbf{Q},\mathbf{p}} \hbar\Omega g_{\mathbf{p}}^{\nu,\nu'} \hat{X}_{\nu,\mathbf{Q}-\mathbf{p}}^{\dagger} \hat{X}_{\nu',\mathbf{Q}} \left(\hat{D}_{-\mathbf{p}} + \hat{D}_{\mathbf{p}}^{\dagger}\right), \tag{E.13}$$

$$\hat{H}_{\mathrm{el-em}} = \hat{H}_{\mathrm{X-em}} \equiv -\sum_{\nu,\mathbf{q}} \mathrm{i}\left[\mathcal{F}_{\mathbf{q}} \phi_{\nu}^{*}(\mathbf{r}=\mathbf{0}) \hat{X}_{\nu,\mathbf{q}}^{\dagger} + \mathcal{F}_{\mathbf{q}}^{*} \phi_{\nu}(\mathbf{r}=\mathbf{0}) \hat{X}_{\nu,-\mathbf{q}}\right] \hat{B}_{\mathbf{q}} + \mathrm{H.C.} \tag{E.14}$$

with the exciton-phonon matrix element

$$g_{\mathbf{p}}^{\nu,\nu'} = \sum_{\mathbf{k}} \phi_{\nu}^{*}(\mathbf{k}) \left[g_{\mathrm{c},\mathbf{p}} \phi_{\nu'}(\mathbf{k}+\mathbf{p}_{\mathrm{h}}) - g_{\mathrm{v},\mathbf{p}} \phi_{\nu'}(\mathbf{k}-\mathbf{p}_{\mathrm{e}})\right]. \tag{E.15}$$

E.2 Boson approximation

Owing to the fermionic substructure of the electron-hole pairs, the exciton operators $\hat{X}_{\nu,\mathbf{Q}}$, $\hat{X}_{\nu,\mathbf{Q}}^{\dagger}$ do not obey bosonic commutation relations. While

$$[\hat{X}_{\nu,\mathbf{Q}}, \hat{X}_{\nu',\mathbf{Q}'}]_{-} = 0 = [\hat{X}_{\nu,\mathbf{Q}}^{\dagger}, \hat{X}_{\nu',\mathbf{Q}'}^{\dagger}]_{-}, \tag{E.16}$$

we have

$$[\hat{X}_{\nu,\mathbf{Q}}, \hat{X}_{\nu',\mathbf{Q}'}^{\dagger}]_{-} = \delta_{\nu,\nu'}\delta_{\mathbf{Q},\mathbf{Q}'} + \hat{C}_{\mathbf{Q},\mathbf{Q}'}^{\nu,\nu'} \tag{E.17}$$

with the additional contribution

$$
\hat{C}_{\mathbf{Q},\mathbf{Q}'}^{\nu,\nu'} \equiv -\sum_{\mathbf{k}} \Big[\phi_{\nu}^{*}(\mathbf{k}-\mathbf{Q}_{\mathrm{e}})\phi_{\nu'}(\mathbf{k}-\mathbf{Q}_{\mathrm{e}}')\hat{h}_{\mathbf{Q}'-\mathbf{k}}^{\dagger}\hat{h}_{\mathbf{Q}-\mathbf{k}}
$$
$$
+ \phi_{\nu}^{*}(\mathbf{k}+\mathbf{Q}_{\mathrm{h}})\phi_{\nu'}(\mathbf{k}+\mathbf{Q}_{\mathrm{h}}')\hat{e}_{\mathbf{k}+\mathbf{Q}'}^{\dagger}\hat{e}_{\mathbf{k}+\mathbf{Q}} \Big]. \tag{E.18}
$$

For the dynamics of the exciton operators due to $\hat{H}_{\mathrm{X}}$ and $\hat{H}_{\mathrm{X-phon}}$, we thus obtain

$$
\mathrm{i}\hbar \frac{\mathrm{d}}{\mathrm{d}t} \hat{X}_{\nu,\mathbf{Q}} \Big|_{\hat{H}_{\mathrm{X}}} = [\hat{X}_{\nu,\mathbf{Q}}, \hat{H}_{\mathrm{X}}]_{-}
$$
$$
= E_{\nu}(\mathbf{Q})\hat{X}_{\nu,\mathbf{Q}} + \sum_{\nu',\mathbf{Q}'} E_{\nu'}(\mathbf{Q}')\hat{C}_{\mathbf{Q},\mathbf{Q}'}^{\nu,\nu'}\hat{X}_{\nu',\mathbf{Q}'}, \tag{E.19}
$$

$$
\mathrm{i}\hbar \frac{\mathrm{d}}{\mathrm{d}t} \hat{X}_{\nu,\mathbf{Q}} \Big|_{\hat{H}_{\mathrm{X-phon}}} = [\hat{X}_{\nu,\mathbf{Q}}, \hat{H}_{\mathrm{X-phon}}]_{-}
$$
$$
= \sum_{\nu'} \sum_{\mathbf{p}} \hbar\Omega g_{\mathbf{p}}^{\nu,\nu'} \hat{X}_{\nu',\mathbf{Q}+\mathbf{p}} \left(\hat{D}_{-\mathbf{p}} + \hat{D}_{\mathbf{p}}^{\dagger} \right)
$$
$$
+ \sum_{\nu',\nu''} \sum_{\mathbf{Q}',\mathbf{p}} \hbar\Omega g_{\mathbf{p}}^{\nu',\nu''} \hat{C}_{\mathbf{Q},\mathbf{Q}'}^{\nu,\nu'} \hat{X}_{\nu'',\mathbf{Q}'+\mathbf{p}} \left(\hat{D}_{-\mathbf{p}} + \hat{D}_{\mathbf{p}}^{\dagger} \right). \tag{E.20}
$$

The first terms on the right-hand sides originate from bosonic commutation relations while the second terms give the deviations from the perfectly bosonic behavior. In the low-density limit, we may neglect the latter contributions because they consist of terms that contain two electron- or two hole-annihilation operators in a row. This argument does not apply to

$$
\mathrm{i}\hbar \frac{\mathrm{d}}{\mathrm{d}t} \hat{X}_{\nu,\mathbf{Q}} \Big|_{\hat{H}_{\mathrm{X-em}}} = [\hat{X}_{\nu,\mathbf{Q}}, \hat{H}_{\mathrm{X-em}}]_{-}
$$
$$
= \mathrm{i}\mathcal{F}_{\mathbf{Q}}\phi_{\nu}^{*}(\mathbf{r}=\mathbf{0}) \left(\hat{B}_{-\mathbf{Q}}^{\dagger} + \hat{B}_{\mathbf{Q}} \right)
$$
$$
+ \sum_{\nu',\mathbf{Q}'} \mathrm{i}\mathcal{F}_{\mathbf{Q}'}\phi_{\nu'}^{*}(\mathbf{r}=\mathbf{0})\hat{C}_{\mathbf{Q},\mathbf{Q}'}^{\nu,\nu'} \left(\hat{B}_{-\mathbf{Q}}^{\dagger} + \hat{B}_{\mathbf{Q}} \right). \tag{E.21}
$$

However, the phonon-assisted semiconductor luminescence equations in the exciton picture describe the evolution of correlations of the form $\Delta\langle \hat{D}^{\dagger}\cdots\hat{D}^{\dagger}\hat{B}^{\dagger}\hat{X}\rangle$. Here, the dynamics of the exciton operators due to $\hat{H}_{\mathrm{X-em}}$ leads to the stimulated-emission source terms that are neglected in the analysis. We therefore expect that the excitonic contribution to the luminescence spectrum is computed correctly when the excitons are treated as genuine bosons, i.e., when the correction terms $\hat{C}_{\mathbf{Q},\mathbf{Q}'}^{\nu,\nu'}$ are omitted.

E.3 Exciton-phonon scattering

Because the $\mathbf{k}$ sum in Eq. (E.15) is a convolution in momentum space, the exciton-phonon matrix element $g_{\mathbf{p}}^{\nu,\nu'}$ can be written as

$$
g_{\mathbf{p}}^{\nu,\nu'} = \frac{1}{\mathscr{L}^{3}} \int \phi_{\nu}^{*}(\mathbf{r})\phi_{\nu'}(\mathbf{r}) \left(g_{\mathrm{c},\mathbf{p}}\mathrm{e}^{-\mathrm{i}\mathbf{p}_{\mathrm{h}}\cdot\mathbf{r}} - g_{\mathrm{v},\mathbf{p}}\mathrm{e}^{\mathrm{i}\mathbf{p}_{\mathrm{e}}\cdot\mathbf{r}} \right) \mathrm{d}^{3}r \tag{E.22}
$$

in terms of the (dimensionless) low-density excitonic wave functions in position space [1]

$$\phi_\nu(\mathbf{r}) = -\sqrt{\left(\frac{2\mathscr{L}}{na_{\mathrm{B}}}\right)^3 \frac{(n-l-1)!}{2n[(n+l)!]^3}}\, \rho^l \mathrm{e}^{-\rho/2} L_{n+l}^{2l+1}(\rho) Y_{l,m}(\theta,\varphi). \tag{E.23}$$

Here, (r,θ,φ) are the spherical coordinates of $\mathbf{r}$ and $\rho \equiv 2r/na_{\mathrm{B}}$ with the exciton Bohr radius $a_{\mathrm{B}} \equiv \hbar^2\epsilon_0\epsilon_{\mathrm{b}}/e^2 m_{\mathrm{red}}$. The subscript $\nu = (n,l,m)$ includes the principal quantum number $n = 1,2,\ldots$, the angular-momentum quantum number $l = 0,1,\ldots,n-1$, and the magnetic quantum number $m = -l,-l+1,\ldots,l$. With $L_{n+l}^{2l+1}(\rho)$, we denote the generalized Laguerre polynomial [105].

When Fröhlich and optical deformation-potential interaction are to be compared, it is helpful to separate the part of the exciton-phonon matrix element that vanishes for band-independent electron-phonon matrix elements $g_{\mathrm{c},\mathbf{p}} = g_{\mathrm{v},\mathbf{p}}$. Explicitly, we obtain

$$g_{\mathbf{p}}^{\nu,\nu'} = \frac{g_{\mathrm{c},\mathbf{p}} + g_{\mathrm{v},\mathbf{p}}}{2}\,\chi_{\nu,\nu',\mathbf{p}}^{(+)} + \frac{g_{\mathrm{c},\mathbf{p}} - g_{\mathrm{v},\mathbf{p}}}{2}\,\chi_{\nu,\nu',\mathbf{p}}^{(-)} \tag{E.24}$$

with

$$\chi_{\nu,\nu',\mathbf{p}}^{(\pm)} \equiv \frac{1}{\mathscr{L}^3}\int \phi_\nu(\mathbf{r})^*\phi_{\nu'}(\mathbf{r})\left(\mathrm{e}^{-\mathrm{i}\mathbf{p}_{\mathrm{h}}\cdot\mathbf{r}} \mp \mathrm{e}^{\mathrm{i}\mathbf{p}_{\mathrm{e}}\cdot\mathbf{r}}\right) \mathrm{d}^3r. \tag{E.25}$$

If $\phi_\nu(\mathbf{r})$ and $\phi_{\nu'}(\mathbf{r})$ have the same parity, a Taylor expansion of $\mathrm{e}^{\pm\mathrm{i}\mathbf{p}_{\mathrm{e,h}}\cdot\mathbf{r}}$ yields

$$\chi_{\nu,\nu',\mathbf{p}}^{(+)} = \frac{m_{\mathrm{e}} - m_{\mathrm{h}}}{2M}\, I_{\nu,\nu'}^{(2)}\!\left(\tfrac{\mathbf{p}}{|\mathbf{p}|}\right) |\mathbf{p}|^2 + \mathcal{O}(|\mathbf{p}|^4), \tag{E.26}$$

$$\chi_{\nu,\nu',\mathbf{p}}^{(-)} = 2\delta_{\nu,\nu'} - \frac{m_{\mathrm{e}}^2 + m_{\mathrm{h}}^2}{2M^2}\, I_{\nu,\nu'}^{(2)}\!\left(\tfrac{\mathbf{p}}{|\mathbf{p}|}\right) |\mathbf{p}|^2 + \mathcal{O}(|\mathbf{p}|^4) \tag{E.27}$$

where $\mathcal{O}(|\mathbf{p}|^k)$ stands for terms of the order of $|\mathbf{p}|^k$, and

$$I_{\nu,\nu'}^{(k)}(\mathbf{n}) \equiv \frac{1}{\mathscr{L}^3}\int (\mathbf{n}\cdot\mathbf{r})^k \phi_\nu^*(\mathbf{r})\phi_{\nu'}(\mathbf{r})\, \mathrm{d}^3r. \tag{E.28}$$

For opposite parities, we find

$$\chi_{\nu\nu'\mathbf{p}}^{(+)} = -\mathrm{i}I_{\nu,\nu'}^{(1)}\!\left(\tfrac{\mathbf{p}}{|\mathbf{p}|}\right) |\mathbf{p}| + \mathcal{O}(|\mathbf{p}|^3), \tag{E.29}$$

$$\chi_{\nu,\nu',\mathbf{p}}^{(-)} = \mathrm{i}\,\frac{m_{\mathrm{e}} - m_{\mathrm{h}}}{M}\, I_{\nu,\nu'}^{(1)}\!\left(\tfrac{\mathbf{p}}{|\mathbf{p}|}\right) |\mathbf{p}| + \mathcal{O}(|\mathbf{p}|^3). \tag{E.30}$$

In case of Fröhlich interaction where $g_{\mathrm{c},\mathbf{p}} = g_{\mathrm{v},\mathbf{p}} = g_{\mathbf{p}}^{\mathrm{Fr}} \propto |\mathbf{p}|^{-1}$, the small-$|\mathbf{p}|$ behavior of the exciton-phonon matrix elements is thus given by

$$\left|g_{\mathbf{p}}^{\nu,\nu'}\right|^2 = \left|g_{\mathbf{p}}^{\mathrm{Fr}}\chi_{\nu,\nu',\mathbf{p}}^{(+)}\right|^2 = \begin{cases} \mathcal{O}(|\mathbf{p}|^2) & \text{for equal parities,} \\ \mathrm{const} + \mathcal{O}(|\mathbf{p}|^2) & \text{for opposite parities.} \end{cases} \tag{E.31}$$

For optical deformation-potential interaction where $g_{\mathrm{v},\mathbf{p}}, g_{\mathrm{c},\mathbf{p}} = \mathrm{const}$, we obtain

$$\left|g_{\mathbf{p}}^{\nu,\nu'}\right|^2 = \begin{cases} g_{\mathrm{c},\mathbf{p}} - g_{\mathrm{v},\mathbf{p}} + \mathcal{O}(|\mathbf{p}|^2) & \text{for } \nu = \nu', \\ \mathcal{O}(|\mathbf{p}|^4) & \text{for equal parities and } \nu \neq \nu', \\ \mathcal{O}(|\mathbf{p}|^2) & \text{for opposite parities.} \end{cases} \tag{E.32}$$

It turns out that with Fröhlich coupling, only scattering between states with opposite parity has allowed character whereas for optical deformation-potential coupling, the scattering has forbidden character unless the phonon affects only the center-of-mass but not the relative motion of the electron-hole pair.

Analogously to the hydrogen problem, the exciton states are often referred to as $1s \equiv (1,0,0)$, $2s \equiv (2,0,0)$, $2p \equiv (2,1,0)$, etc. As discussed in Sec. 4.4.1.2, the matrix elements appearing in the steady-state luminescence formula for the second phonon sideband have the form $g_{\mathbf{p}}^{1s,\nu}$. For $\nu = 1s, 2s, 2p$, we explicitly obtain

$$g_{\mathbf{p}}^{1s,1s} = \frac{g_{c,\mathbf{p}}}{\left[1 + \left(\frac{a_B|\mathbf{p}_h|}{2}\right)^2\right]^2} - \frac{g_{v,\mathbf{p}}}{\left[1 + \left(\frac{a_B|\mathbf{p}_e|}{2}\right)^2\right]^2}, \tag{E.33}$$

$$g_{\mathbf{p}}^{1s,2s} = \sqrt{2}\frac{2^7}{3^6}\left\{\frac{g_{c,\mathbf{p}}(a_B|\mathbf{p}_h|)^2}{\left[1 + \left(\frac{2a_B|\mathbf{p}_h|}{3}\right)^2\right]^3} - \frac{g_{v,\mathbf{p}}(a_B|\mathbf{p}_e|)^2}{\left[1 + \left(\frac{2a_B|\mathbf{p}_e|}{3}\right)^2\right]^3}\right\}, \tag{E.34}$$

$$g_{\mathbf{p}}^{1s,2p} = -\mathrm{i}\sqrt{2}\frac{2^8}{3^6}\cos\theta(\mathbf{p})\left\{\frac{g_{c,\mathbf{p}}a_B|\mathbf{p}_h|}{\left[1 + \left(\frac{2a_B|\mathbf{p}_h|}{3}\right)^2\right]^3} + \frac{g_{v,\mathbf{p}}a_B|\mathbf{p}_e|}{\left[1 + \left(\frac{2a_B|\mathbf{p}_e|}{3}\right)^2\right]^3}\right\}. \tag{E.35}$$

Here, $\theta(\mathbf{p})$ denotes the angle between $\mathbf{p}$ and the z axis. The matrix elements are plotted for Fröhlich and deformation-potential interaction in Fig. 24.

E.4 Phonon-assisted excitonic correlations

When the quantum-optical correlations are omitted, the equations of motion for the spontaneous-emission source terms in the phonon-assisted luminescence equations (4.33) take the form

$$\mathrm{i}\hbar\frac{\mathrm{d}}{\mathrm{d}t}\langle\hat{D}_{\mathbf{p}_n}^\dagger\cdots\hat{D}_{\mathbf{p}_1}^\dagger\hat{X}_{\nu',\mathbf{q}}^\dagger\hat{X}_{\nu,\mathbf{q}+\mathbf{p}_1+\cdots+\mathbf{p}_n}\rangle =$$

$$\left[E_\nu(\mathbf{q}+\mathbf{p}_1+\cdots+\mathbf{p}_n) - E_{\nu'}(\mathbf{q}) - n\hbar\Omega - \mathrm{i}\eta_X^{(n)}\right]\langle\hat{D}_{\mathbf{p}_n}^\dagger\cdots\hat{D}_{\mathbf{p}_1}^\dagger\hat{X}_{\nu',\mathbf{q}}^\dagger\hat{X}_{\nu,\mathbf{q}+\mathbf{p}_1+\cdots+\mathbf{p}_n}\rangle$$

$$-\hbar\Omega\sum_{\nu'',\nu'''}\sum_{\mathbf{Q}}\sum_{j=1}^n(g_{\mathbf{p}_j}^{\nu''',\nu''})^*\langle\Big(\prod_{i\neq j}^n\hat{D}_{\mathbf{p}_i}^\dagger\Big)\hat{X}_{\nu'',\mathbf{Q}+\mathbf{p}_j}^\dagger\hat{X}_{\nu''',\mathbf{Q}}\hat{X}_{\nu',\mathbf{q}}^\dagger\hat{X}_{\nu,\mathbf{q}+\mathbf{p}_1+\cdots+\mathbf{p}_{j-1}+\mathbf{p}_{j+1}+\cdots+\mathbf{p}_n}\rangle$$

$$+\hbar\Omega\sum_{\nu''}\sum_{\mathbf{Q}}\langle\hat{D}_{\mathbf{p}_n}^\dagger\cdots\hat{D}_{\mathbf{p}_1}^\dagger\big(\hat{D}_{\mathbf{Q}}^\dagger+\hat{D}_{-\mathbf{Q}}\big)\big[g_{\mathbf{Q}}^{\nu,\nu''}\hat{X}_{\nu',\mathbf{q}}^\dagger\hat{X}_{\nu'',\mathbf{q}+\mathbf{Q}+\mathbf{p}_1+\cdots+\mathbf{p}_n}$$

$$-\big(g_{-\mathbf{Q}}^{\nu',\nu''}\big)^*\hat{X}_{\nu',\mathbf{q}-\mathbf{Q}}^\dagger\hat{X}_{\nu,\mathbf{q}+\mathbf{p}_1+\cdots+\mathbf{p}_n}\big]\rangle \tag{E.36}$$

As mentioned in Sec. 4.4.1.1, we only consider those contributions to a given replicum that are of lowest order in the electron-phonon coupling constants. In other words, the last line of Eq. (E.36) is neglected in the following analysis. The cluster expansion in the incoherent regime with vanishing expectation values for pure phonon-operator combinations yields the general structure $\langle(\hat{D}^\dagger)^n\hat{X}_1^\dagger\hat{X}_2\hat{X}_3^\dagger\hat{X}_4\rangle = \delta_{2,3}\Delta\langle(\hat{D}^\dagger)^n\hat{X}_1^\dagger\hat{X}_4\rangle + \left\{\Delta\langle(\hat{D}^\dagger)^{n-k}\hat{X}^\dagger\hat{X}\rangle\Delta\langle(\hat{D}^\dagger)^k\hat{X}^\dagger\hat{X}\rangle\right\} + \Delta\langle(\hat{D}^\dagger)^n\hat{X}_1^\dagger\hat{X}_3^\dagger\hat{X}_2\hat{X}_4\rangle$ where some of the terms in the curly brackets have to be subtracted

when only the truly correlated part of the expectation value on the left-hand side of Eq. (E.36) is considered. We exclusively retain the first factorization term because it will provide the contribution to the sideband emission that is of lowest order in the exciton populations. Starting from

$$\Delta\langle \hat{D}^\dagger_{\mathbf{p}_1} \hat{X}^\dagger_{\nu',\mathbf{q}} \hat{X}_{\nu,\mathbf{q}+\mathbf{p}_1}\rangle = \frac{\hbar\Omega \big(g^{\nu',\nu}_{\mathbf{p}_1}\big)^* \Delta N_\nu(\mathbf{q}+\mathbf{p}_1)}{E_\nu(\mathbf{q}+\mathbf{p}_1) - E_{\nu'}(\mathbf{q}) - \hbar\Omega - \mathrm{i}\eta^{(1)}_{\mathrm{X}}},$$ (E.37)

the phonon-assisted carrier correlations can be evaluated recursively, which yields

$$
\langle \hat{D}^\dagger_{\mathbf{p}_n} \cdots \hat{D}^\dagger_{\mathbf{p}_1} \hat{X}^\dagger_{\nu',\mathbf{q}} \hat{X}_{\nu,\mathbf{q}+\mathbf{p}_1+\cdots+\mathbf{p}_n}\rangle \simeq
$$
$$
\sum_{\mu_1,\ldots,\mu_{n-1}} \sum_{j_1=1}^{n} \sum_{\substack{j_2=1 \\ j_2 \neq j_1}}^{n} \cdots \sum_{\substack{j_n=1 \\ j_n \neq j_1,\ldots,j_{n-1}}}^{n} (\hbar\Omega)^n \big(g^{\nu',\mu_1}_{\mathbf{p}_{j_1}}\big)^* \big(g^{\mu_1,\mu_2}_{\mathbf{p}_{j_2}}\big)^* \cdots \big(g^{\mu_{n-1},\nu}_{\mathbf{p}_{j_n}}\big)^*
$$
$$
\times \Delta N_\nu(\mathbf{q}+\mathbf{p}_1+\cdots+\mathbf{p}_n)
$$
$$
\times \Bigg\{ \Big[E_\nu(\mathbf{q}+\mathbf{p}_1+\cdots+\mathbf{p}_n) - E_{\mu_{n-1}}(\mathbf{q}+\mathbf{p}_{j_1}+\cdots+\mathbf{p}_{j_{n-1}}) - \hbar\Omega - \mathrm{i}\eta^{(1)}_{\mathrm{X}}\Big]
$$
$$
\times \Big[E_\nu(\mathbf{q}+\mathbf{p}_1+\cdots+\mathbf{p}_n) - E_{\mu_{n-2}}(\mathbf{q}+\mathbf{p}_{j_1}+\cdots+\mathbf{p}_{j_{n-2}}) - 2\hbar\Omega - \mathrm{i}\eta^{(2)}_{\mathrm{X}}\Big]
$$
$$
\vdots
$$
$$
\times \Big[E_\nu(\mathbf{q}+\mathbf{p}_1+\cdots+\mathbf{p}_n) - E_{\nu'}(\mathbf{q}) - n\hbar\Omega - \mathrm{i}\eta^{(n)}_{\mathrm{X}}\Big] \Bigg\}^{-1}.
$$
(E.38)

For small dephasing constants $\eta^{(n)}_{\mathrm{X}}$, the final results barely depend on $\eta^{(n)}_{\mathrm{X}}$ because the real parts of the energy denominators are far from zero in the relevant momentum range. In Eq. (E.37), we have only included the population $\Delta N_\nu(\mathbf{Q}) = \Delta\langle \hat{X}^\dagger_{\nu,\mathbf{Q}} \hat{X}_{\nu,\mathbf{Q}}\rangle$ since off-diagonal expectation values $\langle \hat{X}^\dagger_{\nu,\mathbf{Q}} \hat{X}_{\nu',\mathbf{Q}}\rangle$ with $\nu \neq \nu'$ can usually be neglected [7] and $\langle \hat{X}^\dagger_{\nu,\mathbf{Q}} \hat{X}_{\nu',\mathbf{Q}}\rangle \simeq \Delta\langle \hat{X}^\dagger_{\nu,\mathbf{Q}} \hat{X}_{\nu,\mathbf{Q}}\rangle$ in the low-density regime. In order to calculate the n-th phonon sideband, the infinite hierarchy (4.33) of luminescence equations is truncated on the $(n+2)$-particle level. The phonon-assisted recombination correlation $\Pi^{(n)}_\nu$ can thus be solved in steady state after inserting the Markov solution (E.38) for the spontaneous-emission source term. The lower-order recombination correlations $\Pi^{(n-1)}_\nu$, ..., $\Pi^{(0)}_\nu$ can then be calculated successively where in the k-th step, the steady-state/Markov solutions for $\Pi^{(k+1)}_\nu$ and $\Delta\langle(\hat{D}^\dagger)^k \hat{X}^\dagger \hat{X}\rangle$ have to be inserted. When we perform a partial-fraction decomposition for the arising energy denominators and carefully identify the lowest-order contributions in $|g^{\nu,\nu'}_{\mathbf{p}}|^2$, we finally obtain the closed luminescence formula (4.35).

F Polaron transformation

We show in Sec. F.1 how the polaron transformation defined in Sec. 4.4.2 acts on the electron, phonon, and photon operators. In Sec. F.2, we derive the normal ordering of the exponential operators appearing in the Hamiltonians (4.38) and (4.42). The results are used in Sec. F.3 to calculate the polaron dispersion at $T = 0\,\mathrm{K}$. The explicit transformation rules (F.8), (F.10) and the polaron energies (F.31) have already been presented in Ref. [59] but no proofs are given in that paper. Finally, we demonstrate in Sec. F.4 how the polaron transformation can be generalized to confined carrier systems.

F.1 Explicit transformation rules

We start from the electron-phonon-photon Hamiltonian (4.5). The polaron picture is introduced when every operator undergoes the unitary transformation

$$\hat{\bar{x}} = \hat{T}\hat{x}\hat{T}^\dagger \tag{F.1}$$

where $\hat{T} = \mathrm{e}^{\hat{U}}$ with the anti-Hermitian (i.e. $\hat{U}^\dagger = -\hat{U}$) operator

$$\hat{U} = \sum_{\lambda,\mathbf{k},\mathbf{p}} g_{\lambda,\mathbf{p}} \hat{a}^\dagger_{\lambda,\mathbf{k}-\mathbf{p}} \hat{a}_{\lambda\mathbf{k}} \hat{Q}_\mathbf{p}. \tag{F.2}$$

For a compact notation, we have introduced the abbreviation $\hat{Q}_\mathbf{p} \equiv \hat{D}^\dagger_\mathbf{p} - \hat{D}_{-\mathbf{p}}$. Equation (F.1) can be evaluated by means of the *Baker-Campbell-Hausdorff formula*

$$\mathrm{e}^{\hat{U}}\hat{x}\mathrm{e}^{-\hat{U}} = \hat{x} + [\hat{U},\hat{x}]_- + \frac{1}{2!}[\hat{U},[\hat{U},\hat{x}]_-]_- + \frac{1}{3!}[\hat{U},[\hat{U},[\hat{U},\hat{x}]_-]_-]_- + \cdots, \tag{F.3}$$

that is

$$\hat{\bar{x}} = \sum_{j=0}^{\infty} \frac{1}{j!}\hat{\bar{x}}^{(j)}, \tag{F.4}$$

$$\hat{\bar{x}}^{(0)} \equiv \hat{x}, \tag{F.5}$$

$$\hat{\bar{x}}^{(j+1)} \equiv [\hat{U},\hat{\bar{x}}^{(j)}]_- \quad (j = 0, 1, 2, \ldots). \tag{F.6}$$

For the fermionic operators, we thus obtain

$$\hat{\bar{a}}^{(0)}_{\lambda,\mathbf{k}} = \hat{a}_{\lambda,\mathbf{k}}, \tag{F.7a}$$

$$\hat{\bar{a}}^{(1)}_{\lambda,\mathbf{k}} = -\sum_{\lambda',\mathbf{k}'}\sum_{\mathbf{p}_1} g_{\lambda,\mathbf{p}_1}[\hat{a}_{\lambda,\mathbf{k}}, \hat{a}^\dagger_{\lambda',\mathbf{k}'-\mathbf{p}_1}]_+ \hat{a}_{\lambda',\mathbf{k}'}\hat{Q}_{\mathbf{p}_1}$$

$$= -\sum_{\mathbf{p}_1} g_{\lambda,\mathbf{p}_1}\hat{a}_{\lambda,\mathbf{k}+\mathbf{p}_1}\hat{Q}_{\mathbf{p}_1}, \tag{F.7b}$$

$$\hat{\bar{a}}_{\lambda,\mathbf{k}}^{(2)} = \sum_{\lambda',\mathbf{k}'} \sum_{\mathbf{p}_1,\mathbf{p}_2} g_{\lambda,\mathbf{p}_1} g_{\lambda',\mathbf{p}_2} [\hat{a}_{\lambda,\mathbf{k}+\mathbf{p}_1}, \hat{a}_{\lambda',\mathbf{k}'-\mathbf{p}_2}^\dagger]_+ \hat{a}_{\lambda',\mathbf{k}'} \hat{Q}_{\mathbf{p}_1} \hat{Q}_{\mathbf{p}_2}$$

$$= \sum_{\mathbf{p}_1,\mathbf{p}_2} g_{\lambda,\mathbf{p}_1} g_{\lambda,\mathbf{p}_2} \hat{a}_{\lambda,\mathbf{k}+\mathbf{p}_1+\mathbf{p}_2} \hat{Q}_{\mathbf{p}_1} \hat{Q}_{\mathbf{p}_2}, \tag{F.7c}$$

$$\vdots$$

$$\hat{\bar{a}}_{\lambda,\mathbf{k}}^{(j)} = (-1)^j \sum_{\mathbf{p}_1,\ldots,\mathbf{p}_j} g_{\lambda,\mathbf{p}_1} \cdots g_{\lambda,\mathbf{p}_j} \hat{Q}_{\mathbf{p}_1} \cdots \hat{Q}_{\mathbf{p}_j} \hat{a}_{\lambda,\mathbf{k}+\mathbf{p}_1+\cdots+\mathbf{p}_j}$$

$$= (-1)^j \sum_{\mathbf{k}_1,\ldots,\mathbf{k}_j} g_{\lambda,\mathbf{k}_1-\mathbf{k}} g_{\lambda,\mathbf{k}_2-\mathbf{k}_1} \cdots g_{\lambda,\mathbf{k}_j-\mathbf{k}_{j-1}} \hat{Q}_{\mathbf{k}_1-\mathbf{k}} \hat{Q}_{\mathbf{k}_2-\mathbf{k}_1} \cdots \hat{Q}_{\mathbf{k}_j-\mathbf{k}_{j-1}} \hat{a}_{\lambda,\mathbf{k}_j}. \tag{F.7d}$$

In a compact notation, this can be written as

$$\hat{\bar{a}}_{\lambda,\mathbf{k}} = \sum_{\mathbf{k}'} \left(\mathrm{e}^{-\hat{C}_\lambda} \right)_{\mathbf{k},\mathbf{k}'} \hat{a}_{\lambda,\mathbf{k}'} \tag{F.8}$$

with the operator-valued matrix $(\hat{C}_\lambda)_{\mathbf{k},\mathbf{k}'} = g_{\lambda,\mathbf{k}'-\mathbf{k}} \hat{Q}_{\mathbf{k}'-\mathbf{k}}$ that has been introduced in Sec. 4.4.2. For the phonon operators, we find

$$\hat{\bar{D}}_{\mathbf{p}}^{(0)} = \hat{D}_{\mathbf{p}}, \tag{F.9a}$$

$$\hat{\bar{D}}_{\mathbf{p}}^{(1)} = -\frac{\partial \hat{U}}{\partial \hat{D}_{\mathbf{p}}^\dagger} = -\sum_{\lambda,\mathbf{k}} g_{\lambda,\mathbf{p}} \hat{a}_{\lambda,\mathbf{k}-\mathbf{p}}^\dagger \hat{a}_{\lambda,\mathbf{k}}, \tag{F.9b}$$

$$\hat{\bar{D}}_{\mathbf{p}}^{(2)} = -\sum_{\mathbf{k},\mathbf{k}',\mathbf{p}'} g_{\lambda,\mathbf{p}} g_{\lambda',\mathbf{p}'} [\hat{a}_{\lambda',\mathbf{k}'-\mathbf{p}'}^\dagger \hat{a}_{\lambda',\mathbf{k}'}, \hat{a}_{\lambda,\mathbf{k}-\mathbf{p}}^\dagger \hat{a}_{\lambda,\mathbf{k}}]_- \hat{Q}_{\mathbf{p}'} = 0 \tag{F.9c}$$

such that

$$\hat{\bar{D}}_{\mathbf{p}} = \hat{D}_{\mathbf{p}} - \sum_{\lambda,\mathbf{k}} g_{\lambda,\mathbf{p}} \hat{a}_{\lambda,\mathbf{k}-\mathbf{p}}^\dagger \hat{a}_{\lambda,\mathbf{k}}. \tag{F.10}$$

Since the photon operators commute with $\hat{U}$, they are not affected by the transformation,

$$\hat{\bar{B}}_{\mathbf{q}} = \mathrm{e}^{\hat{U}} \hat{B}_{\mathbf{q}} \mathrm{e}^{-\hat{U}} = \hat{B}_{\mathbf{q}}. \tag{F.11}$$

If a function $f(x)$ can be written as a power series in x, the unitary transformation of $f(\hat{x})$ yields $\mathrm{e}^{\hat{U}} f(\hat{x}) \mathrm{e}^{-\hat{U}} = f(\mathrm{e}^{\hat{U}} \hat{x} \mathrm{e}^{-\hat{U}})$. Consequently, the functional dependence of the transformed Hamiltonian $\hat{\bar{H}} = \mathrm{e}^{\hat{U}} \hat{H} \mathrm{e}^{-\hat{U}}$ on the transformed operators coincides with the functional dependence of the original Hamiltonian on the original operators. The new picture is established when the new Hamiltonian is rewritten in terms of the old operators. In view of $(\mathrm{e}^{\pm C_\lambda})_{\mathbf{k},\mathbf{k}'}^\dagger = (\mathrm{e}^{\mp C_\lambda})_{\mathbf{k}'\mathbf{k}}$ and $(\mathrm{e}^{\pm C_\lambda})_{\mathbf{k}-\mathbf{p},\mathbf{k}'} = (\mathrm{e}^{\pm C_\lambda})_{\mathbf{k},\mathbf{k}'+\mathbf{p}}$, we find

$$\hat{\bar{H}}_{\mathrm{el}} = \sum_{\lambda,\mathbf{k},\mathbf{k}'} \left(\mathrm{e}^{\hat{C}_\lambda} \mathcal{E}_\lambda \mathrm{e}^{-\hat{C}_\lambda} \right)_{\mathbf{k},\mathbf{k}'} \hat{a}_{\lambda,\mathbf{k}}^\dagger \hat{a}_{\lambda,\mathbf{k}'}, \tag{F.12}$$

$$\hat{\bar{H}}_{\mathrm{vib}} = \sum_{\mathbf{p}} \hbar \Omega_{\mathbf{p}} \left(\hat{D}_{\mathbf{p}}^\dagger \hat{D}_{\mathbf{p}} + \frac{1}{2} \right)$$

$$+ \sum_{\lambda,\mathbf{k},\mathbf{p}} \hbar\Omega_{\mathbf{p}} g_{\lambda,\mathbf{p}} \left(\hat{D}_{-\mathbf{p}} + \hat{D}_{\mathbf{p}}^\dagger \right) \hat{a}_{\lambda,\mathbf{k}}^\dagger \hat{a}_{\lambda,\mathbf{k}+\mathbf{p}}$$

$$+ \sum_{\lambda,\mathbf{k},\mathbf{p}} \hbar\Omega_{\mathbf{p}} |g_{\lambda,\mathbf{p}}|^2 \hat{a}_{\lambda,\mathbf{k}}^\dagger \hat{a}_{\lambda,\mathbf{k}}$$

$$+ \sum_{\substack{\lambda,\lambda' \\ \mathbf{k},\mathbf{k}',\mathbf{p}}} \hbar\Omega_{\mathbf{p}} g_{\lambda,\mathbf{p}}^* g_{\lambda',\mathbf{p}} \hat{a}_{\lambda,\mathbf{k}}^\dagger \hat{a}_{\lambda',\mathbf{k}'}^\dagger \hat{a}_{\lambda',\mathbf{k}'+\mathbf{p}} \hat{a}_{\lambda,\mathbf{k}-\mathbf{p}}, \tag{F.13}$$

$$\hat{\bar{H}}_{\mathrm{em}} = \hat{H}_{\mathrm{em}}, \tag{F.14}$$

$$\hat{\bar{H}}_{\mathrm{el-el}} = \hat{H}_{\mathrm{el-el}}, \tag{F.15}$$

$$\hat{\bar{H}}_{\mathrm{el-vib}} = - \sum_{\lambda,\mathbf{k},\mathbf{p}} \hbar\Omega_{\mathbf{p}} g_{\lambda,\mathbf{p}} \left(\hat{D}_{-\mathbf{p}} + \hat{D}_{\mathbf{p}}^\dagger \right) \hat{a}_{\lambda,\mathbf{k}}^\dagger \hat{a}_{\lambda,\mathbf{k}+\mathbf{p}}$$

$$- 2 \sum_{\lambda,\mathbf{k},\mathbf{p}} \hbar\Omega_{\mathbf{p}} |g_{\lambda,\mathbf{p}}|^2 \hat{a}_{\lambda,\mathbf{k}}^\dagger \hat{a}_{\lambda,\mathbf{k}}$$

$$- 2 \sum_{\substack{\lambda,\lambda' \\ \mathbf{k},\mathbf{k}',\mathbf{p}}} \hbar\Omega_{\mathbf{p}} g_{\lambda,\mathbf{p}}^* g_{\lambda',\mathbf{p}} \hat{a}_{\lambda,\mathbf{k}}^\dagger \hat{a}_{\lambda',\mathbf{k}'}^\dagger \hat{a}_{\lambda',\mathbf{k}'+\mathbf{p}} \hat{a}_{\lambda,\mathbf{k}-\mathbf{p}}, \tag{F.16}$$

$$\hat{\bar{H}}_{\mathrm{el-em}} = - \sum_{\mathbf{k},\mathbf{k}',\mathbf{q}} \mathrm{i} \left[\mathcal{F}_{\mathbf{q}} \left(\mathrm{e}^{\hat{C}_\mathrm{c}} \mathrm{e}^{-\hat{C}_\mathrm{v}} \right)_{\mathbf{k},\mathbf{k}'} \hat{a}_{\mathrm{c},\mathbf{k}+\mathbf{q}}^\dagger \hat{a}_{\mathrm{v},\mathrm{v},\mathbf{k}'} + \mathcal{F}_{\mathbf{q}}^* \left(\mathrm{e}^{\hat{C}_\mathrm{c}} \mathrm{e}^{-\hat{C}_\mathrm{v}} \right)_{\mathbf{k}',\mathbf{k}}^\dagger \hat{a}_{\mathrm{v},\mathbf{k}}^\dagger \hat{a}_{\mathrm{c},\mathbf{k}'-\mathbf{q}} \right] \hat{B}_{\mathbf{q}}$$

$$+ \mathrm{H.C.} \tag{F.17}$$

Regrouping yields the Hamiltonian (4.37).

F.2 Normal ordering of the exponential operators

The exponential operator $\mathrm{e}^{\hat{C}_\lambda}$ explicitly reads

$$\left(\mathrm{e}^{\hat{C}_\lambda} \right)_{\mathbf{k},\mathbf{k}'} = \sum_{j=0}^\infty \frac{1}{j!} (\hat{C}_\lambda^j)_{\mathbf{k},\mathbf{k}'} \tag{F.18}$$

where the j-th power of $\hat{C}_\lambda$ has the matrix elements

$$\begin{aligned} (\hat{C}_\lambda^j)_{\mathbf{k},\mathbf{k}'} &= \sum_{\mathbf{k}_1,\ldots,\mathbf{k}_{j-1}} (\hat{C}_\lambda)_{\mathbf{k},\mathbf{k}_1} (\hat{C}_\lambda)_{\mathbf{k}_1,\mathbf{k}_2} \cdots (\hat{C}_\lambda)_{\mathbf{k}_{j-1},\mathbf{k}'} \\ &= \sum_{\mathbf{k}_1,\ldots,\mathbf{k}_{j-1}} g_{\lambda,\mathbf{k}_1-\mathbf{k}} g_{\lambda,\mathbf{k}_2-\mathbf{k}_1} \cdots g_{\lambda,\mathbf{k}'-\mathbf{k}_{j-1}} \hat{Q}_{\mathbf{k}_1-\mathbf{k}} \hat{Q}_{\mathbf{k}_2-\mathbf{k}_1} \cdots \hat{Q}_{\mathbf{k}'-\mathbf{k}_{j-1}}. \end{aligned} \tag{F.19}$$

For the following derivations, it proves useful to rewrite this as

$$(\hat{C}_\lambda^j)_{\mathbf{k},\mathbf{k}'} = \sum_{\mathbf{p}_1,\ldots,\mathbf{p}_j} \delta_{\sum_{l=1}^j \mathbf{p}_l, \mathbf{k}'-\mathbf{k}} \, g_{\lambda,\mathbf{p}_1} \cdots g_{\lambda,\mathbf{p}_j} \hat{Q}_{\mathbf{p}_1} \cdots \hat{Q}_{\mathbf{p}_j}. \tag{F.20}$$

For instance, in view of $[\hat{D}_{\mathbf{p}}, \hat{Q}_{\mathbf{p}'}]_- = \delta_{\mathbf{p},\mathbf{p}'}$, we immediately obtain

$$[\hat{D}_{\mathbf{p}}, (\hat{C}_\lambda^j)_{\mathbf{k},\mathbf{k}'}]_- = j (\hat{C}_\lambda^{j-1})_{\mathbf{k},\mathbf{k}'-\mathbf{p}} g_{\lambda,\mathbf{p}}, \tag{F.21}$$

$$[\hat{D}_{\mathbf{p}}, \left(\mathrm{e}^{\pm\hat{C}_\lambda} \right)_{\mathbf{k},\mathbf{k}'}]_- = \pm g_{\lambda,\mathbf{p}} \left(\mathrm{e}^{\pm\hat{C}_\lambda} \right)_{\mathbf{k},\mathbf{k}'-\mathbf{p}}. \tag{F.22}$$

In order to write $(e^{\hat{C}_\lambda})_{\mathbf{k},\mathbf{k}'}$ as a series of normally ordered terms, we start from observing that

$$
\hat{Q}_{\mathbf{p}_1} \cdots \hat{Q}_{\mathbf{p}_j} =
$$
$$
\sum_{m=0}^{\lfloor \frac{j}{2} \rfloor} \sum_{n=0}^{j-2m} (-1)^{m+n} \sum_\pi \frac{1}{2^m m! n! (j-2m-n)!} \delta_{\mathbf{p}_{\pi(1)}, -\mathbf{p}_{\pi(2)}} \cdots \delta_{\mathbf{p}_{\pi(2m-1)}, -\mathbf{p}_{\pi(2m)}}
$$
$$
\times \hat{D}^\dagger_{\mathbf{p}_{\pi(2m+1)}} \cdots \hat{D}^\dagger_{\mathbf{p}_{\pi(2m+n)}} \hat{D}_{\mathbf{p}_{\pi(2m+n+1)}} \cdots \hat{D}_{\mathbf{p}_{\pi(j)}} \tag{F.23}
$$

where the π sum extends over all permutations of the set $\{1, 2, \ldots, j\}$. The symbols $\lfloor x \rfloor$ and $\lceil x \rceil$ denote the floor and the ceiling function, respectively, i.e. $\lfloor x \rfloor$ is the largest integer number $\leq x$ and $\lceil x \rceil$ the smallest integer number $\geq x$. Formula (F.23) can be proven by induction. Inserting into Eq. (F.20) yields

$$
(e^{\hat{C}_\lambda})_{\mathbf{k},\mathbf{k}'} = \sum_{j=0}^\infty \sum_{m=0}^{\lfloor \frac{j}{2} \rfloor} \sum_{n=0}^{j-2m} \frac{(-1)^{m+n} \tilde{G}_\lambda^m}{2^m m! n! (j-2m-n)!} \left([\hat{d}_\lambda^\dagger]^{j-2m-n} \hat{d}_\lambda^n \right)_{\mathbf{k},\mathbf{k}'} \tag{F.24}
$$

where $\tilde{G}_\lambda \equiv \sum_\mathbf{p} |g_{\lambda,\mathbf{p}}|^2$ while $(\hat{d}_\lambda)_{\mathbf{k},\mathbf{k}'} \equiv g^*_{\lambda,\mathbf{k}-\mathbf{k}'} \hat{D}_{\mathbf{k}-\mathbf{k}'}$ and $(\hat{d}^\dagger_\lambda)_{\mathbf{k},\mathbf{k}'} = [(\hat{d}_\lambda)_{\mathbf{k}',\mathbf{k}}]^\dagger$. The expression on the right-hand side is already normally ordered but still difficult to evaluate. By means of the decomposition $\sum_{j=0}^\infty z_j = \sum_{i=0}^\infty (z_{2i} + z_{2i+1})$, we find a handier version of Eq. (F.24),

$$
(e^{\hat{C}_\lambda})_{\mathbf{k},\mathbf{k}'} = \sum_{i=0}^\infty (-1)^i \sum_{m=0}^i \frac{\left(\frac{\tilde{G}}{2}\right)^{i-m}}{(i-m)!}
$$
$$
\times \sum_{b=-(2m+1)}^{2m+1} \frac{(-1)^{\lfloor \frac{b}{2} \rfloor}}{(m-\lfloor \frac{b}{2} \rfloor)! (m+\lceil \frac{b}{2} \rceil)!} \left([\hat{d}_\lambda^\dagger]^{m+\lceil \frac{b}{2} \rceil} \hat{d}_\lambda^{m-\lfloor \frac{b}{2} \rfloor} \right)_{\mathbf{k},\mathbf{k}'}
$$
$$
= e^{-\tilde{G}/2} \sum_{m=0}^\infty \sum_{b=-(2m+1)}^{2m+1} \frac{(-1)^{m-\lfloor \frac{b}{2} \rfloor}}{(m-\lfloor \frac{b}{2} \rfloor)! (m+\lceil \frac{b}{2} \rceil)!} \left([\hat{d}_\lambda^\dagger]^{m+\lceil \frac{b}{2} \rceil} \hat{d}_\lambda^{m-\lfloor \frac{b}{2} \rfloor} \right)_{\mathbf{k},\mathbf{k}'} \tag{F.25}
$$

where we have used Cauchy's formula for the product of infinite series.

F.3 Polaron dispersion

In many applications of the polaron picture, it is a good approximation to replace each phonon-operator combination $\hat{O}$ appearing in Eq. (4.38) by its thermal average $\langle \hat{O} \rangle_{\mathrm{TD}}$. This procedure yields

$$
\hat{\tilde{H}}_{\mathrm{pol}} = \sum_{\lambda,\mathbf{k}} e_{\lambda,\mathbf{k}} \hat{a}^\dagger_{\lambda,\mathbf{k}} \hat{a}_{\lambda,\mathbf{k}} \tag{F.26}
$$

with the polaron dispersion

$$
e_{\lambda,\mathbf{k}} = \left\langle (e^{\hat{C}_\lambda} \mathcal{E}_\lambda e^{-\hat{C}_\lambda})_{\mathbf{k},\mathbf{k}} \right\rangle_{\mathrm{TD}} - \sum_\mathbf{q} \hbar \Omega_\mathbf{q} |g_{\lambda\mathbf{q}}|^2
$$
$$
= \sum_{\mathbf{k}'} \varepsilon_{\lambda,\mathbf{k}'} \left\langle (e^{\hat{C}_\lambda})_{\mathbf{k},\mathbf{k}'} (e^{-\hat{C}_\lambda})_{\mathbf{k}',\mathbf{k}} \right\rangle_{\mathrm{TD}} - \sum_\mathbf{q} \hbar \Omega_\mathbf{q} |g_{\lambda\mathbf{q}}|^2. \tag{F.27}
$$

This formula can explicitly be evaluated for a phonon bath at temperature $T = 0\,\mathrm{K}$ where $\langle \hat{O} \rangle_{\mathrm{TD}} = \langle \mathrm{vac}|\hat{O}|\mathrm{vac}\rangle$. With Eq. (F.25), it is straightforward to apply $\mathrm{e}^{\hat{C}_\lambda}$ to the phonon vacuum $|\mathrm{vac}\rangle$. Because non-vanishing terms are only obtained for $m = \lfloor b/2 \rfloor$, we immediately get

$$\left(\mathrm{e}^{\hat{C}_\lambda}\right)_{\mathbf{k}',\mathbf{k}}|\mathrm{vac}\rangle = \mathrm{e}^{-\tilde{G}/2}\left(\mathrm{e}^{d^\dagger}\right)_{\mathbf{k}'\mathbf{k}}|\mathrm{vac}\rangle \tag{F.28}$$

such that

$$\langle\mathrm{vac}|\left(\mathrm{e}^{-\hat{C}_\lambda}\right)_{\mathbf{k},\mathbf{k}'}\left(\mathrm{e}^{\hat{C}_\lambda}\right)_{\mathbf{k}',\mathbf{k}}|\mathrm{vac}\rangle = \mathrm{e}^{-\tilde{G}}\sum_{n=0}^{\infty}\left(\frac{1}{n!}\right)^2\langle\mathrm{vac}|(\hat{d}_\lambda^n)_{\mathbf{k},\mathbf{k}'}([d_\lambda^\dagger]^n)_{\mathbf{k}',\mathbf{k}}|\mathrm{vac}\rangle. \tag{F.29}$$

By writing the powers of $\hat{d}_\lambda$ and $\hat{d}_\lambda^\dagger$ analogously to Eq. (F.20), we find that

$$\left(\hat{d}_\lambda^m\right)_{\mathbf{k},\mathbf{k}'}([\hat{d}_\lambda^\dagger]^n)_{\mathbf{k}'',\mathbf{k}'''}|\mathrm{vac}\rangle = \Theta(n \geq m)\frac{n!}{(n-m)!}(G_\lambda^m)_{\mathbf{k},\mathbf{k}'}([\hat{d}_\lambda^\dagger]^{n-m})_{\mathbf{k}-\mathbf{k}',\mathbf{k}'''-\mathbf{k}''}|\mathrm{vac}\rangle \tag{F.30}$$

where $(G_\lambda)_{\mathbf{k},\mathbf{k}'} = |g_{\lambda,\mathbf{k}-\mathbf{k}'}|^2$ while $\Theta(n \geq m)$ is unity for $n \geq m$ and vanishes otherwise. When inserting this result into Eq. (F.29), we immediately obtain the polaron dispersion

$$e_{\lambda,\mathbf{k}} = \mathrm{e}^{-\tilde{G}_\lambda}\sum_{\mathbf{k}'}\left(\mathrm{e}^{G_\lambda}\right)_{\mathbf{k},\mathbf{k}'}\varepsilon_{\lambda,\mathbf{k}'} - \hbar\Omega\tilde{G}_\lambda. \tag{F.31}$$

F.4 Hetero structures

The polaron transformation (F.2) can be generalized to confined systems. We assume that the energy spacing between the eigen states of the confinement potential is so large that only the lowest eigen state in each band has to be included in the analysis. The subband index β can thus be suppressed such that the phonon part of the Hamiltonian takes the form

$$\hat{H}_{\mathrm{vib}} = \hbar\Omega\sum_{p_\parallel,p_\perp}\left(\hat{D}_{p_\parallel,p_\perp}^\dagger\hat{D}_{p_\parallel,p_\perp} + \frac{1}{2}\right), \tag{F.32}$$

$$\hat{H}_{\mathrm{el-vib}} = \hbar\Omega\sum_{\lambda,k_\parallel}\sum_{p_\parallel,p_\perp}g_{\lambda,p_\parallel,p_\perp}\hat{a}_{\lambda,k_\parallel-p_\parallel}^\dagger\hat{a}_{\lambda,k_\parallel}\left(\hat{D}_{-p_\parallel,p_\perp} + \hat{D}_{p_\parallel,p_\perp}^\dagger\right) \tag{F.33}$$

Compared to the bulk case, the interaction matrix elements $g_{\lambda,p_\parallel,p_\perp}$ are modified by the confinement as shown in Sec. 2.2.4.1. To simplify the interaction Hamiltonian from (F.33), we further assume that the matrix element can be separated into a real-valued band-dependent and a complex momentum-dependent part, $g_{\lambda,p_\parallel,p_\perp} = \alpha_\lambda g_{p_\parallel,p_\perp}$. Such a separation is possible, e.g., for infinitely high potential wells where the confinement functions become band-independent. We can then introduce new bosonic operators

$$\hat{\tilde{D}}_{p_\parallel} \equiv \frac{1}{h_{p_\parallel}}\sum_{p_\perp}g_{p_\parallel,p_\perp}^*\hat{D}_{p_\parallel,p_\perp} \tag{F.34}$$

with $h_{p_\parallel} \equiv \sqrt{\sum_{p_\perp}|g_{p_\parallel,p_\perp}|^2} = h_{-p_\parallel}$. In terms of these operators, the interaction Hamiltonian can be written as

$$\hat{H}_{\mathrm{el-vib}} = \hbar\Omega\sum_{\lambda,k_\parallel}\sum_{p_\parallel}\tilde{g}_{\lambda,p_\parallel}\hat{a}_{\lambda,k_\parallel-p_\parallel}^\dagger\hat{a}_{\lambda,k_\parallel}\left(\hat{\tilde{D}}_{-p_\parallel} + \hat{\tilde{D}}_{p_\parallel}^\dagger\right) \tag{F.35}$$

with real-valued matrix elements $\tilde{g}_{\lambda,p_\parallel} = \alpha_\lambda h_{p_\parallel} = \sqrt{\sum_{p_z} |g_{\lambda,p_\parallel,p_z}|^2}$. The Hamiltonian of the free lattice-vibration field becomes

$$\hat{H}_{\text{vib}} = \hbar\Omega \sum_{p_\parallel} \left(\hat{\tilde{D}}_{p_\parallel}^\dagger \hat{\tilde{D}}_{p_\parallel} + \frac{1}{2} \right) + \hat{H}_{\text{phon}}' \tag{F.36}$$

where the extra term $\hat{H}_{\text{phon}}'$ commutes with $\hat{\tilde{D}}_{p_\parallel}$, $\hat{\tilde{D}}_{p_\parallel}^\dagger$ and $\hat{a}_{\lambda,k_\parallel}$, $\hat{a}_{\lambda,k_\parallel}^\dagger$ such that it does not contribute to the dynamics of the electron-phonon system. The polaron picture can now be introduced via the unitary transformation

$$\hat{T} = \exp \sum_{\lambda,k_\parallel,p_\parallel} \tilde{g}_{\lambda,p_\parallel} \hat{a}_{\lambda,k_\parallel-p_\parallel}^\dagger \hat{a}_{\lambda,k_\parallel} \left(\hat{\tilde{D}}_{p_\parallel}^\dagger - \hat{\tilde{D}}_{-p_\parallel} \right). \tag{F.37}$$

Equations of motion describing phonon-sideband luminescence can then be derived analogously to the bulk case. We can immediately write down the quantum-well luminescence formula:

$$I_{\text{PL}}^{(n)}(\omega) = \frac{2}{\hbar} \left| \mathcal{F}\phi_{1s}^{\text{QW}}(\mathbf{r} = \mathbf{0}) \right|^2 e^{-\tilde{G}} \frac{1}{n!} \operatorname{Im} \sum_{Q_\parallel} \frac{\tilde{\mathcal{G}}_{Q_\parallel}^{(n)} N_{1s}^{\text{QW}}(Q_\parallel)}{E_{1s}^{\text{QW}}(Q_\parallel) - n\hbar\Omega - \hbar\omega - \mathrm{i}\gamma_n}. \tag{F.38}$$

Here, ϕ_{1s}^{QW} and $E_{1s}^{\text{QW}}(Q_\parallel)$ are the ground-state wave function and eigen energy, respectively, for quasi two-dimensional quantum-well excitons, and $N_{1s}^{\text{QW}}(Q_\parallel)$ denotes the corresponding distributions. The constant $\tilde{G}$ and the weight factors $\tilde{\mathcal{G}}_{Q_\parallel}^{(n)}$ are defined analogously to the quantities G and $\mathcal{G}_{Q_\parallel}^{(n)}$ in the bulk case, one only needs to replace $\Delta g_{\mathbf{p}}$ by the effective quantum-well matrix element $\Delta\tilde{g}_{p_\parallel} = \tilde{g}_{\text{v},p_\parallel} - \tilde{g}_{\text{c},p_\parallel}$.

As derived in Sec. 2.2.4.1, the quantum-well matrix element $g_{\lambda,p_\parallel,p_z} = \gamma(p_z)g_{\lambda,\mathbf{p}}$ deviates from the bulk case by a form factor that can be written as

$$\gamma(p_z) = \int |\xi(r_z)|^2 e^{\mathrm{i}p_z r_z} \, dr_z \tag{F.39}$$

for a band-independent confinement function $\xi(r_z)$.

G Influence of disorder on the phonon-sideband emission

Several of the measured spectra that we have used for the theory-experiment comparison show considerable inhomogeneous broadening due to disorder in the sample. We outline in this appendix how that effect can be taken into account when phonon sidebands are evaluated numerically.

It is often a good approximation to assume that only the energies are subject to disorder. Thus, the total luminescence signal $I_{\mathrm{PL}}^{\mathrm{tot}}(\hbar\omega)$ originates from an ensemble of emitters with statistically distributed transition energies. If the emission spectrum for a fixed resonance $\mathcal{E}$ is given by $I_{\mathrm{PL}}(\hbar\omega;\mathcal{E})$, we have

$$I_{\mathrm{PL}}^{\mathrm{tot}}(\hbar\omega) = \int I_{\mathrm{PL}}(\hbar\omega;\mathcal{E})p(\mathcal{E})\,\mathrm{d}\mathcal{E} \tag{G.1}$$

in the disordered case where $p(E)$ denotes the probability distribution for the energies. All the above mentioned spectra could be fitted by assuming Gaussian distributions

$$p(E) = \Phi_\sigma(E - E_0) \equiv \frac{1}{\sigma\sqrt{2\pi}}\exp\left(\frac{-[E-E_0]^2}{2\sigma^2}\right) \tag{G.2}$$

with width σ and mean value E_0. The simple phenomenological dephasing γ that we have introduced in the luminescence equations leads to a homogeneously broadened, Lorentzian line shape for the ZPL. The n-th replicum is composed of a series of shifted Lorentzians with central positions $\mathcal{E}_{1s} + \hbar^2|\mathbf{Q}|^2/2M - n\hbar\Omega$. Hence, it is sufficient to consider the generic case $I_{\mathrm{PL}}(\hbar\Omega;\mathcal{E}) \propto L_\gamma(\hbar\omega - \mathcal{E})$ with then normalized Lorentzian

$$L_\gamma(E) \equiv \frac{1}{\pi}\frac{\gamma}{E^2 + \gamma^2}. \tag{G.3}$$

For this choice, Eq. (G.1) becomes the convolution of a Lorentzian and a Gaussian function,

$$I_{\mathrm{PL}}^{\mathrm{tot}}(\hbar\omega) \propto \int L_\gamma(\hbar\omega - E_0 - E)\Phi_\sigma(E)\,\mathrm{d}E = V_{\gamma,\sigma}(\hbar\omega - E_0), \tag{G.4}$$

i.e. a *Voigt profile*

$$V_{\gamma,\sigma}(E) \equiv \left.\frac{\mathrm{Re}w(z)}{\sigma\sqrt{2\pi}}\right|_{z=\frac{E+\mathrm{i}\gamma}{\sigma\sqrt{2}}} \tag{G.5}$$

where $w(z) \equiv \mathrm{e}^{-z^2}\mathrm{erfc}(-\mathrm{i}z)$ with the complementary error function $\mathrm{erfc}(z) \equiv \frac{2}{\sqrt{\pi}}\int_z^\infty \mathrm{e}^{-t^2}\,\mathrm{d}t$.

This result is illustrated in Fig. 31 for a ZnO bulk spectrum at temperature $T = 30\,\mathrm{K}$. The shaded area represents the measured data [132], the lines correspond to non-linear fit results for the ZPL. While the best fitting Lorentzian (dashed line) decays too slowly at large distances
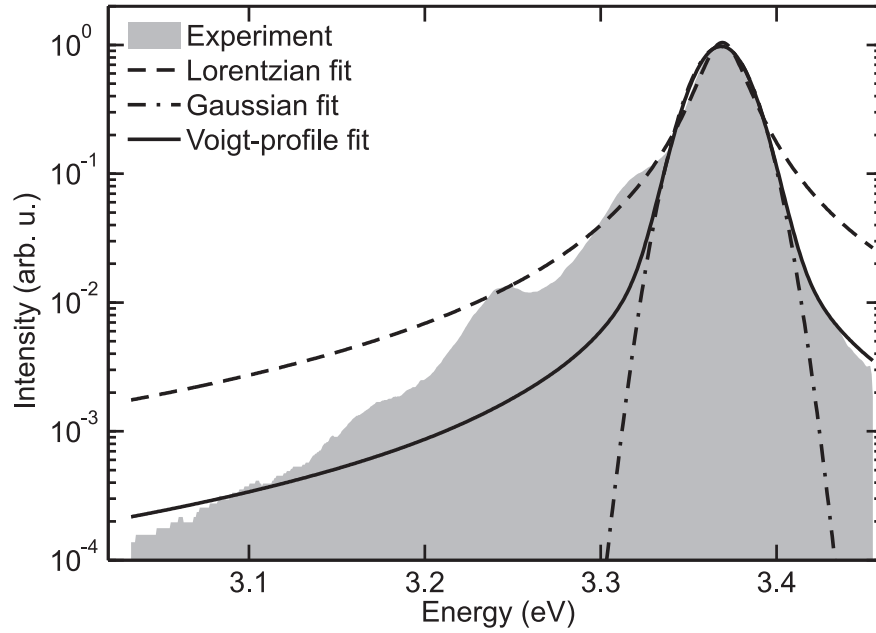
Figure 31: Inhomogeneous broadening due to disorder. See the text for further explanation.

from the central frequency and the best-fitting Gaussian too fast, a reasonable agreement is achieved with a Voigt profile.

Because both the Lorentzian (G.3) and the Voigt profile (G.5) are normalized, the spectrally integrated sideband intensities are not affected by the inhomogeneous broadening. The main results of our theory can thus equally well be tested with disordered systems.

Bibliography

[1] H. Haug and S. W. Koch. *Quantum Theory of the Optical and Electronic Properties of Semiconductors*. World Scientific, Singapore, 5th edition, 2009.

[2] H. W. Wyld and B. D. Fried. Quantum mechanical kinetic equations. *Ann. Phys.*, **23**(3):374, 1963.

[3] J. Čížek. On the correlation problem in atomic and molecular systems. Calculation of wavefunction components in Ursell-type expansion using quantum-field theoretical methods. *J. Chem. Phys.*, **45**(11):4256, 1966.

[4] G. D. Purvis III and R. J. Bartlett. A full coupled-cluster singles and doubles model: The inclusion of disconnected triples. *J. Chem. Phys.*, **76**(4):1910, 1982.

[5] F. E. Harris, H. J. Monkhorst, and D. L. Freeman. *Algebraic and Diagrammatic Methods in Many-Fermion Theory*. Oxford University Press, New York, 1992.

[6] M. Kira, W. Hoyer, T. Stroucken, and S. W. Koch. Exciton formation in semiconductors and the influence of a photonic environment. *Phys. Rev. Lett.*, **87**(17):176401, 2001.

[7] M. Kira and S. W. Koch. Many-body correlations and excitonic effects in semiconductor spectroscopy. *Prog. in Quant. Electr.*, **30**(5):155, 2006.

[8] M. Kira and S. Koch. Microscopic theory of optical excitations, photoluminescence, and terahertz response in semiconductors. *Eur. Phys. J. D*, **36**(2):143–157, August 2005.

[9] M. Kira and S. W. Koch. Quantum-optical spectroscopy of semiconductors. *Phys. Rev. A*, **73**(1):013813, 2006.

[10] P. Michler, A. Imamoğlu, M. D. Mason, P. J. Carson, G. F. Strouse, and S. K. Buratto. Quantum correlation among photons from a single quantum dot at room temperature. *Nature*, **406**:968, 2000.

[11] P. Michler, A. Kiraz, C. Becher, W. V. Schoenfeld, P. M. Petroff, L. Zhang, E. Hu, and A. Imamoğlu. A quantum dot single-photon turnstile device. *Science*, **290**:2282, 2000.

[12] E. Dekel, D. Regelman, D. Gershoni, E. Ehrenfreund, W. V. Schoenfeld, and P. M. Petroff. Cascade evolution and radiative recombination of quantum dot multiexcitons studied by time-resolved spectroscopy. *Phys. Rev. B*, **62**:11038, 2000.

[13] C. Santori, M. Pelton, G. Solomon, Y. Dale, and Y. Yamamoto. Triggered single photons from a quantum dot. *Phys. Rev. Lett.*, **86**:1502, 2001.

[14] C. Becher, A. Kiraz, P. Michler, A. Imamoğlu, W. V. Schoenfeld, P. M. Petroff, L. Zhang, and E. Hu. Nonclassical radiation from a single self-assembled InAs quantum dot. *Phys. Rev. B*, **63**:121312(R), 2001.

[15] E. MOREAU, I. ROBERT, L. MANIN, V. THIERRY-MIEG, J. M. GERARD, AND I. ABRAM. Quantum cascade of photons in semiconductor quantum dots. *Phys. Rev. Lett.*, **87**:183601, 2001.

[16] C. H. BENNETT AND G. BRASSARD. Quantum cryptography: public key distribution and coin tossing. In *Proceedings of the IEEE International Conference on Computers, Systems, and Signal Processing, Bangalore, India, 1984*, New York, 1984. IEEE.

[17] D. LOSS AND D. P. DIVINCENZO. Quantum computation with quantum dots. *Phys. Rev. A*, **57**(1):120, 1998.

[18] F. TROIANI, U. HOHENESTER, AND E. MOLINARI. Quantum-information processing in semiconductor quantum dots. *Phys. Stat. Sol. (b)*, **224**:849, 2001.

[19] E. BEHAM, M. BETZ, S. TRUMM, M. KROUTVAR, Y. DUCOMMUN, H. KRENNER, M. BICHLER, A. LEITENSTORFER, J. FINLEY, A. ZRENNER, AND G. ABSTREITER. Physics and applications of self-assembled quantum dots. *Phys. Stat. Sol. (c)*, **1**:2131, 2004.

[20] Y. Z. HU, M. LINDBERG, AND S. W. KOCH. Theory of optically excited intrinsic semiconductor quantum dots. *Phys. Rev. B*, **42**(3):1713, 1990.

[21] A. BARENCO AND M. A. DUPERTUIS. Quantum many-body states of excitons in a small quantum dot. *Phys. Rev. B*, **52**(4):2766, 1995.

[22] Y. Z. HU, H. GIESSEN, N. PEYGHAMBARIAN, AND S. W. KOCH. Microscopic theory of optical gain in small semiconductor quantum dots. *Phys. Rev. B*, **53**(8):4814, 1996.

[23] A. WOJS AND P. HAWRYLAK. Theory of photoluminescence from modulation-doped self-assembled quantum dots in a magnetic field. *Phys. Rev. B*, **55**(19):13066, 1997.

[24] P. HAWRYLAK. Excitonic artificial atoms: Engineering optical properties of quantum dots. *Phys. Rev. B*, **60**(8):5597, 1999.

[25] E. DEKEL, D. GERSHONI, E. EHRENFREUND, J. M. GARCIA, AND P. M. PETROFF. Carrier-carrier correlations in an optically excited single semiconductor quantum dot. *Phys. Rev. B*, **61**(16):11009, 2000.

[26] U. HOHENESTER AND E. MOLINARI. Role of coulomb correlations in the optical spectra of semiconductor quantum dots. *Phys. Stat. Sol. (b)*, **221**(1):19, 2000.

[27] N. BAER, P. GARTNER, AND F. JAHNKE. Coulomb effects in semiconductor quantum dots. *Eur. Phys. J. B*, **42**(2):231, 2004.

[28] M. BRASKÉN, M. LINDBERG, D. SUNDHOLM, AND J. OLSEN. Spatial carrier-carrier correlations in strain-induced quantum dots. *Phys. Rev. B*, **64**(3):035312, 2001.

[29] S. CORNI, M. BRASKÉN, M. LINDBERG, J. OLSEN, AND D. SUNDHOLM. Size dependence of the electron-hole recombination rates in semiconductor quantum dots. *Phys. Rev. B*, **67**(4):045313, 2003.

[30] S. CORNI, M. BRASKÉN, M. LINDBERG, J. OLSEN, AND D. SUNDHOLM. Electron-hole recombination density matrices obtained from large configuration-interaction expansions. *Phys. Rev. B*, **67**(8):085314, 2003.

[31] L. BANYAI AND S. W. KOCH. *Semiconductor Quantum Dots.* World Scientific, Singapore, 1993.

[32] U. WOGGON. *Optical Properties of Semiconductor Quantum Dots.* Springer, Berlin, 1996.

[33] L. JACAK, P. HAWRYLAK, AND A. WOJS. *Quantum Dots.* Springer, Berlin, 1998.

[34] H. C. SCHNEIDER, W. W. CHOW, AND S. W. KOCH. Many-body effects in the gain spectra of highly excited quantum-dot lasers. *Phys. Rev. B*, **64**(11):115315, 2001.

[35] H. C. SCHNEIDER, W. W. CHOW, AND S. W. KOCH. Anomalous carrier-induced dispersion in quantum-dot active media. *Phys. Rev. B*, **66**(4):041310, 2002.

[36] T. R. NIELSEN, P. GARTNER, AND F. JAHNKE. Many-body theory of carrier capture and relaxation in semiconductor quantum-dot lasers. *Phys. Rev. B*, **69**(23):235314, 2004.

[37] H. C. SCHNEIDER, W. W. CHOW, AND S. W. KOCH. Excitation-induced dephasing in semiconductor quantum dots. *Phys. Rev. B*, **70**(23):235308, 2004.

[38] S. HAMEAU, Y. GULDNER, O. VERZELEN, R. FERREIRA, G. BASTARD, J. ZEMAN, A. LEMAÎTRE, AND J. M. GÉRARD. Strong electron-phonon coupling regime in quantum dots: Evidence for everlasting resonant polarons. *Phys. Rev. Lett.*, **83**(20):4152, 1999.

[39] P. BORRI, W. LANGBEIN, U. WOGGON, V. STAVARACHE, D. REUTER, AND A. D. WIECK. Exciton dephasing via phonon interactions in InAs quantum dots: Dependence on quantum confinement. *Phys. Rev. B*, **71**(11):115328, 2005.

[40] J. SEEBECK, T. R. NIELSEN, P. GARTNER, AND F. JAHNKE. Quantum kinetic theory of phonon-assisted carrier transitions in nitride-based quantum-dot systems. *Eur. Phys. J. B*, **49**(2):167, 2006.

[41] M. LORKE, T. R. NIELSEN, J. SEEBECK, P. GARTNER, AND F. JAHNKE. Influence of carrier-carrier and carrier-phonon correlations on optical absorption and gain in quantum-dot systems. *Phys. Rev. B*, **73**(8):085324, 2006.

[42] M. SOLTANI, M. CERTIER, R. EVRARD, AND E. KARTHEUSER. Photoluminescence of CdTe doped with arsenic and antimony acceptors. *J. Appl. Phys.*, **78**(9):5626–5632, 1995.

[43] C. KLINGSHIRN. Linear and nonlinear optics of wide-gap II-VI semiconductors. *phys. stat. sol. (b)*, **202**(2):857–871, August 1997.

[44] M. KOZHEVNIKOV, B. M. ASHKINADZE, E. COHEN, AND A. RON. LO-phonon sideband photoluminescence in pure GaAs. *Sol. Stat. Comm.*, **106**(2):73–76, 1998.

[45] X. B. ZHANG, T. TALIERCIO, S. KOLLIAKOS, AND P. LEFEBVRE. Influence of electron-phonon interaction on the optical properties of III nitride semiconductors. *J. Phys.: Condens. Matter*, **13**:7053, 2001.

[46] L. T. TAN, R. W. MARTIN, K. P. O'DONNELL, AND I. M. WATSON. Photoluminescence and phonon satellites of single InGaN/GaN quantum wells with varying GaN cap thickness. *Appl. Phys. Lett.*, **89**(10):101910, September 2006.

[47] H. Zhao, S. Moehl, and H. Kalt. Energy relaxation during hot-exciton transport in quantum wells: Direct observation by spatially resolved phonon-sideband spectroscopy. *Appl. Phys. Lett.*, **81**(15):2794–2796, October 2002.

[48] W. Shan, W. Walukiewicz, J. W. Ager III, K. M. Yu, H. B. Yuan, H. P. Xin, G. Cantwell, and J. J. Song. Nature of room-temperature photoluminescence in ZnO. *Appl. Phys. Lett.*, **86**:191911, 2005.

[49] S. Permogorov. Optical emission due to exciton scattering by LO phonons in semiconductors. In E. I. Rashba and M. D. Sturge, Eds., *Excitons*, chapter 5, pages 177–203. North-Holland, Amsterdam, 1982.

[50] M. Kira, F. Jahnke, and S. W. Koch. Microscopic theory of excitonic signatures in semiconductor photoluminescence. *Phys. Rev. Lett.*, **81**(15):3263, 1998.

[51] S. Chatterjee, C. Ell, S. Mosor, G. Khitrova, H. M. Gibbs, W. Hoyer, M. Kira, S. W. Koch, J. P. Prineas, and H. Stolz. Excitonic photoluminescence in semiconductor quantum wells: Plasma versus excitons. *Phys. Rev. Lett.*, **92**(6):067402, 2004.

[52] I. Galbraith, R. Chari, S. Pellegrini, P. J. Phillips, C. J. Dent, A. F. G. van der Meer, D. G. Clarke, A. K. Kar, G. S. Buller, C. R. Pidgeon, B. N. Murdin, J. Allam, and G. Strasser. Excitonic signatures in the photoluminescence and terahertz absorption of a $GaAs/Al_xGa_{1-x}As$ multiple quantum well. *Phys. Rev. B*, **71**(7):073302, 2005.

[53] W. Hoyer, C. Ell, M. Kira, S. W. Koch, S. Chatterjee, S. Mosor, G. Khitrova, H. M. Gibbs, and H. Stolz. Many-body dynamics and exciton formation studied by time-resolved photoluminescence. *Phys. Rev. B*, **72**(7):075324, 2005.

[54] M. Kira, F. Jahnke, S. W. Koch, J. D. Berger, D. V. Wick, T. R. Nelson, G. Khitrova, and H. M. Gibbs. Quantum theory of nonlinear semiconductor microcavity luminescence explaining Boser experiments. *Phys. Rev. Lett.*, **79**(25):5170, 1997.

[55] L. Li, H. Yang, G. Qi, J. Ma, X. Xie, H. Zhao, and F. Gao. Synthesis and photoluminescence of hollow microspheres constructed with ZnO nanorods by H_2 bubble templates. *Chem. Phys. Lett.*, **455**(1-3):93, 2008.

[56] W. Liu, M. F. Li, S. J. Xu, K. Uchida, and K. Matsumoto. Phonon-assisted photoluminescence in wurtzite GaN epilayer. *Semicond. Sci. Technol.*, **13**(7):769–772, 1998.

[57] H. Zhao and H. Kalt. Energy-dependent Huang-Rhys factor of free excitons. *Phys. Rev. B*, **68**:125309, 2003.

[58] R. Hauschild, H. Priller, M. Decker, J. Brckner, H. Kalt, and C. Klingshirn. Temperature dependent band gap and homogeneous line broadening of the exciton emission in ZnO. *Phys. Stat. Sol. (c)*, **3**(4):976, 2006.

[59] K. Hannewald and P. A. Bobbert. Nonperturbative theory of exciton-phonon resonances in semiconductor absorption. *Phys. Rev. B*, **72**(11):113202, 2005.

[60] M. Lindberg and S. W. Koch. Effective Bloch equations for semiconductors. *Phys. Rev. B*, **38**(5):3342, 1988.

[61] M. Kira, F. Jahnke, W. Hoyer, and S. W. Koch. Quantum theory of spontaneous emission and coherent effects in semiconductor microstructures. *Prog. in Quant. Electr.*, **23**(6):189, 1999.

[62] G. Bastard. *Wave Mechanics Applied to Semiconductor Heterostructures*. Les Edition de Physique, Paris, 1988.

[63] M. G. Burt. The justification for applying the effective-mass approximation to microstructures. *J. Phys.: Condens. Matter*, **4**:6651, 1992.

[64] M. Born and R. Oppenheimer. Zur Quantentheorie der Molekeln. *Ann. Phys. (Leipzig)*, **84**:457, 1927.

[65] N. W. Ashcroft and N. D. Mermin. *Festkörperphysik*. Oldenbourg, München, 2001.

[66] G. Czycholl. *Theoretische Festkörperphysik*. Vieweg, Braunschweig, 2000.

[67] J. Sólyom. *Fundamentals of the Physics of Solids*, volume 2. Springer, Berlin, 2009.

[68] L. D. Landau and E. M. Lifschitz. *Statistische Physik Teil 1*, volume V of *Lehrbuch der Theoretischen Physik*. Akademie, Berlin, 7$^{\text{th}}$ edition, 1987.

[69] J. Sólyom. *Fundamentals of the Physics of Solids*, volume 2. Springer, Berlin, 2007.

[70] K. A. Alim, V. A. Fonoberov, and A. A. Balandin. Origin of the optical phonon frequency shifts in ZnO quantum dots. *Appl. Phys. Lett.*, **86**(5):053103, 2005.

[71] J. Zi, X. Wan, G. Wei, K. Zhang, and X. Xie. Lattice dynamics of zinc-blende GaN and AlN: I. Bulk phonons. *J. Phys.: Condens. Matter*, **8**(35):6323, 1996.

[72] H. Siegle, G. Kaczmarczyk, L. Filippidis, A. P. Litvinchuk, A. Hoffmann, and C. Thomsen. Zone-boundary phonons in hexagonal and cubic GaN. *Phys. Rev. B*, **55**(11):7000, 1997.

[73] M. Kira. Lecture notes. Private communication.

[74] L. Nordheim. Electron theory of metals I. *Ann. Phys. (Leipzig)*, **9**(5):607, 1931.

[75] S. Schmitt-Rink, D. A. B. Miller, and D. S. Chemla. Theory of the linear and nonlinear optical properties of semiconductor microcrystallites. *Phys. Rev. B*, **35**(15):8113, 1987.

[76] U. Bockelmann and G. Bastard. Phonon scattering and energy relaxation in two-, one-, and zero-dimensional electron gases. *Phys. Rev. B*, **42**(14):8947, 1990.

[77] H. Rücker, E. Molinari, and P. Lugli. Microscopic calculation of the electron-phonon interaction in quantum wells. *Phys. Rev. B*, **45**(12):6747, 1992.

[78] J. M. Ziman. *Electrons and Phonons*. Clarendon Press, Oxford, 1960.

[79] P. Y. Yu and M. Cardona. *Fundamentals of Semiconductors*. Springer, Berlin, 2$^{\text{nd}}$ edition, 1999.

[80] D. G. Thomas. Excitons and band splitting produced by uniaxial stress in CdTe. *J. Appl. Phys.*, **32**(10):2298, 1961.

[81] A. Blacha, H. Presting, and M. Cardona. Deformation potentials of $k = 0$ states of tetrahedral semiconductors. *Phys. Stat. Sol. (b)*, **126**(1):11, 1984.

[82] G. D. Mahan. *Many-Particle Physics*. Plenum, New York, 2nd edition, 1990.

[83] H. Fröhlich. Electrons in lattice fields. *Adv. Phys.*, **3**:325, 1954.

[84] H. Haken. *Quantenfeldtheorie des Festkörpers*. Teubner, Stuttgart, 1973.

[85] W. A. Harrison. Scattering of electrons by lattice vibrations in nonpolar crystals. *Phys. Rev.*, **104**(5):1281, 1956.

[86] H. Ehrenreich and A. W. Overhauser. Scattering of holes by phonons in Germanium. *Phys. Rev.*, **104**(2):331, 1956.

[87] K. Reimann, R. A. Kaindl, and M. Woerner. Optical deformation-potential scattering of holes in multiple quantum well structures. *Phys. Rev. B*, **65**(4):045302, 2001.

[88] M. Cardona, M. Grimsditch, and D. Olego. Theoretical and experimental determination of Raman scattering cross sections in simple solids. In J. L. Birman, H. Z. Cummins, and K. K. Rebane, Eds., *Light Scattering in Solids*, pages 249–256. Plenum, New York, 1979.

[89] D. Braun, W. W. Rühle, C. Trallero-Giner, and J. Collet. Spectroscopic determination of the optical deformation-potential constant in semiconductors. *Phys. Rev. Lett.*, **67**(17):2335, 1991.

[90] D. Braun. *Exzitondynamik in CdSe*. PhD thesis, Universität Stuttgart, 1991.

[91] W. Pötz and P. Vogl. Theory of optical-phonon deformation potentials in tetrahedral semiconductors. *Phys. Rev. B*, **24**(4):2025, 1981.

[92] P. Vogl. Microscopic theory of electron-phonon interaction in insulators or semiconductors. *Phys. Rev. B*, **13**(2):694, 1976.

[93] C. Cohen-Tannoudji, J. Dupont-Roc, and G. Grynberg. *Photons and Atoms*. Wiley Interscience, New York, 1989.

[94] M. Göppert-Mayer. Über Elementarakte mit zwei Quantensprüngen. *Ann. Phys. (Leipzig)*, **9**(3):273, 1931.

[95] W. Schäfer and M. Wegener. *Semiconductor Optics and Transport Phenomena*. Springer, Berlin, 2002.

[96] M. Shim and P. Guyot-Sionnest. n-type colloidal semiconductor nanocrystals. *Nature*, **407**:981, 2000.

[97] M. F. Bertino, R. R. Gadipalli, L. A. Martin, L. E. Rich, A. Yamilov, B. R. Heckman, N. Leventis, S. Guha, J. Katsoudas, R. Divan, and D. C. Mancini. Quantum dots by ultraviolet and X-ray lithography. *Nanotechnology*, **18**(31):315603, 2007.

[98] P. M. Petroff and S. P. DenBaars. MBE and MOCVD growth and properties of self-assembling quantum dot arrays in III-V semiconductor structures. *Superlatt. Microstr.*, **15**(1):15, 1994.

[99] H. Drexler, D. Leonard, W. Hansen, J. P. Kotthaus, and P. M. Petroff. Spectroscopy of quantum levels in charge-tunable InGaAs quantum dots. *Phys. Rev. Lett.*, **73**(16):2252, 1994.

[100] S. Fafard, D. Leonard, J. L. Merz, and P. M. Petroff. Selective excitation of the photoluminescence and the energy levels of ultrasmall InGaAs/GaAs quantum dots. *Appl. Phys. Lett.*, **65**(11):1388, 1994.

[101] E. Bauer. Phänomenologische Theorie der Kristallabscheidung an oberflächen i. *Z. Kristall.*, **110**:372, 1958.

[102] I. Stranski and L. von Krastanow. *Abhandlungen der Mathematisch-Naturwissenschaftlichen Klasse. Akademie der Wissenschaften und der Literatur in Mainz*, **146**:797, 1939.

[103] S. Raymond, S. Fafard, P. J. Poole, A. Wojs, P. Hawrylak, S. Charbonneau, D. Leonard, R. Leon, P. M. Petroff, and J. L. Merz. State filling and time-resolved photoluminescence of excited states in $In_xGa_{1-x}As$/GaAs self-assembled quantum dots. *Phys. Rev. B*, **54**(16):11548, 1996.

[104] A. Wojs, P. Hawrylak, S. Fafard, and L. Jacak. Electronic structure and magneto-optics of self-assembled quantum dots. *Phys. Rev. B*, **54**(8):5604, August 1996.

[105] M. Abramowitz and I. A. Stegun. *Handbook of Mathematical Functions*. Dover, New York, 9$^{\text{th}}$ edition, 1970.

[106] R. J. Elliott. Theory of excitons–I. In C. G. Kuper and G. D. Whitfield, Eds., *Polarons and Excitons*, Edinburgh and London, 1962. Scottish Universities' Summer School, Oliver and Boyd.

[107] F. Jahnke, M. Kira, S. W. Koch, G. Khitrova, E. K. Lindmark, T. R. Nelson, Jr., D. V. Wick, J. D. Berger, O. Lyngnes, H. M. Gibbs, and K. Tai. Excitonic nonlinearities of semiconductor microcavities in the nonperturbative regime. *Phys. Rev. Lett.*, **77**(26):5257, 1996.

[108] S. W. Koch, M. Kira, W. Hoyer, and V. Filipinov. Exciton ionization in semiconductors. *Phys. Stat. Sol. (b)*, **238**(3):404, 2003.

[109] G. S. Solomon, M. Pelton, and Y. Yamamoto. Single-mode spontaneous emission from a single quantum dot in a three-dimensional microcavity. *Phys. Rev. Lett.*, **86**(17):3903, 2001.

[110] P. Lodahl, A. F. van Driel, I. S. Nikolaev, A. Irman, K. Overgaag, D. Vanmaekelbergh, and W. L. Vos. Controlling the dynamics of spontaneous emission from quantum dots by photonic crystals. *Nature*, **430**:654, 2004.

[111] M. Kira, F. Jahnke, and S. W. Koch. Microscopic theory of excitonic signatures in semiconductor photoluminescence. *Phys. Rev. Lett.*, **81**(15):3263, 1998.

[112] I. I. Rabi. Space quantization in a gyrating magnetic field. *Phys. Rev.*, **51**(8):652, 1937.

[113] I. I. Rabi, S. Millman, P. Kusch, and J. R. Zacharias. The molecular beam resonance method for measuring nuclear magnetic moments. *Phys. Rev.*, **55**(6):526, 1939.

[114] M. Sargent III, M. O. Scully, and W. Lamb. *Laser Physics.* Addison Wesley, New York, 1974.

[115] C. Cohen-Tannoudji, B. Diu, and F. Laloë. *Quantum Mechanics*, volume I. Wiley Interscience, New York, 1977.

[116] R. Binder, S. W. Koch, M. Lindberg, N. Peyghambarian, and W. Schäfer. Ultrafast adiabatic following in semiconductors. *Phys. Rev. Lett.*, **65**(7):899, 1990.

[117] S. T. Cundiff, A. Knorr, J. Feldmann, S. W. Koch, E. O. Göbel, and H. Nickel. Rabi flopping in semiconductors. *Phys. Rev. Lett.*, **73**(8):1178, Aug 1994.

[118] H. Benisty. Reduced electron-phonon relaxation rates in quantum-box systems: Theoretical analysis. *Phys. Rev. B*, **51**(19):13281, 1995.

[119] O. Verzelen, R. Ferreira, G. Bastard, T. Inoshita, and H. Sakaki. Polaron effects in quantum dots. *Phys. Stat. Sol. (a)*, **190**(1):213, 2002.

[120] T. Inoshita and H. Sakaki. Electron relaxation in a quantum dot: Significance of multiphonon processes. *Phys. Rev. B*, **46**(11):7260, 1992.

[121] T. Inoshita and H. Sakaki. Density of states and phonon-induced relaxation of electrons in semiconductor quantum dots. *Phys. Rev. B*, **56**(8):R4355, 1997.

[122] H. Jiang and J. Singh. Self-assembled semiconductor structures: Electronic and optoelectronic properties. *IEEE J. Qu. Electr.*, **34**(7):1188, 1998.

[123] T. R. Nielsen. *Carrier-Carrier and Carrier-Phonon Scattering in Self-Assembled Quantum Dots.* PhD thesis, Universität Bremen, 2005.

[124] M. Goodman. Zeno-based Opto-Electronics (ZOE). Internet resource, `http://www.darpa.mil/dso/solicitations/baa09-19.htm`, 2008. Solicitation by Defense Advanced Research Projects Agency, USA.

[125] Y. Z. Hu, S. W. Koch, M. Lindberg, N. Peyghambarian, E. L. Pollock, and F. F. Abraham. Biexcitons in semiconductor quantum dots. *Phys. Rev. Lett.*, **64**(15):1805, 1990.

[126] F. Jahnke, M. Kira, and S. W. Koch. Linear and nonlinear optical properties of quantum confined excitons in semiconductor microcavities. *Z. Phys. B*, **104**(2):559, 1997.

[127] I. A. Akimov, J. T. Andrews, and F. Henneberger. Stimulated emission from the biexciton in a single self-assembled II-VI quantum dot. *Phys. Rev. Lett.*, **96**(6):067401, 2006.

[128] U. Woggon, M. Portun, C. Klingshirn, H. Giessen, B. Fluegel, G. Mohs, and N. Peyghambarian. Dephasing processes in II-VI quantum dots. *Phys. Stat. Sol. (b)*, **188**(1):221, 1995.

[129] B. Patton, W. Langbein, and U. Woggon. Trion, biexciton, and exciton dynamics in single self-assembled CdSe quantum dots. *Phys. Rev. B*, **68**(12):125316, 2003.

[130] D. S. Bulyanitsa. *Sov. Phys. Semicond.*, **4**:1081, 1970.

140

[131] S. Zollner, S. Gopalan, and M. Cardona. Intervalley deformation potentials and scattering rates in zinc blende semiconductors. *Appl. Phys. Lett.*, **54**(7):614, 1989.

[132] A. Chernikov, S. Horst, and S. Chatterjee. Private communication, May 2009. Experiments performed at the Philipps-University Marburg.

[133] B. Segall. Optical absorption edge in CdTe: Theoretical. *Phys. Rev.*, **150**(2):734, 1966.

[134] O. Verzelen, R. Ferreira, and G. Bastard. Excitonic polarons in semiconductor quantum dots. *Phys. Rev. Lett.*, **88**(14):146803, 2002.

[135] W. Shan, X. C. Xie, J. J. Song, and B. Goldenberg. Time-resolved exciton luminescence in GaN grown by metalorganic chemical vapor deposition. *Appl. Phys. Lett.*, **67**(17):2512, 1995.

[136] E. Gross, S. Permogorov, and B. Razbirin. Free exciton motion in crystals and exciton-phonon interaction. *J. Phys. Chem. Solids*, **27**:1647, 1966.

[137] C. Klingshirn. *Semiconductor Optics*. Springer, Berlin, 2nd edition, 2005.

[138] H.-C. Hsu and W.-F. Hsieh. Excitonic polaron and phonon assisted photoluminescence of ZnO nanowires. *Sol. State Comm.*, **131**(6):371, 2004.

[139] M. Sabathil. Private communication, July 2008. Data provided by OSRAM Opto Semiconductors.

[140] K. Huang and A. Rhys. Theory of light absorption and non-radiative transitions in F-centers. *Proc. R. Soc. London, Ser. A*, **204**(1078):406–423, December 1950.

[141] M. A. Stroscio and M. Dutta. *Phonons in Nanostructures*. Cambridge University Press, Cambridge, 2001.

[142] T. Voss. Private communication, June 2008. Experiments performed at the University of Bremen.

[143] C. Klingshirn. Private communication, May 2009.

Mein Dank gilt. . .

...Mackillo Kira und Stephan W. Koch für das interessante Promotionsthema sowie die freundliche, motivierende und perfekt organisierte[1] Betreuung,

...Florian Gebhard für die Übernahme des Zweitgutachtens unter erschwerten Bedingungen,

...Lukas Schneebeli, Walter Hoyer und Christoph Böttge für hilfreiche Diskussionen und erfrischendes Um-die-Wette-kommutieren,

...Alexej Chernikov, Swantje Horst und Matthias Sabathil für die schönen Spektren,

...dem Graduiertenkolleg „Electron-Electron Interactions in Solids" für die Seminare und Workshops, an denen ich teilnehmen durfte,

...Peter Thomas für die Organisation der Pfalzwanderungen sowie den regelmäßigen Austausch von Altersweisheiten,

...Renate Schmid für die Unterstützung bei den alltäglichen bürokratischen Dramen,

...Sascha Becker, Christoph Schlichenmaier, Sven Siggelkow, Sebastian Imhof, Eckhard A. Kühn, Daniel H. Golde und Michael Walther für das innere Lächeln, mit dem ich jeden Morgen das Büro betrete, sowie das Durchfüttern auf unzähligen Hochzeiten,

...ausdrücklich auch *jedem* anderen Mitglied der Gruppe für ihren oder seinen Beitrag zu dem einmalig guten Arbeitsklima,

...meinen Studenten für die gestrenge Kollegin, die seit einem Jahr aus einem Ehrenplatz im Bücherregal über meine Arbeit wacht,

...Anna Stümke für die Entdeckung, Erforschung und grafische Darstellung des unterscheidbaren Hausphonons,

...Familie Becker für den gemeinsamen Versuch, in der hessischen Diaspora ein wenig maritime Lebensart aufrechtzuerhalten,

...Matthias Reichelt für seine regelmäßigen Ermahnungen, sich mehr mit den wichtigen Dingen im Leben zu beschäftigen,

...und schließlich meiner Familie für ihre arg strapazierte Geduld!

---

[1]Die *message rules* beherzige ich inzwischen auch beim Schreiben von Geburtstagseinladungen, Urlaubskarten und Liebesbriefen.